Mobile Information Systems

Ambient Intelligence for Massive Communication in Mobile Information Systems

Lead Guest Editor: Zhu Han
Guest Editors: Yajuan Tang and Jie Wang

Ambient Intelligence for Massive Communication in Mobile Information Systems

Mobile Information Systems

Ambient Intelligence for Massive Communication in Mobile Information Systems

Lead Guest Editor: Zhu Han
Guest Editors: Yajuan Tang and Jie Wang

Contents

Hindawi
Mobile Information Systems
Volume 2023, Article ID 9793406, 1 page
https://doi.org/10.1155/2023/9793406

Retraction

Retracted: Naive Bayes Algorithm Mining Mobile Phone Trojan Crime Clues

Mobile Information Systems

Received 26 September 2023; Accepted 26 September 2023; Published 27 September 2023

This article has been retracted by Hindawi following an investigation undertaken by the publisher [1]. This investigation has uncovered evidence of one or more of the following indicators of systematic manipulation of the publication process:

(1) Discrepancies in scope
(2) Discrepancies in the description of the research reported
(3) Discrepancies between the availability of data and the research described
(4) Inappropriate citations
(5) Incoherent, meaningless and/or irrelevant content included in the article
(6) Peer-review manipulation

The presence of these indicators undermines our confidence in the integrity of the article's content and we cannot, therefore, vouch for its reliability. Please note that this notice is intended solely to alert readers that the content of this article is unreliable. We have not investigated whether authors were aware of or involved in the systematic manipulation of the publication process.

Wiley and Hindawi regrets that the usual quality checks did not identify these issues before publication and have since put additional measures in place to safeguard research integrity.

We wish to credit our own Research Integrity and Research Publishing teams and anonymous and named external researchers and research integrity experts for contributing to this investigation.

The corresponding author, as the representative of all authors, has been given the opportunity to register their agreement or disagreement to this retraction. We have kept a record of any response received.

References

[1] F. Zhao, "Naive Bayes Algorithm Mining Mobile Phone Trojan Crime Clues," *Mobile Information Systems*, vol. 2022, Article ID 6262147, 11 pages, 2022.

Hindawi
Mobile Information Systems
Volume 2023, Article ID 9768158, 1 page
https://doi.org/10.1155/2023/9768158

Retraction

Retracted: Research on Vessel Speed Heading and Collision Detection Method Based on AIS Data

Mobile Information Systems

Received 8 August 2023; Accepted 8 August 2023; Published 9 August 2023

This article has been retracted by Hindawi following an investigation undertaken by the publisher [1]. This investigation has uncovered evidence of one or more of the following indicators of systematic manipulation of the publication process:

(1) Discrepancies in scope
(2) Discrepancies in the description of the research reported
(3) Discrepancies between the availability of data and the research described
(4) Inappropriate citations
(5) Incoherent, meaningless and/or irrelevant content included in the article
(6) Peer-review manipulation

The presence of these indicators undermines our confidence in the integrity of the article's content and we cannot, therefore, vouch for its reliability. Please note that this notice is intended solely to alert readers that the content of this article is unreliable. We have not investigated whether authors were aware of or involved in the systematic manipulation of the publication process.

Wiley and Hindawi regrets that the usual quality checks did not identify these issues before publication and have since put additional measures in place to safeguard research integrity.

We wish to credit our own Research Integrity and Research Publishing teams and anonymous and named external researchers and research integrity experts for contributing to this investigation.

The corresponding author, as the representative of all authors, has been given the opportunity to register their agreement or disagreement to this retraction. We have kept a record of any response received.

References

[1] G. Wang, E. Fan, G. Zheng, K. Li, and H. Huang, "Research on Vessel Speed Heading and Collision Detection Method Based on AIS Data," *Mobile Information Systems*, vol. 2022, Article ID 7257075, 10 pages, 2022.

Hindawi
Mobile Information Systems
Volume 2023, Article ID 2074890, 9 pages
https://doi.org/10.1155/2023/2074890

Research Article

IoT Networks-Aided Perception Vocal Music Singing Learning System and Piano Teaching with Edge Computing

Qian Li, Heng Liu, and Xiaoming Zhao

College of Art, Hebei Agricultural University, Baoding 071001, Hebei, China

Correspondence should be addressed to Heng Liu; liu123heng456@stu.cpu.edu.cn

Received 14 July 2022; Revised 8 September 2022; Accepted 29 September 2022; Published 28 April 2023

Academic Editor: Yajuan Tang

The research on Internet of Things (IoT) network and edge computing has been a research hotspot in both industry and academia in recent years, especially for the ambient intelligence and massive communication. As a typical form of IoT network and edge computing, the intelligent perception vocal music singing learning system has attracted the attention of researchers in education and academia. Piano teaching is an important course for music majors in higher education. Strengthening piano teaching can cultivate outstanding piano talents for the country and promote the development of music art. This paper applies IoT perception technology to piano teaching, constructs an intelligent piano teaching system, and uses edge computing algorithms to accurately deploy sensors into the system by exploiting the ambient intelligence and massive communication. The system includes data acquisition, data perception, data monitoring, and other modules, making piano teaching more humanized and intelligent. Experiments show that the research in this paper provides important guidance for the application of IoT networks and edge computing, especially for the ambient intelligence and massive communication.

1. Introduction

The research on IoT network and edge computing has been a research hotspot in both industry and academia in recent years, especially for the ambient intelligence and massive communication. As a typical form of IoT network and edge computing, the intelligent perception vocal music singing learning system has attracted the attention of researchers in education and academia. This paper applies IoT perception technology to piano teaching, constructs an intelligent piano teaching system, and uses edge computing algorithms to accurately deploy sensors into the system. The system includes data acquisition, data perception, data monitoring, and other modules, making piano teaching more humanized and intelligent, through the ambient intelligence and massive communication. It is an attempt and an innovation to apply IoT technology and edge computing to piano teaching.

Based on the IoT network technology and edge computing, many scholars have carried out research work. Rao made a comprehensive analysis of piano teaching by using the fuzzy comprehensive evaluation method. The results have shown that the idea based on fuzzy mathematics promotes the progress of piano teaching [1]. Demrayak and Temel applied sensor technology to the piano teaching system, which effectively evaluated the arm movements of piano students [2]. Hamond et al. introduced automatic information technology into piano teaching, making piano teaching more vivid [3]. Zhao discussed the development status of piano teaching in the context of "micro-era". Practice has shown that the teaching method under the "micro era" has realized the upgrading of piano professional teaching from teaching concept to evaluation system [4]. Ryu analyzed the problems existing in today's piano teaching classroom and proposes corresponding solutions to these problems [5]. These studies on the application of the IoT network in piano teaching are rich, but lack pertinence.

With the progress of the times, there are more and more application scenarios of edge computing. Kouziokas and Perakis proposed a collaboration-based industrial intelligent perception framework that realizes intelligent and efficient industrial production services [6]. Liang et al. designed an

intelligent perception system for battlefield intelligence, which can accurately analyze the military requirements, combat operations and mission requirements of the joint battlefield [7]. Akinsunmade and Ejieji applied the Bluetooth sensor and Bluetooth adapter to the intelligent perception recognition system. The experimental results have shown that the system has strong stability and fast sensing speed [8]. Yan et al. proposed a crowdsourcing-based industrial intelligent perception system, using which factories improved productivity and workplace safety [9]. Liang et al. applied IntelliSense technology to home sleep monitoring. Experimental results have shown that this technique is effective in detecting irregular sleep [10]. Xiao et al. proposed an edge detection algorithm based on IntelliSense. Experiments show that the algorithm is effective for edge detection of color remote sensing images [11]. Du et al. developed a distributed cooperative spectrum sensing algorithm based on IntelliSense. Simulation results have shown that the algorithm improves the detection efficiency to a certain extent [12]. The above research on edge computing is relatively detailed, but less related to the IoT.

IoT networks have come a long way in recent years. As an important part of the Internet of Things, edge computing has also attracted the attention of many researchers. This paper applies the IoT network to the piano teaching system, and then uses the edge computing algorithm to accurately deploy the sensors into the system. The research found that the new piano teaching system proposed in this paper has important reference significance for the next development of the Internet of Things and edge computing, especially for the ambient intelligence and massive communication.

2. IoT-Based Intelligent Perception and Vocal Singing

2.1. IoT-Based Intelligent Perception Technology. Based on the IoT network and edge computing, this paper studies the intelligent sensing technology. Intelligent perception is the process of acquiring and processing external information using sensors and network technology. The specific content of intelligent perception is shown in Figure 1. "Sense" refers to sensing technology, and "knowledge" refers to recognition technology. Among them, sensing technologies include sensor sensing, radar sensing, and satellite sensing, and recognition technologies include image processing, image analysis, and image understanding. At present, the intelligent sensing technology is quite mature, and the applications in enterprises include intelligent access control and intelligent front desk [13]. Smart access control is to enable the machine to have the ability to perceive, to capture the face through the camera for perceptual recognition, and to compare with the database face image, so as to perform attendance access control check-in. The smart front desk mainly uses face recognition for appointment registration.

2.2. IoT Based Intelligent Perception Vocal Music Singing Learning System. Based on the IoT network and edge computing, this paper builds an intelligent perception vocal learning system as shown in Figure 2. In this system, learning resources refer to all available teaching resources related to vocal music learning. It includes vocal data, PPT courseware, audio, and video, and each resource is set with a corresponding identification keyword. Learning feeling refers to the use of mobile positioning technology to build a virtualized resource navigation map of cyberspace, to perceive, locate, and extract relevant vocal music learning information of an application, so as to provide effective intelligent perception application services. Learning feeling is to use intelligent perception technology to acquire and locate vocal music learning information, and then provide corresponding services for learners.

With the help of the IoT network and edge computing, vocal music learning resources can also form a three-dimensional personalized knowledge perception map. Among them, the first dimension is the resource-aware navigation for learners entering the learning resource platform, the second dimension is to accurately locate the learning content and related information, and the third dimension is to complete the matching between learners' learning needs and potential resources.

3. IoT Network and Edge Computing-Based Piano Teaching Model

Assisted by the IoT networks and edge computing, vocal singing and piano accompaniment are interrelated, and a good piano accompaniment can make vocal singing more musical. In this paper, the application of the intelligent perception vocal music singing learning system to the piano teaching mode can also be said to complement each other.

3.1. IoT-Based Intelligent Piano Teaching System. Combined with the IoT network and edge computing, this paper draws the architecture diagram of the piano teaching system shown in Figure 3. First, establish the connection between the vocal music singing learning system and piano teaching, so that students can play with a purpose. Piano accompaniment music itself and vocal singing are interdependent in melody, and the fusion of the two can complete a more beautiful melody. Then, there is the realization of the perception function. In order to realize the perception function, there must be certain software and hardware to support it. Therefore, sensors are arranged in the learning process of piano teaching, and the learner wears an intelligent induction bracelet. The bracelet can monitor the learner's technique and playing process in real time, and record the whole process. Finally, according to the piano teaching data on the bracelet, piano teachers and students can make an assessment of the piano learning efficiency.

3.2. IoT-Based Realization Process of Intelligent Perception. Combined with the IoT network, this paper constructs the realization process of intelligent perception as shown in Figure 4, including three parts: sensing unit, computing unit, and interface unit.

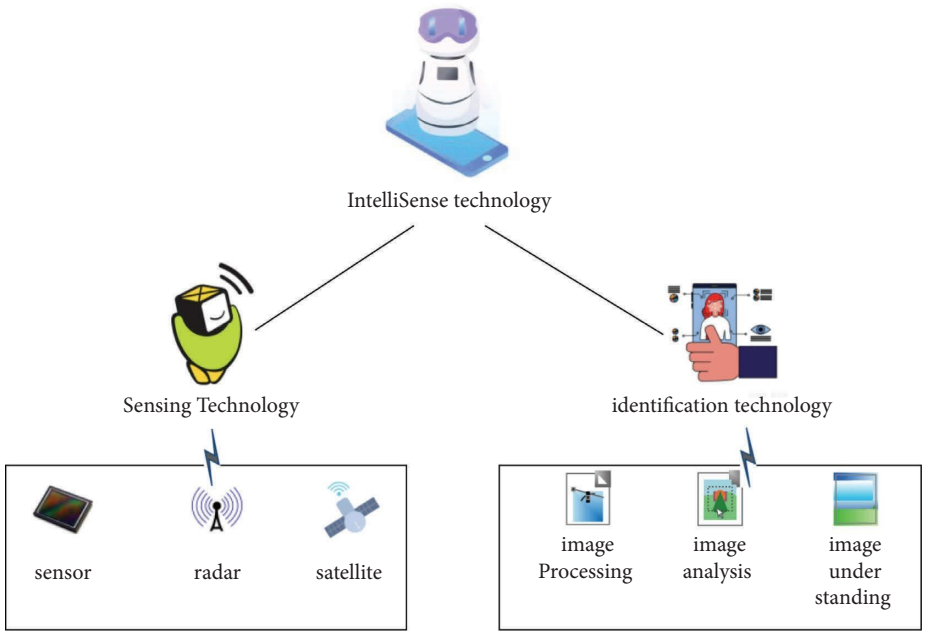

Figure 1: IoT-based intelligent technology framework.

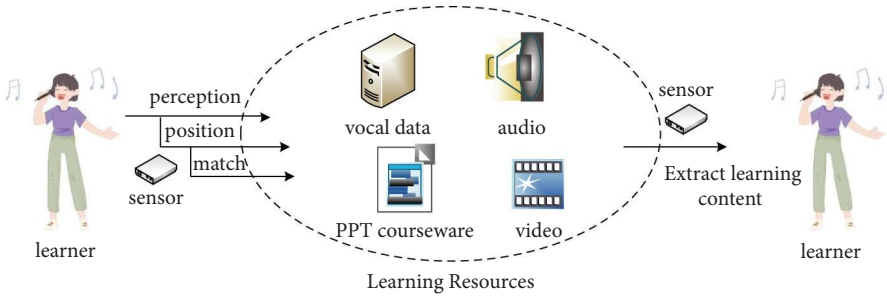

Figure 2: IoT network and edge computing based intelligent perception vocal learning system based on.

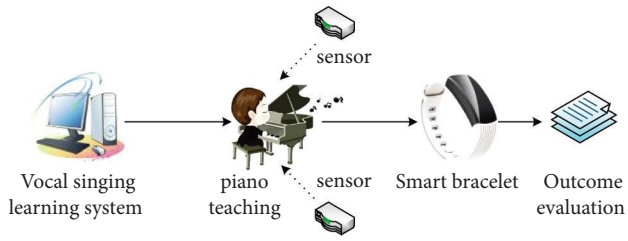

Figure 3: IoT network and edge computing-based architecture of piano teaching system.

Several sensors are arranged in the sensing unit to monitor and record the entire teaching process. The data in the sensor will be transmitted to the computing unit in time, and the computing process of the unit includes signal acquisition, data processing, and data storage. The signal collection is divided into image collection and audio collection. The image collection collects the position, depth, and foot movement of the fingers pressing the piano keys through multiple cameras, and the audio collection collects the piano playing sound through the omnidirectional microphone. Data processing is the modeling of piano temperament and piano score, and the processing and analysis of audio. Data storage is to save all the data generated in the process of piano teaching. Both ends of the interface unit are connected with intelligent sensors and external network systems to ensure the smooth operation of the entire intelligent sensing work.

3.3. IoT Networks-Based Application Demonstration of Intelligent Piano Teaching System. Combined with the IoT network and edge computing, this paper constructs the application process of the intelligent piano teaching system as shown in Figure 5, which mainly includes three parts: acquisition module, perception module, and processing center. In piano teaching, playing technique and audio output are the two most important links [14], so the acquisition module also focuses on these two when collecting data. Through the network server, the acquisition module transmits the relevant data to the perception module, and then the processing center compares the fingering images and audio information in the data, and finally forms a new piano teaching mode.

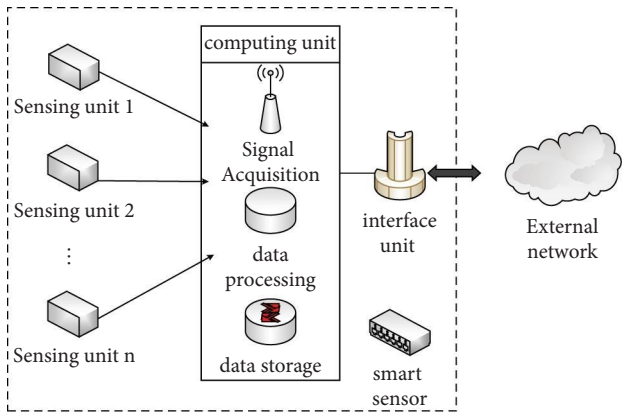

Figure 4: IoT network and edge computing-based realization process of intelligent perception in piano teaching system.

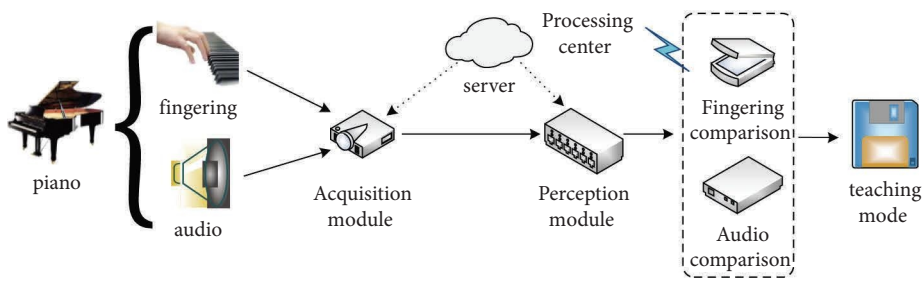

Figure 5: IoT network and edge computing-based application process of intelligent piano teaching system.

3.4. IoT-Based Organic Combination of Vocal Singing and Piano Teaching. Based on the IoT networks, in order to promote the better cooperation between vocal singing and piano teaching, this paper improves the teaching mode in the piano teaching classroom, that is, let the piano learners accompany the vocal singers to strengthen their cooperation consciousness. The specific content is as follows: first, the piano accompaniment and vocal singers analyze and understand the background and style of the work together under the guidance of the teacher, and the two must reach a consensus on understanding the work. Then, the piano accompanist also needs to understand the singing style of the singer. The more comprehensive he knows about the singer, the more he will be able to control the overall situation with certainty, and put into practice without accident, so that the processing of the work can achieve better results. Finally, the accompanist and the singer must be emotionally consistent, and the two must have a common purpose in their hearts, which is to finally express the emotion of the work correctly and jointly create a perfect musical image.

4. Application of Edge Computing Algorithm in Piano Teaching

Combined with the edge computing method of Gaussian mixture model, this paper deploys and locates the sensor equipment in piano teaching. According to the idea of Gaussian distribution [15], the distribution form of device nodes can be expressed as follows:

$$f(x, \alpha, \beta) = \frac{1}{\sqrt{2\pi\beta}} e^{-1/2(x-\alpha)^2\beta^2}. \tag{1}$$

In formula (1), α is the mean value of the Gaussian distribution, which describes the center position of the Gaussian distribution and β^2 is the variance of the Gaussian distribution, which describes the degree of concentration of the data in the distribution. The larger the β^2, the more dispersed the distribution, the smaller the β^2, the more concentrated. It can be known from this formula that the closer the sample node is to the center, the higher the probability will be, and the smaller the β^2, the more concentrated the sample node will be.

Assuming that all sample nodes are generated by Gaussian component, the distribution of sensor devices in piano teaching can be regarded as the problem that the sample nodes obey the Gaussian mixture model distribution. The calculation method is $G = \{g_1, g_2, g_3, \ldots g_k\}$.

$$p(x_a, \alpha, \beta) = \sum_{b=1}^{k} \alpha_b * f(x_a, \alpha_b, \beta_b). \tag{2}$$

Where α_b represents the weight of each Gaussian model component and satisfies the following equation:

$$\sum_{b=1}^{k} \alpha_b = 1, \tag{3}$$

$$0 \le \alpha_b \le 1, \forall_b \in [1, k]. \tag{4}$$

After calculating the probability distribution of each sample node, the probability values of all sample distributions can be obtained by multiplying the probability of each sample node. The calculation method is as follows:

$$\max\prod_{a=1}^{N} = \sum_{b=1}^{k} \alpha_v * f\left(x_a, \alpha_b, \beta_b\right). \tag{5}$$

The previous Gaussian mixture model simply compares the probability to cluster the sample nodes, which often results in the imbalance between some Gaussian components [16]. In order to ensure that the load belonging to each Gaussian component is relatively balanced, the following mathematical model is established:

$$B_b = \sum_{a=1}^{N} p_{ab} * c_{ab} * y_{ab}. \tag{6}$$

In the formula, B_b represents the total load of the Gaussian component g_b, p_{ab} represents the probability of the node b on the Gaussian component g_b, c_{ab} represents the load required by the sensor device g_b to connect the terminal device x_a, and y_{ab} is a binary variable. The loading of the entire Gaussian mixture model can be written as follows:

$$B = \frac{1}{k}\sum_{b=1}^{k}\sum_{a=1}^{N} p_{ab} * c_{ab} * y_{ab}. \tag{7}$$

In order to ensure the load balancing of the entire Gaussian mixture model [17], the objective function is as follows:

$$\min\sqrt{\frac{1}{k-1}} = \sum_{b=1}^{k}\left(B_b - B\right)^2, \tag{8}$$

$$s.t\ y_{ab} \in \{0, 1\}, 1 \le a \le N, 1 \le b \le k, \tag{9}$$

$$\sum_{b=1}^{k} y_{ab} = 1, \quad \beta_{ab}^{t+1} = \frac{\sum_{a=1}^{N} \omega_{ab}^{t+1}}{N}, \tag{10}$$

$$\sum_{b=1}^{N} y_{ab} * c_{ab} \le c_b. \tag{11}$$

The restriction formula (9) represents the indicator variable of y_{ab}, which can only take values between 0 and 1. Formula (10) indicates that each sensor device can only be clustered into one gateway.

Generally, in the problem of parameter estimation of edge devices, variable selection is a primary problem to be solved, because the selection of variables is related to whether the subsequent model parameter estimation can be performed accurately. Variable selection must be performed when estimating parameters of edge devices. The selection of variables should be based on some information criteria. Commonly used information criteria include AIC (Akaike information criterion) criterion and BIC (Bayesian information criterion) criterion. The criterion expression is as follows:

$$AIC = -2 * \log H + 2K, \tag{12}$$

$$BIC = -2 * \log H + K * \log N. \tag{13}$$

In the formula, K represents the number of parameters to be estimated in the selected model, N represents the length of the selected model data sample, and H represents the maximum likelihood estimate of the model established with the sample node as a variable.

This paper uses the BIC criterion to solve the maximum likelihood estimate of the Gaussian mixture model, namely,

$$BIC = -2 * \max\sum_{a=1}^{N}\log\left(p\left(x_a, \alpha, \beta\right)\right) + K * \log N. \tag{14}$$

Firstly, different initial parameters are selected, and the maximum likelihood estimation value of Gaussian mixture model is obtained by the algorithm. Substituting into formula (14), the BIC value can be obtained, and then the smaller BIC value is selected as the number of Gaussian models in the Gaussian mixture model, so as to ensure the optimal number of edge sensor devices.

The last step of edge computing is to solve the objective function. The objective function expression above can be expressed as follows:

$$\max\sum_{a=1}^{N}\log\sum_{b=1}^{k}\alpha_b * f\left(x_a, \alpha_b, \beta_b\right). \tag{15}$$

Because of the Gaussian mixture model involved, it is very troublesome to directly find the derivative of the objective function, so this paper adopts the expectation-maximum iterative algorithm (EM) for calculation [18]. According to the above, the iteration expression can be expressed as follows:

$$\omega_{ab}^{t+1} = \frac{\alpha_b^t * f\left(x_a, \alpha_b^t, \beta_b^t\right)}{\sum_{b=1}^{K}\alpha_b^t * f\left(x_a, \alpha_b^t, \beta_b^t\right)}. \tag{16}$$

In the formula, t represents the number of iterations. The parameters of each Gaussian model component can be estimated from the probability data. The specific process is as follows:

$$\alpha_b^{t+1} = \frac{\sum_{a=1}^{N}\omega_{ab}^{t+1} * x_a}{\sum_{a=1}^{N}\omega_{ab}^{t+1}}, \tag{17}$$

$$\beta_b^{t+1} = \frac{\sum_{i=1}^{N}\omega_{ab}^{t+1}\left(x_a - \alpha_b^t\right)\left(x_a - \alpha_b^t\right)^T}{\sum_{i=1}^{N}\omega_{ab}^{t+1}}, \tag{18}$$

$$\alpha_{ab}^{t+1} = \frac{\sum_{a=1}^{N}\omega_{ab}^{t+1}}{N}. \tag{19}$$

The parameters of each Gaussian model are denoted as $\theta = \{\theta_1, \theta_2, \theta_3, \ldots\theta_k\}$, and each model as $\theta_b = (\alpha_b, \beta_b)$, according to the number of iterations, the parameters of

Table 1: IoT network and edge computing-based adaptability of teachers and students in the piano teaching model.

Degree of adaptation	Teacher		Student	
	Number of people	Proportion	Number of people	Proportion
Cannot adapt	4	1.3%	8	2.7%
Not very suitable	7	2.4%	13	4.3%
General adaptation	23	7.7%	46	15.3%
Well adapted	96	32%	103	34.4%

each Gaussian model component can be expressed as follows:

$$\theta_b^{T+1} = \left(\alpha_b^{t+1}, \beta_b^{t+1}\right). \tag{20}$$

By multiplying the parameter values of each Gaussian component, and then calculating the sample node value of each Gaussian component, the sensor device can be arranged at the edge of the path of the piano teaching system.

5. IoT Network and Edge Computing-Based Practice Results and Analysis of Piano Teaching Mode

Combining the IoT network and edge computing, this paper proposes a new piano teaching model. In order to analyze whether the new piano teaching mode can make students and piano teachers adapt, this paper investigates the degree of adaptation of 300 teachers and students in a certain college to the new piano teaching mode. The survey results are shown in Table 1.

From IoT networks as well as the number and proportion of the adaptation level in Table 1, it can be clearly seen that there are very few people who cannot adapt to this model. Generally, there are relatively more people who adapt, and the number of teachers and students accounts for 23% of the total number. People accounted for the majority, and the number of teachers and students accounted for 66.4% of the total number, which also shows from the side that it is relatively successful to apply the IoT network and edge computing to piano teaching.

The most important thing in the IoT based piano teaching is students' autonomy. In addition to the teaching content in the classroom, it is also very necessary for students to practice piano after class. In order to verify whether the new piano teaching mode can improve students' autonomy, the time spent practicing piano after class under the traditional piano teaching mode and the new piano teaching mode was investigated. The specific period is five weeks, and the survey results are shown in Figure 6.

As can be seen from the histogram in Figure 6, the practice time of the new mode in the first two weeks was only a little higher than that of the traditional mode, and there was a downward trend. This corresponds to the degree of adaptation mentioned above, and there must be a process for students to change between the two modes. From the third week, the students' piano practice time has increased significantly. The third week is nearly 15 hours longer than the second week, and the next two weeks have also maintained

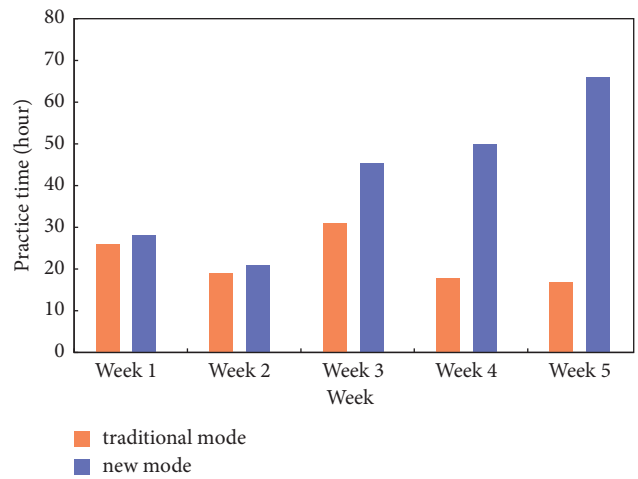

Figure 6: IoT network and edge computing-based after-class piano practice time under the traditional piano teaching mode and the piano teaching mode.

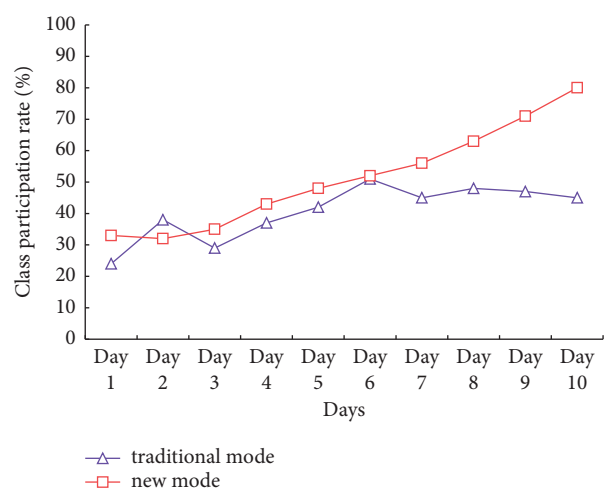

Figure 7: IoT network and edge computing-based classroom participation rate in traditional piano teaching mode and piano teaching mode.

an upward trend. In contrast to the traditional model, although the duration of piano practice in the last three weeks has greatly increased in the third week, there has been a downward trend in the next two weeks. Generally speaking, the piano practice time under the new piano teaching mode is much longer than that in the traditional piano teaching mode, and as time goes by, the time is always on the rise.

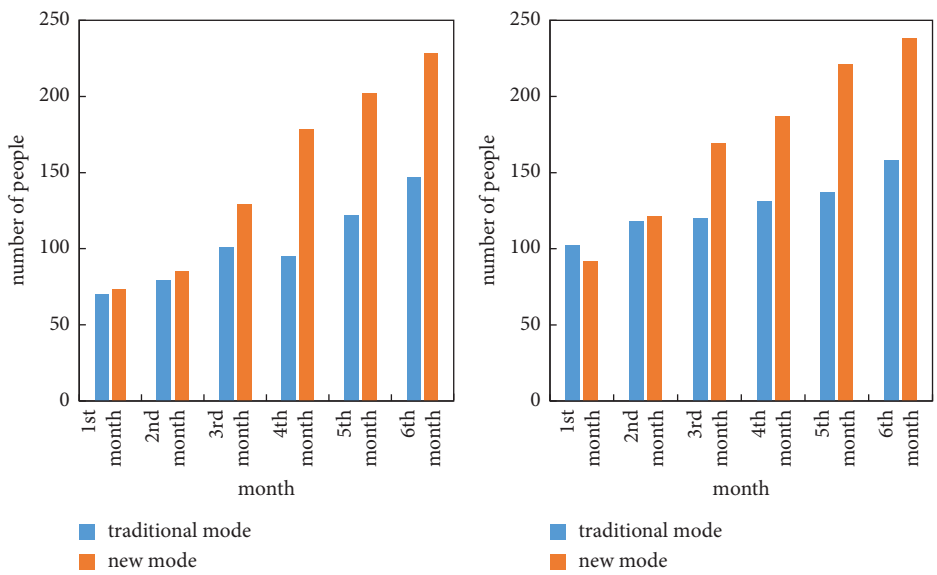

Figure 8: IoT network and edge computing-based status of piano grading under the piano teaching mode.

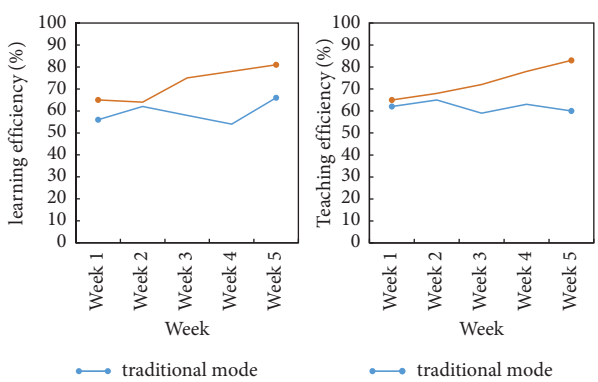

Figure 9: IoT network and edge computing-based learning efficiency and teaching efficiency under the traditional piano teaching mode and the piano teaching mode.

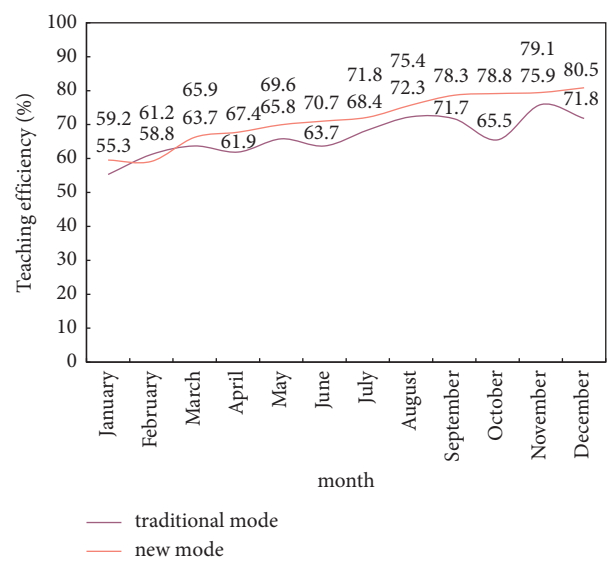

Figure 10: IoT network and edge computing-based teaching efficiency of traditional piano teaching mode and piano teaching mode within one year.

To measure the quality of an IoT based teaching model, the classroom participation rate is undoubtedly one of the best indicators. Figure 7 shows the classroom participation rate of the traditional piano teaching model and the new piano teaching model within 10 days.

It can be seen from the line chart in Figure 7 that the difference in the IoT based classroom participation rates between the two modes within 10 days is still relatively large. The first three days of classroom participation rates were relatively low, and on the second day, the participation rate under the traditional teaching model was even a little higher than that of the new teaching model. This is understandable, after all, it takes a certain process for students to accept the new teaching model. From the fourth day, the class participation rate in both modes started to rise, but the status of the rise was different in the following days. The classroom participation rate under the new teaching model has always been on the rise, while the participation rate of the classroom participation rate under the traditional teaching model fluctuates greatly and has a downward trend. Comparing the line charts, it is easy to draw that the classroom participation rate under the new teaching model is much higher than that of the traditional teaching model, and it is relatively stable.

In order to better demonstrate the practical effect of the new IoT based piano teaching mode, the students' piano grading test in the classroom was investigated. The specific period is the first 6 months, and the total number of people is 500. The survey results are shown in Figure 8.

From the perspective of edge computing, the first small histogram in Figure 8 represents the passing result of the piano teaching test based on the Internet of Things mode, and the second small histogram represents the passing result of the piano teaching test based on the edge computing mode. It can be seen that in the first two months, the number

of people who passed the test under the two modes were not much different, and the number of people who passed the test did not even exceed 100 in the first two weeks. With the passage of time, from the third month onwards, the number of passing grades and the number of passing grades in both modes have increased, but the difference in the growth rate is still obvious. The growth rate under the new model can be said to be soaring. In the sixth month, the number of people who passed the exam and passed the grades reached more than 200. In contrast to the traditional model, its growth rate is relatively small, and there is still a decline in individual months.

From the basis of IoT networks and edge computing, the purpose of integrating intelligent perception technology and vocal singing in the piano teaching mode is to improve the learning efficiency of students on the one hand, and to improve the teaching efficiency of piano teachers on the other hand. Figure 9 presents the learning efficiency and teaching efficiency of the two modes over five weeks.

The first small line graph in Figure 9 shows the edge computing-based learning efficiency in the two modes over five weeks, and the second shows the teaching efficiency. The learning efficiency under the traditional piano teaching mode did not exceed 70% at the highest level within five weeks, and was basically between 50% and 60%, and fluctuated greatly. From the first week of the new piano teaching mode, the learning efficiency has reached about 65%, and in the second week, there was a slight decline, and then it has maintained a steady increase. In terms of teaching efficiency, the traditional model is relatively stable, and the efficiency is maintained at around 60%, while the new model has been on the rise, which is also due to the adaptability of piano teachers to the new model.

Unlike other teaching, the IoT based piano teaching is a relatively slow process, which requires that the teaching mode must be matched with teachers and students. In order to better verify the practical effect of the new piano teaching mode, the teaching efficiency of this mode within one year was analyzed, and compared with the traditional piano teaching mode. The specific comparison results are shown in Figure 10.

From the graph in Figure 10, it can be seen that there is still a large gap in the efficiency of IoT based piano teaching under the two modes within one year. In the first two months, due to the conversion and adaptation of the two modes, the teaching efficiency has shown a crossover trend. Since March, the teaching efficiency test under the new piano teaching mode has gradually increased, and it has maintained a trend of no decline until December. In contrast to the traditional piano teaching model, although there is an upward trend in the middle months, the overall fluctuation is too great. In contrast, it is easy to conclude that the teaching efficiency of the new piano teaching mode is 7.31% higher than that of the traditional piano teaching mode within one year.

6. Conclusion

The research on IoT network and edge computing has been a research hotspot in both industry and academia in recent years, especially for the ambient intelligence and massive communication. As a typical form of IoT network and edge computing, the intelligent perception vocal music singing learning system has attracted the attention of researchers in education and academia. This paper applies IoT perception technology to piano teaching, constructs an intelligent piano teaching system, and uses edge computing algorithms to accurately deploy sensors into the system, through exploiting the ambient intelligence and massive communication. The final results show that the research in this paper provides important guidance for the application of IoT network and edge computing, especially for the ambient intelligence and massive communication.

Data Availability

The data that support the findings of this study are available from the corresponding author upon reasonable request.

Conflicts of Interest

The authors declare that they have no conflicts of interest.

References

[1] T. Rao, "The exploration of integrating piano teaching into ideological and political education from the perspective of morality building and people cultivating," *Region-Educational Research and Reviews*, vol. 3, no. 1, pp. 1–5, 2021.

[2] E. Demirayak and T. Temel, "An action research on the use of therapeutic stories as a new method of piano education," *Rast Müzikoloji Dergisi*, vol. 9, no. 1, pp. 2673–2706, 2021.

[3] L. Hamond, E. Himonides, and G. Welch, "The nature of feedback in higher education studio-based piano learning and teaching with the use of digital technology," *Orfeu*, vol. 6, no. 1, pp. 1–31, 2021.

[4] P. Zhao, "An optimized ability model construction of skill training in piano performance teaching," *Revista de la Facultad de Ingenieria*, vol. 32, no. 9, pp. 636–641, 2017.

[5] J. Y. Ryu, "I wish, I wonder, and everything I like: living stories of piano teaching and learning with young children," *LEARNing Landscapes*, vol. 11, no. 2, pp. 319–330, 2018.

[6] G. N. Kouziokas and K. Perakis, "Decision support system based on artificial intelligence, GIS and remote sensing for sustainable public and judicial management," *European Journal of Sustainable Development*, vol. 6, no. 3, pp. 397–404, 2017.

[7] X. Liang, R. Ghannam, and H. Heidari, "Wrist-worn gesture sensing with wearable intelligence," *IEEE Sensors Journal*, vol. 19, no. 3, pp. 1082–1090, 2019.

[8] A. E. Akinsunmade and C. N. Ejieji, "Land suitability and crop pattern model using integrated pollination intelligence algorithm and remote sensing," *Earthline Journal of Mathematical Sciences*, vol. 5, no. 1, pp. 1–15, 2020.

[9] R. Yan, A. Nandi, P. Wang, and W Li, "Guest editorial special issue on smart sensing and artificial intelligence-enabled data analytics for health monitoring of engineering systems," *IEEE Sensors Journal*, vol. 20, no. 15, p. 8203, 2020.

[10] Q. Liang, G. G. Yen, and T. S. Durrani, "Guest editorial: special issue on computational intelligence for communications and sensing," *IEEE Transactions on Emerging Topics in Computational Intelligence*, vol. 4, no. 1, pp. 1–4, 2020.

[11] F. Xiao, Z. Guo, Y. Ni, X. Xie, S. Maharjan, and Y. Zhang, "Artificial intelligence empowered mobile sensing for human flow detection," *IEEE Network*, vol. 33, no. 1, pp. 78–83, 2019.
[12] Y. Du, V. Issarny, and F. Sailhan, "When the power of the crowd meets the intelligence of the middleware: the mobile phone sensing case[J]," *ACM SIGOPS - Operating Systems Review*, vol. 53, no. 1, pp. 85–90, 2019.
[13] L. Li, "Study on the innovation of piano teaching in normal colleges and universities," *Creative Education*, vol. 09, no. 05, pp. 697–701, 2018.
[14] C. Liu and Q. Zhang, "Optimized application of network resources in college piano teaching reform under the background of innovation and entrepreneurship education," *Boletin Tecnico/Technical Bulletin*, vol. 55, no. 8, pp. 225–231, 2017.
[15] Y. Shao, "The influence of psychological factors on piano performance," *International Journal of Social Science and Education Research*, vol. 2, no. 12, pp. 83–87, 2020.
[16] D. A. Alexandrovna, L. S. Sergeevich, and P. M. Viktorovna, "Piano music of composers-minimalists in the teaching repertoire of higher music education," *Opción*, vol. 34, no. 17, pp. 149–162, 2018.
[17] A. M. Dudeque Pianovski Vieira, "Teaching in the history of education: a transdisciplinary perspective," *International Journal of Action Research*, vol. 13, no. 1, pp. 39–50, 2017.
[18] I. N. Okeke, "The ambiguity of musical expression marks and the challenges of teaching and learning keyboard instruments: the nnamdi azikiwe university experience," *UJAH Unizik Journal of Arts and Humanities*, vol. 18, no. 1, pp. 131–148, 1970.

Hindawi
Mobile Information Systems
Volume 2023, Article ID 2896471, 12 pages
https://doi.org/10.1155/2023/2896471

Research Article

Deconstruction of Related Technologies of Ground Image Processing Based on High-Resolution Satellite Remote Sensing Images

Kai Feng, Yi Wu, and Rui Zhang

Shaanxi Academy of Aerospace Technology Application Co. Ltd, Xi'an 710100, Shaanxi, China

Correspondence should be addressed to Kai Feng; fengkai1980@st.btbu.edu.cn

Received 18 July 2022; Revised 5 August 2022; Accepted 22 August 2022; Published 18 February 2023

Academic Editor: Yajuan Tang

The Earth observation system heavily relies on sophisticated remotely sensed satellites, an important means to obtain global high-precision geospatial products and an important strategic area for the world's major scientific and technological powers to develop. Although China's satellites currently have real-time or quasi-real-time observations with a high temporal resolution, there are still a lot of gaps between their positioning accuracy and the world's advanced level. This essay aims to study an efficient ground image processing technology and apply it to high-resolution satellite remote sensing images. The convolutional neural network is an efficient deep learning method for image recognition and feature extraction. In this essay, people use a convolutional neural network (CNN) to identify ground images, use a support vector machine (SVM) to classify and summarize images, and then use a Kalman filter for noise reduction, so as to obtain sophisticated remotely sensed images. In the experiment, 100 satellite remote sensing images in the GeoImageDB database were selected for the simulation test, the images were divided into 5 types, and their recognition accuracy, classification accuracy, image signal-to-noise ratio, and resolution were analyzed. The results show that the accuracy of CNN's recognition of different types of images is up to about 94%, and the lowest is about 85%. The accuracy of the SVM for image classification is above 80%, and the highest is about 95%. The SNR of the image after noise reduction is basically above 6.5, and some even reach above 8.0. The resolution of the image is basically above 800ppi, and the highest even reaches an ultra-high resolution of 1400ppi. Overall, the processed images are of high quality. This shows that this essay uses CNN for image recognition and then uses an SVM for classification, and finally, the method of denoising the image has certain feasibility and has achieved good results through experiments.

1. Introduction

As space launch technology, satellite platforms, sensors, and other technologies advance, the "four highs" characteristics (that is, high space, high spectrum, high temporal resolution, and high positioning accuracy) of earth observation satellites become prominent. High-resolution remote sensing satellites have been widely used in global surveying and mapping, national defense surveillance, intelligence collection, accurate mapping, and other fields and are important strategic, forward-looking, and infrastructure facilities for countries. The construction of a high-resolution satellite remote sensing system has many characteristics, for example, high technology content, large capital investment, long construction cycle, obvious industry drive, etc. The system and corresponding data resources have become a crucial pillar of a state's financial, military, and social progress. However, the current images obtained by satellite remote sensing systems are not clear enough compared to those of other countries, and the image quality still needs to be improved. Therefore, it is of great value and significance to study the ground image processing technology in this essay to improve the image quality of the high-resolution satellite remote sensing system.

Ground image processing technology is the key to improving the quality of satellite remote sensing images. At present, many scholars have carried out related research on it. Among them, in order to distinguish vegetation from the

backdrop, Wang A created several color indices and classification strategies and provided a summary of the development of weed identification utilizing ground-based machine vision and image processing techniques, such as color index-based, threshold-based, and learning-based classification methods [1]. Xuan designed an ISAL receive channel layout that combines an orthogonal short baseline in the inner field with an orthogonal long baseline in the outer field. The significance is to improve the focus of the two-dimensional image and obtain high-precision three-dimensional imaging results [2]. Wang F. proposed an improved region-growing image processing method with modifications to the region-growing seeds and growing criteria obtained by the background subtraction method. This method can obtain the integral area of the cloud, which can be used to extract geometric parameters [3]. Demi developed and described a method for calculating ground-specific tire pressure using image processing theory [4]. However, most of these methods emphasize the theoretical basis but little for practical application and effect analysis, so further practice and exploration are needed.

In order to further study satellite remote sensing images, some scholars have conducted more in-depth exploration. Gong C. suggested a sizable dataset named NWPU-RESISC45 after studying several datasets and methodologies for scene categorization from remote sensing photos. The dataset contains 31,500 images covering 45 scene classes with 700 images per class [5]. Wang proposed a new kernel clustering algorithm to segment sophisticated remotely sensed images. The effectiveness and reliability of the proposed algorithm were verified by comparing the experimental results with the mean-shift algorithm and the watershed algorithm [6]. Wenjie proposed a technique for segmenting sophisticated remotely sensed images that combines the RHMRF-FCM algorithm with static minimal spanning tree (MST) subdivision, taking shape information into account [7]. Jiang suggested a sealed approach where a length signal in the form is induced using both multispectral data [8]. Although these methods have achieved some research results, the effect of improving the quality of remote sensing images is not obvious, so these methods need to be further improved and innovated.

In the era of continuous development of science and technology, the previous satellite remote sensing images require higher quality because high-quality images can be more conducive to serving society. The innovation of this essay is that it proposes a method of using CNN for ground image recognition and combining it with SVM for ground image classification, so that the image obtained from remote sensing images is more stable. Then the Kalman filter is used to denoise the image so that the image quality is higher and a higher-resolution satellite remote sensing image can be obtained.

2. Ground Image Processing Technology for Satellite Remote Sensing

2.1. Satellite Remote Sensing Technology. At present, China's satellite development has achieved good results, but the gap between satellite remote sensing technology and developed countries is not small [9], as shown in Figure 1, from China's first artificial near-Earth satellite, Dong Fang Hong-1, to the moon-orbiting satellite Chang'e-1, and then to the space station and Mars probe, which is undoubtedly the best proof of technological improvement. Although some achievements have been made in the remote sensing technology of Chinese satellites, and the high-resolution satellites manufactured have many characteristics (such as stable operation, efficient detection, global coverage, and other characteristics), currently, it is challenging to fulfill large-scale mapping and high-precision reconstruction of ground objects demands. Taking sophisticated remotely sensed images for precision-guided weapon strikes in national defense applications as an example, it is not only necessary to solve the problem of "seeing clearly," but also the problem of "accurate positioning" [10, 11].

At present, high-resolution mapping satellites generally use the linear array push-broom imaging mode, as shown in Figure 2. The key to realizing its high-precision geometric positioning is to restore the photographic light and orientation parameters at the imaging time and establish a strict imaging model according to the three-point collinear principle of the image point, the projection center, and the ground point at the imaging time. The core of this is to accurately obtain satellite orbit and attitude data at the time of imaging. The high-precision geometric positioning of high-resolution satellite remote sensing images has always been concerned and favored by aerospace photogrammetry scholars [12, 13]. At present, satellites for photogrammetry with good resolution at home and abroad all use line array cameras as imaging sensors. During photography, along the flight direction of the satellite, push-broom imaging is performed row by row, and the detected image is the projection image at the center of the row. That is, each line of scanned image has a strict geometric imaging relationship with the ground, and each line has an independent external orientation element. However, when the satellite is actually in orbit, due to platform flutter, equipment aging, gravitational perturbation, temperature change, and other reasons, the position and attitude of the satellite image often have systematic errors. It is difficult to describe the azimuth elements outside each scan line with a standard and unified model, and it is even more difficult to use conventional framed aerial photogrammetry methods to process them. Therefore, in view of the geometric characteristics of sophisticated remotely sensed image imaging systems such as linear array push-broom and line center projection, the study of high-precision positioning models and methods has always been a hot and difficult issue in the field of aerospace photogrammetry [14].

The beam method commonly used in satellite remote sensing technology, which uses internal and external azimuth elements, model point coordinates, and self-checking parameters as parameters for overall adjustment, is the most rigorous method and theoretical basis for the high-precision positioning of remote sensing images. This method is an effective way to achieve a fast, accurate, and reliable solution. High-resolution remote sensing satellite linear array push-

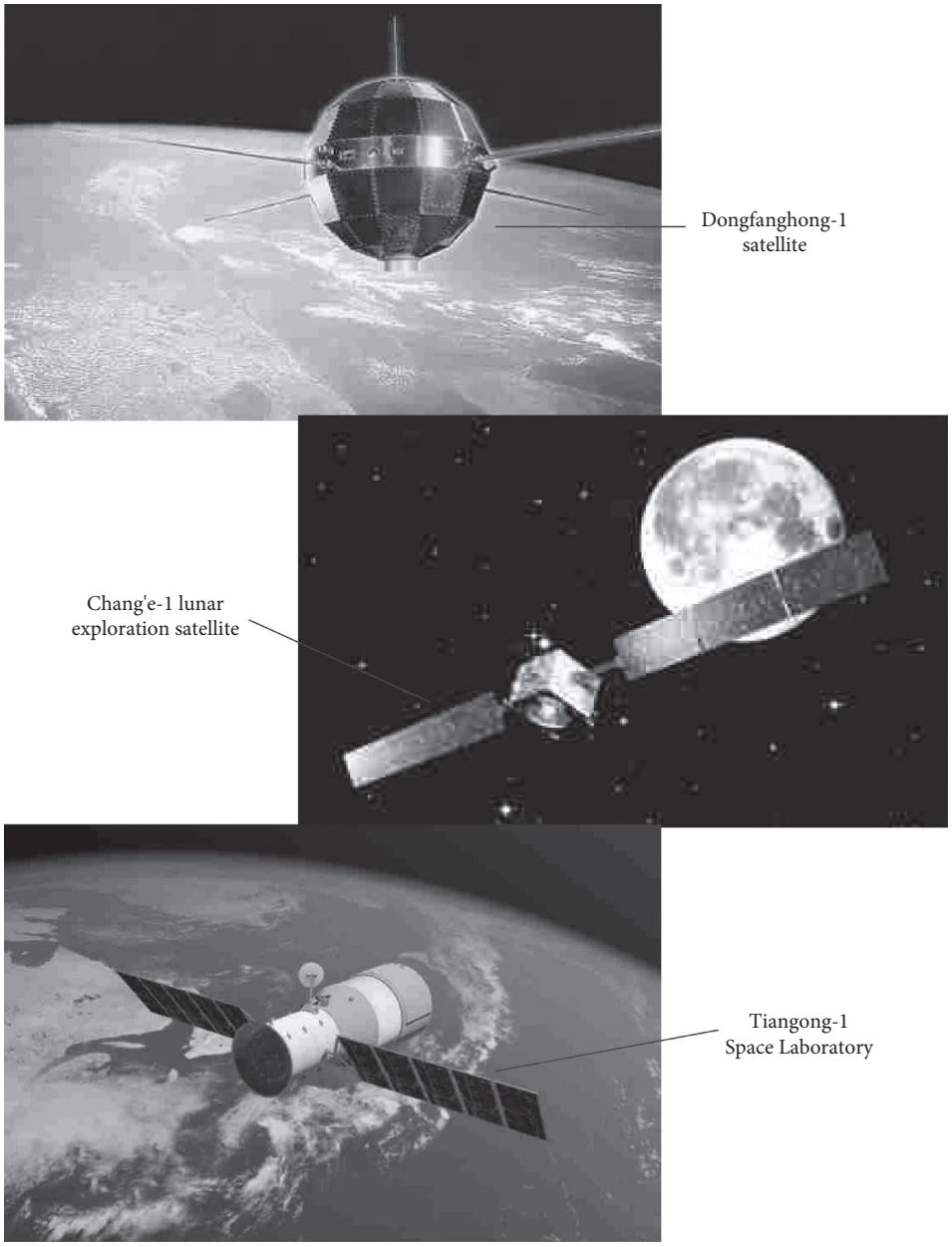

Figure 1: Chinese satellite.

broom imaging has the characteristics of high orbital operation, high dynamic photography, narrow beam imaging, small field of view detection, short time exposure, etc. There is a strong correlation between the external azimuth and the orientation parameters. When the external orientation is characterized based on the classical Euler angles and quaternions, the problems of ill-conditioned formulas, poor iterative efficiency, and low solution accuracy in the adjustment algorithm often appear. In addition, self-calibration parameter polynomials and a large number of connection points are introduced in the linear satellite image beam adjustment. There are many unknowns to be solved and huge normal formulas, so there is an urgent need for fast, reliable, and stable solutions [15].

In addition, for satellite remote sensing images, there are generally hyperspectral images and high-resolution images, as shown in Figure 3. The so-called hyperspectral image is the image formed according to the spectral information, which can distinguish the ground objects in more detail according to the spectral information. High-resolution images refer to high-definition images with a resolution of 720p or higher. In high-resolution images, the human eye can have a more intuitive perception of the image and can acquire target information more quickly. The advantage of the high-scoring Earth observation system is that it can obtain global remote sensing data, but there are still underdeveloped areas in the world that belong to the unmapped area. Especially in difficult or unmanned areas such

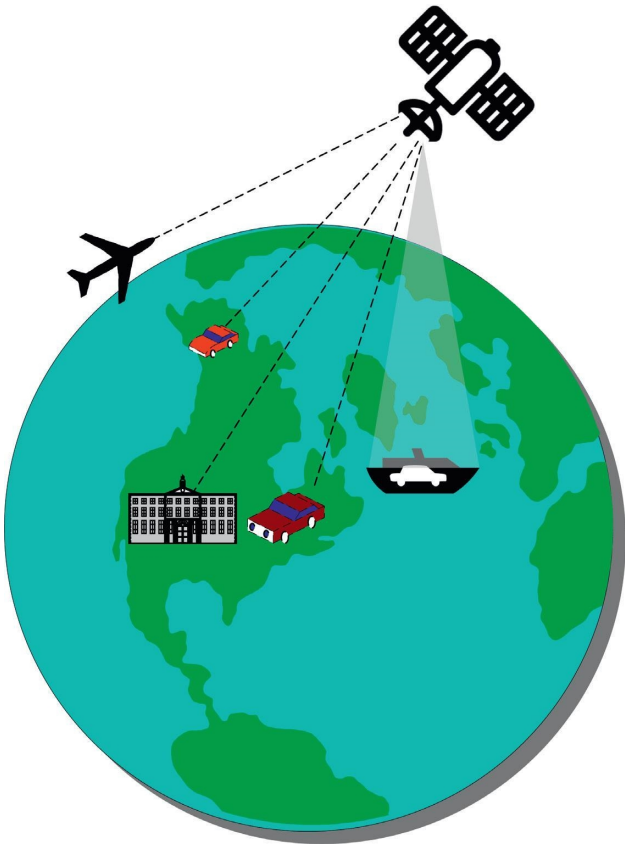

Figure 2: Schematic figure of satellite remote sensing technology.

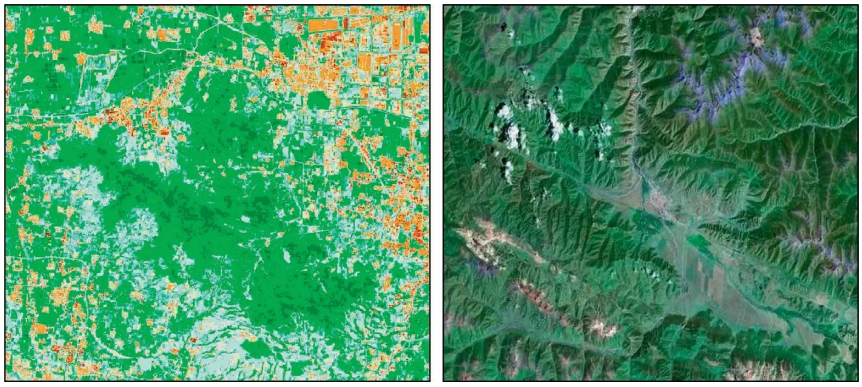

Satellite imagery spectral data High-resolution satellite imagery

Figure 3: Satellite remote sensing image.

as oceans, deserts, and overseas, it is often difficult to implement topographic map surveying due to the lack of ground features and the inability of personnel to carry out surveys. Therefore, the most effective way to solve the problems of surveying and mapping in these difficult areas or areas without maps is to implement photogrammetry without ground control points. When using remote sensing satellite images to measure topographic maps of different scales, there are specific requirements for elevation accuracy and plane accuracy. The actual satellite engineering shows that after the high-precision orbit determination of the satellite platform is realized based on the single-frequency or dual-frequency receiver system, the plane positioning accuracy can be better guaranteed. Therefore, to realize topographic map surveying without ground control points, it is necessary to improve the elevation positioning accuracy [16, 17].

From single-star independent observation on a large platform to multi-star/constellation network detection on a small platform, it has become a new trend in the development of high-resolution Earth observation systems, so as to meet the new requirements for the application and development of Earth observation systems with shorter revisit times, wider detection range, and faster response. The use of

large satellite platforms to move towards universal small satellite platforms is another development frontier of high-resolution Earth observation systems. At the International Forum on Small Satellites held in the Silicon Valley of the United States a long time ago, well-known experts and scholars in the aerospace field from various countries pointed out that, due to the further maturity of technology, the small satellite platform will play an important role from a single professional application to several formations networking, and then to large-scale cluster applications. In the future, the small satellite platform will achieve clustered shared launch [18].

2.2. Ground Image Processing. During the joint observation of satellites in orbit, nearly hundreds of images and auxiliary data are obtained every day. This kind of massive data requires satellite and ground coprocessing, and new intelligent processing mechanisms will become an urgent problem for high-resolution Earth observation systems. According to the different task requirements of users, such as real-time imaging, high-precision positioning, and change monitoring, optimize the allocation of satellite-to-ground computing resources, realize intelligent processing of the satellite-to-ground data, and provide quasi-real-time, high-precision, and highly reliable information services. It is a crucial strategy for raising the usability of the process of Earth observation systems, so it is necessary to study the efficient processing of high-resolution satellite images under the condition of limited resources. In order to meet the requirements of the future joint processing technology for earth observation, it is necessary to expand and supplement the ground image processing technology [19, 20].

For the processing of ground images, the process is shown in Figure 4. Firstly, the data preprocessing is carried out, the data is transferred to the remote sensing image management, and the features are extracted from the images. Then, the classification model is used to classify and aggregate them into cloud images, and then the cloud images are filtered and denoised to generate high-resolution images. At present, China is constrained by the level of hardware such as star sensors, and its attitude determination technology is relatively backward. After the camera parameters are calibrated in orbit, the positioning accuracy is insufficient without ground control points, and there is a gap with foreign satellite positioning accuracy, which makes it difficult to meet the current needs of high-precision positioning and mapping of satellite images. The lack of accurate satellite remote sensing images cannot provide accurate three-dimensional positioning and cannot use the ground control point beam method adjustment theory [21].

For image processing methods, CNN can be used to extract features from ground images, and then various classification models can be used to classify and summarize images. The similarity of grayscale information and spatial information between regional elements in the image can also be used to measure the correlation of ground objects. In satellite remote sensing images, the grayscale changes between pixels are gentle, the similarity between pixels with small spacing is greater, and the image as a whole also exhibits a certain spatial correlation, while the types of ground objects are quite different, and the correlation is small. Therefore, the correlation can also be used to distinguish clouds from ground objects. The inverse moment is a feature quantity that describes the same or similar local materials in the image. The basic principle of CNN image feature extraction used in this essay can be shown in Figure 5. The original image is extracted by the convolution process to obtain the feature image, and the feature image is then pooled and then preferably fully connected to obtain the final image to be extracted.

In recent years, the domestic three-dimensional surveying and mapping satellite "Tianhui-1" has been successfully launched and is running normally in orbit. By adopting certain technical methods, improving current work has focused heavily on the spatial placement precision of local satellite and aerial figures, and very rich research results have been achieved. Because there is no ground information for reference in uncontrolled positioning of high-resolution satellite remote sensing images, only a certain system error compensation model and an appropriate adjustment method can be used to correct the observed values based on the strict imaging model of satellite remote sensing images. And the ground information is complex and diverse, including building information, terrain relief, and traffic information. As shown in Figure 6, to display and process this information in real-time and with high resolution, more precise location and image processing technology is required.

Attitude accuracy is the core index that affects the positioning accuracy of linear array satellite images without ground control, and it is necessary to introduce altimetry auxiliary data to make the elevation accuracy error less than meters in uncontrolled positioning. At present, higher-resolution satellite remote sensing images and higher ephemeris attitude measurement accuracy provide important prerequisites for obtaining higher-precision target position information. Aerospace photogrammetry technology is based on a strict mathematical theory, through the modeling of satellite attitude and orbit data. According to the imaging collinear condition formula and the appropriate error modeling theory, the spatial position information of the camera shooting area can be calculated, and the target position can be determined. Due to the practical application of high-precision sensors such as high-resolution three-line array cameras and arcsecond-level star sensors, the positioning method of high-resolution earth observation satellites is gradually developing towards a direction that does not depend on control points, that is, control-free positioning. In addition, the uncertain vibration of the space-based platform makes the attitude measurement of the spaceborne sensor inaccurate. In the actual engineering process, it is necessary to perform interpolation, modeling, and other processing on the external orientation and attitude information collected by the star sensor according to the characteristics of the linear array image [22]. The processing method adopted will introduce different degrees of systematic errors, which will affect the accuracy of subsequent

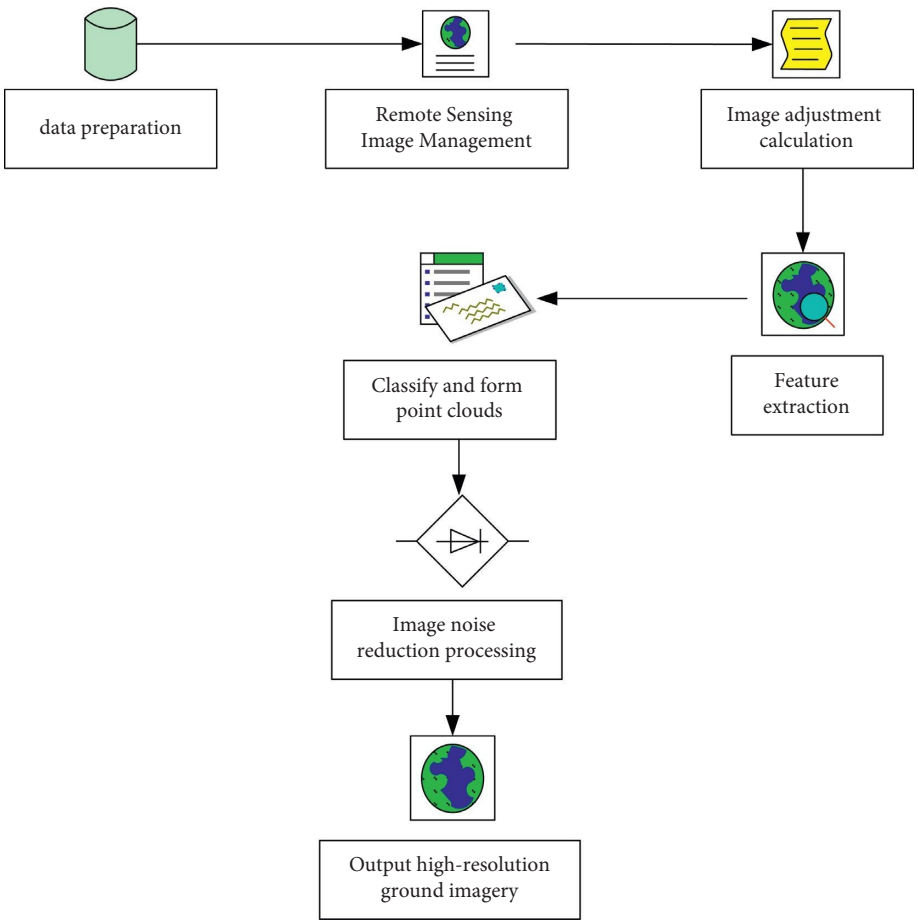

Figure 4: Ground image processing flow.

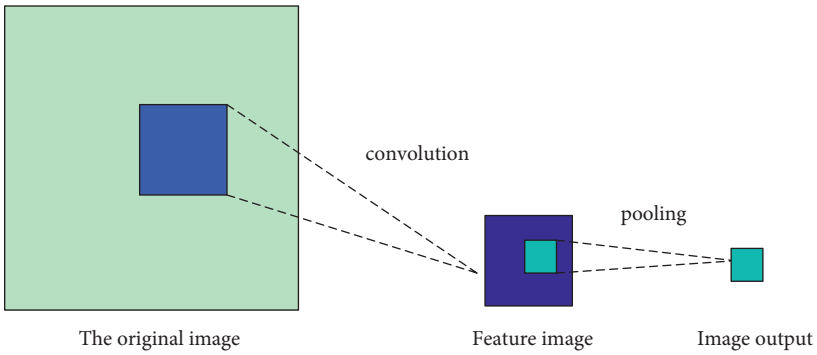

Figure 5: CNN image processing principle.

spatial positioning. The processing method adopted will introduce different degrees of systematic errors, which will affect the accuracy of the subsequent spatial positioning [23].

In addition to image processing techniques, determining satellite attitude is also critical. A high-precision satellite attitude is the primary condition for high-resolution satellite remote sensing images to build a rigorous model and achieve high-precision positioning. In high-resolution satellite push-broom imaging, the image line transfer period is much lower than the sampling time of the attitude determination equipment, so it needs to be based on the operating characteristics of the satellite. To build a suitable attitude interpolation and fitting model to obtain the trajectory and attitude data of each linear image imaging time, high-precision attitude determination is an important prerequisite for high-precision positioning. The satellite attitude was first characterized and processed using Euler angles. According to the "rotation theorem" proposed by the mathematician Euler, any rotation can be characterized by the three independent rotation angles around a certain axis, thereby determining the current attitude of an object.

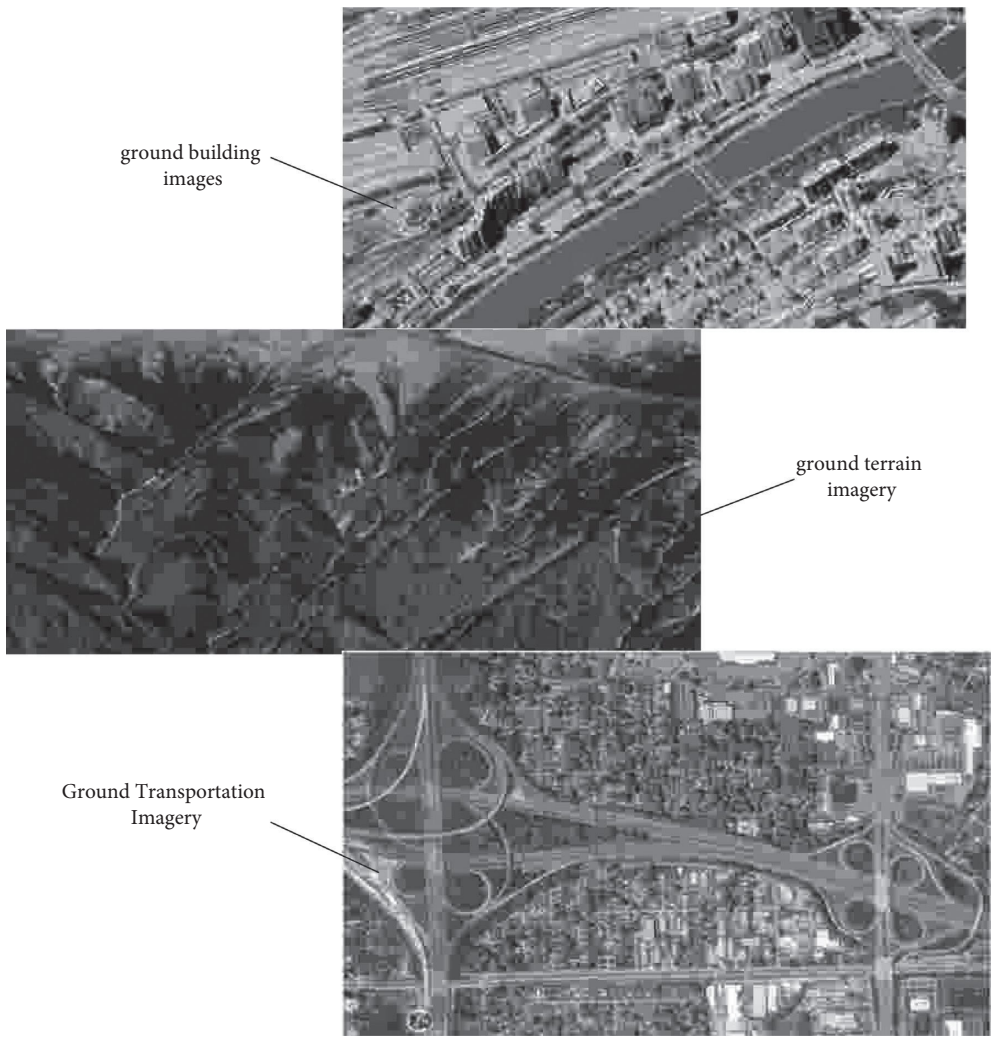

Figure 6: Ground image classification.

2.3. SVM Classification. The classification model used in this essay is the commonly used SVM, and its classification principle is shown in Figure 7. The SVM classifier has the qualities of higher accuracy, dependability, and durability when used to categorize ground figures. The model's formal program process involves the following steps.

It is assumed that when the input image information set can be linearly classified, and the classification decision surface is represented by w, it satisfies the following:

$$y_i \cdot \left[\left(w, x_i\right) + d\right] \geq 1. \tag{1}$$

If the nonlinearity is separable, then the extended field λ is introduced to satisfy the following:

$$\left(w, x_i\right) + d \geq 1 - \lambda_i \left(w, x_i\right) + d \geq -1 + \lambda_i. \tag{2}$$

Then, the optimal decision surface should meet the conditions is given as follows:

$$\left[w, f\left(x_i\right)\right] + d \geq 1 - \lambda_i \min S\left(w, \lambda\right) = \frac{1}{2}\left(w, w\right) + c \cdot \sum_{i=1}^{l} \lambda_i. \tag{3}$$

That is, use Lagrangian to solve the following:

$$\max_{\alpha} \sum_{i=1}^{l} \alpha_i - \frac{1}{2} \sum_{i=1}^{l} \sum_{j=1}^{l} y_i y_j \alpha_i \alpha_j \left[f\left(x_i\right), f\left(x_j\right)\right] s.t. \sum_{i=1}^{l} y_i \alpha_i = 0. \tag{4}$$

In any data, there is a vector formula satisfied by the corresponding factor α.

$$\sum_{x_i \in SV} y_i \alpha_i \left[f\left(x_i\right), f\left(x_j\right)\right] + d = 0. \tag{5}$$

The dataset is represented by a function $f(x)$ in a high-dimensional space, and is given as follows:

$$\left[f\left(x_i\right), f\left(x_j\right)\right] = k\left(x, x'\right). \tag{6}$$

From this, the optimal decision surface formula can be obtained in the following:

$$\sum_{x_i \in SV} y_i \alpha_i k\left(x_i, x_j\right) + d = 0. \tag{7}$$

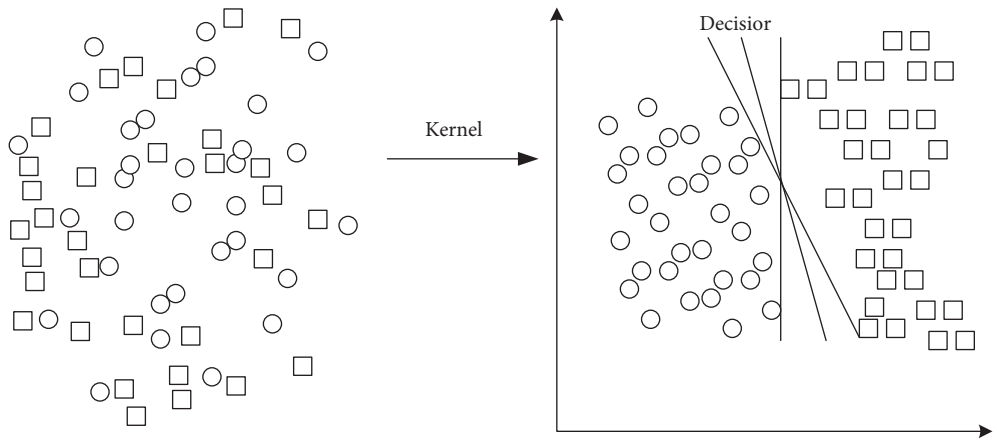

Figure 7: SVM classification principle.

Among them,

$$d = -0.5\left[\max_{\alpha}\left(\sum_{x \in SV}^{l} y_i\alpha_i k\left(x_i, x_j\right) + \sum_{x \in SV}^{l} y_j\alpha_j k\left(x_i, x_j\right)\right)\right]. \tag{8}$$

The SVM function is given as follows:

$$y = sgn\left[\sum_{x \in SV}^{l} y_i\alpha_i k\left(x_i, x\right) + d\right]. \tag{9}$$

Among them, sgn represents a symbolic function.

2.4. Image Filtering and Noise Reduction. After the CNN image recognition and classification, the image is filtered and denoised to make the image clearer. The denoising process is shown in Figure 8. The Kalman filter noise reduction selected in this essay is as follows.

In image processing, the relationship between the real state of the system at time k and noise can be expressed as follows:

$$x(k) = ax(k-1) + bu(k) + w_k. \tag{10}$$

Among them, w_k represents system noise.

Then, the prior value at time k–1 is given as follows:

$$\hat{x}(k|k-1) = a\hat{x}(k-1) = bu(k). \tag{11}$$

The sensor state is represented by z, and its relationship to noise is given as follows:

$$z(k) = H \cdot x(k) + v_k. \tag{12}$$

Among them, v_k represents sensor noise.

From this, the posterior value can be obtained by weighting is given as follows:

$$\hat{x}(k) = \hat{x}(k|k-1) + K[z(k) - H \cdot \hat{x}(k|k-1)]. \tag{13}$$

Then, according to the difference between the actual value and the posterior value, the mean square error is obtained in following formula:

$$\min E\left[x(k) - \hat{x}(k)^2\right]. \tag{14}$$

The covariance is given as follows:

$$P(k) = E\left\{[x(k) - \hat{x}(k)][x(k) - \hat{x}(k)]^T\right\}. \tag{15}$$

The Kalman increment K can be obtained in the following:

$$K = P'(k)H^T\left[Hp'(k)H^T + R\right]^{-1}. \tag{16}$$

Finally, substitute K into Formula (15) to get the covariance is given as follows:

$$P(k) = (1 - KH)p'(k). \tag{17}$$

3. Simulation Test of Ground Image Processing Effect

3.1. Experimental Design. This essay selects 100 satellite remote sensing images from the GeoImageDB database, which include different types of images such as agriculture, military, transportation, and urban buildings, as shown in Table 1.

In addition, the image size of each type of image is shown in Table 2.

The test environment of the simulation experiment is shown in Table 3. OpenCV is a cross-platform computer vision and machine learning software library that can run on Linux, Windows, and other operating systems. It is lightweight and efficient, and provides interfaces in languages such as Python, Ruby, and MATLAB, and implements many common algorithms in image processing and computer vision.

In the testing process, the selected 100 images are first scrambled and randomly input into the image processing software. The feature extraction of the image is performed by CNN, and then the SVM is used to classify and summarize the feature-extracted image, and finally a high-resolution image is obtained by filtering and denoising.

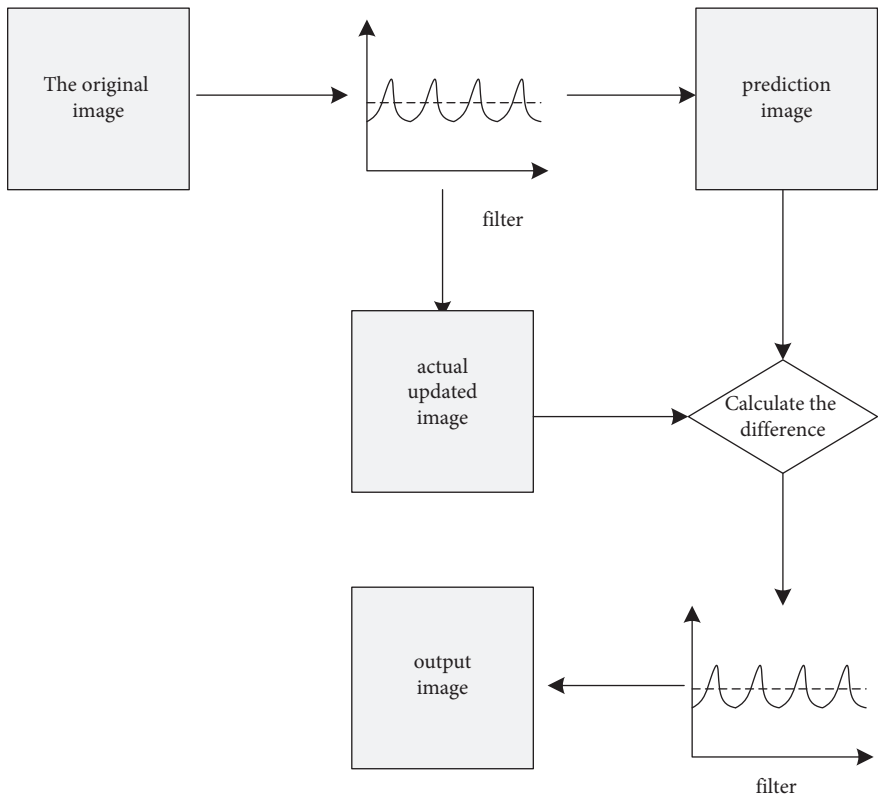

Figure 8: Image filtering for noise reduction.

3.2. Experimental Results. First of all, this essay uses CNN to identify and extract features from the selected 100 satellite remote sensing images and records the accuracy of identification. It then uses SVM to classify the extracted images and summarizes the accuracy of SVM classification. The results are shown in Figure 9.

As the figure demonstrates, the recognition accuracy of CNN for these 100 images is generally above 85%, and the highest is about 97%. It shows that the effect of CNN recognition is relatively good, and from the accuracy of these five types of images, CNN has the highest recognition accuracy for the C3 type, that is, agricultural type image recognition, reaching about 94%. For C1 and C5, the recognition degree is lower, but both exceed 85%. From the results of SVM classification of images, it can be observed that the classification accuracy is above 80%, and the highest is about 95%. From the comparison of these five types of images, it can be observed that the classification accuracy of SVM for buildings is the highest, at about 95%, and the classification degree for agriculture is the lowest, at only 83.6%. It may be that there are many types of agriculture and the similarity between many crops is high, resulting in a high rate of classification errors, while buildings are generally more prominent and may be easier to identify. Overall, the recognition effect of CNN and the classification effect of SVM are quite good, and both have high accuracy.

After the images are more accurately classified, the classified images are filtered and denoised. The image SNR and image resolution obtained by the Kalman filter denoising in this essay are shown in Figure 10.

Table 1: Image information.

Category number	Classification name	Include number of images
C1	Transportation	28
C2	Building	36
C3	Agriculture	25
C4	Military	8
C5	Other	3

Table 2: Image size.

Classification name	Biggest size: MB	Average size: MB
Transportation	400	102 MB
Building	382	138
Agriculture	352	123
Military	299	88
Other	324	139

Table 3: Simulation test environment.

Code	Item	Model
T1	Test computer	WIN 7 intel core i7
T2	Web environment	5G,wifi
T3	Test power	30 W
T4	Image processing software	OpenCV

As can be observed from the figure, the SNR of the image after noise reduction is basically above 6.5, and some even reach above 8.0. With the high quality, the

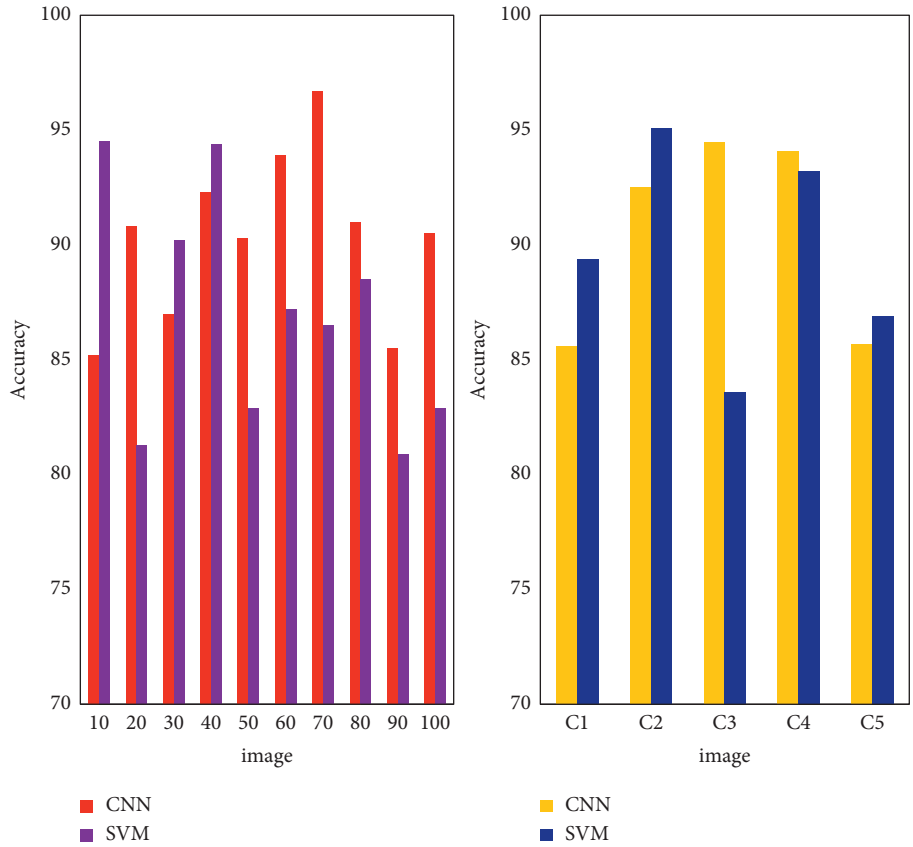

Figure 9: Accuracy of image recognition and classification.

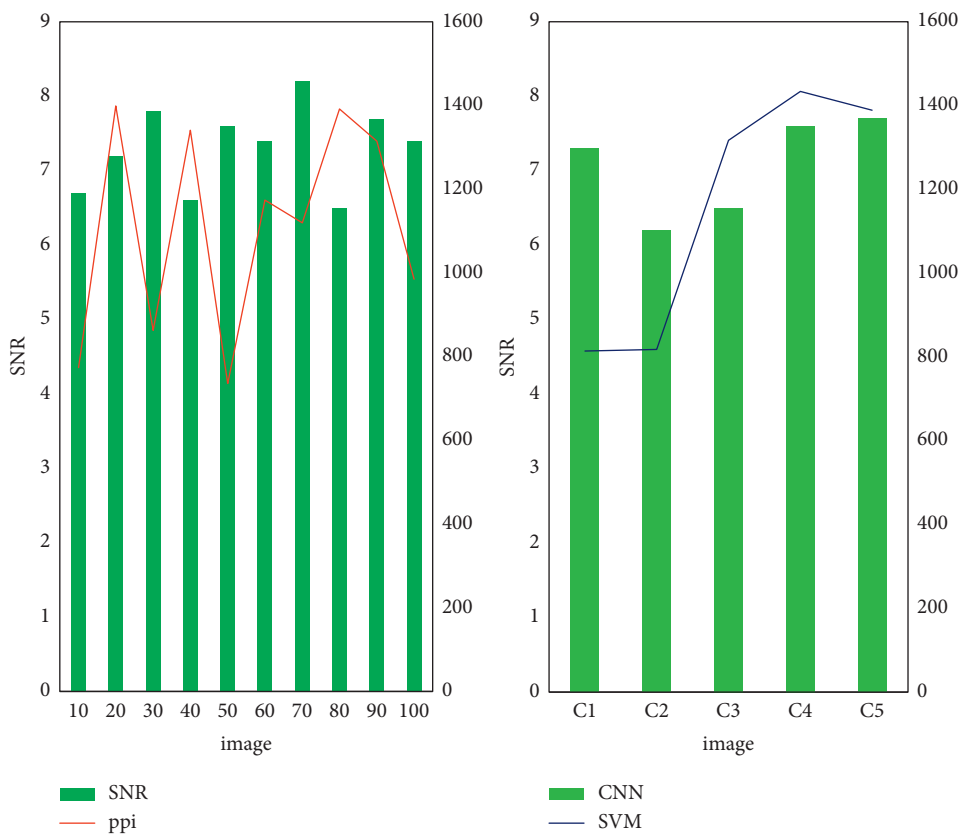

Figure 10: Image SNR and resolution.

resolution of the image is basically above 800ppi, which is a high-resolution, and the highest even reaches an ultra-high-resolution of 1400ppi. For different types of images, it can be observed that the C2 type, that is, the building type, has a lower SNR and resolution, only about 800ppi. The SNR and resolution of C4 and C5 are higher, at around 7.6 and 1400ppi, which may be due to the fact that there are more light reflections in buildings, which are not as good as glass reflections, wall reflections, etc., which cause image distortion. So the SNR and resolution will be lower. But on the whole, the quality of the processed images is very high, and the resolution of the images is above 720ppi, which are high-resolution or ultra-high-resolution images. The experimental test shows that this essay uses the Kalman filter for noise reduction to achieve good results.

Although this essay uses CNN feature extraction, SVM classification, and filtering noise reduction methods, some results have been achieved in the experiment. However, there is not much research on the imaging technology of remote sensing satellites, and it is necessary to realize the mutual conversion between the strict imaging model and the rational function model. The strict imaging model is used in the uncontrolled positioning of sophisticated remotely sensed satellite images, and it is used in professional processing. The strict geometric relationship of satellite imaging time is constructed through orbit modeling, system error elimination, and other methods to achieve high-precision positioning processing. However, for professional users, obtaining strict imaging geometry data is of great practical significance for studying satellite imaging characteristics, multi-sensor fusion processing, and long-strip regional network adjustment under uncontrolled conditions.

4. Conclusions

It is of great significance to study the formation of high-resolution satellite remote sensing images and the processing of ground images. Among them, linear array satellite single image positioning, two-strip image positioning, multiple-strip image positioning, and regional network adjustment methods under uncontrolled conditions are the basis of high-resolution satellite remote sensing images. The research on these topic has important reference value for realizing sophisticated remotely sensed satellite image positioning processing. This essay firstly studies satellite remote sensing images and finds that the current satellite remote sensing images cannot meet the needs of large-scale mapping and high-precision reconstruction of ground objects. Through the research of satellite remote sensing technology, it is found that most remote sensing satellites currently use linear array push-broom imaging, and the quality of remote sensing images obtained by this method needs to be improved. Then this essay analyzes the current processing technology of ground images and finds that it is a good method to use CNN for image feature extraction and SVM for image recognition. Therefore, this essay selects multiple satellite remote sensing images in the database and divides them into different types for image processing and testing. The results show that the recognition accuracy of CNN for these 100 images is generally above 85%. Among them, the image recognition accuracy of agricultural types is the highest, the accuracy of SVM classification is above 80%, and the classification accuracy of buildings is the highest. The quality of the images after noise reduction is very high, and the resolution of the images is above 720ppi. This shows that the image processing method in this essay has achieved good results. However, there are still some deficiencies in this essay. Among them, the specific principles of satellite remote sensing image imaging are not described clearly enough, the research in the experimental part is not complete enough, and the overall needs to be improved.

Data Availability

The data for this paper can be obtained through e-mail to the authors.

Conflicts of Interest

The authors declare that there are no conflicts of interest regarding the publication of this work.

References

[1] A. Wang, W. Zhang, and X. Wei, "A review on weed detection using ground-based machine vision and image processing techniques," *Computers and Electronics in Agriculture*, vol. 158, pp. 226–240, 2019.

[2] X. Hu, J. Du, and D. Li, "Image processing for GEO object with 3D rotation based on ground-based InISAL with orthogonal baselines," *Applied Optics*, vol. 58, no. 15, pp. 3974–3985, 2019.

[3] F. Wang, Y. Z. Li, and L. P. Li, "Research on FAE cloud image processing method based on background subtraction and region growing," *International Journal of Pattern Recognition and Artificial Intelligence*, vol. 32, no. 7, pp. 1854019.1–1854019.14, 2018.

[4] M. Demi, S. Mudeka, and A. Uri, "Contribution to the application of the image processing theory in determining the middle specific tire pressure on ground at motor vehicles," *IMK-14 - Istrazivanje i razvoj*, vol. 26, no. 2, pp. 25–28, 2020.

[5] C. Gong, J. Han, and X. Lu, "Remote sensing image scene classification: benchmark and state of the art," *Proceedings of the IEEE*, vol. 105, no. 10, pp. 1865–1883, 2017.

[6] Y. Wang and C. Wang, "High resolution remote sensing image segmentation based on multi-features fusion," *Engineering Review*, vol. 37, no. 3, pp. 289–297, 2017.

[7] L. I. N. Wenjie, L. I. Yu, and Z. H. A. O. Quanhua, "High-resolution remote sensing image segmentation using minimum spanning tree tessellation and RHMRF-FCM algorithm," *Journal of Geodesy and Geoinformation Science*, vol. 3, no. 1, pp. 54–65, 2020.

[8] J. Jiang, C. Chen, Y. Yu, X. Jiang, and J. Ma, "Spatial-aware collaborative representation for hyperspectral remote sensing image classification," *IEEE Geoscience and Remote Sensing Letters*, vol. 14, no. 3, pp. 404–408, 2017.

[9] H. Lu, Q. Liu, X. Liu, and Y. Zhang, "A survey of semantic construction and application of satellite remote sensing

images and data," *Journal of Organizational and End User Computing*, vol. 33, no. 6, pp. 1–20, 2021.

[10] C. Gong, Z. Li, X. Yao, G. Lei, and Z. Wei, "Remote sensing image scene classification using bag of convolutional features," *IEEE Geoscience and Remote Sensing Letters*, vol. 14, no. 10, pp. 1735–1739, 2017.

[11] M.-lvarez Pablo and Adrianl, "Remote sensing image classification with large-scale Gaussian processes," *IEEE Transactions on Geoscience and Remote Sensing*, vol. 56, no. 2, pp. 1103–1114, 2017.

[12] H. Xie, A. Zhao, S. Huang et al., "Unsupervised hyperspectral remote sensing image clustering based on adaptive density," *IEEE Geoscience and Remote Sensing Letters*, vol. 15, no. 4, pp. 632–636, 2018.

[13] D. Jiang, F. Wang, Z. Lv et al., "QoE-Aware efficient content distribution scheme for satellite-terrestrial networks," *IEEE Transactions on Mobile Computing*, vol. 1, 2021.

[14] S. Gou, S. Liu, S. Yang, and L Jiao, "Remote sensing image super-resolution reconstruction based on nonlocal pairwise dictionaries and double regularization," *Ieee Journal of Selected Topics in Applied Earth Observations and Remote Sensing*, vol. 7, no. 12, pp. 4784–4792, 2014.

[15] C. Shi, J. Zhang, and H. Chen, "A novel hybrid method for remote sensing image approximation using the tetrolet transform," *Ieee Journal of Selected Topics in Applied Earth Observations and Remote Sensing*, vol. 7, no. 12, pp. 4949–4959, 2017.

[16] M. Long, B. Du, and C. He, "Region-of-Interest detection via superpixel-to-pixel saliency analysis for remote sensing image," *IEEE Geoscience and Remote Sensing Letters*, vol. 13, no. 12, pp. 1–5, 2017.

[17] T. Mei, L. An, and Q. Li, "Supervised segmentation of remote sensing image using reference descriptor," *IEEE Geoscience and Remote Sensing Letters*, vol. 12, no. 5, pp. 938–942, 2017.

[18] L. Wang, X. Huang, C. Zheng, and Y Zhang, "A Markov random field integrating spectral dissimilarity and class co-occurrence dependency for remote sensing image classification optimization," *ISPRS Journal of Photogrammetry and Remote Sensing*, vol. 128, pp. 223–239, 2017.

[19] J. Munoz-Mari, E. Izquierdo-Verdiguier, and C.-T. M. HyperLabelMe, "A web platform for benchmarking remote-sensing image classifiers," *IEEE Geoence & Remote Sensing Magazine*, vol. 5, no. 4, pp. 79–85, 2017.

[20] H. Li, S. Zhang, C. Zhang, P. Li, and R Cropp, "A novel unsupervised Levy flight particle swarm optimization (ULPSO) method for multispectral remote-sensing image classification," *International Journal of Remote Sensing*, vol. 38, no. 23, pp. 6970–6992, 2017.

[21] S. Wang, D. Quan, X. Liang, M. Ning, Y. Guo, and L Jiao, "A deep learning framework for remote sensing image registration," *ISPRS Journal of Photogrammetry and Remote Sensing*, vol. 145, pp. 148–164, 2018.

[22] R. Dr Pandi Selvam, "Earthworm optimization with deep transfer learning enabled aerial image classification model in IoT enabled UAV networks," *Fusion: Practice and Applications*, vol. 7, no. 1, pp. 41–52, 2022.

[23] Y. Guo, X. Jia, and D. Paull, "Effective sequential classifier training for SVM-based multitemporal remote sensing image classification," *IEEE Transactions on Image Processing*, vol. 27, no. 6, pp. 3036–3048, 2017.

Hindawi
Mobile Information Systems
Volume 2022, Article ID 2760131, 7 pages
https://doi.org/10.1155/2022/2760131

Research Article

Research on Augmented Reality College English Listening and Speaking Teaching Mode Supported by Wearable Technology

Na Li

Shool of Foreign Languages, Weinan Normal University, Weinan 714000, Shaanxi, China

Correspondence should be addressed to Na Li; hn2916@wfd.edu.ug

Received 1 July 2022; Revised 5 August 2022; Accepted 17 August 2022; Published 11 October 2022

Academic Editor: Yajuan Tang

With the rapid development of Internet technology, two new terms, such as wearable devices and AR, have begun to appear in front of people. AR technology refers to things that are difficult to experience in reality. It appears in front of people's eyes in space and time, and these things actually exist in the real world. The development process of AR technology shows that the boundary between teachers and students is gradually disappearing. If the school purchases a wearable device, they can use this device for university English listening and speaking teaching. This article will discuss the advanced equipment of AR supported by wearable technology applied in the field of university English teaching and complete the discussion and analysis of the following aspects: first, analyze the current situation of the application of AR technology in education and collect some domestic research cases outside, finding the problems. Then, this article introduces the theoretical basis and technical support for the education application of wearable AR technology, and a total of 110 students in the experimental class and control class of a university's English department are interviewed and investigated. Finally, this article applies wearable AR technology to the university. In the English listening and speaking teaching model, we use questionnaire surveys, interviews, and quasi-experimental research methods to understand the teaching model of wearable devices. We used AR technology in English listening and speaking learning and discussed the application of mobile AR technology in education and found that wearable AR technology is of great help to college English listening and speaking teaching.

1. Introduction

1.1. Background. At present, the teaching mode of college English listening and speaking is divorced from real life and away from its context, so that students can only passively accept it. With the rapid development of Internet technology, AR technology has slowly entered people's lives. AR is a technology that calculates the position and angle of a camera in real time and adds the corresponding image. The goal of this technology is to display and interact with virtual worlds on the screen. However, AR technology has not yet been fully popularized in the fields of education and teaching, so in this article, we will discuss how AR technology will make new major breakthroughs in the field of education.

1.2. Significance. The process of educational information development is constantly advancing, and more and more new technologies and tools are being introduced into classroom teaching to solve the problems existing in traditional classrooms. The continuous innovation of educational concepts and teaching methods has increased the demand for new technologies in the design of modern classroom learning activities. The classroom environment supported by technology has become a trend in educational research and development. Therefore, the exploratory significance of wearable AR technology to the teaching model of English listening and speaking is divided into two aspects: academic value and application value.

1.3. Related Work. Foreign research on AR technology in daily teaching started relatively early, and a series of research results have been achieved. A team of scientists headed by Akcayir et al. has explored the effects of using AR in scientific laboratories and adopted standards. The experimental pretest and post-test control group design of AR technology

enhances the development of college students' laboratory skills and helps them establish a positive attitude towards the physics laboratory [1], but their research has not been applied to daily teaching management mode. So experts like Jaramillo and Solano began to study using YouTube English music videos and AR mobile technology as a teaching resource to improve the listening and speaking skills of college students [2], but they only studied English for other languages, such as English as a popular language, and they have not carried out any related research and reports. Although Roesner et al. proposed that AR systems would bring potential security issues that should be resolved before the system is widely used [3], most people in the education sector believe that AR systems should be more widely used. These studies have guiding significance for virtual reality in college English audio-visual teaching, but the research on AR technology is not deep enough.

1.4. Innovation. Mobile AR devices have been so successful, in part, because AR marketing only requires the use of a smartphone. Wearable AR technology for university English listening and speaking teaching can not only recognize images and superimpose information but also provide students with a more realistic learning environment so that they have an immersive feeling. The teaching mode can not only stimulate students' interest in learning and bring them into the historical and cultural connotations of English but also allows students to travel through thousands of years of cultural history and have face-to-face language exchanges with ancient English scholars, thereby improving the learning efficiency. This kind of university English listening and speaking teaching mode is unprecedented. AR technology can take content off the screen and put it back in the book, making it entertaining and interactive.

2. Research Methods of AR for University English Listening and Speaking Education Model under Wearable Technology

2.1. Interview Method. Use the interview method to understand college students' feelings about using wearable AR devices in the learning process and the benefits and disadvantages of wearable technology-based AR for university English listening and speaking [4].

2.2. Questionnaire Survey. The general differences among students in different regions and genders were investigated through questionnaires. Use questionnaire research methods to understand students' acceptance of AR technology and AR equipment requirements, and use questionnaire survey methods to collect students' technical acceptance of wearable device AR technology based on AR models [5, 6]. AR education superimposes virtual information into the real world through AR technology, making the original boring education and teaching knowledge points into vivid images, enhancing students' interest in things, and attracting them to actively participate in teaching.

2.3. Quasi-Experimental Research Method. Quasi-experimental research refers to a research method that uses the original group to conduct experimental treatment in a relatively natural situation without randomly arranging subjects. Use quasi-experimental research to apply mobile AR technology to the learning of university English listening and speaking courses. After the completion of the experiment, according to Davis's technology acceptance model, the influence of wearable device AR technology on learning English listening and speaking was confirmed, and its problems were confirmed [7, 8]. Davis' acceptance model is a usage intention and attitude of users through perceived usefulness and perceived ease of use in the presence of external variables. The overall technical model is shown in Figure 1.

2.4. Mathematical Statistics. Mathematical statistics is a branch of mathematics divided into descriptive statistics and inferential statistics. It is based on probability theory and studies the statistical regularity of a large number of random phenomena.

(1) Levene's test of homogeneity of variance

$$S = \frac{1}{NWJ} \frac{\sum_{m=1}^{i} Bm\left(Xm-\right)_{2}}{i-1}. \tag{1}$$

(2) T-test

$$\mathrm{t} = \frac{-\mu}{\sigma \mathrm{n}/\sqrt{\mathrm{m}-1}}. \tag{2}$$

(3) Synthesis of sample difference

$$\theta x = \sqrt{\frac{\sum_{j=1}^{k}\left(mj\,\theta j_{2}\right) + \sum_{j=1}^{k} mj\,\left(-Yx\right)_{2}}{m1+m2+\ldots+mk}}. \tag{3}$$

(4) Sample size estimation

$$\mathrm{m} = \left(\frac{\mathrm{t}\left(\alpha/2\right)\bullet S}{\mathrm{d}_{2}}\right). \tag{4}$$

(5) Confidence interval of the overall mean

$$\left[-\frac{Z\left(\alpha/2\right)\bullet\sigma}{\sqrt{\mathrm{n}}}, +\frac{Z\left(\alpha/2\right)\bullet\sigma}{\sqrt{\mathrm{n}}}\right]. \tag{5}$$

(6) Product difference correlation coefficient

$$Z\mathrm{MN} = \frac{\sum \mathrm{MiNi}—1/\mathrm{x}\left(\sum \mathrm{Mi}\right)\left(\sum \mathrm{Ni}\right)}{\sqrt{Mi_{2}-1/x\left(\sum Mi_{2}\right)}\sqrt{Ni_{2}-1/x\left(\sum \mathrm{Ni}_{2}\right)}}. \tag{6}$$

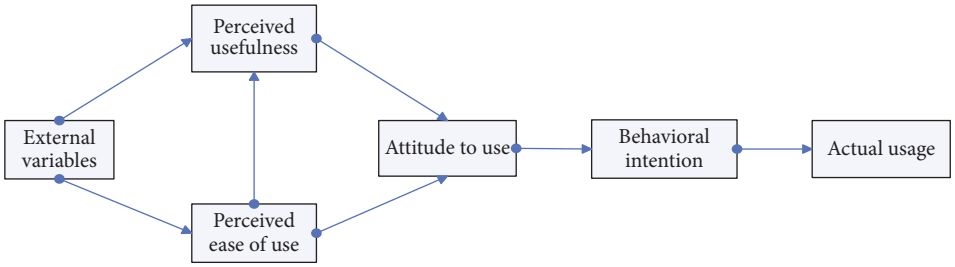

Figure 1: Davis' acceptance model.

3. Experiments Related to the Influence of AR Technology on College English Listening and Speaking Classes Supported by Wearable Technology

3.1. Test Subject. In order to verify the learning effect of the college English listening and speaking teaching based on wearable technology and AR technology in this study, we selected two classes in the first year of the English department of a university, one as an experimental class, and the second as a control class, with 55 students in each class. These students have the basic operating ability of the software. The English courses are also at the same level [9, 10]. Before the experiment, first, conduct a test with students in two classes; the test content is to understand the English content put on the player and express it fluently [11]. In traditional classrooms, teachers teach new knowledge on the podium, and students listen carefully, take notes, answer questions, and complete paperwork assigned by the teachers on time after class (as shown in Figure 2).

3.2. Implementation Process. AR listening and speaking teaching is adopted for experimental class teaching, which is a learning method corresponding to traditional receiving learning [12]. With students as the main body of learning, students can make their own decisions and achieve learning goals through relatively independent analysis, exploration, practice, inquiry, and student creation [13, 14]. As shown in Figure 3, learners learn independently through AR English listening and speaking teaching, which promotes learning in the AR environment and helps improve classroom learning efficiency. The improvement of learning efficiency is the key to implementing quality education [15]. Teachers and students can communicate on the Internet in a timely manner, and problems can be solved through mutual discussions within the group; if they encounter problems that cannot be solved, they will conduct intergroup discussions and ask teachers for advice.

Traditional teaching methods such as blackboard writing design and practice, lesson preparation and transformation, and so on that use multimedia cannot achieve the desired effect and may even diminish the prestige of the teacher. In the implementation, the first class of the English Department adopts the teaching method of AR education application and teacher guidance under the guidance of the teacher. In the second class of the English Department, the same teacher used traditional teaching methods to teach and did not use wearable AR devices. AR education has the characteristics of simulation and interaction, which can present abstract and obscure knowledge in a more vivid, intuitive, and comprehensive way and enhance students' sense of substitution with immersive experience. The study time is 2 weeks with 5 lessons per week.

4. Experimental Results of the Inquiry into the Teaching Mode of English Listening and Speaking in AR Universities Supported by Wearable Technology

4.1. Results of the Interview Method. When asked whether the students in class 1 find the current class more interesting than before, most of them expressed affirmation and believed that by using wearable AR devices, the difficulty of listening can be reduced by enhancing the rendering of the pictures, and they all said they are also willing to speak English, which greatly enhances students' interest in English learning. We think it will be more interesting after using these resources in class [16, 17]. When asked if they were confident in their ability to learn better and achieve better results in the test, most of the interviewed students expressed confidence that they could get better results in the test, which shows that wearable AR devices can listen to English well and have a good teaching effect.

4.2. Questionnaire Results. The questionnaire was entrusted to the first-year counselor of the English Department. A total of 110 questionnaires were sent out, and 110 were returned. A total of 5 questionnaires were excluded from blank and incomplete questionnaires, and 105 valid questionnaires were received. The interview has strong flexibility, using a relatively complex interview outline; the standardization of the questionnaire survey process; the scope of the survey is wide; and the efficiency is high. Our survey subjects included students from different parts of the country and different genders in the experimental class and the control class. There are also some differences in the understanding of virtual reality and AR technology. From the statistical data, there are general differences in AR technology. Out of the number of boys and girls who "do not understand," one-third of boys and girls choose to "know a little bit," and only a small number of people choose "very well" (as shown in Figure 4). Considering that they are students majoring in English

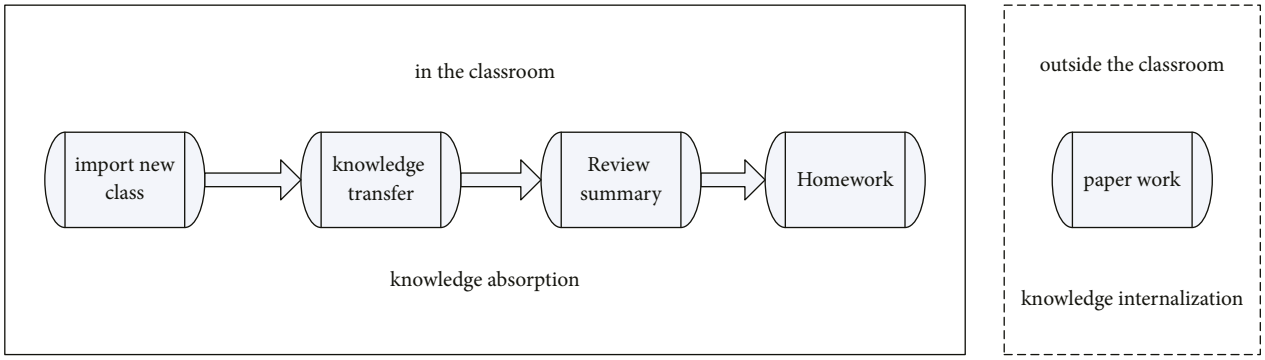

Figure 2: Traditional teaching.

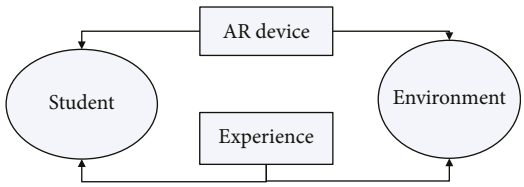

Figure 3: Listening and speaking teaching method based on AR technology.

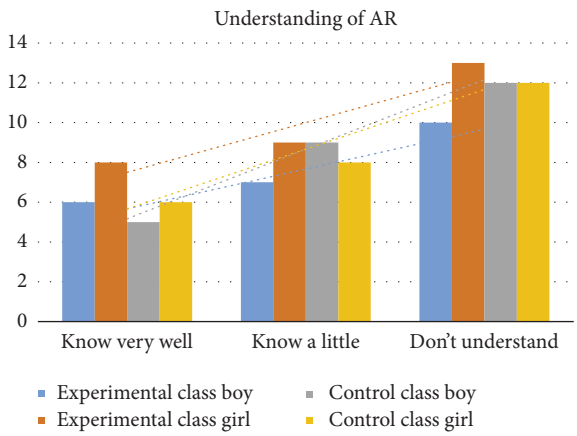

Figure 4: The level of English students' understanding of AR technology.

education, we can think that among college students, fewer people understand AR technology. It can be seen that the popularity of AR technology in the field of education in our country is far from enough [18]. It can be seen from these surveys that few people understand AR technology, which shows that the application of AR technology to English education is very rare.

In addition, we also investigated the deficiencies of the use of wearable technology AR devices for university English listening and speaking teaching from the experimental class students. The results of the survey are shown in Figure 5. There are three main aspects: AR equipment is too bulky, AR equipment is complicated to use, and frequent use of AR equipment will cause students' vision loss [19]. In future technological development, product developers will definitely optimize these problems and bring us more brand-new experiences.

4.3. Result of Quasi-Experimental Research Method

4.3.1. Statistics and Analysis of Pretest and Post-Test Data. Collect and analyze the data in the pretest and post-test experiments. First of all, with the help of the school's educational administration information system, the final English listening and speaking test scores of the students in two classes were obtained in the first semester of admission. There was no significant difference in English proficiency in the control class before the experiment. The experimental class uses the wearable AR technology teaching mode, while the control class uses the traditional university English listening and speaking teaching modes. Both the two classes took part in the university's English listening and speaking tests after the completion of the study course. The listening and speaking test results before and after the experiment are shown in Tables 1 and 2.

After the experiment, the average score change curve of the listening and speaking levels of the experimental group and the control group is shown in the following Figure 6:

At that time, it was about two weeks before the two classes applied their respective teaching modes. The listening and speaking tests contain questions such as listening, interpreting, and written translation and are authoritative and professional [20]. Judging from the changes in the two balance scores before and after the test, the changes in the test group's scores were more obvious than those in the control group, and the results were authoritative and professional. Therefore, the results of the university's English listening and speaking tests are post-test data to analyze the difference in English proficiency between two classes after different English listening and speaking teaching modes. At the same time, we conducted a review of the experimental class students. The learners conducted a questionnaire survey on the receiving data model of the teaching mode of wearable AR technology, and the statistical results are shown in Table 3.

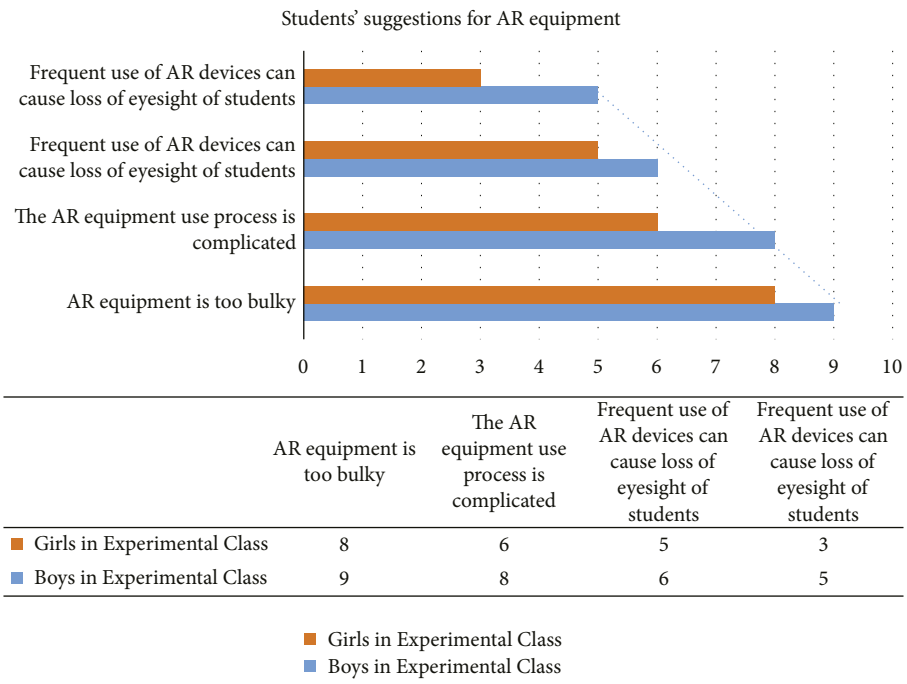

Figure 5: Students' suggestions for wearable technology AR devices.

Table 1: Pre-experiment test levels.

Group	Test group	Control group
Listening section average score	46	44
Average score for the oral part	39	42
Average score	85	86

Table 2: Postexperiment test levels.

Group	Test group	Control group
Listening section average score	48	46
Average score for the oral part	42	43
Average score	90	89

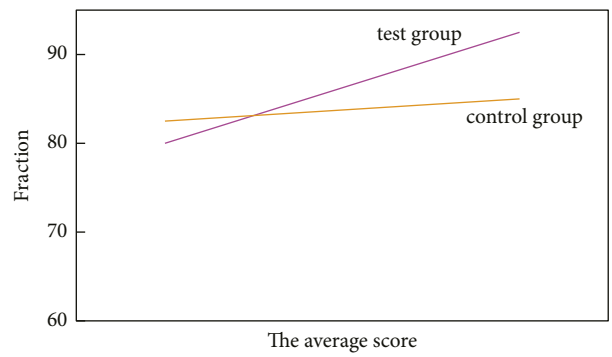

Figure 6: Comparison chart of changes in the average scores of the two groups before and after the test.

Analysis of the data shows that the evaluation scores of the number of people who choose perceived usefulness learning are relatively high. Perceived usefulness refers to learners who have a certain understanding of AR technology after using wearable AR devices. The average score for the two questions is 4.5. The highest score is that AR technology can promote English listening and speaking learning, and the lowest score is that we have more confidence in the final English listening and speaking tests after using the wearable AR device. In the statistics of the behavioral intention dimension data, we can find that the option with the lowest score is "I will use other AR devices in the future". Since our wearable AR device still has some shortcomings, we can obviously find that the scores on the option of "hope to continue to use the wearable AR device for English listening and speaking learning" are low, but after the wearable use of AR and the understanding of AR technology by the interviewees, they showed great concern about the application of AR technology in other courses.

(1) Pretest. Through the use of SPSS software, the first semester and end of the first semester English listening and speaking test scores (converted into a hundred-point system) of two classes are statistically analyzed .

① Homogeneity of Variance Test (as shown in Table 4).

② *T*-test with equal mean (as shown in Table 5).

(2) Post-Test. The SPSS software is used to analyze the English listening and speaking scores (converted into a hundred-point system) after the two-week study course of the experimental group and the control group, that is, the post-test (as shown in Table 6).

According to the above independent *t*-test sample data, sng is 0.045, which is less than 0.05, indicating that there is a significant difference between the English listening and speaking scores of the two classes. The average score of the experimental class is better than that of the control class.

Table 3: Technical acceptance model statistics.

Dimension	Serial number	Number of people	The average score
Perceived usefulness	A1	33	4.2
	A2	22	4.8
Perceived ease of use	B1	14	4.1
	B2	23	3.6
Behavioral intention	C1	18	3.4
	C2	34	3.7
Use behavior	D1	4	2.5

Table 4: Levene's test of homogeneity of variance.

		F	Sng
Grades	Assuming equal variances	0.458	0.486
	Assuming that the variances are not equal		

Table 5: T-test for equal means.

		t	df	Sng	Mean error	Standard error difference	95% difference confidence interval	
							Lower limit	Upper limit
Pretest score	Assuming equal variances	−0.245	59	0.745	−0.4416	1.4852	−3.145	2.345
	Assuming that the variances are not equal	−0.236	53.124	0.745	−0.4416	1.4852	−3.145	2.345

Table 6: Independent sample t test and Levene's test for post-test results.

		Post-test score variance equation Levene's test		T-test for the mean equation						
		F	Sng	t	df	Sng	Mean error	Standard error difference	95% difference confidence interval	
									Lower limit	Upper limit
Post-test score	Assuming equal variances	2.584	0.135	−0.245	59	0.045	3.5471	1.6578	−3.145	6.3245
	Assuming that the variances are not equal			−0.236	56	0.045	3.5471	1.6578	−3.145	8.3355

Therefore, the use of wearable AR devices can improve students' overall English listening and speaking skills and improve learning efficiency.

5. Conclusions

There are still many problems with our research. First, we only studied the teaching of English listening and speaking with wearable device AR technology. Does this technology have the same effect on reading and writing as it does on teaching in other languages? Second, this wearable AR device also has many shortcomings, and it is still necessary to wait for R&D personnel to improve the device. It is believed that as more demand based on AR technology continues to emerge, this technology will surely mature and its application in education and teaching will also be popularized. It can be predicted that in the next 10 years, educational applications based on AR technology will reach a new height.

Data Availability

This article does not cover data research. No data were used to support this study.

Conflicts of Interest

The authors declare that they have no conflicts of interest.

Acknowledgments

This work was supported by the Shaanxi Province Education Science "14th Five-Year Plan" 2021 Annual Project.

References

[1] M. Akcayir, G. Akcayir, H. M. Pektas, and M. A Ocak, "Augmented reality in science laboratories: the effects of

augmented reality on university students' laboratory skills and attitudes toward science laboratories," *Computers in Human Behavior*, vol. 57, no. apr, pp. 334–342, 2016.

[2] M. Jaramillo and L. Solano, "Youtube English music videos as educational resource to teach vocabulary and improve the listening and speaking skills[J]," pp. 103–106, 2019, https://zenodo.org/record/3283788#.YywsxD1BzIU.

[3] F. Roesner, T. Kohno, and D. Molnar, "Security and privacy for augmented reality systems," *Communications of the ACM*, vol. 57, no. 4, pp. 88–96, 2014.

[4] E. Marchand, H. Uchiyama, and F. Spindler, "Pose estimation for augmented reality: a hands-on survey," *IEEE Transactions on Visualization and Computer Graphics*, vol. 22, no. 12, pp. 2633–2651, 2016.

[5] I. Masaki, "Erratum to: reduced health-related quality of life among English college students with visual impairment[J]," *BioPsychoSocial Medicine*, vol. 10, no. 1, pp. 1–7, 2016.

[6] Y. Kokubo, K. Kisara, Y. Yokoyama et al., "Habitual dietary protein intake affects body iron status in Japanese female college rhythmic gymnasts: a follow-up study," *SpringerPlus*, vol. 5, no. 1, p. 862, 2016.

[7] J. M. T. Van Uem, T. Isaacs, A. Lewin et al., "A viewpoint on wearable technology-enabled measurement of wellbeing and health-related quality of life in Parkinson's disease," *Journal of Parkinson's Disease*, vol. 6, no. 2, pp. 279–287, 2016.

[8] J. M. Jakicic, K. K. Davis, R. J. Rogers et al., "Effect of wearable technology combined with a lifestyle intervention on long-term weight loss: the IDEA randomized clinical trial[J]," *JAMA*, vol. 316, no. 11, pp. 1161–1171, 2016.

[9] A. Daniel and H. Hashimoto, "A blinded assessment of video quality in wearable technology for telementoring in open surgery: the Google Glass experience[J]," *Surgical Endoscopy*, vol. 30, no. 1, pp. 372–378, 2016.

[10] J. Wu, H. Li, S. Cheng, and Z. Lin, "The promising future of healthcare services: when big data analytics meets wearable technology," *Information & Management*, vol. 53, no. 8, pp. 1020–1033, 2016.

[11] M. A. Hentschel, M. L. Haaksma, and T. van de Belt, "Wearable technology for the elderly: u," *European geriatric medicine*, vol. 7, no. 5, pp. 399–401, 2016.

[12] L. D. Ellingson, J. D. Meyer, and D. B. Cook, "Wearable technology reduces prolonged bouts of sedentary behavior," *Translational Journal of the American College of Sports Medicine*, vol. 1, no. 2, pp. 10–17, 2016.

[13] R. Lindberg, J. Seo, and T. H. Laine, "Enhancing physical education with exergames and wearable technology," *IEEE Transactions on Learning Technologies*, vol. 9, no. 4, pp. 328–341, 2016.

[14] M. H. Iqbal, A. Aydin, O. Brunckhorst, P. Dasgupta, and K. Ahmed, "A review of wearable technology in medicine," *Journal of the Royal Society of Medicine*, vol. 109, no. 10, pp. 372–380, 2016.

[15] S. L. Halson, J. M. Peake, and J. P. Sullivan, "Wearable technology for athletes: information overload and pseudo-science?[J]," *International Journal of Sports Physiology and Performance*, vol. 11, no. 6, pp. 705-706, 2016.

[16] A. V. Shelgikar, P. F. Anderson, and M. R. Stephens, "Sleep tracking, wearable technology, and opportunities for research and clinical care," *Chest*, vol. 150, no. 3, pp. 732–743, 2016.

[17] J. A. Bunn, J. W. Navalta, C. J. Fountaine, and J. D. Reece, *International Journal of Exercise Science*, vol. 11, no. 7, pp. 503–515, 2018.

[18] S. Nemati, M. M. Ghassemi, V. Ambai et al. in *Proceedings of the Annual International Conference of the IEEE Engineering in Medicine and Biology Society. IEEE Engineering in Medicine and Biology Society. Annual International Conference*, vol. 2016, pp. 3394–3397, Mexico, North America, November 2016.

[19] J. Blumenthal, A. Wilkinson, and M. Chignell, "Physiotherapists' and physiotherapy students' perspectives on the use of mobile or wearable technology in their practice," *Physiotherapie Canada*, vol. 70, no. 3, pp. 251–261, 2018.

[20] I. Awolusi, E. Marks, and M. Hallowell, "Wearable technology for personalized construction safety monitoring and trending: review of applicable devices," *Automation in Construction*, vol. 85, no. JAN, pp. 96–106, 2018.

Hindawi
Mobile Information Systems
Volume 2022, Article ID 1642790, 12 pages
https://doi.org/10.1155/2022/1642790

Research Article

Online and Offline Mixed Teaching Mode Based on Multimedia Computer-Aided Music Lessons during the Epidemic

Hongmei Ding

Tourism and Trade College, Lishui Vocational and Technical College, Lishui 323000, Zhejiang, China

Correspondence should be addressed to Hongmei Ding; 201902012127@stu.zjsru.edu.cn

Received 2 July 2022; Revised 10 August 2022; Accepted 24 August 2022; Published 3 October 2022

Academic Editor: Yajuan Tang

In recent years, due to the repeated outbreak of the epidemic, the normal teaching of students has been affected, and many schools have conducted mixed online and offline teaching for students, so that students can carry out teaching activities anytime and anywhere without delaying course learning due to class suspension. This paper mainly studies the online and offline mixed teaching mode of multimedia computer-assisted music lessons under the epidemic situation and then selects two classes of students as experimental objects to carry out traditional online and offline teaching behaviors and online and offline teaching as the main, multimedia computer teaching as the main object, and compares the performance differences of the two classes in music courses to reflect the effect of multimedia computer-assisted online and offline teaching. This paper introduced the algorithm use of multimedia computer in detail and then applied it to teaching activities to improve the shortcomings of the existing teaching mode. In order to reflect the effect of the mixed teaching mode assisted by multimedia computer, this paper selected two classes of an experimental middle school to conduct experiments on their music class performance. Before the experiment, the algorithm was evaluated and tested, and the accuracy rate of the algorithm was 91.333%. By carrying out teaching activities in different modes and analyzing the data of the test results, it can be seen that the results of the teaching mode assisted by multimedia computer are much higher than the existing teaching mode. Compared with the traditional classroom learning, the scores of the first class in the music class under the two modes were 0.32 points and 4.74 points higher than those of the traditional classroom learning, and the second class was 0.25 points and 7.01 points higher, respectively. In terms of improvement rate, the improvement rates of Class 1 and Class 2 in the multimedia computer-assisted teaching mode were 6.593% and 9.432%, respectively, which indicated that multimedia computers played a positive role in the assisted mixed teaching mode.

1. Introduction

With the rapid development of information technology, people are not simply using computers to surf the Internet. In the current environment where the epidemic is still severe, the normal teaching activities of students in many countries have been seriously affected. Under this circumstance, many schools use a combination of online and offline teaching mode to conduct daily teaching for students, so that students can enjoy the normal teaching of the school at home. In the past online and offline teaching mode, the school only taught students through the online platform, the platform did not analyze the problems of the students, and the teachers could not understand the specific situation of the students and could only teach according to the prepreparation behavior. Although it did not delay the students' learning progress, the students' course performance did not improve much under this traditional model, and the learning effect was even lower than the traditional offline teaching. In this case, it is necessary to make full use of the powerful functions of multimedia computers, and let the computers take advantage of the advantages of personalized recommendation algorithms to improve the past online and offline teaching mode. Accurately locate the problems in the teaching activities, perform data conversion processing on the text information generated in the teaching activities, feed the students' problems back to the teacher in time, and then make corresponding changes to the curriculum according to the results. Finally, an experimental analysis of the improved teaching mode was carried out, and

it was concluded that the online and offline mixed teaching mode assisted by multimedia computer has a positive effect on students' performance in music class. This conclusion also provided a reliable experimental basis for the subsequent changes in mixed teaching. Aiming at the shortcomings of the traditional online and offline mixed teaching mode, this paper mainly lets the multimedia computer learn the personalized recommendation algorithm and then processed the key information such as text information and digital information generated in the teaching activities according to the characteristics of the algorithm. Then, the processing results were fed back to the teaching teachers, and the remaining courses can be improved in time to improve the quality and efficiency of teaching. The application of this thinking provides certain ideas for changing the existing online and offline teaching mode.

In recent years, affected by the epidemic, not only schools have carried out online and offline teaching activities, but some companies have also carried out business training and other activities for employees through online and offline teaching. The wide application of online and offline teaching has aroused the interest of many scholars and conducted research on it. Through research and analysis, Wu found that the online and offline hybrid teaching mode can change the traditional classroom teaching mode. Its advantages can help to realize the transformation between languages and promote the understanding of Chinese culture by foreign students [1]. Xu believed that the effect of online and offline teaching on college computer courses is obvious. This mixed teaching model can bring a new teaching experience to boring computer courses and increase students' interest in boring coding courses [2]. Yen conducted an experimental analysis of online, offline, and online-offline mixed teaching for undergraduate child development courses to determine whether there are differences in students' course performance and satisfaction with different modes of teaching [3]. It can be seen from the research work of previous scholars that online and offline teaching can not only carry out teaching activities anytime and anywhere, but also improve students' learning. The interest in learning brings instructive significance to the development of the new teaching model.

The application of multimedia computer-assisted teaching breaks the shortcomings of traditional online and offline teaching, and provides certain convenience for daily teaching. The advantages of multimedia computers are not only reflected in students' teaching activities. Based on the wavelet transform theory, Zhu studied the speed of image compression and coding of multimedia computers in news technology and concluded that under this technology, image compression and coding are more convenient and faster [4]. Li analyzed the application of multimedia computer interactive education in preschool teacher training and found that multimedia computer interactive teaching can not only meet individual differences but also provide interactive functions, which greatly improves children's learning ability and interest [5]. Rachmadtullah studied the degree of effect of multimedia computer interaction in basic education. Through the analysis of students' learning materials, learning progress, and additional learning materials, it was known that the effect is positive and effective, and suitable for basic education activities [6]. Simarmata found that in daily teaching activities, the effectiveness of teaching activities is reduced due to the limitation of materials. Now with the help of multimedia computers, students can be broadened by playing videos and pictures to explain, and the teaching behaviors that could not be carried out before can be vividly displayed to students, so that students can have a deep understanding and improve their learning efficiency [7]. Sun studied the application of the multimedia computer teaching platform in the reform of university education. In the process of using multimedia computers, the teachers' teaching situation, the students' course learning situation, and other factors were fully considered, and the problems existing between the two were systematically dealt with, which greatly improve the quality of teaching [8]. It can be seen that multimedia computers can not only be used for interactive teaching, but also to open students' eyes and increase their interest in learning based on the rich teaching resources of multimedia computers, etc. The multi-functionality of multimedia computers provides new ideas for the change of the current teaching mode, and the advantages of multimedia computers can make up for the shortcomings of the current teaching and provide some help for the subsequent teaching reform.

The innovation of this paper is to combine multimedia computers with offline teaching, breaking the old teaching model, giving full play to the advantages of multimedia computers, implementing personalized recommendation algorithms for computer learning, allowing computers to analyze the course based on students' online and offline learning, and giving real-time feedback to the teaching teacher on the actual situation of students, and then the teacher makes improvements based on the results of the course analysis. The teacher then makes improvements to the shortcomings of the teaching process based on the results of the course analysis, and through the rich multimedia teaching resources and other features, the students are given targeted training, which not only improves the students' course performance but also stimulates their interest in learning, and this idea is proposed to provide certain guiding suggestions for the subsequent online and offline courses.

2. Personalized Recommendation Algorithm Theory

The traditional online and offline mixed teaching mode simply uses MOOC and SPOC and other network platforms to conduct daily teaching activities for students. This teaching mode has shortcomings such as low efficiency and inability to follow up students' learning progress in a timely manner. Now there are multimedia computers to improve the shortcomings of traditional online and offline mixed teaching. How does the multimedia computer realize it? In daily teaching activities, students' mastery of learning content and absorption efficiency are not the same. The traditional hybrid teaching mode can be improved through computer assistance. With the help of personalized

recommendation algorithms, teachers can teach according to the actual situation of students, and teachers can also receive the personalized learning results of students fed back by the computer in time, so that teachers can improve the quality of teaching. Personalized recommendation algorithms can provide users with an accurate profile to guide product recommendations, and their product recommendation accuracy is better than other algorithms. Next, the related theory of personalized recommendation algorithm was introduced [9].

2.1. Collaborative Filtering Recommendation Algorithm. Implementing personalized recommendation for users is actually algorithmic recommendation, and the applicability of the algorithm determines whether it can recommend suitable content to users [10]. The main operation process is as follows: firstly, calculate the similarity measure between users or between items, and secondly calculate the similarity between users and items. Finally, find the K most similar items, and generalize the previous N most frequent items to all target objects in the same field.

The first thing needs to be considered is whether there is similarity between users. To put it simply, if the distance between the two is closer, the similarity is higher and vice versa [11]. Here are some common similarity functions:

(1) The similarity function based on the Pearson coefficient is to calculate the similarity $w_{u,v}$ between user u and user v, and its calculation is

$$w_{u,v} = \frac{\sum_{i\in I}\left(r_{u,i} - \overline{r_{u,v}}\right)\left(r_{v,i} - \overline{r_v}\right)}{\sqrt{\sum_{i\in I}\left(r_{u,i} - \overline{r_u}\right)^2 \sum_{i\in I}\left(r_{v,i} - \overline{r_v}\right)^2}}. \quad (1)$$

Among them, I is the product evaluated by users u and v at the same time, and $\overline{r_u}$ is the average score of all products evaluated by the u-th user.

(2) The similarity function based on cosine vector assumes that each evaluation of students is processed into a vector with its corresponding score, and then the similarity between students can be measured by calculating the cosine angle between these vectors. Assuming that a matrix R of $m \times n$ is used to measure students, then the cosine value of the n-dimensional vector corresponding to the i-th row and the j-th row in this matrix can be calculated, and this value can be expressed as the similarity between students. The range of similarity intervals for cosine vectors is [-1, 1]. The calculation is

$$w_{i,j} = \cos\left(\overrightarrow{i}, \overrightarrow{j}\right) = \frac{\overrightarrow{i} \bullet \overrightarrow{j}}{\left\|\overrightarrow{i}\right\| * \left\|\overrightarrow{j}\right\|}. \quad (2)$$

Among them, "•" represents the inner product of two vectors. In other words, if vector $\overrightarrow{X} = \{x_1, x_2, ..., x_n\}$, vector $\overrightarrow{Y} = \{y_1, y_2, ..., y_n\}$, then (3) is the cosine similarity between vectors $\overrightarrow{X}$ and $\overrightarrow{Y}$:

$$w_{X,Y} = \frac{x_1 x_2 ... x_n + y_1 y_2 ... y_m}{\sqrt{x_1^2 + x_2^2 + ... + x_n^2}\sqrt{y_1^2 + y_2^2 + ... + y_n^2}}. \quad (3)$$

2.2. Algorithms Based on Content Recommendation. Content-based recommendation algorithms are good at overcoming sparsity and cold-start problems, and are good at interpreting recommendation results, while having high algorithm execution efficiency. The specific operation is to first extract the object features, and the extracted features are enough to describe the object and then record the user's usual preferences to generate a specific descriptive file. Finally, calculate the similarity between the user's real hobby object and the recommended object, and then recommend content according to the similarity [12].

When constructing the recommended object model, it is necessary to first evaluate the frequency of a certain keyword (the description of object feature extraction) appearing in the recommended object, which is expressed by importance here, and the calculation is

$$tf_{i,j} = \frac{n_{i,j}}{\sum_k n_{k,j}}. \quad (4)$$

In (4), $n_{i,j}$ is the number of times the keyword appears in the recommended object d_j, and $\sum_k n_{k,j}$ is the sum of all words in the recommended object.

$$i\,df_i = \log\frac{|D|}{\left|\left\{j\colon t_i \in d_j\right\}\right|}. \quad (5)$$

In (5), t_i represents the inverse document frequency, $|D|$ represents the total number of recommended objects in the corpus, and $|\{j\colon t_i \in d_j\}|$ represents the number of recommended objects containing keyword t_i.

In order to judge whether the recommended object meets the user's expectation, the utility function is used to calculate and explain it. The specific representation is

$$\mu(c, j) = \frac{\sum_{i=1}^{P} w_{i,c} w_{i,j}}{\sqrt{\sum_{i=1}^{P} w_{i,c}^2}\sqrt{\sum_{i=1}^{P} w_{i,j}^2}}. \quad (6)$$

In (6), P is the number of keywords. The smaller the value of $\mu(c, j)$, the better the recommended object meets the user's ideal expectations.

3. Implementation Process of the Algorithm

3.1. User Features. User features are generally divided into attribute features and behavioral features [13]. The content of personalized recommendation for users depends on the accuracy of user characteristic information. The specific user characteristics-related content is shown in Figure 1.

Different users have corresponding characteristic information. The recommendation system collected and then mined information according to this characteristic information, analyzed the favorite preferences of different users, timely pushed personalized content to users, and

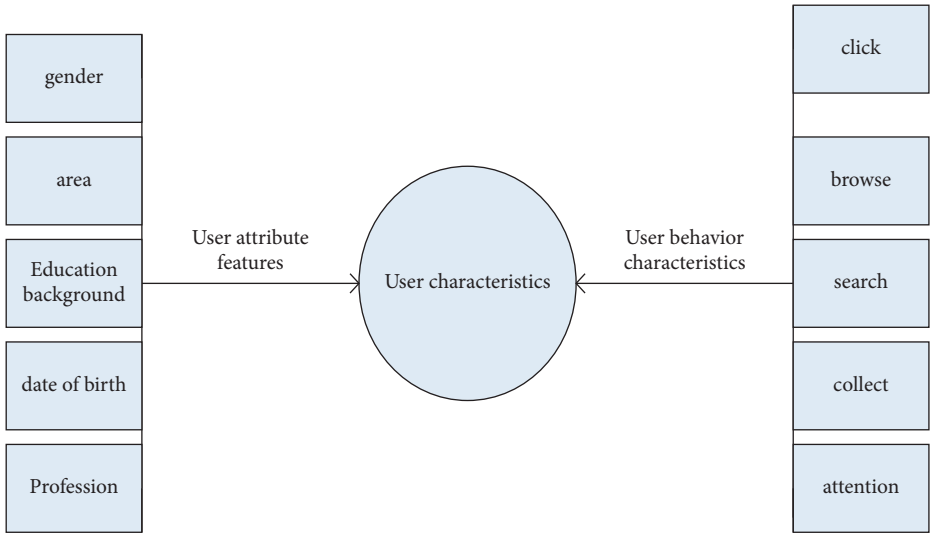

Figure 1: User feature classification.

met their needs. It can be seen that the extraction of feature information plays a crucial role in personalized service [14]. The source of user characteristic information is shown in Table 1.

The attribute characteristics of the user are generally the information registration of the user when the account is registered. This basic information is highly accurate and has obvious dominant characteristics representing the user, which is convenient for the system to identify and analyze. The user's behavioral characteristics mainly include the user's browsing, clicks, comments, and other related information, and this part of the information includes the user's favorite preference. However, this part of the information is both explicit and implicit. Explicit information can directly derive user needs, but implicit information needs to be studied and analyzed with the help of corresponding algorithms to obtain useful information for users. For example, when a student registers for an account, the account will have information such as the exact course name and course content, and not only that, but when a student is studying online, the videos they repeatedly watch or the questions they ask during the course will reflect some information about the course that is relevant to them.

3.2. Labels. When students conduct online and offline learning, a large amount of data will be generated in the learning process. The information and data are highly free and unconstrained. The occurrence of this phenomenon will bring difficulties to the subsequent system analysis work, and it is difficult to extract object features from this complex text information. Information is standardized by means of abstract symbols such as numbers or characters, mainly because computers can process these abstract symbols more accurately and conveniently than, for example, verbal texts. Therefore, in order to better reflect the effect of multimedia computer assistance on online and offline teaching, it is necessary to standardize these text information data before the experiment, so as to facilitate the feature extraction of the system, and to achieve the enhancement effect of multimedia computer assistance [15]. For example, Zhang San is a second-year student majoring in music education at xx University, majoring in music literacy courses such as sheet music reading, sight-reading, listening, rhythm, harmony, writing, music appreciation, and music history, then the key information related to Zhang San is can be extracted from these texts.

Table 1: User feature source.

User characteristics	Source
Attribute feature	Registration message
Favorite feature	Click, browse, bookmark
Active login features	Purchase of related courses
Social characteristics	Evaluated by teachers

When students conduct online and offline learning, the generated text information data may appear to be marked by users with one or more tags. The following images can be used to describe the relationship composition as shown in Figure 2.

Although multimedia computers cannot directly recognize and understand the semantics of tags like the human brain, according to Figure 2, the meaning of tags can be reflected from the marked course content. In order to better understand the standardization of labels, some concepts are now defined to facilitate subsequent work.

Definition 1. Label standardization: the process of mapping students' custom labels to semantic labels that can be recognized by the system.

Definition 2. Standard tags: tags with clear semantics and recognized by everyone, there is no correlation between each tag, and all tags form a tag set.

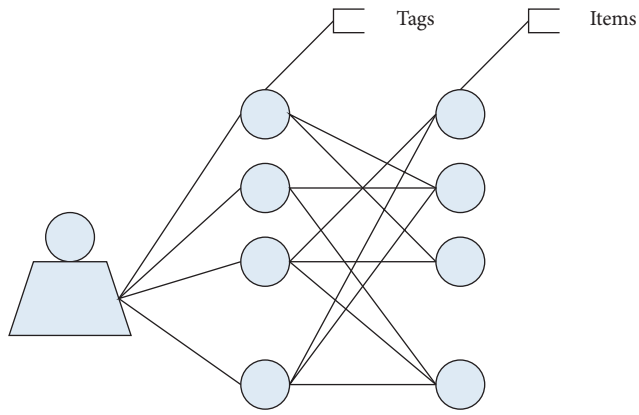

Figure 2: Relationship between labels and courses.

Definition 3. Word co-occurrence rate: it is assumed that during the online and offline learning process, the frequency of a word occurs repeatedly in each sentence, such as comments or active questions.

However, there will be semantic ambiguity in the process of label standardization. To solve this problem, three improvement methods were proposed: the first is tag matching, which matches and analyzes student-defined tags and tag sets; the second is to standardize words with high word co-occurrence rates; the third is to standardize tags with similar similarity. The combined use of these three methods can greatly improve the accuracy and work efficiency that cannot be standardized due to unclear semantics. The label standardization process is shown in Figure 3.

3.3. Operation Process of Two Kinds of Label Standardization

3.3.1. Label Standardization Based on Attribute Co-Occurrence Rate. When students are learning online and offline, their custom labels may have labeling errors. At this time, it is necessary to use the label standardization of the attribute co-occurrence rate to perform corresponding operations. By using the commonality of all resource objects in a marked set to express the true meaning of the label, combined with Definition 3, it can be seen that the condition that this attribute value satisfies is that the co-occurrence rate of the attribute value in this label set is 100% [16], and its calculation process is as follows:

Assume that the label to be standardized is *t*, resource set $P_t = \{p_1, p_2, \ldots p_l\}$ marked by *t*, and a certain resource $p_k = \{p_{k_1}, p_{k_2}, \ldots p_{k_n}\}$, $1 \le k \le l$, and p_{k_i} $(1 \le i \le n)$ are the attribute values of the i-th attribute of the resource. Then, the label normalization process based on attribute co-occurrence rate of label *t* is described as follows:

Now perform co-occurrence analysis on the resources marked in P; if $p_{1_i} = p_{2_i} = \ldots = p_{k_i} = \ldots = p_{l_i} = 1$, then take p_{k_i} as the standard label of all resources in this set; if $p_{k_i} \neq 1$, treat this p_{k_i} as a new standard tag and import it into the standard tag library.

3.3.2. Cluster-Based Label Normalization. Clustering plays an important role in the data mining process. Simply put, clustering is to classify several similar objects into clusters. Each cluster is independent, and there is a similarity or correlation between objects within a cluster [17]. In the clustering process of label standardization, this theory is also used for research and analysis.

In the usual research process, similarity is generally used to measure the similarity between two objects. But this is only studied based on numeric vectors, and this calculation method is not applicable when analyzing between words in the text. Therefore, used the method based on MI to calculate the similarity between different labels. MI is an evaluation criterion of information measurement. In short, it is to describe the value of Y that reflects the amount of information of *X* [18]. Assuming discrete random variables, then the expression is

$$I(X;Y) = H(X) - H(X \mid Y) = \sum_{x,y} p(x,y)\log\frac{p(x,y)}{p(x)p(y)}. \quad (7)$$

In (7), $H(X)$ is the entropy of the random variable *X*, and $H(X \mid Y)$ is the conditional entropy of the random variable *X* given the random variable Y. The expressions of the two are

$$H(X \mid Y) = -\sum_{x \in X}\sum_{y \in Y} p(x,y)\log p(x \mid y). \quad (8)$$

The mutual information $I(t_i, t_j)$ and entropy $H(t_i)$ of labels t_i and t_j are calculated as

$$H(t_i) = -p(t_i)\log p(t_i). \quad (9)$$

Theoretically speaking, the larger the value of mutual information, the greater the correlation between the two labels; if t_i and t_j are related, $I(t_i, t_j) > 0$; otherwise $I(t_i, t_j) = 0$ [19]. That is to say, the value of mutual information can be used to represent the similarity of labels. In order to prevent the value from exceeding the theoretical range, it is normalized before comparison [20]. The similarity between those two labels is expressed as

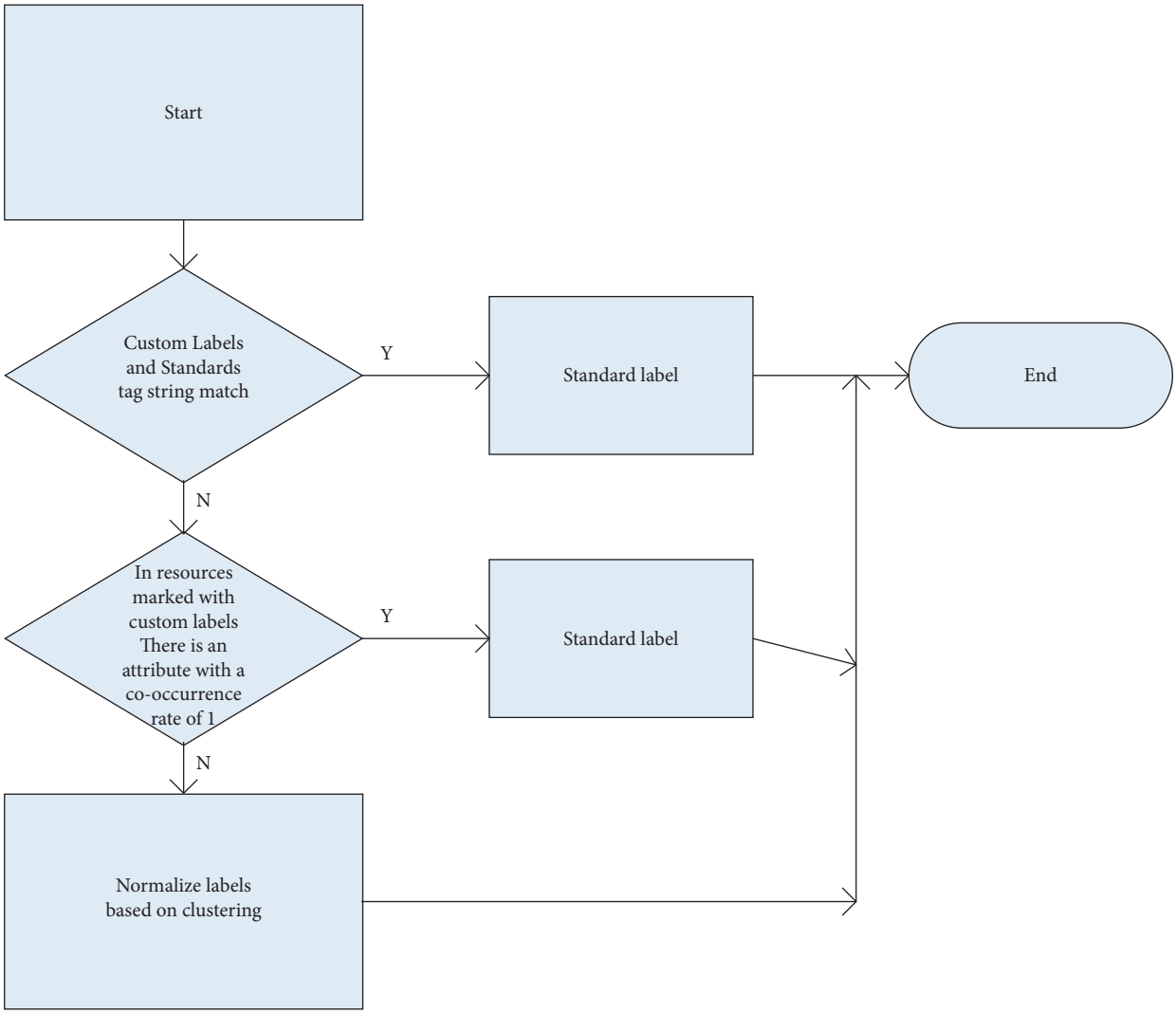

Figure 3: Label standardization process.

$$r_{i,j} = \frac{I(t_i, t_j)}{H(t_i) + H(t_j)/2}. \tag{10}$$

Among them, when $t_i = t_j$ and $r_{i,j} = 1$, there is a correlation between t_i and t_j and the two are completely correlated; when $t_i \neq t_j$ and $r_{i,j} = 0$, there is no correlation between t_i and t_j; in other cases, the value of $r_{i,j}$ is on the interval $[0, 1]$.

After analyzing and studying the similarity of labels, the next step is to cluster the labels on the basis of MI.

The clustering process of the personalized recommendation algorithm is similar to other clustering processes. It first determines a cluster center, that is, a standard label, and then calculates the distance between other labels and this standard label. Here, the size of the similarity was used to replace the size of the distance, the other tags with high similarity to the standard tag were grouped into a data set until the similarity between the remaining tags, the standard tag was less than a given value, and then the clustering process ends. Finally, the remaining labels were clustered with each other to obtain a new standard label, the new standard label was incorporated into the standard label data set, and the above operations were repeated until all custom labels complete the clustering operation. (11) is the definition of the similarity matrix R of labels:

$$R = \begin{bmatrix} r_{11} & r_{12} & \cdots & r_{1n} \\ r_{21} & r_{22} & \cdots & r_{2n} \\ \cdots & \cdots & \cdots & \cdots \\ r_m & r_{m2} & \cdots & r_{mn} \end{bmatrix} = (r_{ij})_{m\times n}. \tag{11}$$

Among them, n is the number of standard signatures, m is the number of custom labels, and $r_{i,j}$ is the label similarity.

The implementation process of the MI algorithm is as follows:

Assuming that there is a standard label set of $T_S = \{t_{s1}, t_{s2}, \ldots, t_{sn}\}$, other labels are represented by $T_P = \{t_{p1}, t_{p2}, \ldots, t_{pm}\}$, and δ is used to represent the above given value and then operate the following:

(i) Operation 1: Take the label in T_S as the cluster center, and then calculate the similarity of all elements in the two sets according to (10).

(ii) Operation 2: Calculate the similarity matrix R of the tags according to (11).

(iii) Operation 3: Select the largest element r_{ij} in the calculated matrix R. If it is $r_{ij} \geq \delta$, then aggregate label t_{pi} into the class centered on label t_{sj}, and then delete the i-th row of R to obtain a $(m - l) * n$-dimensional matrix.

(iv) Operation 4: Repeat the steps of Operation 3 for the new matrix obtained in Operation 3. When the value of the largest element in the finally obtained matrix is less than the given value, the clustering process is terminated. The clusters obtained in the above process are classified into a set $C_1 = (c_1, c_2, ..., c_n)$, in which the cluster center of the standard label t_{si} $(1 \leq i \leq n)$ can be represented by c_i.

(v) Operation 5: Cluster the labels with the remaining similarity less than the given value again, then reconstruct the standard labels, and then perform the steps of Operations 1 and 2 to obtain a new matrix. Find the maximum value of the main diagonal of this matrix, finally repeat the process of Operations 3 and 4, and finally form a new cluster set $D_1 = (d_1, d_2, ..., d_n)$.

The finally obtained clustering result expression is

$$M = C_1 + D_1 = \{c_1, c_2, ..., c_n, d_1, ..., d_n\}. \quad (12)$$

It can be seen that the labels in each class form a mapping relationship with the standard labels of the class, and the custom labels that fail to cluster use themselves as the standard labels. The above two methods were used in combination to make up for each other's deficiencies and improve the accuracy of standardization. The attribute co-occurrence rate can make up for the problems of similar labels and too many labels in the clustering process when standardizing labels. The combination of the two improved the operating speed and accuracy of the system.

4. Experiments on Label Normalization Algorithms

4.1. Data Selection and Algorithm Evaluation Criteria

4.1.1. Experimental Data. This paper collects 1,000 comment records of 10 movies from 100 users on the Douban platform. In this data set, movies were divided into 8 categories, namely, action, adventure, animation, logical, truth, funny, thriller, and horror. During the experiment, the movie-related plot category, the main actor's preference for participating in the film, and the movie's tidbits were used as the labels of the movie. According to the algorithm, the tags of 100 users' comments are standardized, then compared and analyzed according to the processing results and the standard tags, and then combined with the evaluation results of the audience. In the process of processing, in order to form a comparison, 70% of the selected data set was used as the training set, and the remaining 30% was used as the test set. There was no correlation between the two data sets and both data sets contain the normalized results of all user and review labels.

4.1.2. Evaluation Criteria. In order to test the performance of the above algorithms, the corresponding evaluation criteria should be established. In this experiment, P@N (accuracy rate) was selected as the standard to measure the accuracy of the prediction results, and its calculation is

$$P@N = \frac{N_{max}}{N}. \quad (13)$$

In (13), N_{max} is #relevant items in top N items.

4.2. Experimental Results. In order to verify the advantages of the above algorithms, the slope one algorithm (method 1), the recommendation algorithm based on association rules (method 2), and the personalized recommendation algorithm (method 3) were selected for comparative analysis. The information data in the above data sets were randomly divided into 9 groups, then each data set was analyzed separately using the above algorithm, then the accuracy was compared according to the calculation, and the experimental results are shown in Table 2.

Then, the results of Table 2 were analyzed graphically, as shown in Figure 4.

As can be seen from Figure 4, the personalized recommendation algorithm had a higher accuracy of label standardization than the other two algorithms. Now calculate the mean of the data, and the result is shown in Figure 5 (three decimal places are reserved for the mean value).

Combining Figures 4 and 5, it can be seen that the accuracy of the personalized recommendation algorithm was higher than that of the other two algorithms in the 9 experimental data sets. After the average calculation of the 9 data results, the accuracy of the personalized recommendation algorithm was obtained. The rates were 3.444% and 4.222% higher than the other two algorithms, respectively, indicating that the personalized recommendation algorithm is effective in standardizing labels.

5. Multimedia Computer-Aided Music Class Online and Offline Mixed Teaching Mode

Based on the above experimental verification of the personalization algorithm, it was concluded that the personalized recommendation algorithm is better than other algorithms in terms of standardization of textual information and related content recommendations. After the matching was completed, the students' music course learning situation was fed back to the teacher in real time through computer analysis, so that the teacher could improve the teaching content based on the results and then use the rich teaching resources of multimedia computers to

Table 2: Accuracy data of different methods.

	Method 1	Method 2	Method 3
Group 1	87	86	90
Group 2	91	89	92
Group 3	89	86	93
Group 4	85	85	89
Group 5	96	95	98
Group 6	83	83	89
Group 7	79	83	88
Group 8	91	90	92
Group 9	90	87	91

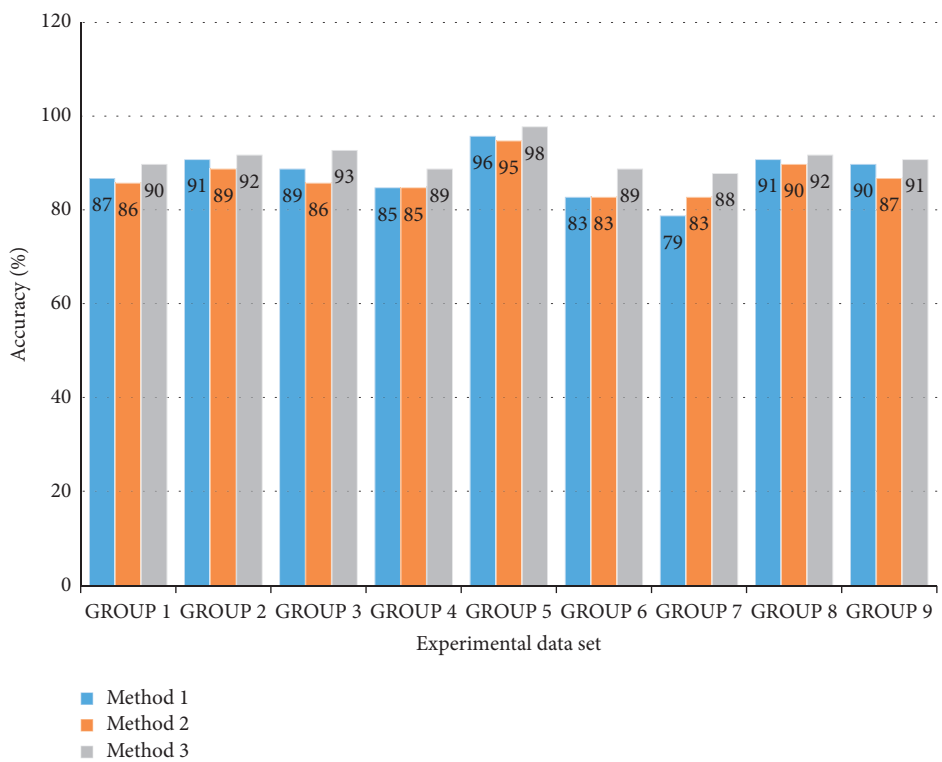

Figure 4: Accuracy data chart of different methods.

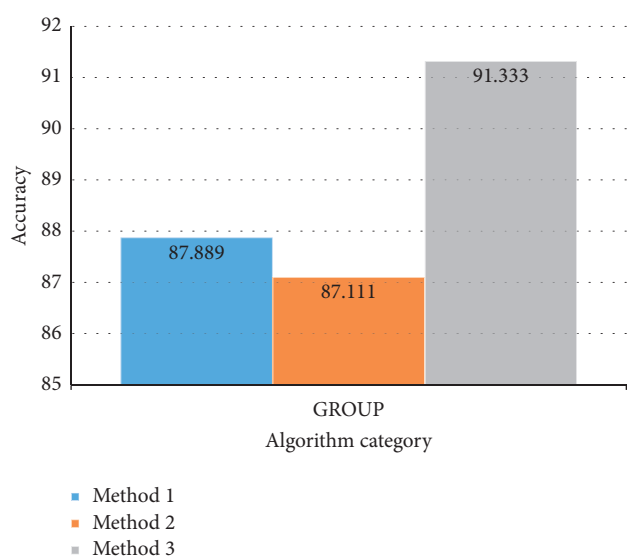

Figure 5: Average accuracy comparison chart.

teach students in a mixed way. In order to better reflect the acceptance rate, this paper mainly conducts a postlesson quiz on students to study and analyze the results.

5.1. Experimental Subjects and Methods. The research objects are two ordinary classes of grade 20 in a selected experimental middle school, taking the test scores of the music class as the research object. Before the experiment, the students in the two classes who participated in the experiment were checked whether they were interested in music lessons, and whether there was a large fluctuation in the scores of the music lessons before. After relevant investigations, it was found that there was no significant difference between the two classes, which met the basic conditions of this experiment. In this experiment, the number of students in the two classes is 45, of which the first class is the control group, and the second class is the experimental group.

During the experiment, it is necessary to clarify the experimental variables and other irrelevant variables in the experimental process. The irrelevant variables are the learning pace and receptivity of each student, etc. The independent variables of this paper are the traditional online and offline mixed teaching mode and the multimedia computer-assisted online and offline mixed teaching mode. Class one uses traditional online and offline mixed teaching, and the second class uses multimedia computer-assisted online and offline mixed teaching. The dependent variable is the students' test scores after completing the teaching activities of the music class.

5.2. Experimental Data. Before the experiment, the two classes should be tested on the course performance (the results of this experiment are the test results of traditional offline teaching) to ensure that the indicators of the two classes are at the same level. Only the conclusions drawn in this way are true and valid.

Use SPSS to process and analyze the grade data of the two classes, and the results are shown in Tables 3 and 4 (the full score is 100 points).

As can be seen from Table 4, the average score of the pre-experiment music class of the general class 1 was 72.21 points, the average score of the music class of the general class 2 was 74.56 points, and the average score of the second class was 2.35 points higher than that of the first class. In the comparative analysis of the standard deviation of the two classes, it was found that the standard deviation of the second class was smaller than that of the first class, which indicated that the grades of the second class students are relatively concentrated.

Next, a t-test is performed on the two classes, and the test results are shown in Table 5.

As can be seen from Table 5, the t-test is performed on the scores of the ordinary Class 1 and Class 2 before the experiment. In the case of equal variances, $p = 0.094 > 0.05$; in the case of different variances, $p = 0.093 > 0.05$. It shows that no matter whether the variances are equal or not, the difference between the two classes is not significant; that is, the average grades of the two classes are the same, which means that the two classes can be analyzed experimentally.

In order to ensure the validity of the experiment, the average of the mid-term scores of the two classes was taken as the reference value (the average is the average of all the scores of the two classes and the scores are in a stable state, not subject to sharp fluctuations due to distracting factors), the reference scores are the scores obtained from the tests conducted in the traditional offline teaching mode, and the scores of the music courses in the different teaching modes were compared and analyzed after the experiment. After conducting two kinds of teaching experiments in music class, the students in the two classes were tested for course performance, and then the obtained scores were analyzed by SPSS. The results obtained are shown in Tables 6 and 7.

As can be seen from Table 6, the average scores of the two classes after the two modes of teaching were 76.67 and 81.32, respectively, and the average score of the second class was 4.65 points higher than that of the first class. It showed that the online and offline mixed teaching mode assisted by multimedia computer is more effective than the traditional online and offline teaching, which is conducive to improving students' performance. Not only that, the standard deviation of the average scores of the two classes was smaller than the previous test data, which made the scores of the two classes relatively concentrated, indicating that the mixed teaching mode assisted by multimedia computers is reliable.

Table 7 shows a t-test for the scores of the two classes after the test. In the case of equal and unequal variances, the p value is less than 0.05, indicating that the difference between the two samples is significant. That is to say, there is a significant difference in the scores of ordinary classes 1 and 2 after the conventional online and offline mixed teaching and the online and offline mixed teaching assisted by multimedia computers. The average grades of the students in the second class have improved more than the average grades of the first class, which showed that the multimedia computer-aided teaching has a positive effect on online and offline mixed teaching activities.

In order to better reflect the effect of multimedia computer-aided online and offline mixed teaching, this paper, respectively, analyzes the performance of traditional teaching music class in nononline and offline teaching mode (experimental group 1), the traditional online and offline teaching music class performance (experimental group 2), and the results of multimedia computer-assisted online and offline teaching music class (experimental group 3). The experimental data results are shown in Figure 6 (the average scores are taken, respectively).

In Figure 6, it can be seen intuitively that after adopting different teaching modes for the music lessons of the two classes, their scores were improved compared with the traditional offline teaching. Among them, the music class scores of the first class were 0.32 points and 4.74 points higher than the traditional offline teaching scores under the two modes, and the music class scores of the second class were 0.25 points and 7.01 points higher than the traditional offline teaching scores, respectively. It showed that in the two

Table 3: The operating standard of the group experiment.

Class	Test subject	Pre-experimental state	Experimental factor	Experimental operation	Post-test status	Experimental results
Experimental class	A1	B1	C1	B1Q1	B1′	$D1 = B1'\text{-}B1$
Control class	A2	B2	C2	B2Q2	B2′	$D2 = D1'\text{-}D1$
Condition	A1 = A2		C1 ≠ C2			
	Result		C = C1–C2			

Table 4: Statistics of the basic situation group in the pretest for the first and second shifts.

	Pretest scores	
Class	1	2
Average value	72.21	74.56
Standard deviation	6.178	5.415
Standard error of the mean	0.932	0.835

Table 5: *T*-test.

			Assuming equal variances	Assuming unequal variances
Levene test for variance equation		F	1.32	
		Sig.	0.254	
t-test for the mean equation		t	−1.692	−1.698
		df	84	83.398
		Sig.(bilateral)	0.094	0.093
		Mean difference	−2.124	−2.124
		Standard error value	1.255	1.251
	95% confidence interval for difference	Lower limit	−4.621	-4.613
		Upper limit	0.372	0.364

Table 6: Postexperiment results.

	Postexperiment results	
Class	1	2
Average value	76.67	81.32
Standard deviation	5.814	5.013
Standard error of the mean	1.096	1.387

Table 7: Postexperiment *t*-test.

			Assuming equal variances	Assuming unequal variances
Levene test for variance equation		F	4.503	
		Sig.	0.038	
t-test for the mean equation		t	−2.366	−2.361
		df	83	78.356
		Sig.(bilateral)	0.02	0.21
		Mean difference	−4.175	−4.175
		Standard error value	1.762	1.765
	95% confidence interval for difference	Lower limit	−7.688	−7.698
		Upper limit	−0.668	−0.658

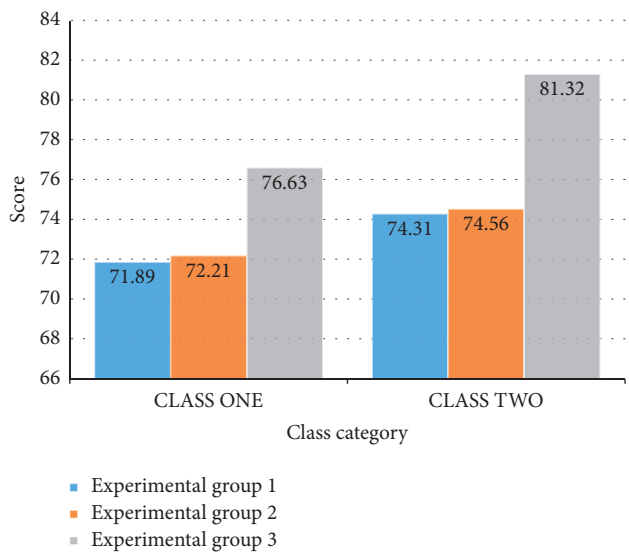

Figure 6: Comparison chart of scores before and after the experiment.

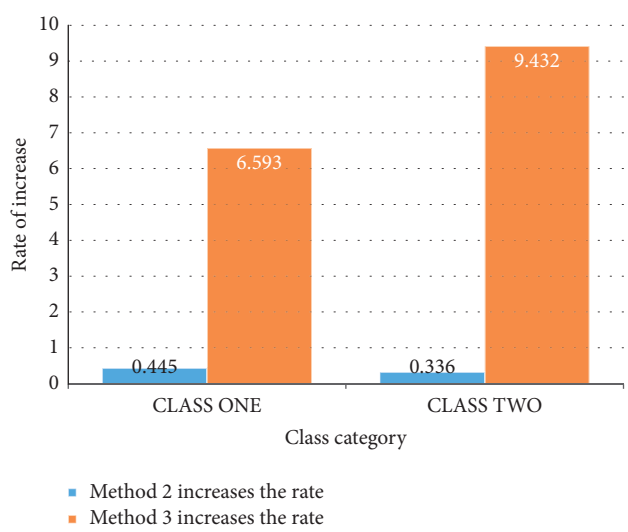

Figure 7: The graph of the improvement rate of the grades of the two classes.

classes under the multimedia computer-assisted teaching mode, the students' performance in music class has been improved.

In order to better reflect the improvement of grades, the improvement rate on the basis of the original data is calculated, and the results obtained are shown in Figure 7 (using the grades under the traditional teaching mode as the basic data).

As can be seen from Figure 7, the improvement rates of the music class scores of the first and second classes under the traditional online and offline mixed teaching were 0.445% and 0.336%, respectively, and the increase is not large; the improvement rate of music class performance in the online and offline mixed teaching mode assisted by multimedia computer is 6.593% and 9.432%, respectively, and the increase is far greater than that of the traditional online and offline mixed teaching mode. In short, the increase is 14.8 and 28.1 times the original, which indicated that the effect of online and offline mixed teaching of music lessons based on multimedia computer assistance is significant.

6. Conclusion

In recent years, many people have completed their learning tasks through online and offline teaching. The application of online and offline teaching mode allows people to carry out learning activities anywhere and anytime, providing people with great convenience. This paper mainly conducted auxiliary research on online and offline mixed teaching based on multimedia computers. In the research process, two classes of an experimental middle school are selected to conduct a comparative analysis of the changes in music class performance before and after the experiment. Before the experiment, the accuracy of the algorithm was tested experimentally, and it was concluded that the algorithm was effective; then, two classes were taught in different modes of teaching activities, and after the teaching activities were completed, curriculum tests were conducted. Then, the results of the test were researched and analyzed, and it was concluded that the multimedia computer-assisted education model has a positive effect on the existing teaching model. The main work of this paper can be divided into three points.

6.1. Theoretical Introduction to Algorithms in Multimedia Computers. This paper mainly applied the personalized recommendation algorithm to the multimedia computer. First, the content recommendation algorithm and the collaborative filtering algorithm of the personalized recommendation algorithm were introduced theoretically, and the implementation process of the algorithm was described accordingly.

6.2. Test of Personalized Recommendation Algorithm. This paper mainly used the personalized recommendation algorithm to improve the online and offline mixed mode teaching. Before the experiment, the accuracy of the algorithm needed to be tested to ensure that the algorithm can quickly and accurately judge and analyze the information in the subsequent process.

6.3. Multimedia Computer-Aided Online and Offline Mode Analysis. This section focuses on the experimental comparative analysis of traditional offline, traditional online, and multimedia computer-assisted online and offline teaching. Students in two classes are studied in different teaching modes, then the comparative analysis of teaching modes is based on the results of music course performance tests, and it is concluded that the multimedia computer-assisted online and offline hybrid teaching mode is superior to other teaching modes.

Due to the influence of the experimental environment, the experimental data in this paper were not perfect and the

data range was not large enough. The test results may fluctuate violently due to irresistible factors, which made certain flaws in the final score analysis process, and the handling of these factors was also the focus of subsequent work improvement.

Data Availability

The data that support the findings of this study can be obtained from the author upon reasonable request.

Conflicts of Interest

The author declares that there are no potential conflicts of interest with respect to the research, authorship, and/or publication of this article.

References

[1] Y. Wu and J. Wang, "Three-stage blended Chinese teaching online and offline for international students: a case study on Chinese teaching for international students in S university," *Journal of Higher Education Research*, vol. 3, no. 2, pp. 207–211, 2022.

[2] C. Xu, "Thoughts on the implementation of online and offline hybrid teaching of university computer courses," *Region - Educational Research and Reviews*, vol. 3, no. 2, pp. 1–4, 2021.

[3] S. C. Yen, Y. Lo, A. Lee, and J. Enriquez, "Learning online, offline, and in-between: comparing student academic outcomes and course satisfaction in face-to-face, online, and blended teaching modalities," *Education and Information Technologies*, vol. 23, no. 5, pp. 2141–2153, 2018.

[4] Y. Zhu, "Research on the application of multimedia computer in news technology," *Revista de la Facultad de Ingenieria*, vol. 32, no. 14, pp. 183–187, 2017.

[5] L. Li, "Research on application of multimedia computer interactive education in preschool teacher training," *Revista de la Facultad de Ingenieria*, vol. 32, no. 12, pp. 1007–1013, 2017.

[6] R. Rachmadtullah, Z. Ms, and M. Syarif Sumantri, "Development of computer-based interactive multimedia: study on learning in elementary education," *International Journal of Engineering & Technology*, vol. 7, no. 4, pp. 2035–2038, 2018.

[7] J. Simarmata, T. Limbong, E. Napitupulu et al., "Learning application of multimedia-based-computer network using computer assisted instruction method," *International Journal of Engineering & Technology*, vol. 7, no. 2.13, pp. 341–344, 2018.

[8] M. Sun, R. Hao, and B. Wang, "Research on the computer assisted multimedia teaching platform application in university education reform," *Boletin Tecnico/Technical Bulletin*, vol. 55, no. 4, pp. 544–550, 2017.

[9] F. Long, "Improved personalized recommendation algorithm based on context-aware in mobile computing environment," *Wireless Communications and Mobile Computing*, vol. 2020, no. 1, pp. 1–10, 2020.

[10] L. Xiaojun, "An improved clustering-based collaborative filtering recommendation algorithm," *Cluster Computing*, vol. 20, no. 2, pp. 1281–1288, 2017.

[11] G. Wei and Y. Wei, "Similarity measures of Pythagorean fuzzy sets based on the cosine function and their applications," *International Journal of Intelligent Systems*, vol. 33, no. 3, pp. 634–652, 2018.

[12] L. Cui, L. Dong, X. Fu, Z. Wen, N. Lu, and G. Zhang, "A video recommendation algorithm based on the combination of video content and social network," *Concurrency and Computation: Practice and Experience*, vol. 29, no. 14, pp. e3900–20, 2017.

[13] D. C. Hernandez-Bocanegra and J. Ziegler, "Explaining review-based recommendations: effects of profile transparency, presentation style and user characteristics," *I-Com*, vol. 19, no. 3, pp. 181–200, 2021.

[14] Y. Liu, X. Yi, R. Chen, Z. Zhai, and J. Gu, "Feature extraction based on information gain and sequential pattern for English question classification," *IET Software*, vol. 12, no. 6, pp. 520–526, 2018.

[15] R. Jenke, A. Peer, and M. Buss, "Feature extraction and selection for emotion recognition from EEG," *IEEE Transactions on Affective Computing*, vol. 5, no. 3, pp. 327–339, 2014.

[16] Z. Li, Y. Shen, and J. Chen, "Iterative bootstrapping attribute knowledge base extension algorithm based on word Co-occurrence graph," *Moshi Shibie yu Rengong Zhineng/Pattern Recognition and Artificial Intelligence*, vol. 31, no. 12, pp. 1143–1150, 2018.

[17] R. E. Chandler, K. Juhlin, J. Fransson, O. Caster, I. R. Edwards, and G. N. Noren, "Current safety concerns with human papillomavirus vaccine: a cluster Analysis of reports in VigiBase," *Drug Safety*, vol. 40, no. 1, pp. 81–90, 2017.

[18] Q. Zhu and B. K. Jesiek, "A pragmatic approach to ethical decision-making in engineering practice: characteristics, evaluation criteria, and implications for instruction and assessment," *Science and Engineering Ethics*, vol. 23, no. 3, pp. 663–679, 2017.

[19] R. Cui, Y. Li, and W. Yan, "Mutual information-based multi-AUV path planning for scalar field sampling using multidimensional RRT," *IEEE Transactions on Systems, Man, and Cybernetics: Systems*, vol. 46, no. 7, pp. 993–1004, 2016.

[20] H. Zhang, H. Lin, and Y. Li, "Impacts of feature normalization on optical and SAR data fusion for land use/land cover classification," *IEEE Geoscience and Remote Sensing Letters*, vol. 12, no. 5, pp. 1061–1065, 2017.

Hindawi
Mobile Information Systems
Volume 2022, Article ID 8635335, 6 pages
https://doi.org/10.1155/2022/8635335

Research Article

Innovation and Design of Physical Teaching Resource Intelligent Distribution Platform Based on Blockchain Technology

Jing Wang,[1] Peng Ran,[1] and Zhe Xie[1,2]

[1]*College of Physical Education, Jeonju University, Jeonju 55060, Jeollabuk-do, Republic of Korea*
[2]*Sports Department, Zhengzhou Business Colleage, Gongyi 451200, Henan, China*

Correspondence should be addressed to Peng Ran; 2021214948@ecut.edu.cn

Received 19 July 2022; Revised 19 August 2022; Accepted 31 August 2022; Published 22 September 2022

Academic Editor: Yajuan Tang

This article aims to study the innovation and design of an intelligent distribution platform for physical teaching resources based on blockchain technology (BT). With the continuous shrinking of teaching, the problem of balanced shrinking of teaching has become a hot issue in the field of teaching. In the distribution of physical education resources, there are problems such as lack of physical equipment and not fully open teaching, which as an important and shrinking point in the overall shrinking of society, will inevitably be included in the ranks of the overall shrinking of urban and rural areas. Physical teaching should be mentioned in the proposal as an important content of the school's teaching. It can make teaching resources more distinctive and personalized, closer to life, and can also make more sports resources become school materials. School physical teaching resources are the basis for all school physical teaching. However, for historical and practical reasons, the gap in the allocation of physical teaching resources in urban and rural primary and secondary schools is gradually increasing. This problem has always restricted the modernization of school sports. To achieve the coordinated shrinking of urban and rural school sports, the balanced shrinking of urban and rural school sports resources is a prerequisite. It enables users to build portrait and content intelligent recommendation algorithms to build a cross-platform and geographic one-stop teaching resource intelligent distribution platform. Through experiments, the statistical data of the questionnaire survey results after the design and test show that 80% of the primary and middle school students are satisfied with the subplatform and believe that the design of this platform has a role in enhancing physical exercise.

1. Introduction

1.1. Background. Physical teaching is an important part of school teaching and a prerequisite for students to improve their cultural scores. Physical teaching reform is the key to continuously improve the quality and effectiveness of physical teaching, and physical teaching resources affect the progress and quality of physical teaching reform to a large extent. Therefore, the design of an intelligent distribution platform for physical teaching resources can reasonably allocate physical teaching resources and promote the reform of how physical teaching is taught in the elementary and secondary schools.

1.2. Significance. At present, in China's physical teaching system, more and more physical teaching teachers are unable to conduct physical teaching. Even if they have better teaching methods and teaching concepts, they do not have a good platform. The distribution of teaching resources can fully implement the modernization of physical education teaching in the general direction. It can cultivate students' physical education literacy, integrate teaching resources, optimize teaching structure, reflect school teaching characteristics, and improve teaching efficiency.

1.3. Related Work. Sikorski et al. and other scholars highlighted BT's research and application potential in relation to the fourth industrial revolution [1]. Zhang and Wen proposed a IoT e-commerce model specifically designed for IoT e-commerce, redesigned many elements in the traditional e-commerce model, and finally realized it on the IoT with the help of P2P transactions based on blockchain and smart contracts for smart property and payment data transactions

[2]. Their research has played a pivotal role in my country's e-commerce industry, but their research has not been implemented in the teaching industry. The reforms have led to a gradual increase in the relative performance of students in low-income school districts, which is consistent with the goal of increasing teaching opportunities for these students. The hidden influence of school resources on teaching achievement is great. Researchers such as Lafortune *J* found that reforms have led to a gradual increase in the relative performance of students in low-income school districts, which is consistent with the goal of increasing teaching opportunities for these students. School resources have a great influence behind the scenes of teaching achievements. The school has abundant teaching resources, which is also conducive to teachers' teaching. Teaching resources are integrated with teaching results. If the teaching resources cannot be satisfied, the teaching results will also be affected [3]. But they have not conducted in-depth analysis and research on the intelligent distribution of physical teaching resources.

1.4. Innovation. This paper proposes an innovative design of an intelligent distribution platform for sports resource based on BT. The focus of this model is decentralized/intermediate blockchain trust, collective maintenance, smart contracts, security, and reliability. The system itself does not need external access to ensure the reliability and authenticity of the data, and the data are stored, transmitted, and verified in a distributed structure, so the node can still operate normally if the data are lost, which helps to solve the problem of different regions and regions under the traditional model. The problem of the uneven distribution of school physical teaching teachers and the serious imbalance of teachers provides a transparent and fair circulation environment for the distribution of physical teaching resources.

2. BT and Teaching Related Professional Concepts

In this paper, the POW algorithm and the POS algorithm in the BT technology are mainly explained, and the two algorithms are explained in the teaching resources. The two methods are described below.

2.1. PoW Algorithm. The shape of the block H supplied by the node must meet the following requirements: H (A) target, where B is a specified hash algorithm, and T is a defined integer [4, 5]. That is, the hash value in its entirety. The block must be less than the supplied amount and include a predetermined number of targets [6, 7]. If the node finds such a lawful zone, it will reward the mines excavated with a particular digital money [8, 9]. The hash function is proper and random. The hash value may be substantially different than earlier in the event of slight modifications to the source data [10, 11]. The hash value may appear out of the predicted range, or the value may be too large, which may make the calculation impossible. The probability P of discovering a valid block in each test is as follows:

$$P = \frac{T\,(\text{target})}{H\,(\max)}. \tag{1}$$

The following formula will be used to change the value of T in Bitcoin:

$$T\,(\text{new}) = \frac{T2016}{2W}.T\,(tar). \tag{2}$$

Formula (3) may be used to calculate the difficulty value of the created block.

$$D\,(\text{difficulty}) = \frac{T1}{T\,(\text{current})}. \tag{3}$$

2.2. PoS Algorithm. Finding a legal block in PoW requires a lot of calculation, a lot of energy, and time. In order to speed up the creation of blocks, PoS also considers the node's share in the digital currency.

$$H\,(B, \text{t}) \leq \text{b} * T\,(\text{target}). \tag{4}$$

2.3. The LFM Recommendation Algorithm

$$m\,(x, y) = m_x^T n_y = \sum_{i=1}^{I} m_{xi} n_{yi}, \tag{5}$$

m (x,y) represents the pair of user and item. If the user clicks on the item, then m (x,y) is 1, otherwise it is 0. The model finally outputs the user vector and the item vector, namely Mu and Ni. The i in the formula represents the dimension of the vector, which is the number of factors that affect whether the user likes the item or not [12, 13]. Supplement: This formula is to calculate user m's interest in item n, which is a certain value of a matrix, and i is the number of hidden categories.

The LFM loss function

$$L = \sum_{(\text{x,y})\in D} \left(\text{m}\,(x, y) - m^{LFM}\,(x, y)\right)^2,$$

$$L = \sum_{(\text{x,y})\in D} \left(\text{m}\,(x, y) - \sum_{\text{i}=1}^{I} MxiNyi\right)^2 + \beta|Mx|^2 + \beta|Ny|^2. \tag{6}$$

In the formula, m (x, y) is the label of our training sample, which means that if the user clicks on the item, then the label is 1, otherwise the label is 0. The latter item is the user-to-item estimated by our model. The degree of preference is the product of the transposed parameters M (x) and N (y) of the model output, where D is the set of all training samples [14, 15]. It can be seen that if the product evaluated by the model is close to the label, the value of the loss function is small, and vice versa. In the second formula, the model estimation type is expanded according to the LFM modeling formula, where β is the normalization factor, which is used to balance the secondary loss and normalization conditions. If the type evaluation is the same as the label, then the value of the function-valued loss is almost 0.

The purpose of normalization is to simplify the model so that M (x) and N (y) match the data in the training sample, which will make the model parameters more complicated and weaken the normalization ability. In this paper, the two algorithms are used to explain the calculation of the internal operation of the platform. Through these two calculations, the required resources can be determined for reasonable allocation.

2.4. Physical Teaching Resources. So far, the concept of physical teaching resources has not been clearly defined, and they are all derived from the concept of teaching resources [16]. All the resources that can be used in teaching practice can be called teaching resources. That is to say: teaching resources are the general term for various resources needed in teaching practice. Therefore, it can be seen from the above fact that physical teaching resources refer to all kinds of resources required for physical teaching practice. At present, domestic physical education resources are insufficient superficial inquiry learning, physical education is too relaxed, and students are too obedient. By comparing the research results of physical teaching resources at home and abroad, it can be seen that the outstanding advantages of foreign elementary school physical teaching are mainly concentrated in different aspects, such as lifelong, healthy, individualized, and innovative. In terms of material resources, foreign sports venues are rich in resources, which can not only meet the needs of daily teaching but also advocate reasonable and full use of existing resources in society, schools, and so on and continuously improve the utilization rate of sports resources. For physical teaching teachers' resources, foreign countries advocate that physical teaching teachers have multiple skills, understand multiple fields of knowledge, and are good at adjusting teaching content flexibly according to the school's geographic conditions and teaching needs [17].

2.5. BT. The so-called blockchain technology, referred to as BT, also known as distributed ledger technology, is an Internet database technology that is characterized by decentralization, openness, and transparency, allowing everyone to participate in database records. BT is an emerging technology in recent years. Its application fields have completely exceeded finance and digital currency and have stepped into other fields. The application of BT to the field of teaching BD is a new kind of try. The application of BT in the field of teaching, due to its own characteristics, makes it possible to build a high level of confidentiality, not easily tamper with, and to record a series of data collected by the subject.

The data owner's ownership of the data is guaranteed, and the owner can decide with whom his data can be shared. These can promote the wide sharing and dissemination of teaching resources in society, ensure that teaching resources are not lost, and improve resource utilization [18].

However, due to the immature shrinking of BT, it is just starting to get involved in the nonfinancial field. Judging from the present level of technological shrinking and actual conditions, there will be some shortcomings and problems:

(1) Security issues. BT will publish the collected data in the entire network, that is, each block will record and store the data, which on the one hand ensures the safety and nonloss of the data; but on the other hand, whether it is students, teachers or teaching institutions such as schools, their basic information and related data will be recorded in public accounts.

(2) The problem of data storage space. The blockchain database records every transaction from the genesis block, and every new node needs to participate in the chain, download and update the data package that has been continued since the beginning [14]. The BT itself cannot be deleted. On the one hand, its nondeletable and unalterable characteristics lead to learning records and learning behavior data that can only be increased and cannot be modified. There are great requirements for storage capacity and search capacity, which will restrict its key issue of shrinking.

(3) The issue of technology landing. BT has always been used in the financial and currency fields, and the application of blockchain is still in its infancy. To implement it into real-world applications, a lot of technical details need to be considered. At the same time, the shrinking of big data technology (BDT) in the teaching field is not yet fully mature. The construction is also in the preliminary stage.

The shortcomings of blockchain technology are that it cannot be tampered with, can be cancelled, and the transaction ledger is easy to disclose. The larger the data, the higher the performance requirements and the delay.

2.6. Information Security Technology. Information security is very important in all aspects of the cloud platform software system, especially in the field of unified-identity authentication. Once the user identity information is leaked, the less serious it will cause personal privacy leakage, and the more serious it will cause serious damage to the entire cloud platform, because the first consideration in cloud platform design is information security. The information security of the cloud platform must ensure the confidentiality of the data, ensure the integrity of the data in the transmission process, in order to ensure the consistency of the user's identity and its declaration, and the nonrepudiation of the user's operations on the data. The information security technology used by the cloud platform is accepted below [19].

2.6.1. Assertion Information Is Transmitted in the Single Sign-On Systems, We Need to Encrypt the Assertion to Achieve Confidentiality of the Information. The so-called encryption is to organize the original plaintext information according to a certain algorithm and transform the plaintext information into an unrecognizable code, that is, ciphertext. Except for the legal recipient, no one can obtain the original information (plain text), nor can they read the encrypted information (ciphertext). On the contrary, we call the process of recovering the ciphertext into plaintext through a

specific algorithm as decryption. Both data encryption and decryption require keys, and they are called encryption keys and decryption keys, respectively.

2.6.2. Symmetric Encryption Algorithm. If the encryption key and the decryption key are the same, or if the decryption process can be derived from the encryption process, we call it a symmetric encryption algorithm. Commonly used are AES, RC4, and DES. Key management is the biggest problem of symmetric encryption algorithms. Firstly, the key is only how to ensure the security of the key transmission channel, how to ensure that both parties can ensure that the key is not leaked; secondly, if you send a message to multiple people, you need to make sure if the message is encrypted multiple times, so multiple keys will be generated. The encryption algorithm runs fast and does not consume much computer memory, avoiding a series of problems caused by computer heat.

2.6.3. Asymmetric Encryption Algorithm. Anyone can use the public key to encrypt the plain text. Because the private key cannot be inferred from the public key, the ciphertext is safe even if someone else obtains the public key. Only the person who owns the key can decrypt the ciphertext. The biggest problem with the asymmetric encryption algorithm is that its operation speed is thousands of times slower than that of the symmetric encryption algorithm, which increases the computing load of the server.

3. Design of an Intelligent Distribution Platform for Physical Teaching Resources

3.1. Architecture Design of the Intelligent Distribution Platform of Physical Teaching Resources. The intelligent distribution platform of sports resources adopts a content distribution method based on BT, which changes the existing pooling model of teaching resource platforms and solves the problem of author positioning, distribution, and delivery of high-quality content. Even content consumers, viewers, and others can obtain the corresponding profit share through activities such as promotion and sharing, interactions such as reviews and polls and the intelligent allocation of sports resources encountered by all users. Therefore, the architecture of the intelligent sports resource allocation platform is shown in Figure 1.

3.2. Intelligent Distribution of Physical Teaching Resources. According to the layout of the interface, the content delivery of teaching resources can be divided into two parts: intelligent recommendation and attention. Followed content will only display a list of the latest works of authors that the present user is following and will be distributed in the order of release time. The "smart recommendation" part is based on matching user portraits with content portraits, realizing

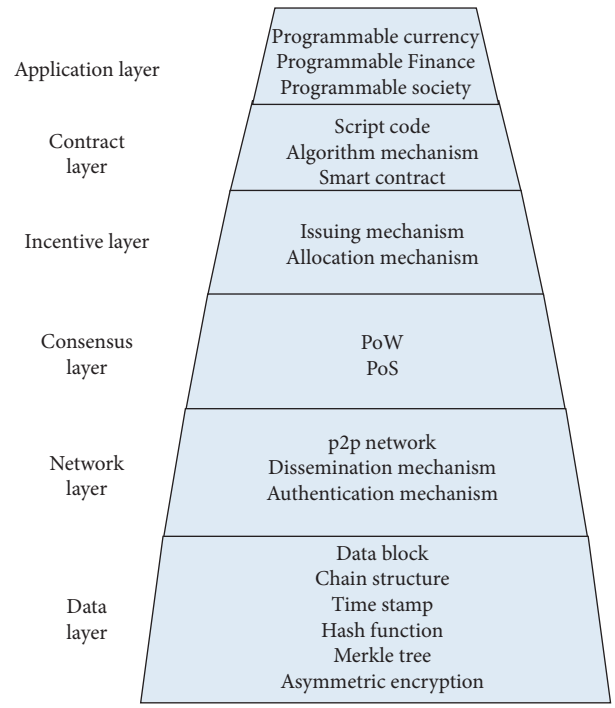

Figure 1: An architecture diagram of the intelligent distribution platform for physical teaching resources.

the personalized distribution of physical teaching resources, and noting that the implementation of the module is relatively simple and nonrepetitive, but the implementation of smart recommendation is relatively complex. The specific algorithm mechanism is as follows:

3.2.1. Build User Portraits. A detailed implementation document is required for the data product before starting to build the user portrait. If the user portrait planning document is about what to do, then the user portrait implementation document is to explain how to do it so that the developer knows the specific logic to proceed. Implementation, such as the weight of each factor of the label affected by multiple factors so that the final label value can be calculated. The tag value determines the weight of the influencing factors, and the user portrait can be established only through the tag value. Figure 2 shows the construction process of the user portrait.

3.2.2. Build Content Profile. The basic principle of the content-based recommendation algorithm is to obtain the user's preference for the type of sports based on the user's previous behavior and recommend sports curriculum resources similar to the sports curriculum that the user is interested in. Readers can intuitively understand the algorithm flow chart of base content recommendation from Figure 3.

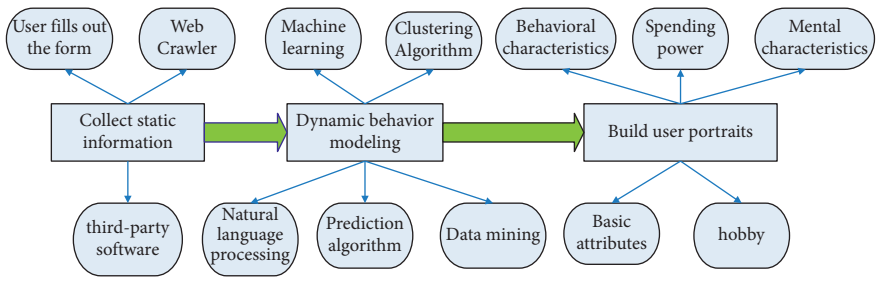

Figure 2: Construction process of a user portrait.

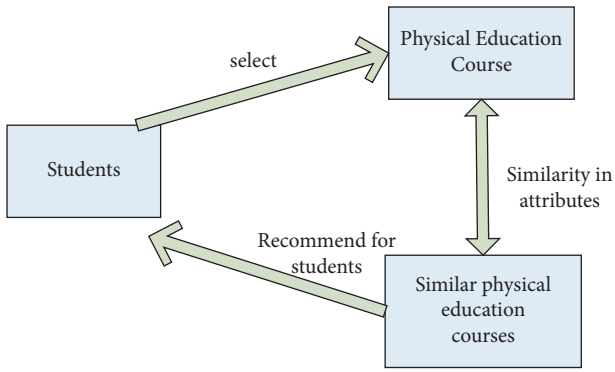

Figure 3: Basic principle of content recommendation algorithm.

Table 1: Primary and secondary school students' satisfaction with platform design.

Satisfaction/number of people	Boys	Girls
Very satisfied	40	35
Quite satisfied	12	16
Dissatisfied	6	6

Table 2: Primary and secondary school students' opinions on the revision of the platform design.

Insufficiency/number of people	There are fewer types of platform sports courses	The platform page design is not beautiful enough	The interactive function of the platform needs to be improved
Boys	22	15	5
Girls	21	10	8

4. Platform Innovation and Design Feed

After the design of the platform, Lee invited 120 middle school students to conduct a questionnaire survey on the design of the intelligent distribution platform for physical teaching. A total of 120 questionnaires were recovered, including 115 valid copies and 5 invalid surveys. Table 1 and Table 2 exhibit statistical findings of the statistical analysis of the feedback form.

It can be seen from Tables 1 and 2 that 80% of primary and middle school students are satisfied or relatively satisfied with the physical teaching resources recommended by the distribution platform and are willing to use the platform as an auxiliary tool for online physical teaching courses. 10% of elementary and middle school students are dissatisfied with the platform design and believe that the functional design of the platform is not perfect. Most students said that the platform sports curriculum resources are too few, and they do not have a sports curriculum they like, and some students think that the platform page design is not beautiful enough.

5. Conclusions

This article designs a brand-new smart distribution platform for physical teaching resources based on BT through the description of the POW algorithm and POS algorithm, as well as the introduction of physical teaching resources and information security technology and passes the

questionnaire investigation and performance test. It found that this system has good performance, which can improve the efficiency of physical teaching resource allocation, and make full use of scarce physical teaching resources. As a new model of distributed encrypted storage technology and applications, blockchain undoubtedly provides unprecedented opportunities. Blockchain can optimize and reshape the distribution system of physical teaching resources through strong security and decentralization. Based on the analysis of the correlation between BT and physical teaching courses, a blockchain-based intelligent distribution platform for physical teaching resources is being researched and designed. The platform uses artificial intelligence algorithms to create content and user portraits and uses related intelligent recommendation algorithms. Resource content transactions are automatically completed by the system in the form of smart contracts, thereby minimizing content delivery costs. By issuing and distributing encrypted digital currency on the side chain, people who publish content and those who watch courses can be encouraged and authorized to voluntarily create and distribute high-quality content in a decentralized manner. User interaction behaviors such as user likes, sharing, and comments will not only affect the matching of sports curriculum resource pushes but also the platform will respond based on the traffic value generated by these behaviors and provide them with rewards. Therefore, in order to make incentives fairer and effective, monitoring measures will further study effective content authentication mechanisms and effective traffic authentication mechanisms. For example, consider using large-scale data analysis techniques to mathematically model the content of interactive reviews. Improve the content quality of physical teaching resources; conduct more accurate assessments; and use manual reward policies to clear and filter traffic to avoid the negative impact of malicious traffic.

Data Availability

The data that support the findings of this study are available from the corresponding author upon reasonable request.

Conflicts of Interest

The authors declare no potential conflicts of interest with respect to the research, authorship, and/or publication of this article.

References

[1] J. J. Sikorski, J. Haughton, and M. Kraft, "Blockchain technology in the chemical industry: machine-to-machine electricity market," *Applied Energy*, vol. 195, no. JUN.1, pp. 234–246, 2017.

[2] Y. Zhang and J. Wen, "The IoT electric business model: using blockchain technology for the internet of things," *Peer-to-Peer Networking and Applications*, vol. 10, no. 4, pp. 983–994, 2017.

[3] J. Lafortune, J. Rothstein, and D. W. Schanzenbach, "School finance reform and the distribution of student achievement," *American Economic Journal: Applied Economics*, vol. 10, no. 2, pp. 1–26, 2018.

[4] M. Buitenhek, "Understanding and applying Blockchain technology in banking: evolution or revolution? [J]," *Journal of Digital Banking*, vol. 1, no. 2, pp. 111–119, 2016.

[5] D. Efanov and P. Roschin, "The all-pervasiveness of the blockchain technology," *Procedia Computer Science*, vol. 123, pp. 116–121, 2018.

[6] G. Andrea, "Blockchain technology: living in a decentralized everything[J]," *Cyberpsychology, Behavior, and Social Networking*, vol. 21, no. 1, pp. 65-66, 2018.

[7] H. Sun, W. Li, and B. Shen, "Learning in physical education: a self-determination theory perspective," *Journal of Teaching in Physical Education*, vol. 36, no. 3, pp. 277–291, 2017.

[8] J. Liu, R. Shangguan, X. D. Keating, J. Leitner, and Y. Wu, "A conceptual physical education course and college freshmen's health-related fitness," *Health Education*, vol. 117, no. 1, pp. 53–68, 2017.

[9] D. Wang, "Improving school physical education to increase physical activity and promote healthy growth of Chinese school-aged children—time for action[J]," *Journal of Sport & Health Science*, vol. 6, no. 04, pp. 10-11+131, 2017.

[10] H. Liu, Y. Liu, and J. Feng, "The realistic dilemma and breakthrough ways of improving the quality of online teaching resources of physical education in colleges and universities," *Advances in Physical Education*, vol. 11, no. 01, pp. 1–11, 2021.

[11] H. H. D. N. P. Opatha, "Teaching ethics in human resource management education: a study in Sri Lanka," *Prabandhan: Indian Journal of Management*, vol. 14, no. 1, pp. 8–24, 2021.

[12] T. Chan, B. Thoma, K. Krishnan et al., "Derivation of two critical appraisal scores for trainees to evaluate online educational resources: a metriq study," *Western Journal of Emergency Medicine*, vol. 17, no. 5, pp. 574–584, 2016.

[13] B. Scott, J. Loonam, and V. Kumar, "Exploring the rise of blockchain technology: towards distributed collaborative organizations," *Strategic Change*, vol. 26, no. 5, pp. 423–428, 2017.

[14] S. Dietze, S. Sanchez-Alonso, and H. Ebner, "Linked teaching: interlinking teachingal resources and the Web of data [J]," *Program Electronic Library & Information Systems*, vol. 47, no. 1, pp. 261–274, 2016.

[15] E. K. Kurelovic, "Advantages and limitations of usage of open teachingal resources in small countries [J]," *International Journal of Real-Time Systems*, vol. 2, no. Issue 1, pp. 136–142, 2016.

[16] H. A. Man, J. Han, and Q. Wu, "Special issue on cryptographic currency and block-chain technology [J]," *Future Generation Computer Systems*, vol. 107, pp. 758-759, 2020.

[17] A. Sharma, D. Jhamb, and A. Mittal, "Food supply chain traceability by using blockchain technology," *Journal of Computational and Theoretical Nanoscience*, vol. 17, no. 6, pp. 2630–2636, 2020.

[18] E. K. Kurelovic, "Advantages and limitations of usage of open educational resources in small countries [J]," *International Journal of Research in Education & Science*, vol. 2, no. Issue 1, pp. 136–142, 2016.

[19] X. J. Edgence, "A blockchain-enabled edgecomputing platform for intelligent IoT-based dApps [J]," *China Communications*, vol. 17, no. 4, pp. 78–87, 2020.

Hindawi
Mobile Information Systems
Volume 2022, Article ID 2546418, 14 pages
https://doi.org/10.1155/2022/2546418

Research Article

Basketball Big Data and Visual Management System under Metaheuristic Clustering

Hailong Xia[1] and Long Liu[2]

[1]*Henan University of Engineering, Zhengzhou 450000, Henan, China*
[2]*Chongqing Preschool Education College, Wanzhou, Chongqing 404100, China*

Correspondence should be addressed to Long Liu; liulong@aynu.edu.cn

Received 12 July 2022; Revised 2 August 2022; Accepted 12 August 2022; Published 21 September 2022

Academic Editor: Yajuan Tang

This study aims to discuss the application value of KMC algorithm optimized by heuristic method in basketball big data analysis and visual management. Because the data in basketball big data is too complicated and incomplete, the extraction of information is not direct and effective enough. Based on the metaheuristic K-Means clustering (KMC) algorithm, the weights and genetic algorithm are introduced to optimize it, and the University of California at Irvine (UCI) data set is applied to analyze the big data clustering performance of the optimized KMC algorithm. The 2018-2019 season National Basketball Association (NBA) shooting guards are selected as the research objects, and the optimized KMC algorithm is used to process the data and analyze the NBA scoring functional factors. It is found that the number of clusters increased from 2 to 16. After optimization, the Between-Within Proportion (BWP) value of the KMC algorithm only drops by 0.35, and the improved BWP (IBWP) value only drops by 0.288, which shows the smallest drop among all the algorithms. When the number of nodes is 4, the running time of the optimized KMC algorithm for processing the COVTYPE data set is 1922 s after optimization, and the running time for processing the IRIS data set is the shortest (113 s). When the number of parallel nodes is 10, the speedup ratio of the optimized KMC algorithm for processing COVTYPE data set is 4.16, and the maximal expansion rate is 0.81. The clustering accuracy of traditional KMC algorithm is 89.33%. After optimization, the clustering accuracy of KMC algorithm is 98.67%. The leader factor, offensive contribution factor, shooting stability factor, and passing ability factor in the core grouping are all at the maximum, which are 0.59, 0.51, 0.47, and 0.43, respectively. The optimized KMC algorithm has been shown to reduce the number of iterations, reduce convergence time, and improve clustering accuracy. The optimized KMC algorithm has been shown to reduce the number of iterations, reduce convergence time, and improve clustering accuracy. The conclusion of this study can provide reference basis for big data clustering and visual management.

1. Introduction

For data research or data application requirements, data visualization is to present specific data in the form of statistical charts and information. Big data analytics refers to the process of extracting potentially valuable information from a large amount of noisy and incidentally incomplete application data [1]. Big data analytics is a poorly multidisciplinary methodology. The main areas are neural networks, pattern recognition, spatial data analysis, image databases, signal processing, artificial intelligence, knowledge base systems, data acquisition, and bioinformatics [2, 3]. Big data analysis has concept description, association analysis, classification and prediction, cluster analysis, external analysis, and evolutionary analysis [4]. Clustering is an unsupervised classification method that automatically divides big data into multiple classes or clusters according to a certain standard. Cluster analysis can preprocess the data by observing the characteristics of each class or concentrating on a certain type of valuable data for further analysis and processing [5]. Cluster analysis is widely used in data analysis, image segmentation, pattern recognition, and other fields [6]. Currently, the common clustering method is the K-Means Clustering (KMC) algorithm based on the

heuristic algorithm. The KMC algorithm is widely used in data statistics, data analysis, and machine analysis due to its short and fast properties [7]. The KMC method based on heuristic algorithm shows significant advantages in small- and medium-scale data analysis. However, when the large-scale data sets are clustered, it is necessary to manually determine the number of clusters, the clustering results are unstable, and the misselecting noise and abnormal points will eventually lead to inefficient data processing and poor clustering quality [8].

The data analysis process is based on a large amount of data, and the ability of human brain to absorb and process information is limited. Visualization technology can transform scientific data into graphic image information that changes with time and space through computer and image processing technology and finally achieve the interactivity, visibility, and multidimensionality of the data [9]. Researchers can analyze the data and its changing trends through graphs and images. Data visualization speeds up data processing and increases the utilization of effective data. Data visualization has been widely used in various fields such as natural sciences, engineering technology, finance, communications, and commerce [10]. Basketball has become a popular sport because of its features such as simplicity, fun, fitness, and education. The depth of basketball is measured by the game. Basketball statistics can make an objective analysis of the data and unearth potential actual combat information. However, there are few studies on applying cluster analysis methods to basketball big data analysis.

In summary, the KMC method based on heuristic algorithm for processing big data has to be further optimized, and there is limited research on applying the clustering data analysis method to basketball data analysis. In this study, the KMC algorithm in the heuristic method is optimized and applied to basketball big data analysis to provide a reference for basketball big data clustering and visual management.

2. Materials and Data

2.1. The Cluster Analysis Methods of Big Data. Big data cluster analysis is the process of grouping a collection of physical or abstract objects into multiple classes composed of similar objects, clustering a collection of data objects in the same cluster. Big data analysis is not a postprocess that obtains effective results after simple analysis of input data. It needs to go through the continuous repetition of a multistep complex process to obtain accurate results. For n vectors in the a-dimensional space Ra, they are assigned to one of the c clusters, so that the distance between each vector and its cluster center is the smallest. Then, the distance between the vectors X_i and X_j can be expressed as follows:

$$d_{ij} = \sqrt{\sum_{k=1}^{a} \left(X_{ik} - X_{jk}\right)^2}, X_i = \{X_{i1}, X_{i2}, \ldots, X_{ia}\}, X_j = \{X_{j1}, X_{j2}, \ldots, X_{ja}\}. \quad (1)$$

Cluster analysis mainly includes two kinds of data matrix and discrepancy matrix [11]. They differ from the matrix diagram method in that they are not filled with symbols on the matrix diagram but filled with data to form a matrix for analyzing the data. The data matrix is a matrix in which d data objects of the entire data set are described with l attributes, and the final data object set is regarded as a $d * l$ matrix. The data matrix can be expressed as follows:

$$\begin{bmatrix} x_{11} \cdots x_{1e} \cdots x_{1p} \\ x_{i1} \cdots x_{ie} \cdots x_{ip} \\ x_{n1} \cdots x_{ne} \cdots x_{np} \end{bmatrix}. \quad (2)$$

The difference matrix refers to the degree of similarity between any two data points in the overall data object set [12], which can be expressed as follows:

$$\begin{bmatrix} 0 & & \\ d(2,1) & 0 & \\ d(n,1) & d(n,2) & 0 \end{bmatrix}, d(i,j) = d(j,i), d(i,j) \geq 0. \quad (3)$$

In (3), n represents the number of data points, and the $d(i, j)$ in the matrix represents the difference degree calculated according to the specified degree of similarity of the data points i and j in the data object collection. The larger the $d(i, j)$ value, the greater the degree of difference between the data objects.

The core of cluster analysis is to obtain the degree of similarity among different data objects [13]. At present, the Minkowski distance calculation method, the Euclidean distance calculation method, and the Chebyshev distance calculation method are commonly used for evaluation [14]. Among them, the data obtained by the Euclidean distance calculation method is not affected by coordinate translation and rotation changes, and it is a commonly used distance similarity measurement method [15]. The calculation method of Euclidean distance is given as follows:

$$d(i,j) = \sqrt{\left|x_{i1} - x_{j1}\right|^2 + \left|x_{i2} - x_{j2}\right|^2 + \cdots + \left|x_{ip} - x_{jp}\right|^2}. \quad (4)$$

In the above equation (4), $d(i, j)$ represents the Euclidean distance between two data points, which satisfies the conditions $d(i,j) \geq 0$, $d(i,j) = d(j,i)$, and $d(i,j) \leq d(i,k) + d(j,k)$.

The similarity factor is mainly used to gauge the similarity among data points [16]. The angle cosine method is a commonly used similarity coefficient calculation method. The value range of the similarity coefficient is [−1, 1]. When

the orthogonal value is 0, it means that the two vectors are completely dissimilar. The calculation method of the similarity coefficient of the angle cosine method is as follows:

$$r_{ij} = \frac{\left|\sum_{k=1}^{p} x_{ik}x_{jk}\right|}{\sqrt{\left(\sum_{k=1}^{p} x_{ik}^2\right)\left(\sum_{k=1}^{p} x_{jk}^2\right)}}. \quad (5)$$

The correlation coefficient method represents the degree of correlation between two data vectors [17], and its value range is $[-1, 1]$. 0 means that they are not correlated, 1 means that positive correlation is found, and -1 means that negative correlation can be seen. The correlation coefficient method can be expressed as follows:

$$r_{ij} = \frac{\sum_{k=1}^{p}\left(x_{ik} - \overline{x_i}\right)\left(x_{jk} - \overline{x_j}\right)}{\sqrt{\sum_{k=1}^{p}\left(x_{ik} - \overline{x_i}\right)^2\left(x_{jk} - \overline{x_j}\right)^2}}. \quad (6)$$

Appropriate criterion function in cluster analysis can further improve the quality of clustering [18]. The criterion functions commonly used in cluster analysis are as follows: squared margin of error, squared weighted mean value distance sum, and interclass distance sum [19]. The error sum of squares is often used for data analysis with dense samples and little difference between samples [20]. The error sum of square (J_a) can be expressed as follows:

$$J_a = \sum_{i=1}^{n}\sum_{j=1}^{k}\left\|x_i - m_j\right\|^2. \quad (7)$$

In the equation above, m_j is the average value of the class C_k, and $m_j = (1/n_j)\sum_{i=1}^{n_j} x_i$. nj refers to the number of objects in the class C_k.

The interclass distance and criterion (J_b) calculates the distance sum of every clustering epicenter to the global epicenter. The higher the similarity of the research data, the less obvious the clustering result, and the results making J_b the largest result have to be found.

$$J_b = \sum_{j=1}^{k}\left(m_j - m\right)^T\left(m_j - m\right). \quad (8)$$

The weighted average squared distance (J_c) is applicable to data objects with a large disparity in the number of samples, and its calculation method can be expressed as follows:

$$\begin{aligned} J_c &= \sum_{j=1}^{p} p_j s_j^*, \\ s_j^* &= \frac{2}{n_j\left(n_j - 1\right)}\sum_{x\in X_j}\sum_{x\in X_j}\|x - \bar{x}\|^2, p_j = \frac{n_j}{n}. \end{aligned} \quad (9)$$

In the above two equations, s_j^* refers to the average squared distance between samples within a class, and P_j is the prior probability.

2.2. Establishment of Cluster Analysis Method Based on Metaheuristic Algorithm. KMC is the most classic and most widely used clustering method in the metaheuristic algorithm. The kinetic Monte Carlo method (KMC) is simple in principle and highly adaptable, so it is the first choice of researchers in many cases. This method takes Euclidean distance as the correlation measure, and the error sum of squares criterion (J_a) as the criterion function to minimize the evaluation index. The KMC algorithm divides the data set A into the closest classes, and its cluster center is $C_1, C_2, C_3, \ldots, C_k$. The calculation method of each cluster center point is shown in equation (11), in which $i = 1, 2, \ldots, k$ and n_i was the number of data objects in the class C_i.

$$C_i^* = \frac{1}{n_i}\sum_{x_j\in C_i} x_j. \quad (10)$$

The traditional KMC method has a great dependence on the selection of the initial clustering center point, and it is susceptible to the interference of local noise data. The different feature weights assigned to the attributes of each data point can improve the KMC results greatly. The feature weights of variable patterns were assigned to data points, which were named KMC based on density, DK-Mean. The attribute feature weight value of the j-th dimension is assigned to the object data. The calculation method is expressed as follows:

$$w_j = \frac{a_j}{\sum_{j-1}^{m} a_j}, w_j \in [0, 1], \sum_{j-1}^{m} w_j = 1. \quad (11)$$

In (11), a_j is the ratio of the distance between the classes of the attribute and the distance within the classes, and $a_j = d_b/d_i$ (d_b refers to the distance between classes, and $d_b = \sum_{k=1}^{K}(m_{kj} - m_j)^2$; d_i refers to the distance within the class, and $d_i = \sum_{k=1}^{K}\sum_{i=1}^{n_k}(x_{ij} - m_{kj})^2$). m_i represents the mean value of the data set on the j-th dimension attribute; K is the number of clusters, and j is the number of attribute bits. Then, the weighted Euclidean distance calculation equation can be written as follows:

$$d(m, n) = \sqrt{\sum_{j=1}^{m} w_j\left(x_{mj} - x_{nj}\right)^2}. \quad (12)$$

The KMC method relies on the cluster center point, which is easy to cause local optimal clustering. Based on the density, the choice of the original aggregation centers is improved accordingly in this study. The clustering criterion function can be denoted as the following equation:

$$J_k = \frac{k_{wi}}{k_{be}}. \quad (13)$$

In (13), k_{wi} represents the distance within the class, and $k_{wi} = \max_{i\in[1,k]}\left\{\min_{j\in[1,C_i]}\left[(1/C_i)\sum_{p=1}^{C_i}\|x_j - x_p\|\right]\right\}$. K_{be} represents the distance between classes, and $k_{be} = \min_{x_p\in C_i, x_q\in C_j, i\neq j}\|x_p - x_q\|$. Then, the density $D(x)$ at sample point X can be expressed as the following equation:

Figure 1: The flow chart of DK-Mean algorithm clustering.

$$D(x) = \left[p \in C \,\middle|\, D_i(x, p) \le r\right]. \tag{14}$$

In (14), D_i represents the weighted Euclidean distance, and r is the specified radius.

Cluster analysis method can solve such problems; cluster analysis method is an exploratory analysis method, which can analyze the inherent characteristics and laws of things and is a commonly used technology in data mining. Genetic algorithm shows good applicability and scalability and can reduce the initialization requirements of traditional clustering algorithms in cluster analysis. The genetic algorithm is introduced further based on the DK-Mean algorithm to increase the accuracy of the clustering algorithm in this study. The genetic algorithm search can minimize the J_k value, and then the fitness feature can be represented as formula (16):

$$f = \frac{1}{J_k} = \frac{k_{be}}{k_{wi}}. \tag{15}$$

The probability of an individual being selected can be expressed as follows:

$$P(x_i) = \frac{f(x_i)}{\sum_{j=1}^{p_s} f(x_j)}. \tag{16}$$

In the above equation, $f(x_i)$ is the fitness value, and $i = 1, 2, \ldots, p_s$.

The crossover operation is performed on two individuals x_1, and x_2, and the new individuals produced by them can be expressed as equations (18)~(19), in which α is the uniform arithmetic crossover parameter.

$$\begin{aligned} \tilde{x}_1 &= \alpha x_1 + (1-\alpha)x_2, \\ \tilde{x}_2 &= \alpha x_2 + (1-\alpha)x_1. \end{aligned} \tag{17}$$

The improved DK-Mean algorithm calculates the data gap matrix and initializes the target eigenvalues to obtain new cluster centers. The specific process of the DK-Mean algorithm is shown in Figure 1.

2.3. Visual Data Analysis and Visualization Based on Clustering Algorithm. The biggest difference between visual analysis and visualization lies in the analysis of this point, the

process of visualizing data for business simulation, correlating multidimensional business data to form a more comprehensive data result, and providing users with auxiliary decision-making process, which is called visual analysis. Parallel coordinate method has the characteristics of mapping high-dimensional data to low-dimensional space and can interact with users at the same time, and it is a commonly used method of visual data analysis at present. In this study, a visual data analysis model based on the KMC algorithm is established based on the optimized KMC algorithm and the parallel coordinate method.

It is assumed that G is a collection of n-dimensional data objects, and $G = \{g_1, g_2, \ldots, g_n\}$, of which gi is an n-dimensional collection $g_i = \{x_{i1}, x_{i2}, \ldots, x_{in}\}$; the basic coordinate axis $\{x_1, x_2, \ldots, x_n\}$ corresponds to the attribute of the i-th dimension, and each n-dimensional vector can be expressed as $H\{h_1, h_2, \ldots, h_n\}$. The polyline H of the n-dimensional data using linearly independent equations is given as follows:

$$\frac{x_1 - \alpha_1}{\mu_1} = \frac{x_2 - \alpha_2}{\mu_2} = \cdots = \frac{x_n - \alpha_n}{\mu_n}. \tag{18}$$

According to the mapping principle from the midpoint of the coordinate system to the parallel coordinate, the following equation can be obtained:

$$x_{i+1} = m_i x_i + b_i, i = 1, 2, \ldots, n - 1. \tag{19}$$

In the equation, m_i is the slope, and b_i represents the intercept on the axis in parallel coordinates x_{i+1}.

The technology and process of data analysis are applied in the basketball data visualization management system, which can be data processing automation. The data analysis visualization process based on the optimized KMC algorithm is shown in Figure 2. After the sample data is processed through selection operations and cross operations, a new visualization population can be formed.

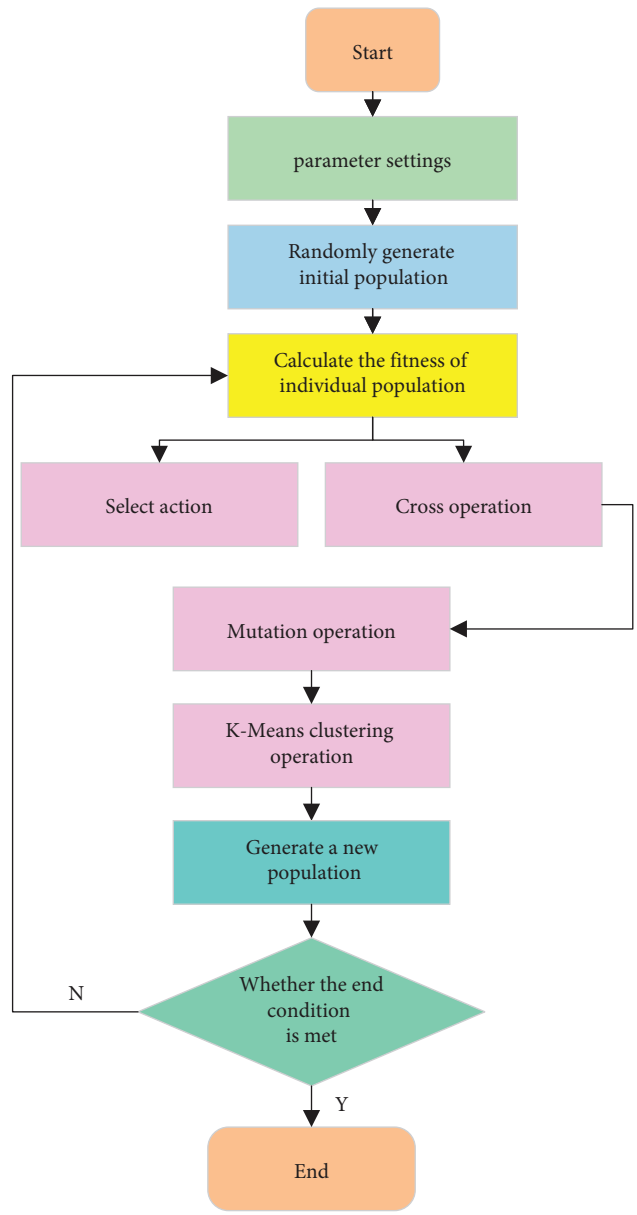

Figure 2: Flow chart of KMC algorithm after optimization.

2.4. The Evaluation Indicators of Cluster Validity. The main indicators in the cluster analysis evaluation are as follows: Accuracy, Precision, Recall, and $F1$ value, four commonly used indicators. The ideal clustering result should reflect the internal structure of the data set as much as possible, so that the sample similarity between classes is the smallest, and the samples within the class are the most similar. In this study, the Between-Within Proportion (BWP) and improved BWP (IBWP) indicators were adopted to analyze the clustering results and performance, where BWP is the ratio of the clustering deviation distance to the clustering distance, and its calculation method is given as follows:

$$\mathrm{BWP}(i, j) = \frac{c(i, j) - w(i, j)}{c(i, j) + w(i, j)}. \tag{20}$$

In the equation, $c(i, j)$ represents the interclass distance of the object i in the j-th class, and $c(i, j)$ represents the intraclass distance of the object i in the j-th class. Among them, $c(i, j) = \min_{a \in [1,k], a \neq j} (1/n_a) \sum_{p=1}^{n_a} \|x_p^a - x_i^j\|^2$, n is the number of data objects, which can be the number of divided clusters, n_a represents the number of elements of the class a, and j represents the class label. The larger the $BWP(i, j)$ value, the more effective the clustering of sample objects.

The IBWP indicators can evaluate the clustering effectiveness of a single data object very well, and its calculation method is shown as follows:

$$\mathrm{IBWP}(i, j) = \frac{ic(i, j) - iw(i, j)}{ic(i, j) + iw(i, j)}. \tag{21}$$

In the (21), $ic(i, j)$ and $iw(i, j)$represent the interclass distance and the intraclass distance of the object i in the j-th class. The larger the value of IBWP index, the more effective the clustering of individual points of the sample.

The speedup ratio and the expansion rate are used to evaluate the parallelization effect and performance of the

Table 1: Data sets under UCI database.

Data sets	IRIS	WINE	SEED	ABALONE	LETTER	COVTYPE
Number of samples	150	178	210	4177	20000	581012
Number of attributions	4	13	8	8	16	54

clustering algorithm in analyzing data. The calculation method of speedup ratio and the expansion rate is given as follows:

$$S = \frac{T_1}{T_m}, \quad S' = \frac{T_n}{T_{mn}}. \tag{22}$$

In the above two equations, T_1 is the data processing time for a single node; T_m is the data processing time for m nodes. N is the size of the processed data; T_n is the time for data to be processed on a child node; and T_{mn} is the time for data of size n to be processed on m nodes.

2.5. Data of Testing Dataset of the Model. In this study, the IRIS, WINE, SEED, ABALONE, LETTER, and COVTYPE data sets in the UCI database are undertaken as the validation sets to verify the algorithm model established. Table 1 shows the total number of samples, dimensions, and categories of the data set. Data analytics is the process of analyzing data sets in order to make decisions about the information they hold, to be used in the business industry to enable organizations to make business decisions.

2.6. Research Objects and Methods of Basketball Big Data. The NBA shooting guards in the 2018-2019 season were selected as the research objects. The relevant indicators included in the study were analyzed statistically using literature data method, logical analysis method, mathematical statistics method, video analysis method, and comparative analysis method. The technical statistical data of the season finals are collected on related websites such as Tencent Sports Video, Hupu NBA, the control video, and official statistics, which were repeatedly confirmed to ensure the authenticity and reliability of the data source. These raw data were adopted for statistical analysis of basketball technical indicators. Data analytics can help businesses better understand their customers, improve their advertising campaigns, personalize their content, and improve their bottom line.

2.7. Analysis on Influencing Factors of Basketball Scoring Based on KMC Algorithm. The 2018-2019 season NBA scoring guards were selected as the research objects. Based on the NBA data query website (https://www.basketball-reference.com/), 17 basic pieces of data such as player scores, rebounds, assists, and steals, as well as advanced data such as passing ability, defensive contribution, and offensive contribution are selected as the original data. The original data removes rebounds, blocks, and fouls and reduces the original data from 36 dimensions to 22 dimensions, including Field goal attempts (FGA), Field goals (FG), Free throws (FT), Free throw attempts (FTA), Assists (AST), Steals (STL), and Points (PTS).

3. Results

3.1. Analysis on Results Based on Metaheuristic Clustering. Using the traditional KMC algorithm to cluster the data in the IRIS data set, the clustering results are divided into 4 clusters, but the clustering results of some data overlap (Figure 3(a)), and the clustering results are significantly different from the real data. The optimized KMC algorithm is used to cluster the data in the IRIS data set. The clustering results are divided into 4 clusters, the data clustering results are of high quality, and there is no crossover phenomenon of different types of data (Figure 3(b)). In addition, there is no difference between the clustering results and the real data.

3.2. Comparison on Classification Indicators of Different Clustering Algorithms. The traditional KMC algorithm is compared with DKMC, the optimized KMC algorithm, self-organizing feature map (SOM) algorithm, quantum evolutionary clustering algorithm (QEAM), and k-medoids algorithm in terms of BWP values (Figure 4(a)). As the number of clusters increases, the BWP values of different algorithms show a downward trend all, and the number of clusters increased from 2 to 16. After optimization, the BWP value of the KMC algorithm only drops by 0.35, which is the smallest drop among all algorithms. The BWP value of an optimized KMC algorithm with the same number of clusters is higher than that of other algorithms. The IBWP values of the different algorithms are compared, and the results are shown in Figure 4(b). As shown in the figure, the IBWP values of the various algorithms show a decreasing trend as the number of clusters increases. The number of clusters increases from 2 to 16. After optimization, the IBWP value of the KMC algorithm only decreases by 0.288, which is the smallest decrease of all algorithms. The IBWP value of an optimized KMC algorithm with the same number of clusters is higher than that of other algorithms.

3.3. Execution Time of Clustering Algorithm. The optimized KMC algorithm was used to perform cluster analysis for six datasets in the UCI database (Figure 5). As the number of nodes increases, the time taken by the KMC algorithm to collect 6 different data sets decreases. If the number of nodes is 4, the COVTYPE dataset output time is 1922 s, and the IRIS dataset output time is 113 s.

3.4. Performance Analysis of Clustering Algorithm in Parallel Data Processing. The speed ratios of the optimized KMC algorithm between the six data sets were analyzed and

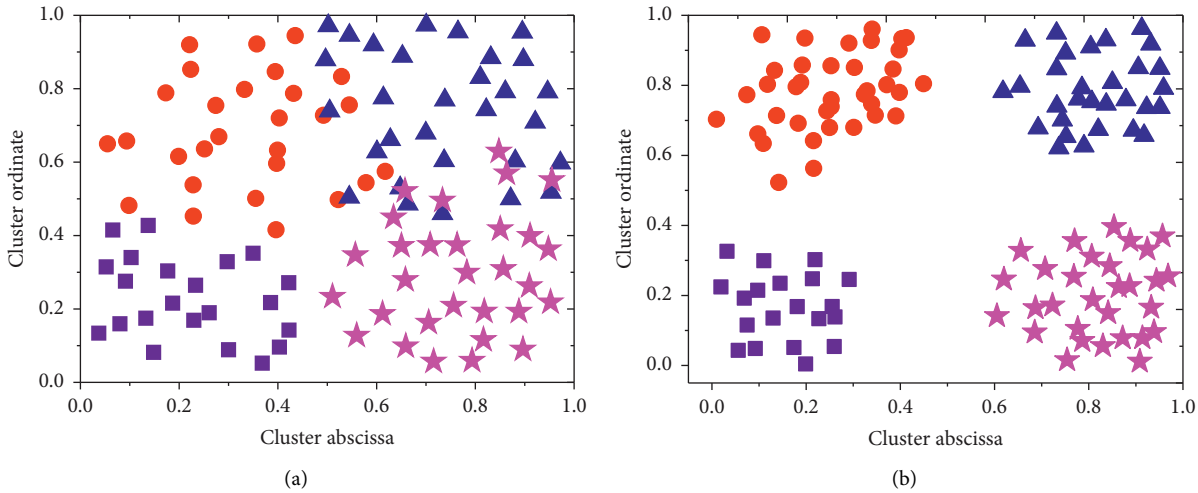

Figure 3: Comparison of cluster results of different algorithms. (a) The clustering results of the traditional KMC algorithm; (b) the clustering results of optimized KMC algorithm.

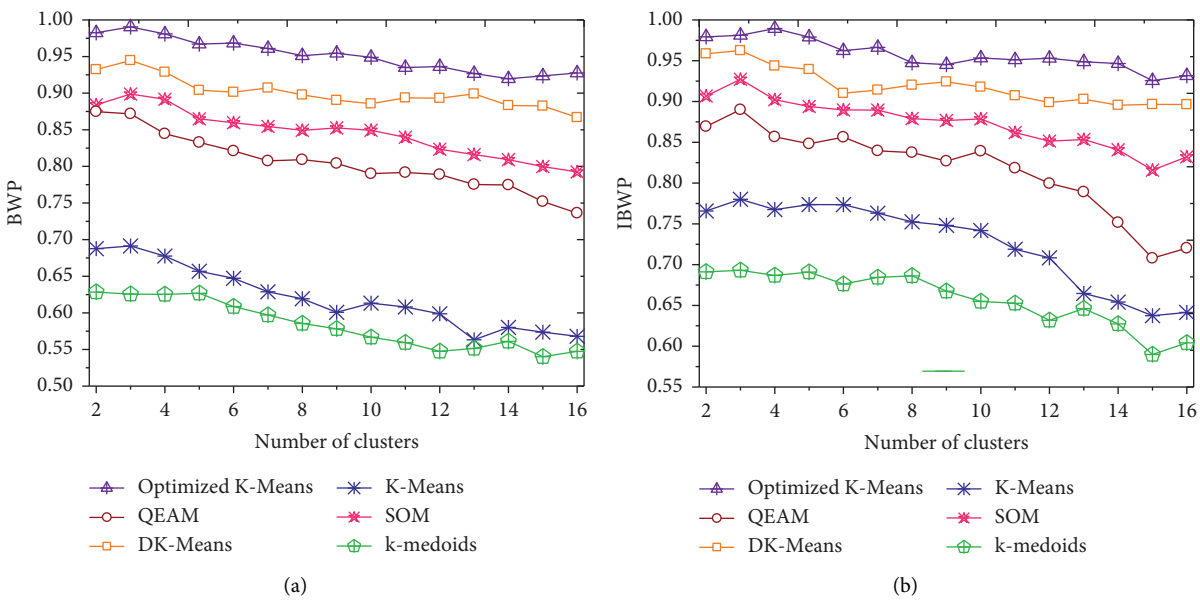

Figure 4: Comparison on classification indicators of different clustering algorithms. (a) Comparison on BWP values of different clustering algorithms; (b) comparison on IBWP values of different clustering algorithms.

compared, and the comparison results are shown in Figure 6(a). As the number of parallel nodes increases, the speed ratio of the KMC 6 algorithm when processing the data set shows an increasing trend. If the number of parallel nodes is 10, the maximum speed ratio of the COVTYPE data set is 4.16. The expansion ratios of the KMC-optimized algorithm between the six data sets were analyzed and compared, and the comparison results are shown in Figure 6(b). As the number of parallel nodes increases, the expansion ratio of the KMC algorithm for processing the six data sets appears to decrease. If the number of parallel nodes is 10, the maximum expansion ratio of the COVTYPE data set is 0.81.

3.5. Analysis on Test Performance Rate of Clustering Algorithm. The group accuracy of the different cluster algorithms across the different datasets is compared, and the results are shown in Figure 7(a). There are three different algorithms for the accuracy of data grouping. After optimization, the accuracy of the KMC algorithm when processing the six data sets was clearly higher than the other two algorithms ($P < 0.05$). The convergence times of the different clustering algorithms in the different data sets are compared, and the results are shown in Figure 7(b). The convergence time of the optimized KMC algorithm in the different data sets was shorter than that of the other algorithms, and the difference was statistically significant ($P < 0.05$). The number

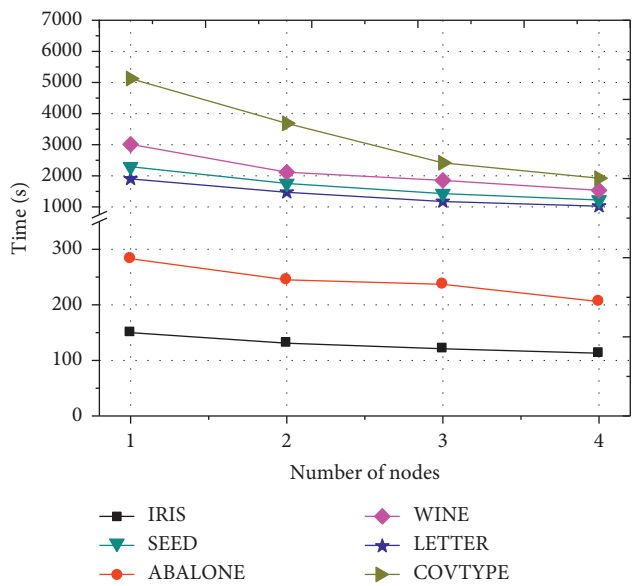

Figure 5: Comparison on execution times of different algorithms under different data sets.

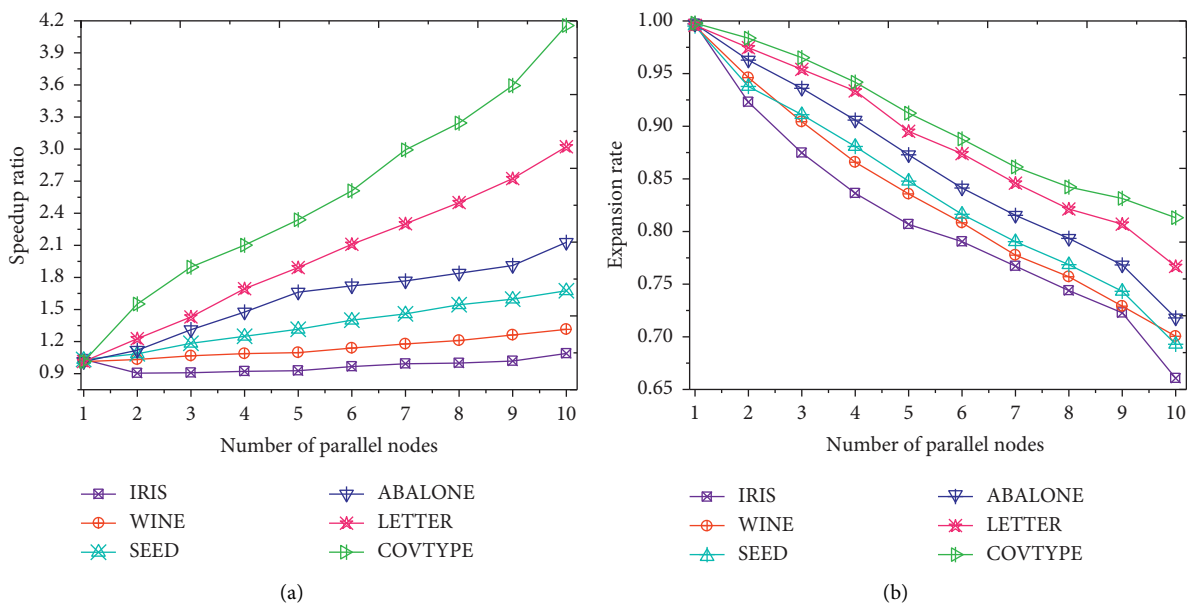

Figure 6: Performance analysis of clustering algorithm in parallel data processing. (a) Comparison on speedup ratio of the optimized algorithm on different data sets; (b) comparison on the expansion rate of the optimized algorithm on different data sets.

of iterations of different clustering algorithms in different datasets is compared, and the results are shown in Figure 7(c). The number of iterations of the optimized KMC algorithm across the different data sets was lower than that of the other algorithms, and the difference was statistically significant ($P < 0.05$).As the convergence time increases, different clustering algorithms are proportional to the data iteration effect.

3.6. Analysis on Cluster Visualization Result. The traditional KMC algorithm and the optimized KMC algorithm are performed with the cluster analysis on the Luanweihua data set in the IRIS data set. The cluster visualization analysis is performed on three types of Luanweihua data in this study. After cluster analysis, all data are divided into 3 clusters, with 50 groups of data in each cluster of original data. After clustering using the traditional KMC algorithm, a total of 16 sets of data have been misclassified, and the clustering accuracy is 89.33%, as illustrated in Figure 8. After clustering using the optimized KMC algorithm, there are two sets of data that are misclassified, and the clustering accuracy is 98.67% (as given in Figure 9). Through the clustering visualization analysis of the traditional KMC algorithm, the

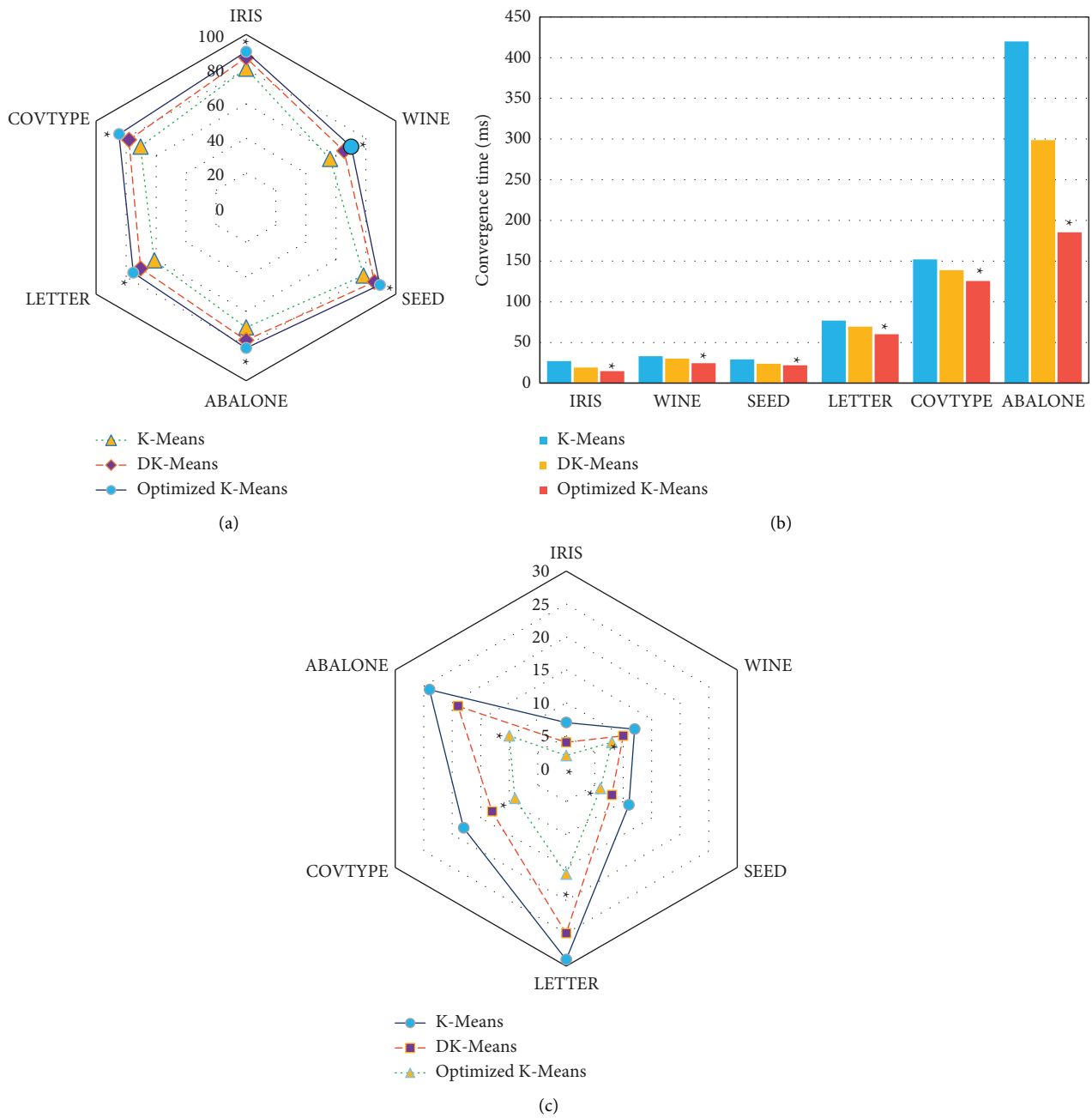

Figure 7: Analysis on test performance rate of clustering algorithm. (a) The clustering accuracy of the clustering algorithm on the test set. (b) The convergence time of the clustering algorithm on the test set. (c) The number of iterations of the clustering algorithm on the test set. Note: $*$ suggested that the difference was statistically great in contrast to the optimized KMC algorithm, $P < 0.05$.

traditional KMC clustering accuracy is about 10% lower than that of the optimized KMC.

3.7. Analysis on the Statistic Results of Basketball Technical Indicators. According to the data from the NBA official website, the technical indicators of the top 10 Eastern teams in the 82 regular seasons in the 2018-2019 season are counted, and the results are shown in Figure 10. The figure illustrates that, except for the significant differences between the lost points and the score items, there is little difference in other indicators. The field goal score of Indiana Pacers is 25.4, which is lower than the first place (Milwaukee Bucks, 38.2 scores), showing a difference of 12.8 between the two. The comparison on the indicators of the first and tenth teams shows that the scores for shots, hits, and rebounds of Milwaukee Bucks are 5.8, 2.8, and 3.4 higher than those of the Miami Heat.

The technical indicators of the top 10 Midwestern teams in 82 regular season games are compared, and the results are given in Figure 11. The free throw of Houston Rockets is as high as 45.4, which is obviously higher than that of other teams. The scores in rebounds and assists of Los Angeles

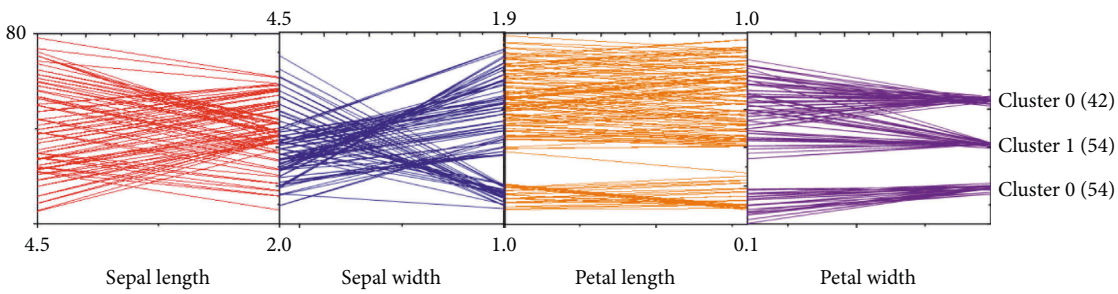

Figure 8: The clustering visualization results of traditional KMC algorithm.

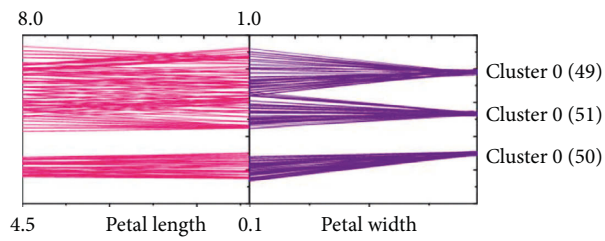

Figure 9: The clustering visualization results of optimized KMC algorithm.

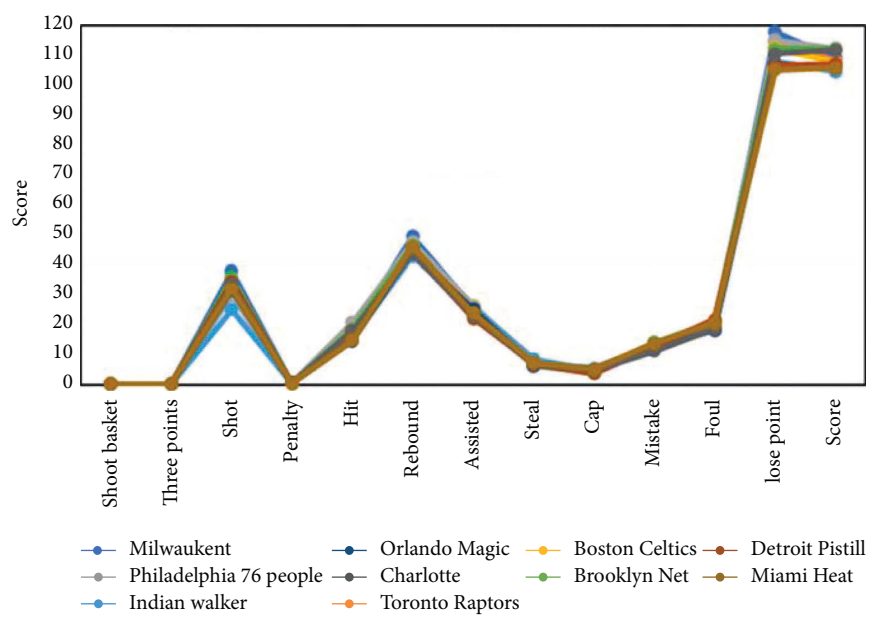

Figure 10: Regular season performance of the top 10 teams in Eastern conference.

Clippers are 22.6 and 28.5, respectively, which are much higher than those of other teams. The shooting percentage of Los Angeles Lakers (the 10th) is 0.7, which is much lower than that of the San Antonio Spurs (0.82) and the Golden State Warriors (0.8).

A cluster analysis is performed in 20 teams in regular games (Figure 12), which shows that 20 teams in the East and West are clustered into 7 categories. Among them, the Golden State Warriors and the Milwaukee Bucks, the first place in the East and West teams, are grouped into the same category. It shows that the top NBA teams have similar characteristics to a certain extent.

The technical indicators of the Golden State Warriors and the Milwaukee Bucks team in the East and West teams are compared, as given in Figure 13. The scores in shooting, attempts, free throws, rebounds, assists, and blocks of the Golden State Warriors and the Milwaukee Bucks are higher than the average scores of all teams. The Milwaukee Bucks and the Golden State Warriors have rebound scores of 49.8 and 46.2, respectively, which are higher 4.6 points and 1 point than the average scores of all teams, respectively, which shows that the rebounding technical indicators of the Milwaukee Bucks have a significant advantage. The scores in assists of the Milwaukee Bucks and the Golden State

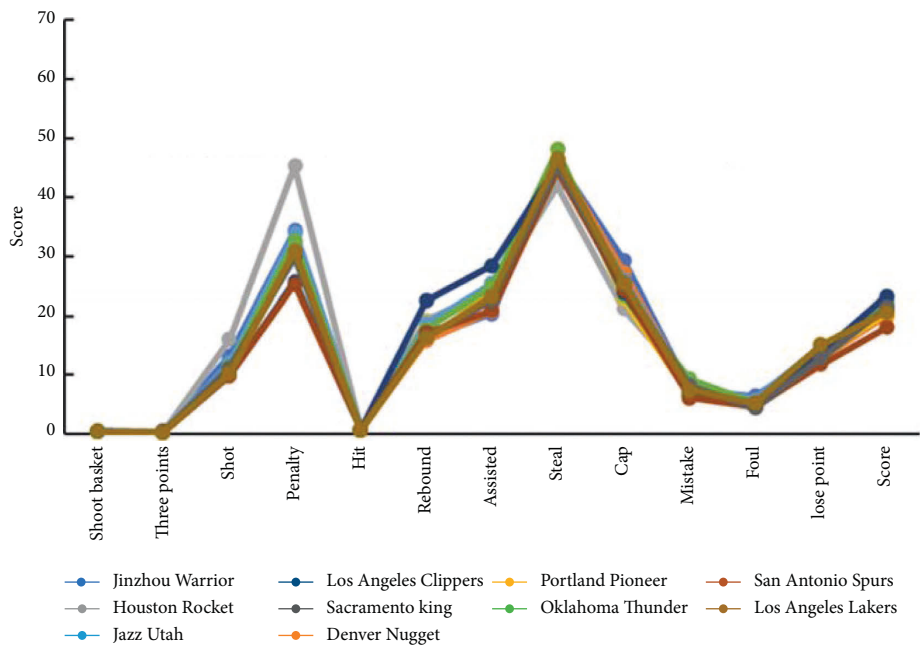

Figure 11: The regular season performance of the top 10 teams in Western.

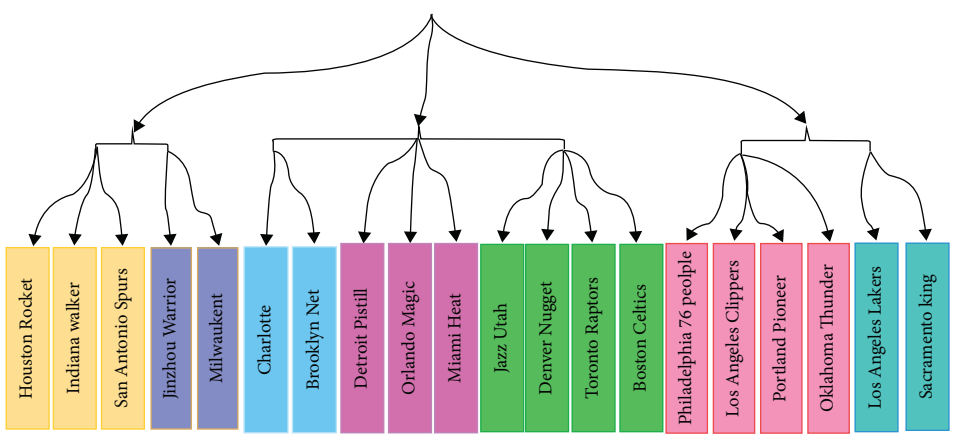

Figure 12: Dendrogram of NBA team clustering results.

Warriors were 26 and 29.4, respectively, showing that the score in assists of the Golden State Warriors has a significant advantage.

3.8. Analysis on the Result of the Influencing Factors of Basketball Scoring. The coefficients of the NBA basketball score scheme in the different groups were compared based on the optimized KMC algorithm. As shown in Figure 14, the cluster boundary factor first increases and then decreases as the number of clusters increases. If the number of clusters is 7, the cluster boundary factor reaches a maximum value of 0.24.

Based on the optimized KMC algorithm, the functional factors of basketball NBA scores are analyzed, and the matrix of different factors after coordinate translation is shown in Table 2. All factor coefficients are close to 0 or 1.

The influencing factors of basketball NBA score are analyzed based on the optimized KMC algorithm, and the distribution of different factor cluster centers is shown in Figure 15. The leader factor, offensive contribution factor, shooting stability factor, and passing ability factor in the absolute core grouping are all the maximum values, which are 0.59, 0.51, 0.47, and 0.43, respectively.

4. Discussion

In this study, the KMC algorithm in the metaheuristic clustering method is optimized, its clustering and visualization performance are analyzed, and it is applied to the analysis of basketball NBA score functional factors. It is found that the clustering results of traditional KMC algorithm have the overlapping of some data clustering results,

Figure 13: Comparison of team technical indicators.

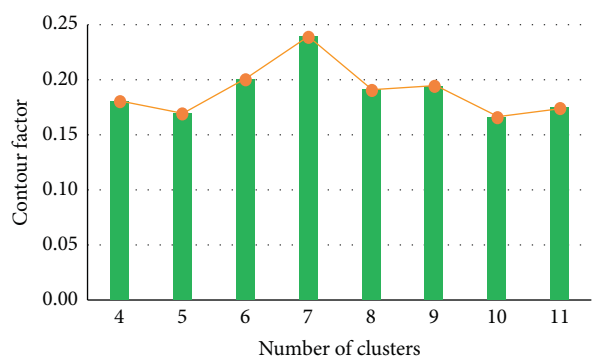

Figure 14: Analysis on changes in cluster profile coefficients.

and there is a big difference with the real data. The optimized KMC algorithm does not have the crossover phenomenon of different types of data, and the clustering results are closer to the real data. Such results prove that the optimized KMC algorithm shows improved quality of clustering results. The clustering centers of the traditional KMC algorithm are randomly selected, which leads to errors in the clustering results, and the clustering analysis of the traditional KMC algorithm requires multiple iterations, so the clustering results are greatly different from the true data distribution. The optimized KMC algorithm has coordinate rotation to select the cluster center, which reduces its randomness, so the initial cluster center can be determined more accurately. The number of clusters increased from 2 to 16. After optimization, the BWP value of the KMC algorithm only drops by 0.35, and the IBWP value only drops by 0.288, which is the smallest drop of all algorithms. Such results suggest that the optimized KMC algorithm shows better clustering results. The BWP and IBWP values of the optimized KMC algorithm are greater than those of other algorithms, indicating that the optimized KMC algorithm shows higher clustering accuracy on the samples. As the number of nodes increases, the time for the KMC algorithm to cluster 6 different data sets shows a downward trend. When the number of nodes is 4, the optimized KMC algorithm can process the COVTYPE data set for a maximum of 1922 s, and the shortest running time for processing the IRIS data set is 113 s. The sample size of the IRIS dataset is observably lower than that of the COVTYPE dataset. Such results indicate that the optimized KMC algorithm takes longer time to process low sample size data. This is because each operation needs to start the Map and Reduce tasks, which takes a certain amount of time, so when the task start time dominates, the small samples are processed. Xu pointed out that as the number of sample nodes increases, the running time of clustering decreases. The larger the data size, the better the acceleration ratio of the algorithm, and the better the algorithm's ability to handle large data. If the number of parallel nodes is 10, the maximum speed ratio of the KMC algorithm optimized for processing the COVTYPE data set is 4.16. He found that the optimized KMC algorithm has several advantages in big data processing. As the number of parallel nodes increases, the level of expansion of the KMC algorithm for processing the six datasets appears to decrease. If the number of parallel nodes is 10, the maximum expansion rate of the COVTYPE data set is 0.81. This is because the amount of communication between each node increases as the number of nodes increases. Some studies have shown that as data size increases, parallel uptime increases, which is similar to the results of this study. This is because the optimized KMC algorithm introduces weights in the calculation of the Euclidean distance, which increases the Euclidean distance between the abnormal point and the cluster center and makes the algorithm iteration result closer to the real data, thereby reducing the number of iterations and

Table 2: Component matrix after coordinate translation.

	Leader factor	Offensive contribution factor	Defensive contribution factor	Three-point ability factor	Shot stability factor	Passing ability factor
FGA	0.942	0.036	−0.058	0.086	−0.053	−0.013
FG%	0.083	0.332	−0.016	−0.22	0.879	−0.059
FT	0.755	0.455	−0.065	−0.259	−0.154	0.074
FTA	0.762	0.414	−0.016	−0.309	−0.146	0.078
AST	0.463	0.127	0.181	−0.164	−0.01	0.78
STL	0.059	0.056	0.91	−0.101	0.029	0.065
PTS	0.906	0.3	−0.098	0.1	0.118	−0.01
AST %	0.563	0.165	0.154	−0.196	−0.018	0.7
STL%	0.042	0.058	0.901	−0.138	0.014	0.049

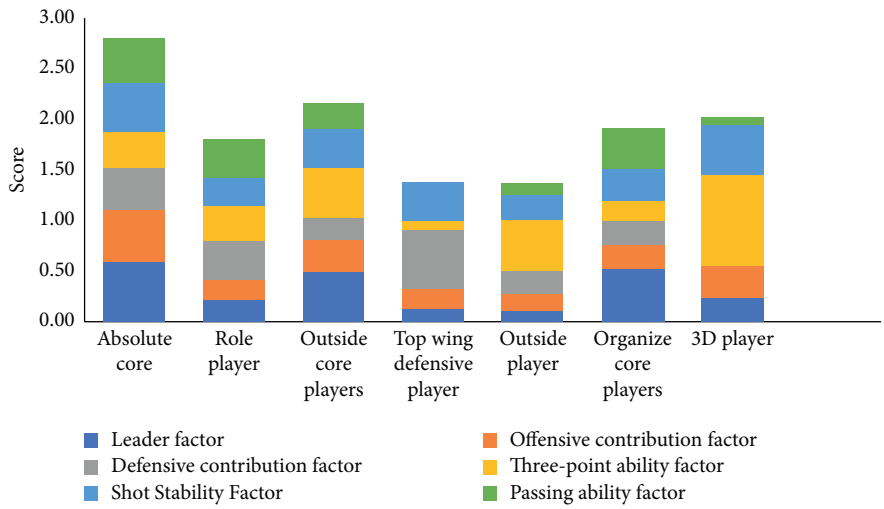

Figure 15: Statistical results for cluster distribution of basketball score influencing factors.

convergence time and improving clustering accuracy. Yin pointed out that the optimized KMC algorithm has improved the clustering efficiency, and its clustering accuracy has not changed greatly. The reason is that the study did not consider the impact of each sample data on the entire clustering result, so the Euclidean distance calculation method was not optimized. The clustering accuracy of the traditional KMC algorithm is 89.33%. After optimization, the clustering accuracy of the KMC algorithm is 98.67%, and the clustering accuracy is improved by 9.34%.

Effective clustering can correctly display the player's status, which is helpful for the rational operation of the team. The research results of this study show that as the number of clusters increases, the cluster contour coefficients first increase and then decrease. When the number of clusters is 7, the cluster contour coefficient reaches the maximum value of 0.24. The leader factor, offensive contribution factor, shooting stability factor, and passing ability factor in the absolute core grouping are all the maximum values, which are 0.59, 0.51, 0.47, and 0.43, respectively. These results show that the absolute core group has an important influence on the team's score. The main influence factors of absolute core are leader factor, offensive contribution factor, shooting stability factor, and passing ability factor.

5. Conclusion

The KMC algorithm in metaheuristic clustering is optimized and applied to the analysis of NBA scoring functional factors in this study. The results of statistical analysis of basketball technical indicators show that there are significant differences in the gain and loss of scores, and other differences are not significant. It turns out that the optimized KMC algorithm reduces the number of iterations and convergence time and improves the clustering accuracy. The leader factor, offensive contribution factor, shooting stability factor, and passing ability factor are functional factors of NBA scoring. However, there are still some shortcomings in this study. Only a preliminary analysis of the functional factors of basketball NBA scores has been carried out, and the clustering results of different players of different teams have not been analyzed and verified. Therefore, it will further increase

the sample size and perform cluster analysis to verify the different players of the team in future. In short, this study provides a reference basis for big data clustering and visual management.

Data Availability

The data used to support the findings of this study can be obtained from the corresponding author upon reasonable request.

Conflicts of Interest

The authors declared no potential conflicts of interest with respect to the research, authorship, and/or publication of this article.

Acknowledgments

This work was supported by 2022 Key Scientific Research Projects of Higher Education Institutions in Henan Province, project no. 22A890001.

References

[1] X. Zhang, E. J. Pérez-Stable, P. E. Bourne et al., "Big data science: opportunities and challenges to address minority health and health disparities in the 21st century," *Ethnicity & Disease*, vol. 27, no. 2, pp. 95–106, 2017.

[2] C. S. Kruse, R. Goswamy, Y. Raval, and S. Marawi, "Challenges and opportunities of big data in health care: a systematic review," *JMIR Medical Informatics*, vol. 4, no. 4, p. e38, 2016.

[3] L. N. Sanchez-Pinto, Y. Luo, and M. M. Churpek, "Big data and data science in critical care," *Chest*, vol. 154, no. 5, pp. 1239–1248, 2018.

[4] A. Madabhushi and G. Lee, "Image analysis and machine learning in digital pathology: challenges and opportunities," *Medical Image Analysis*, vol. 33, pp. 170–175, 2016.

[5] J. S. Beckmann and D. Lew, "Reconciling evidence-based medicine and precision medicine in the era of big data: challenges and opportunities," *Genome Medicine*, vol. 8, no. 1, p. 134, 2016.

[6] J. Xia, J. Wang, and S. Niu, "Research challenges and opportunities for using big data in global change biology," *Global Change Biology*, vol. 26, no. 11, pp. 6040–6061, 2020.

[7] S. Dirmeier, M. Emmenlauer, C. Dehio, and N. Beerenwinkel, "PyBDA: a command line tool for automated analysis of big biological data sets," *BMC Bioinformatics*, vol. 20, no. 1, p. 564, 2019.

[8] S. U. Park, H. Ahn, D. K. Kim, and W. Y. So, "Big data analysis of sports and physical activities among Korean adolescents," *International Journal of Environmental Research and Public Health*, vol. 17, no. 15, p. 5577, 2020.

[9] H. R. Thornton, J. A. Delaney, G. M. Duthie, and B. J. Dascombe, "Developing athlete monitoring systems in team sports: data analysis and visualization," *International Journal of Sports Physiology and Performance*, vol. 14, no. 6, pp. 698–705, 2019.

[10] A. Alonso-Betanzos and V. Bolón-Canedo, "Big-data analysis, cluster Analysis, and machine-learning approaches," *Advances in Experimental Medicine and Biology*, vol. 1065, pp. 607–626, 2018.

[11] A. M. AbdelAziz, T. Soliman, K. K. A. Ghany, and A. Sewisy, "A hybrid multi-objective whale optimization algorithm for analyzing microarray data based on Apache Spark," *PeerJ Computer Science*, vol. 7, p. e416, 2021.

[12] M. M. Saeed, Z. Al Aghbari, and M. Alsharidah, "Big data clustering techniques based on Spark: a literature review," *PeerJ Computer Science*, vol. 6, p. e321, 2020.

[13] H. Mushtaq, N. Ahmed, and Z. Al-Ars, "SparkGA2: production-quality memory-efficient Apache Spark based genome analysis framework," *PLoS One*, vol. 14, no. 12, Article ID e0224784, 2019.

[14] H. Xia, W. Huang, N. Li, J. Zhou, and D. Zhang, "PARSUC: a parallel subsampling-based method for clustering remote sensing big data," *Sensors*, vol. 19, no. 15, p. 3438, 2019.

[15] V. Ravuri and S. Vasundra, "Moth-flame optimization-bat optimization: map-reduce framework for big data clustering using the moth-flame bat optimization and sparse fuzzy C-means," *Big Data*, vol. 8, no. 3, pp. 203–217, 2020.

[16] V. Mayer-Schönberger and E. Ingelsson, "Big Data and medicine: a big deal?" *Journal of Internal Medicine*, vol. 283, no. 5, pp. 418–429, 2018.

[17] M. A. Levin, J. P. Wanderer, and J. M. Ehrenfeld, "Data, big data, and metadata in anesthesiology," *Anesthesia & Analgesia*, vol. 121, no. 6, pp. 1661–1667, 2015.

[18] B. Karmakar, S. Das, S. Bhattacharya, R. Sarkar, and I. Mukhopadhyay, "Tight clustering for large datasets with an application to gene expression data," *Scientific Reports*, vol. 9, no. 1, p. 3053, 2019.

[19] A. A. Qaffas, R. Hoque, and N. Almazmomi, "The internet of things and big data analytics for chronic disease monitoring in Saudi arabia," *Telemedicine and e-Health*, vol. 27, no. 1, pp. 74–81, 2021.

[20] A. Waschkau, D. Wilfling, and J. Steinhäuser, "Are big data analytics helpful in caring for multimorbid patients in general practice? - a scoping review," *BMC Family Practice*, vol. 20, no. 1, p. 37, 2019.

Hindawi
Mobile Information Systems
Volume 2023, Article ID 9768158, 1 page
https://doi.org/10.1155/2023/9768158

Retraction

Retracted: Research on Vessel Speed Heading and Collision Detection Method Based on AIS Data

Mobile Information Systems

Received 8 August 2023; Accepted 8 August 2023; Published 9 August 2023

This article has been retracted by Hindawi following an investigation undertaken by the publisher [1]. This investigation has uncovered evidence of one or more of the following indicators of systematic manipulation of the publication process:

(1) Discrepancies in scope
(2) Discrepancies in the description of the research reported
(3) Discrepancies between the availability of data and the research described
(4) Inappropriate citations
(5) Incoherent, meaningless and/or irrelevant content included in the article
(6) Peer-review manipulation

The presence of these indicators undermines our confidence in the integrity of the article's content and we cannot, therefore, vouch for its reliability. Please note that this notice is intended solely to alert readers that the content of this article is unreliable. We have not investigated whether authors were aware of or involved in the systematic manipulation of the publication process.

Wiley and Hindawi regrets that the usual quality checks did not identify these issues before publication and have since put additional measures in place to safeguard research integrity.

We wish to credit our own Research Integrity and Research Publishing teams and anonymous and named external researchers and research integrity experts for contributing to this investigation.

The corresponding author, as the representative of all authors, has been given the opportunity to register their agreement or disagreement to this retraction. We have kept a record of any response received.

References

[1] G. Wang, E. Fan, G. Zheng, K. Li, and H. Huang, "Research on Vessel Speed Heading and Collision Detection Method Based on AIS Data," *Mobile Information Systems*, vol. 2022, Article ID 7257075, 10 pages, 2022.

Hindawi
Mobile Information Systems
Volume 2022, Article ID 7257075, 10 pages
https://doi.org/10.1155/2022/7257075

Research Article

Research on Vessel Speed Heading and Collision Detection Method Based on AIS Data

Guoqing Wang,[1,2] **En Fan**,[3] **Guohua Zheng**,[1] **Kexiang Li**,[1] **and Haiguang Huang**[4]

[1]*Zhejiang Suosi Technology Co. Ltd, Wenzhou 325000, Zhejiang, China*
[2]*Asia Pacific University of Technology and Innovation, Technoloy Park Malaysia, 57000 Kuala Lumpur, Malaysia*
[3]*Department of Computer Science and Engineering, Shaoxing University, Shaoxing 312000, Zhejiang, China*
[4]*College of Computer Science and Artificial Intelligence, Wenzhou University, Wenzhou 325000, Zhejiang, China*

Correspondence should be addressed to Guoqing Wang; wgq@zjsos.net

Received 12 July 2022; Revised 29 July 2022; Accepted 13 August 2022; Published 16 September 2022

Academic Editor: Yajuan Tang

In order to better predict the sailing information data of fishing boats, make accurate prediction and spacing budget for the sailing status of ships, achieve more accurate coordination and early warning in advance, and ensure the safety of fishing boats' laneway, the essay combined the kinematics equation and artificial neural network model to adapt to the traffic situation of fishing boats in the far sea. A course and collision test technique based on ship AIS data is proposed, and the course collision detection method of fishing boats is studied by means of actual ship beacon collision accident data. Through the practical test, taking the navigation mark 4560.117 as an example, under the detection track of the navigation mark field corresponding to $R = 70$, the two ships have the same track, thus verifying the practicality and feasibility of the ship navigation mark collision detection method.

1. Introduction

In recent years, with the rapid development of China's economy, shipping industry has also developed rapidly. Due to the increasing volume of shipping traffic, the situation of waterway congestion and navigation accidents gradually increased in the shipping area, and even caused huge economic losses. In this case, it is better to predict the propagation trajectory accurately. On the one hand, it can timely find the abnormal trajectory of the ship. On the other hand, it can also effectively prevent ship landing, avoid collision accidents, and provide reliable technical support for the scientific decision-making of fishing vessel collision avoidance and route planning. In order to better strengthen the scientific control and monitoring of maritime shipping traffic, AIS technology began to emerge. This technology, through automatic identification system, can break the disadvantages of traditional radar equipment, has higher positioning accuracy for ships, and is less affected by terrain, weather, and other factors. It can provide reliable data support for ship navigation gathering prediction and collision avoidance.

2. Literature Review

Some scholars proposed a four-element dynamic ship domain model, improved the method of judging safe distance and collision risk with the help of AIS information, and established a set of reasonable and effective ship collision avoidance decision model. It realizes the judgment of collision danger and encounter situation. Some scholars have also made corresponding discussions on collision avoidance of ships and postulated that the AIS system is an effective means to avoid collision. The AIS system in ships will accurately detect the changes in course and speed caused by weather or human factors, which helps ships to determine whether they will encounter the scene; based on dynamic AIS information, an adaptive ship safety domain system with spatial risk function is proposed to identify collision and landing risks, which greatly improves the accuracy of identifying collisions between ships [1]. Some scholars extracted the motion model from the original AIS data and used it to construct the corresponding motion anomaly detector. Gaussian filter and tracking filter are

Table 1: Composition of AIS data structure of ships.

Static data	Dynamic data	Voyage data
MMSI unique identifier	Ground course	The depth of the draft
Callsign hull number	Speed of sailing	The port of destination
Ship type	Longitude	Eta.
The length and breadth of the ship	Latitude	None

Table 2: AIS data information table of ships.

The field names	Field description	The field type	Note
ID	Record line account	Integer	The static message
Ship_ jid	The ship number	Integer	The static message
IMO	IMO ship number	String	The static message
Name	Name of vessel	String	The static message
Callsign	Call sign of ship	String	The static message
Ship_ type	Ship type	Integer	The static message

used to predict ship motion. An incremental learning of ship motion patterns for single AIS ground receivers, regional networks, or global scale tracking is proposed. By providing the relevant characteristics of ship traffic to detect ship anomaly trajectory, ideas for many ship anomaly detection models proposed by many subsequent scholars are provided. Abnormal ship track can be detected from AIS and recorded by feature learning algorithm. This detection method can effectively detect abnormal trajectory and provide an important basis for the realization of maritime intelligent transportation [2]. Some scholars proposed a clustering algorithm related to regional density. However, the neighborhood radius of this method limits the number of line segments required in the clustering process. In order to solve this problem, the algorithm is improved to produce an algorithm that can output many same clustering trajectory segments. However, for a wider range of decision parameters, this method may encounter problems in data sets with circular motion and frequent crossing paths. The DBSCAN algorithm is proposed to cluster ship track, which provides ideas for many subsequent scholars in the study of ship track clustering. The DBSCAN algorithm is improved and a trajectory clustering model based on AIS data is proposed to analyze ship track. The improved density-based DBSCAN clustering algorithm can automatically classify different routes with route characteristics and improve the clustering accuracy of main route extraction of ship track. A probabilistic method based on hidden Markov model is proposed for ship trajectory clustering. This model provides a natural framework, and models the inherent time correlation of data according to the definition, and displays it visually [3, 4].

3. AIS Data Preprocessing and Choice of Flight Path Prediction Model

3.1. Data Structure. AIS has become an essential component of modern ship navigation system. AIS information mainly contains three types of data, namely, static data of ships, dynamic data of ships, and navigation data of ships. Specific data information is shown in Table 1.

These information parameters representing ship navigation state are of great value to the study of ship track prediction. Therefore, detailed analysis of AIS internal data is needed. AIS data update speed is very fast, which can provide real-time dynamics of ships [5, 6]. In order to facilitate the analysis of AIS data information structure and types, the basic format of AIS data is given, as shown in Table 2.

3.2. AIS Data Preprocessing

3.2.1. AIS Data Collection. Ship track prediction is to predict the course of the ship in the next period according to the track of the ship, so it is necessary to obtain the known historical track data. However, currently available AIS data record the track data of all ships, and does not classify and encode individual ship routes, so the track data of a single ship route cannot be directly obtained, and the ship route needs to be identified artificially according to the MMSI unique identification code of ship AIS data. Filter and sort according to MMSI and collection time. Sample table of collected and sorted AIS data is shown in Table 3.

3.2.2. AIS Data Cleaning. The AIS system identifies a ship by the unique identification code MMSI. Based on time series, it is necessary to perform certain data cleaning and processing in case of the following special situations for the ship track data encoded only by MMSI [7].

(1) Illegal data. Illegal data refer to data with multiple round trips at multiple places in the sea area or with large time difference between the ship and the ship due to man-made or environmental reasons. In this case, a clean and stable track period can be selected according to the ship's time interval, speed, and heading as the input data of the track pre-model.

Table 3: Partial AIS data collected.

Ship identification code	Time	Latitude	Longitude	Speed of sailing	Heading course
367617230	2017-12-00 : 00 : 22	19.30434	−65.4934	11.4	96
367617230	2017-12-0100 : 01 : 33	28.30358	−65.4395	11.23	56
367617230	2017-12-0100 : 06 : 03	16.30284	−65.4257	11.00	91
367617230	2017-12-0100 : 07 : 12	15.30138	−65.4188	11.96	90

(2) Drift data. Drift data refer to some abnormal data points that deviate far from the normal course due to positioning errors. In case of drift trajectory data, this point is usually filled by fitting according to the distance between the two points before and after. For data points that cannot be fitted, they can be directly removed.

(3) Sparse data. Sparse data refer to the data with a large distance between two adjacent track points due to information loss. These kind of data need to be discarded directly. In fact, in the COLLECTED AIS data, some track points are close to each other or close to the same straight line. Such data should be processed by compression with appropriate time interval [8].

3.2.3. AIS Data Missing Value Processing. Assume that the ship's track sequence is shown in equation (1):

$$T = \left\{p_t^1, p_t^2, \cdots, p_t^n\right\},$$
$$p_t^i = \{\text{sog}, \text{cog}, \text{lat}, \text{lon}\}, \tag{1}$$

p_t^i represents THE AIS data at time t_i, where sog, cog, lat, lon, respectively, represent the ship's speed, heading, latitude, and longitude at time t. Interpolation methods for ship track data can be roughly divided into the following categories:

First, linear interpolation.

Set the position coordinates of the missing data point as (t_i, p_t^i), and the position coordinates of the front and rear data points as (t_{i-1}, p_t^{i-1}) and (t_{i+1}, p_t^{i+1}), respectively. The missing values are fitted by the coordinate data of the front and rear data points, and the specific linear interpolation fitting diagram is shown in Figure 1.

According to Figure 1, the interpolation formula can be expressed as follows:

$$p_t^i = p_t^{i-1} + \frac{p_t^{i+1} - p_t^{i-1}}{t_{i+1} - t_{i-1}}\left(t_i - t_{i-1}\right). \tag{2}$$

It can be seen from the above equation that the linear interpolation method is only applicable to the trajectory data with a small degree of bending. If the trajectory curvature is large, this method will produce relatively large errors.

Second, Lagrange interpolation.

Assume that the coordinates of $k+1$observed track points of the ship can be expressed as formula (3):

$$\left(t_0, p_t^0\right), \left(t_1, p_t^1\right), \cdots, \left(t_k, p_t^k\right). \tag{3}$$

Suppose that the position of the ship is different at any two moments, $t_i$represents the corresponding time point of the data, and p_t^i represents the value of the ship at the corresponding time point. The Lagrange interpolation polynomial can be expressed as formula (4):

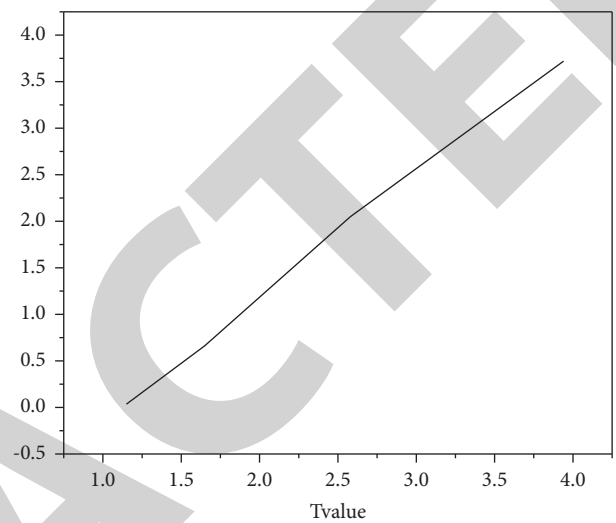

Figure 1: Schematic diagram of linear interpolation.

$$L(t) = \sum_{i=0}^{k} p_t^i l_i(t_i), \tag{4}$$

where $l_i(t)$ represents the interpolation basis function, and its expression is equation (5):

$$l_i(t) = \prod_{j=0, i\neq j}^{k} \frac{t - t_j}{t_i - t_j}. \tag{5}$$

The value of the above formula is 1 at $t = t_i$ and 0 at $t \neq t_i$, so the polynomial can be guaranteed to pass through all observed data points. Because polynomials can fit curves well, this method is more suitable for trajectory interpolation of curved ships.

3.3. Track Prediction Model Based on PSO-LSTM. PSO algorithm is a heuristic global search algorithm based on swarm intelligence. The algorithm compares the optimization problem to bird predation, and the optimal solution is the target food. Each bird is the particle in THE PSO algorithm, and all the particles move at a certain speed and track in space, and guide the behavior of the whole population to approach the target function through the function to be optimized [9]. Its essence is to use individual competition mechanism to generate local optimal solution, and then through information sharing and cooperation

mechanism to generate global optimal solution. The specific process is shown in Figure 2.

PSO algorithm is a method to search for the optimal solution globally. The combination of PSO algorithm and LSTM network can help the model to determine the optimal parameter combination and achieve better prediction effect. Set the number of parameter combinations in LSTM neural network as N, that is, a population composed of N particles is formed. The position of each particle$i$ at any time is an n-dimensional space vector, so the position of particle i at the t-th time period can be represented by equation (6):

$$x_i(t) = \left[x_{i1}(t), x_{i2}(t), \cdots, x_{in}(t)\right]^T. \tag{6}$$

Fitness function determines the direction of particle swarm, which is set as mean square error, as shown in equation (7):

$$F = \sum_{i=1}^{n} \left|y_i - y_i'\right|, \tag{7}$$

where $y_i$is the expected value of the i th particle, and y' is the corresponding predicted value.

In the update stage, the historical optimal x_i^{pb} set at $t$time cycles is expressed in formulas (8)–(10):

$$x_i^{pb}(t) = \left[x_{i1}^{pb}(t), x_{i2}^{pb}(t), \cdots, x_{in}^{pb}(t)\right]^T. \tag{8}$$

The historical optimum of all particles isx_i^{gb}:

$$x_i^{gb}(t) = \left[x_{i1}^{gb}(t), x_{i2}^{gb}(t), \ldots, x_{in}^{gb}(t)\right]^T. \tag{9}$$

Then, in the $t$time period, the updating formula of the individual extreme value x_i^{pb} of particle i is:

$$x_i^{pb}(t+1) = \begin{cases} x_i(t+1), & F\left(x_i(t+1)\right) \le F x_i^{pb}(t), \\ x_i^{pb}(t), & F\left(x_i(t+1)\right) \le F x_i^{pb}(t). \end{cases} \tag{10}$$

The updating formula of the global extreme value $x_i^{gb}$of all particles is equation (11):

$$x_i^{gb}(t+1) = \arg\left\{F_{\min}\left(x_i^{gb}(t+1)\right)\right\}, \tag{11}$$

where arg is the value of independent variable$x$ corresponding to function $F(x)$. The velocity and position of the particle in the$(t+1)$ time period are updated by formulas (12) and (13):

$$\begin{aligned} v_i(t+1) = {} & l \cdot v_i(t) + c_1 \cdot r_1 \cdot \left(x_i^{pb}(t) - x_i(t)\right) \\ & + c_2 \cdot r_2 \cdot \left(x_i^{gb}(t) - x_i(t)\right), \end{aligned} \tag{12}$$

$$x_i(t+1) = x_i(t) + v_i(t+1), \tag{13}$$

where, $v_i(t)$ is the traveling speed of particle $i$in the t time period; l is the linear decreasing weight coefficient; c_1、c_2 represent learning factor; r_1、$r_2$is a uniform random number whose value range is (0, 1). After the particle has obtained the best fitness, the corresponding parameter combination can be put into the LSTM neural network.

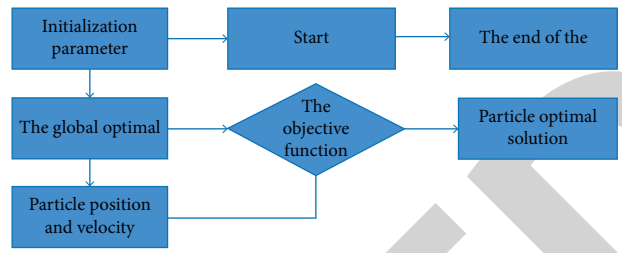

Figure 2: Basic flow of PSO algorithm.

3.4. GA-LSTM Prediction Model. GA algorithm is a computational model of evolutionary process inspired by biological evolution theory and natural genetics principle. It is a global, parallel, and efficient search method in essence. When dealing with related problems, GA algorithm will transform them into the biological evolution process, which will be eliminated according to the survival of the fittest principle. Finally, the evolution model will converge to the optimal individual, namely, the optimal solution of the problem [10]. The specific process is shown in Figure 3.

In the fitness calculation stage, GA algorithm is consistent with PSO algorithm, and the mean square error is used to evaluate the fitness equation (14):

$$F = \sum_{i=1}^{n} \left|y_i - y_i'\right|. \tag{14}$$

In the selection stage, Roulette's rule is adopted as the selection operator. This method can improve the evolutionary weight of individuals with high fitness and keep the evolutionary weight of individuals with low fitness not zero, so as to ensure the diversity of parameters in THE LSTM network and avoid the occurrence of local extreme values. Then the probability p_i of individual$i$ being selected in the selection stage is equation (15):

$$p_i = \frac{(k/F_i)}{\sum_{i=1}^{n}(k/F_i)}, \tag{15}$$

where $F_i$is the fitness value of individual i in the population. In crossover stage, random linear combination of individuals is carried out. The specific real number crossover process is shown in formulas (16) and (17):

$$w_{ij} = w_{ij} \cdot (1-u) + w_{ij} \cdot u, \tag{16}$$

$$w_{kj} = w_{kj} \cdot (1-u) + w_{kj} \cdot u, \tag{17}$$

where w_{ij} is the information of j position on the i th gene; w_{kj} is the information of j position on the kth gene; u is the probability of information crossing, and its value ranges from 0 to 1. In the mutation stage, nonuniform mutation is adopted to conduct random perturbation of existing chromosomes, as shown in formulas (18)–(20):

$$w_{ij}' = w_{ij} + \left(w_{\min} - w_{ij}\right) \cdot F_{(G_1)}, r_3 \ge 0.5, \tag{18}$$

$$w_{ij}' = w_{ij} + \left(w_{ij} - w_{\max}\right) \cdot F_{(G_1)}, r_3 \ge 0.5, \tag{19}$$

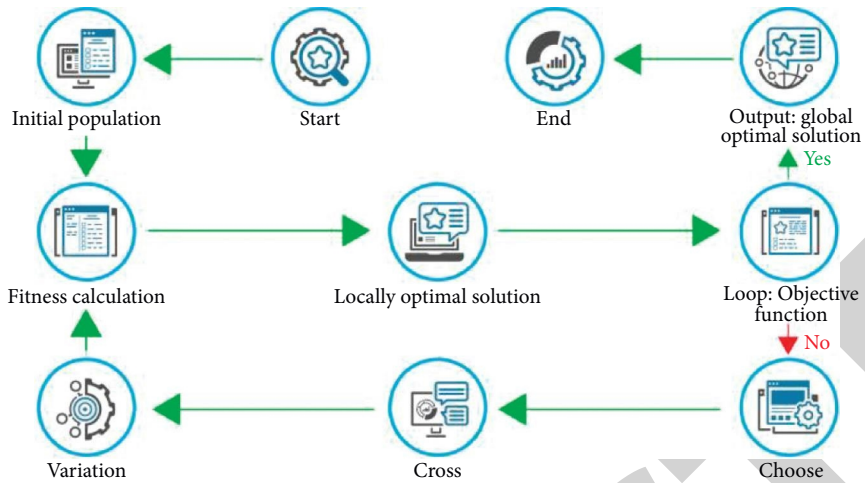

Figure 3: Basic flow of GA algorithm.

$$F_{(G_1)} = r_4\left(1 - \frac{G_1}{G_2}\right)^2, \tag{20}$$

where $w'_{ij}$is the new chromosome after mutation; G_1、G_2 are the current generation and the maximum generation; r_3、r_4 are the disturbance probability, and its value range is [0,1]. After the optimal fitness of the population is obtained, the corresponding parameter combination can be put into the LSTM neural network.

3.5. PSO-LSTM Model and GA-LSTM Model. PSO and GA heuristic algorithms are used to adjust the combination of Units, steps, and EPOchs of LSTM network in each time sequence and feature. The experiment sets the voyage prediction timestamp as {1, 5, 10, 20, 30, 40, 50} uniformly to test the prediction effect of the two models in the long and short periods.

Tables 4–6 show the average absolute percentage errors predicted by LSTM model, PSO-LSTM model, and GA-LSTM model for four kinds of navigational dynamics features: longitude, latitude, speed, and heading. Through the horizontal comparison of data, it can be seen that with the addition of the two optimization algorithms, the prediction errors of the LSTM model in the four types of features are reduced to different degrees. Compared with the LSTM model, PSO-LSTM model and GA-LSTM model have better effects on the prediction of longitude, latitude, and speed in the whole time series. The maximum longitude MAPE decreases to 0.0054, and the maximum latitude MAPE decreases to 0.002. Speed MAPE value decreased to 2.9923; for the prediction of heading characteristics, the two optimization algorithms perform well in the short time sequence, and local error oscillation occurs in the long time sequence prediction, and the maximum MAPE value decreases to 0.4428.

Figures 4 and 5 show the root mean square error of PSO-LSTM model and GA-LSTM model for the prediction of speed and heading characteristics in navigation dynamics. It can be seen that the error of the GA-LSTM model is significantly smaller than that of the PSO-LSTM model in the prediction of ship speed and heading. Therefore, it can be analyzed that there are multiple optimal solutions for "multi-peak regression" problems such as speed and heading characteristics, and more attention is paid to the global search ability. Compared with PSO algorithm, the GA algorithm has higher complexity, better global optimization, and implicit parallelism, which is reflected in the LSTM model framework as stronger search ability. The unique biological evolution process of the algorithm ensures the diversity of the population and can escape the local peak with a certain probability in the iterative process, avoiding the model falling into the local optimum in the iteration [11, 12].

Table 4: Average absolute percentage error of LSTM prediction model.

MAPE	LON	LAT	SoG	CoG
$n = 1$	0.0012	0.269	1.7896	0.5693
$n = 6$	0.0011	0.369	2.6391	0.1269
$n = 12$	0.0016	0.598	8.2369	0.7863
$n = 20$	0.0018	0.756	9.5630	0.4599

Table 5: Average absolute percentage error of PSO-LSTM prediction model.

MAPE	LON	LAT	SoG	CoG
$n = 2$	0.0002	0.369	3.7897	0.5623
$n = 9$	0.0001	0.349	4.6392	0.1369
$n = 10$	0.0006	0.578	7.2359	0.7767
$n = 30$	0.0008	0.856	8.5637	0.4798

Table 6: Average absolute percentage error of GA-LSTM prediction model.

MAPE	LON	LAT	SoG	CoG
$n = 8$	0.0032	0.268	9.7896	0.5593
$n = 7$	0.0011	0.369	8.6391	0.1369
$n = 13$	0.0056	0.548	4.2369	0.7753
$n = 40$	0.0098	0.736	1.5630	0.4572

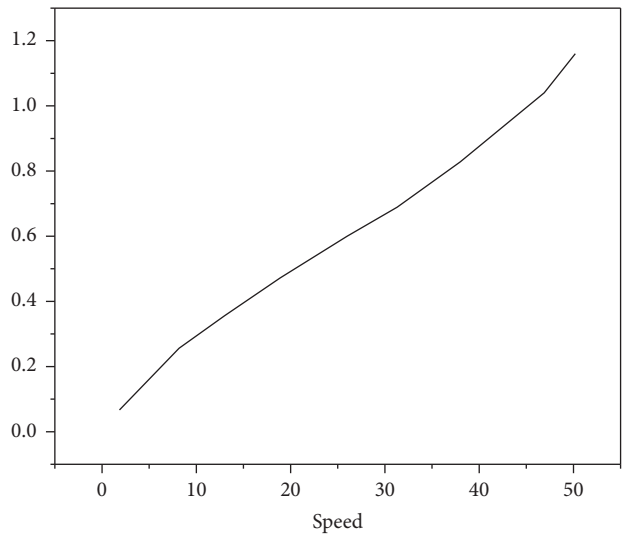

Figure 4: PSO-LSTM model.

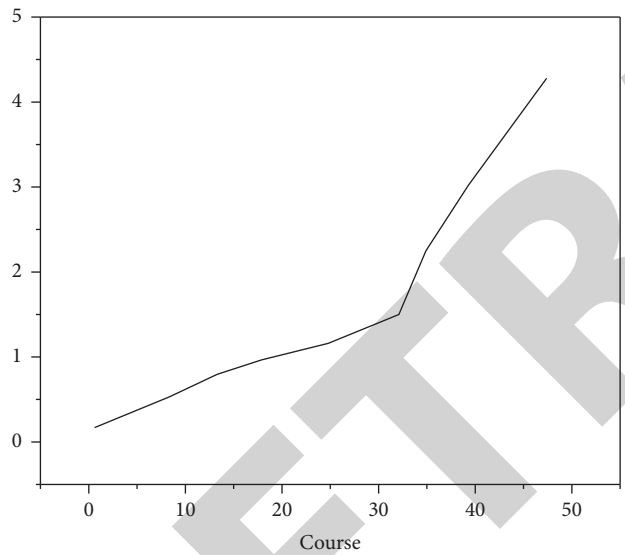

Figure 5: Root mean square error of the GA-LSTM model.

To sum up, both PSO algorithm and GA algorithm can enable LSTM-based navigation dynamic prediction model to find more optimal parameters and improve the prediction accuracy. Among them, the PSO-LSTM model performs better in the prediction of longitude and latitude characteristics, and the GA-LSTM model performs better in the prediction of speed and heading characteristics. Therefore, the two algorithms are combined to provide reference for subsequent model comparison, and the new model after combination is denoted as LSTM*.

4. Ship-Beacon Collision Detection Method Based on Hierarchical Navigation Beacon Field

4.1. Principle of Ship-Beacon Collision Detection. According to the construction methods of the ship domain model, it can be divided into ship domain model based on analysis, ship domain model based on statistical methods, and ship domain model based on intelligent technology. Ship domain based on analysis is mainly expressed as a function expression of ship length, width, and speed. However, due to the influence of ship navigation environment and other aspects of ship domain, ship domain has differences in different waters, resulting in limited portability of the ship domain model. The ship domain model based on intelligent technology integrates fuzzy set theory and neural network technology, and outputs the fuzzy boundary of ship domain by taking the distance between two ships and the relative position as the input of the model. However, because the neural network adopts the "black box" mode to carry out association mapping, the exact relation expression cannot be obtained. The ship domain model construction method based on statistical method is based on maritime observation data, and the ship domain model is constructed by fitting the distribution of ships around the central ship and combining with navigation rules [13]. For example, based on AIS data and network division of the region, single ship grid frequency diagram is extracted by superimposing the distribution of other ships around the central ship, and ship domain model in restricted waters is calculated and analyzed. Therefore, the corresponding ship domain model can be constructed based on AIS data in the situation of designated waters and designated ships [14–16].

Navigation mark is a kind of ship with special purpose in essence. In order to avoid collision with navigational markers, ships in the past keep a safe distance from them in most cases, which means that navigational markers also exist in the realm of ships. Referring to the expression of the ship field, this essay describes it as the navigation mark field. It can be speculated that under normal conditions, the past ships are active in the navigation mark area, and when the ships invade the navigation mark area, they can be considered as suspected of colliding with the navigation mark. On the other hand, in the traditional ship-buoy collision detection method, it is impossible to avoid the situation of missing detection caused by the discontinuous data returned, so the ship-buoy collision detection method based on the navigation buoy field is adopted. Ship suspicion can be judged by detecting whether the ship's navigation track and navigation mark field have intersection, so as to avoid missed detection [17].

At present, the research mainly focuses on the research in the field of ships and less involves the research in the field of navigation markers. Therefore, in order to improve the effectiveness of the ship-beacon collision detection method based on the navigational domain, it is necessary to study the navigational domain first. That is, AIS data under non-accident conditions are taken as the basis. The distribution results of ships in all directions around the navigation mark field were obtained by grid division of the waters near the navigation mark and superposition of the grid distribution of passing ships in the waters near the navigation mark, and the boundary of the navigation mark field was obtained by merging. Then, combined with the model of navigation mark field, the passing ships on the day of navigation mark collision are detected. By judging whether past ships

intruded into the navigation mark area and the extent of intrusion, the suspicious nature of past ships' accidents was determined, and the ships involved were traced, as shown in Figure 6.

4.2. Analysis of the Construction Process in the field of Navigation AIDS. In the field of navigational markers, AIS data of ships are screened through time range and space, and the waters near navigational markers are networked. The distribution of ships in the grid is counted, and the accurate boundary range of navigational markers is obtained by superimposing data of several similar navigational markers, so as to build the navigational domain model.

At the same time, in order to confirm the accurate position of the ship in the waters near the navigation mark, so as to accurately extract the boundary of the navigation mark field, network division is carried out for the waters near navigation markers, and the region is divided into grids with a side length of 10 m [18]. After regional grid division, ships will be in different grids, ships are distributed in different grids, and the corresponding grid frequency increases by 1.

To solve this problem, firstly confirm the scope of the rectangular area where the ship is located and the corresponding grid according to the coordinates of the four vertices of the ship, as shown in the blue rectangular box in Figure7. Then, in order to determine whether each grid in the rectangular frame intersects with the rectangular frame, the separation axis theory is adopted. The separation axis is defined as follows: When polyhedron A and B are projected vertically onto a line L without overlap, the line L is said to be the separation axis of the polyhedron A and B. According to this, there is a separation axis theorem: if and only if polyhedron A and polyhedron B have a separation axis, the closed region formed will not intersect. If there is a separation axis, one of the separation axes must meet one of the following three conditions:

The first condition is that the separation axis is perpendicular to some plane of polyhedron A;

The second condition is that the separation axis is perpendicular to some plane of polyhedron B;

The third condition is that the separation axis is perpendicular to a plane that is parallel to an edge of the convex polyhedron A and an edge of the convex polyhedron B.

Based on the separation axis theorem, the intersection of objects can be determined only by judging whether there is separation axis between objects. When one or more separate axes exist, the bodies must not intersect, otherwise the bodies intersect. The green grids do not intersect the ship projection on the transverse axis of the ship, indicating that the ship is not distributed in two grids. Therefore, the separation axis is constructed along the length and width of the outer tangent rectangular frame of the ship, and the grid within the blue rectangular frame is judged successively whether it intersects with the ship, so as to determine the distribution grid of the ship [19].

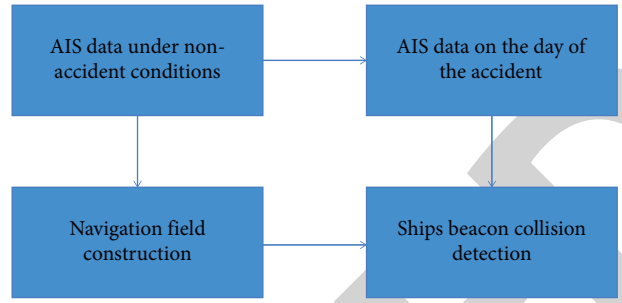

Figure 6: Ship-beacon collision detection flow based on navigation beacon field.

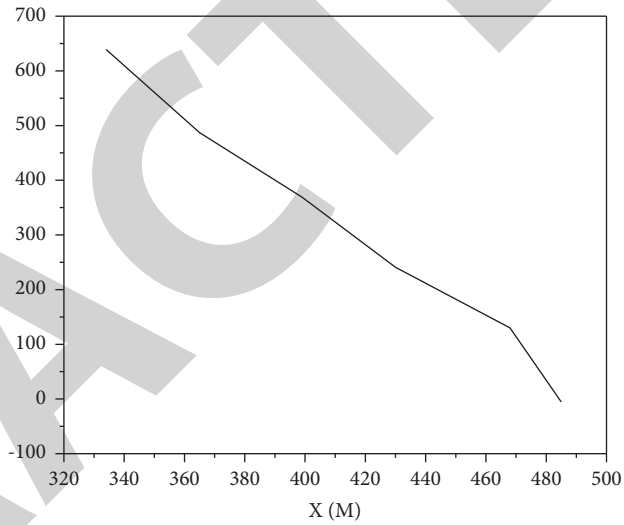

Figure 7: Detection results of the ship involved in the accident of beacon 4431.33.

For the same navigational beacon, the grid distribution results of different ships in the nearby waters were obtained, and the grid distribution results of all ships were superimposed to obtain the statistical results of navigational beacon. Due to the limited data of a single beacon, it is impossible to confirm the range of the beacon field. Multiple grid data of the same size are superimposed to obtain the grid distribution map after being superimposed to ensure the effectiveness of the range of the beacon field. In order to extract the boundary of the navigation mark field, the ship distribution curves in each grid in the four directions of the navigation mark were drawn, respectively, and the critical point of the curve value remaining stable to continuously rising was taken as the distance boundary in each direction. The navigation field is constructed as a circle. The center position of the circle is the position of the navigation beacon, and the radius is confirmed by combining the boundary extraction results and the ship-navigation beacon collision experiment results [20].

4.3. Ship-Beacon Collision Detection Based on Navigation Beacon Field. The navigation mark field constructed above is used to conduct ship-navigation mark collision detection experiment. The experiment includes two contents: collision

detection of all ship tracks matching the track of the ship causing the accident on the day of the navigation mark accident to verify the effectiveness of the range of navigation mark field; Second, collision detection is performed on all ship tracks on the day of the navigation mark accident where the track matching of the ship causing the accident cannot be completed, so as to verify the practicability of the ship-beacon collision detection method based on the navigation mark field. The detection and discrimination of ship-beacon collision can be divided into two types: (1) if the ship point is within the range of $r = 20$ m beacon field or there is an intersection between the ship track and $r = 20$ m beacon field, the ship can basically be judged as the ship in trouble; (2) If the ship point is within the range of navigation mark $r = 70$ m or there is an intersection point between the ship track and navigation mark $R = 70$ m, there is ship-beacon collision aversion. For the determination of the center position of the navigation mark, based on the AIS data return time point, the prediction point is taken as the center and the navigation mark domain model is used for judgment.

4.3.1. Validation Test of the Model in the Navigational Domain. Taking navigational beacon 4431.33 as an example, the navigational beacon fields with $R = 20$ m and $R = 70$ m were tested, respectively, and the results showed that only two ship paths were at the intersection with the navigational beacon fields, as shown in Figure 8. In Figure 8, ship 477269700 is the ship causing the actual ship-buoy collision. The ship first passes through the buoy area and then sails back and forth. Although the ship is close to the buoy, due to its small size (length 40 m, width 12 m), ship-buoy collision does not occur.

Furthermore, the data of the ship's beacon, which cannot be detected in the beacon field of $R = 20$ m, is tested. Take navigational beacon 4431.22 as an example, there is a ship track that intersects with the field of navigational beacon $r = 20$ m, as shown in Figure 7. The ship is 150 m long and 22 m wide, and sails in the bow direction without contacting the central navigational beacon. A total of 9 ship tracks were detected in the field of navigational markers with $r = 70$ m. It is shown that 3 ship tracks were detected with $R = 70$ m, among which are the tracks of the ship causing the accident. It can be seen that most other nonoffending ship tracks can still be detected in the navigation mark field with $R = 70$ m.

4.3.2. Practical Test of Ship: Beacon Collision Method. In order to further verify the practicability of the ship-beacon collision detection method based on the navigation mark field, ship-beacon collision detection is performed on the accident data other than the data matching the ship track and the ship information provided by the navigation mark management department. Taking navigation mark 4560.117 as an example, it is the suspicious ship track detected in the corresponding navigation mark field with $R = 70$ m, and the two ship tracks are both of ship 412378780. Furthermore, the name of the vessel involved in the accident was queried through the information list of the vessel involved in the accident provided by the navigation beacon management department, and the vessel information network MMSI was used according to the name of the vessel. This verifies the practicability of the ship-beacon collision detection method based on the navigation mark field.

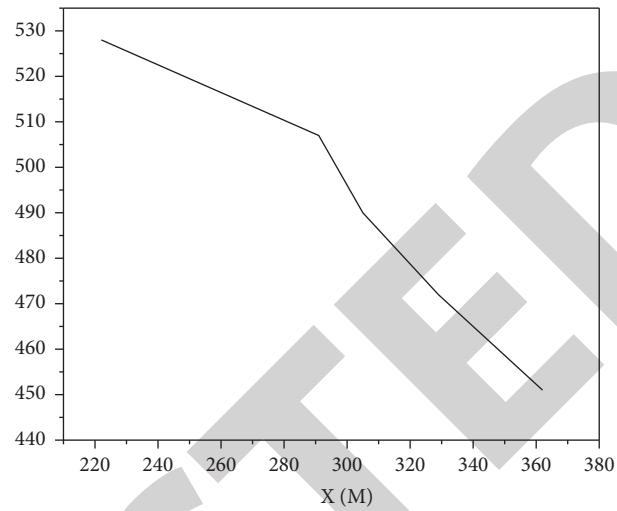

Figure 8: Example of ship detection in accident of navigation beacon 4431.22.

In this article, a ship-buoy collision detection method based on the navigation buoy field is proposed. Through the construction of hierarchical beacon field model, the intersection detection of beacon field and ship track of passing ships is carried out to determine the ship causing the accident. The specific contents include:

(1) The construction process and method of navigational beacon domain based on AIS data are proposed, and the hierarchical navigational beacon domain model is constructed based on ship-buoy collision accident data;

(2) A ship-buoy collision detection method based on hierarchical buoy domain model is proposed, and the effectiveness of the method is verified by actual ship-buoy collision accident data.

However, when multiple ship tracks are detected based on the hierarchical model, it still needs to be judged manually. However, compared with the collision detection method based on trajectory tracking, it avoids the subjective error of relying only on manual judgment, the insufficiency of detecting abnormal data of navigation mark, and the failure of detecting due to the discontinuity of data returned. On the other hand, the collision detection based on fuzzy navigation beacon cannot accurately judge the collision time and location, and does not fully consider the size of the ship.

5. Conclusion

In this article, the lack of systematic and effective detection methods in the actual detection of ship-buoy collision accidents has caused some difficulties in obtaining evidence and tracing responsibility for accidents. Based on the actual ship-beacon collision data and AIS data, ship-beacon

collision methods are studied. The specific research contents and results include the following aspects:

Combining the dynamic characteristics of ship navigation in AIS information with time series, and using longitude, latitude, heading, speed, heading and time increment as inputs, a dynamic prediction model of ship navigation based on LSTM was established. At the same time, PSO-LSTM prediction model based on particle swarm optimization algorithm and GA-LSTM prediction model based on genetic algorithm were constructed to optimize the parameter (step-unit-epoch) optimization in the model, respectively, to help the LSTM network to find the global optimal. The simulation results show that the prediction accuracy of the PROPOSED LSTM model is better than that of the existing BP model. At the same time, the prediction accuracy of the two LSTM models based on heuristic optimization algorithm is better than that of the naive LSTM model, in which the PSO-LSTM model has better performance in the prediction of longitude and latitude, and the GA-LSTM model has better performance in the prediction of ship speed and heading. Therefore, the combination of the two is recorded as LSTM* model to provide a comparative reference for subsequent studies.

Aiming at the deficiency of relying on abnormal data detection and manual judgment in ship-buoy collision detection based on trajectory tracking, a ship-buoy collision detection method based on hierarchical buoy field was proposed based on analyzing the construction process of AIS data–based buoy field. The validity of fuzzy ship domain scope and the practicability of ship-beacon collision detection method are verified by using ship-beacon collision accident data.

Data Availability

The data of this paper can be obtained from the corresponding author upon request.

Conflicts of Interest

The authors declare that they have no conflicts of interest.

Acknowledgments

This work was supported by Zhejiang Province "Ten Thousand Talents Program" Technology Entrepreneurship Leading Talent (2019R53015) and Shaoxing University Research Startup Project (20205048).

References

[1] B. Liu, X. Wu, X. Liu, and M. Gong, "Assessment of ecological stress caused by maritime vessels based on a comprehensive model using ais data: case study of the bohai sea, Assessment of ecological stress caused by maritime vessels based on a comprehensive model using AIS data: Case study of the Bohai Sea, Chinahina," *Ecological Indicators*, vol. 126, no. 1, Article ID 107592, 2021.

[2] M. B. Zaman, E. Kobayashi, and A. Zubaydi, "Traffic analysis for enhancing safety in the Traffic analysis for enhancing safety in the Singapore Straits using AIS dataingapore straits using ais data," *IOP Conference Series: Earth and Environmental Science*, vol. 649, no. 1, Article ID 12065, 2021.

[3] Y. Liang and H. Zhang, "Ship track prediction based on ais data and pso optimized lstm network," *International Core Journal of Engineering*, vol. 6, no. 5, pp. 23–33, 2020.

[4] M. Gao and G. Y. Shi, "Ship collision avoidance anthropomorphic decision-making for structured learning based on ais with seq-cgan," *Ocean Engineering*, vol. 217, no. 13–15, Article ID 107922, 2020.

[5] H. T. Lee, J. S. Lee, H. Yang, and I. S. Cho, "An ais data-driven approach to analyze the pattern of ship trajectories in ports using the dbscan algorithm," *Applied Sciences*, vol. 11, no. 2, p. 799, 2021.

[6] J. Xiong, X. Jin, G. Dong, D. Gu, and C. Yi, "Risk assessment of ship traffic safety in port waters based on ais data," *IOP Conference Series: Earth and Environmental Science*, vol. 638, no. 1, Article ID 12022, 2021.

[7] Y. Dogan, O. Kart, B. Kundakci, and S. Nas, "A novel approach for knowledge discovery from ais data: an application for transit marine traffic in the sea of marmara," *Advances in Electrical and Computer Engineering*, vol. 21, no. 3, pp. 73–80, 2021.

[8] W. He, J. Lei, X. Chu, S. Xie, C. Zhong, and Z. Li, "A visual analysis approach to understand and explore quality problems of ais data," *Journal of Marine Science and Engineering*, vol. 9, no. 2, p. 198, 2021.

[9] M. I. Asborno and S. Hernandez, "Assigning a commodity dimension to ais data: disaggregated freight flow on an inland waterway network," *Research in Transportation Business & Management*, vol. 9, Article ID 100683, 2021.

[10] A. A. Masroeri, A. S. Aisjah, and M. M. Jamali, "Iuu fishing and transhipment identification with the miss of ais data using neural networks," *IOP Conference Series: Materials Science and Engineering*, vol. 1052, no. 1, Article ID 12054, 2021.

[11] S. Chen, F. Wang, X. Wei, Z. Tan, and H. Wang, "Analysis of tugboat activities using ais data for the tianjin port," *Transportation Research Record*, vol. 2674, no. 5, pp. 498–509, 2020.

[12] M. Gao and G. Shi, "Modelling of ship collision avoidance behaviours based on ais data," *International Journal of Simulation and Process Modelling*, vol. 15, no. 1/2, p. 100, 2020.

[13] K. Y. Shen, Y. J. Chu, S. J. Chang, and S. M. Chang, "A study of correlation between fishing activity and ais data by deep learning," *TransNav the International Journal on Marine Navigation and Safety of Sea Transportation*, vol. 14, no. 3, pp. 527–531, 2020.

[14] C. Liu, J. Liu, X. Zhou, Z. Zhao, C. Wan, and Z. Liu, "Ais data-driven approach to estimate navigable capacity of busy waterways focusing on ships entering and leaving port," *Ocean Engineering*, vol. 218, no. 2, Article ID 108215, 2020.

[15] G. Dhiman, V. Vinoth Kumar, A. Kaur, and A. Sharma, "Don: deep learning and optimization-based framework for detection of novel coronavirus disease using x-ray images," *Interdisciplinary Sciences: Computational Life Sciences*, vol. 13, no. 2, pp. 260–272, 2021.

[16] J. Jayakumar, B. Nagaraj, S. Chacko, and P. Ajay, "Conceptual implementation of artificial intelligent based E-mobility controller in smart city environment," *Wireless Communications and Mobile Computing*, vol. 2021, Article ID 5325116, 8 pages, 2021.

[17] J. Chen, J. Liu, X. Liu, X. Xu, and F. Zhong, "Decomposition of toluene with a combined plasma photolysis (cpp) reactor: influence of uv irradiation and byproduct analysis," *Plasma*

Hindawi
Mobile Information Systems
Volume 2022, Article ID 6831049, 7 pages
https://doi.org/10.1155/2022/6831049

Research Article

Research on Satisfaction of Driverless Function Based on the Artificial Intelligence Algorithm

Tianyu Dong,[1] **Qiong Wang**,[2] **and Lingxing Meng**[1]

[1]*Business College, China University of Political Science and Law, Beijing 100088, China*
[2]*Economics College, Beijing International Studies University, Beijing 100024, China*

Correspondence should be addressed to Lingxing Meng; cu202002@cupl.edu.cn

Received 12 July 2022; Revised 29 July 2022; Accepted 18 August 2022; Published 13 September 2022

Academic Editor: Yajuan Tang

With the popularization of driverless technology, more and more vehicles have begun to apply this technology. Under these circumstances, user satisfaction with driverless function begins to have an increasing impact on car sales. This paper adopts the KANO model, a two-dimensional model, to analyze users' attitudes toward driverless functions. It is found that users have a high dependence on functions such as forward collision warning, autonomous emergency braking, and stated-speed sign recognition. Therefore, relevant enterprises should continue to develop these functions. Besides, users have high expectations for functions such as blind spot detection systems and rear cross-traffic alerts. Enterprises can achieve more support from users by optimizing these functions. Functions like lane-keeping assist, lane departure warning, parking distance control, and door open warning systems belong to indifferent attributes of driverless function, which are not cared about by users. There is no need for enterprises to optimize these functions. However, the lane change assist system has been criticized by users and should be improved by corresponding manufacturers.

1. Introduction

In recent years, the rapid development of the Internet and data science has brought profound changes to the automotive industry. Besides, the progress of high definition (HD) maps and the wide application of artificial intelligence have also promoted the maturity of intelligent driving technology. Under this circumstance, car driving is becoming simpler and smarter. As a direction for car driving development in the future, driverless technology has enjoyed considerable development in the latest years. Driverless cars, i.e., autonomous vehicles, are different from traditional cars. The latter needs to be driven by people, while the former perceives the surrounding environment through a sensor system inside the vehicle, including relevant intelligent software and various induction equipment. The driverless car can make its judgment according to perceived road information, vehicle position, and obstacle information to control the speed and steering so that it can be safe on the road. The driverless car breaks through the traditional driver-centered mode and improves safety and stability to a certain extent with the advantage of decreasing the incidence of traffic accidents, as well as reducing exhaust emissions and energy consumption. With high economic and social benefits, the driverless car is becoming an important part of the future development of smart cities.

The driverless car is a new technology and a new product. During the process of forming a new market, understanding and acceptance degree of consumers are unavoidable matters. According to a survey by relevant research institutions in the United States, 75% of drivers keep a cautious attitude toward the driverless car, and some of them are even skeptical [1]. Most people only have a simple understanding of the functions of the driverless car or view it as a novelty. The acceptance degree is still low. As the development direction of technology and product for auto enterprises in the future, whether driverless technology can satisfy users will play a key role in enhancing product attractiveness, thereby increasing sales of auto enterprises. Therefore, it is necessary to conduct research on user satisfaction with driverless

technology so as to provide suggestions for auto enterprises and driverless technology suppliers. The autonomous driving function studied in this paper belongs to the L2 level, which is not fully autonomous and requires the driver to maintain attention.

2. Introduction to Common Driverless Functions

Functions of driverless technology are still increasing, but they are mainly divided into two categories based on an existing framework. One is driverless technology that uses the camera as the data collection tool, and the other uses lidar [2]. However, mixed use of two technologies is the mainstream nowadays. Driverless functions provided mainly include adaptive cruise control, forward collision warning, autonomous emergency braking, lane-keeping assist, lane departure warning, stated-speed sign recognition, blind spot detection system, parking distance control system, rear cross-traffic alert, and door open warning system [2]. Among them, data are provided by cameras in the first six functions due to the visual field, while the data are provided by lidar in the remaining five functions [3].

The specific functions of automatic driving technology mainly have two sets of programs: one is pure visual perception and the other is laser radar. The supporters of the visual plan believe that humans can be qualified drivers through visual information with brain processing. So cameras and deep learning neural networks and computer hardware can achieve a similar effect. Representing companies of the visual plan include Tesla and Baidu.

The radar group uses mechanical radar, millimeter wave radar, ultrasonic radar, and multichannel cameras to achieve commercial production of L4. Representative enterprises include Robotaxi, BYD, and Nio.

The image sensor in the vision scheme can obtain complex environment information with a high frame rate and resolution, and the price is cheap. However, the image sensor is a passive sensor, which does not emit light itself. The imaging quality is greatly affected by the environmental brightness, and the difficulty of completing the perception task will be greatly increased in a harsh environment. However, data obtained by the visual scheme are more similar to the real world perceived by human eyes with characteristics of light hardware and heavy software. Due to the low price of the camera, the visual solution has an obvious cost advantage and is easier to pass the vehicle regulation test. In addition, the image data obtained by the camera are more similar to the real world perceived by human eyes, and the shape is most similar to human driving. The high resolution and high frame rate imaging technology also make the perceived environmental information richer. However, camera perception is limited in a dark environment, and accuracy and security are reduced. Moreover, its requirements for software are significantly increased because of presence of the visual scheme in the background of lower hardware requirements. So it needs to rely on powerful algorithms to ensure the efficiency of image processing, command delivery, and processing.

Laser radar is a kind of precise three-dimensional position sensor, which is essentially laser detection and ranging, and its principle is the precise rendering of the 3 d structure information of the target by transmitting and receiving laser detection and the distance between the target according to the target surface reflection energy, reflection spectrum amplitude, frequency and phase information. As an active sensor, radar can obtain the depth information of the target by emitting a pulse laser and detecting the scattering light characteristics of the target. It has the characteristics of high precision, large range, and strong anti-interference ability. However, the data obtained by radar are sparse and disordered, which are difficult to be directly used, and the monochromatic characteristics of a laser make it unable to obtain color and texture information. Although the ability of ranging description of the surrounding environment is outstanding, it has too fatal shortcomings, so it must be complementary with other sensors.

Adaptive cruise control mainly helps the driver to keep the same speed when the vehicle is in the front and the preset time headway [4]. The driver can set the desired speed and the time headway to the vehicle in the front. When the camera detects that the vehicle in the front is slowing down, the speed will also be automatically decelerated accordingly. If the traffic jam is relieved, the vehicle will steer at the selected speed again.

Forward collision warning warns the driver of pedestrians, bicycles, or vehicles in the front with visual and audible signals [5]. This function can prevent a car from colliding or reducing its speed when a collision happens. Besides, it can also help the driver if the car is at risk of colliding with pedestrians, cyclists, or other vehicles.

Autonomous emergency braking is a kind of auxiliary function, which can help the driver avoid collisions in traffic jams. For example, if the traffic becomes complex while at the same time, the driver is in the condition of low concentration, a collision may possibly happen in this situation [6]. When the vehicle is at imminent risk of collision, this function can assist the driver by automatically braking the vehicle or steering clear of the obstacles if the driver fails to act in time.

Lane-keeping assist aims at preventing the driver from accidental lane departure in certain situations on highways or arterial roads [7].

Lane departure warning uses audible and light signals to warn the driver when the vehicle departs from the lane. Stated-speed sign recognition can help the driver observe speed signs when the vehicle passes by [8]. The difference between a lane-keeping system and a lane departure warning is that one is a system for keeping a straight line, and the other is a system for warning of lane deviation.

The blind spot detection system is an auxiliary function for avoiding the blind spot vision of the driver. The warning lights are put on the outside rear mirror on both sides. It is not a substitute function but a complementary function for safe driving and outside rear mirror usage [6].

Parking distance control systems and door open warning systems use lidar to recognize obstacles so as to help users park or get on and off more safely.

The lane change assist system provides driving assistance when changing lanes to overtake, whether it is your vehicle or other vehicles.

The unmanned driving function introduced in this paper is a combination plan of pure vision and radar, which has no reference for the pure vision plan.

3. Satisfaction Research on Driverless Functions Based on the KANO Model

3.1. Basic Concept. A KANO model is a two-dimensional cognitive model that was established in 1984 by Noriaki Kano, a famous Japanese quality management expert [9]. He was inspired by Herzberg's dual-factor theory. The model is about the relationship between quality attributes and user satisfaction. It breaks the traditional single-dimensional cognition of quality and believes that even when product quality meets user cognition, users may not be satisfied. In this model, the relationship between product quality and user cognition is built, and quality attributes are divided into the following five categories. The first is an attractive quality. In this case, the quality attribute of products makes users feel surprised and user satisfaction will be greatly improved. Even when a certain quality attribute does not meet user cognition, users will not feel dissatisfied. The second is one-dimensional quality, which means when the quality attribute meets user cognition, users will feel satisfied. Otherwise, users will feel dissatisfied. The third is must-be quality. In this case, only when the quality attribute meets user cognition, users will feel satisfied. The fourth is indifferent quality, which means the quality attribute is not concerned by users and is unrelated to user satisfaction. The last is reversal quality. In this case, when the quality attribute meets user cognition, users may feel dissatisfied instead.

3.1.1. Attractive Demand. Attractive demand can be described as the attribute of surprise. Under this circumstance, customers will feel satisfied when their requirements are met; however, they will not feel dissatisfied even when their requirements are not met. For driverless functions, the key to achieving performance excellence and gaining a competitive advantage is to pay more attention to attractive attributes on the basis that the basic attribute is met. For attractive demand, customer satisfaction will rise sharply along with the increase of the satisfaction degree of customer expectation. Furthermore, once customer expectation is met, the customer may still feel very pleased even though the products or services are not that satisfying [10].

3.1.2. One-Dimensional Demand. One-dimensional demand is also called performance demand. It refers to the condition in which customer satisfaction is proportional to the satisfaction degree of customer needs. In this case, the more the customer needs are met, the more the customer will feel satisfied. The more the products or services provided by enterprises exceed customer expectations, the more satisfied customers are [11]. On the contrary, when such needs are not met, customer satisfaction may decrease significantly. Therefore, the driverless function should attach significance to this kind of attribute and meet one-dimensional demand to the greatest extent.

3.1.3. Must-Be Demand. Must-be demand is the essential quality requirements of certain products or services. It refers to the basic requirements of customers for the products or services provided by enterprises. Customers consider that the products must have a certain kind of attribute or function. According to Maslow's hierarchy of needs, when the quality attribute does not meet customer needs, customers feel dissatisfied. However, even when the quality attribute meets customer needs, customers may still feel dissatisfied [12]. Therefore, the driverless function should first meet must-be demand because it is the most basic requirement of users.

3.1.4. Indifferent Demand. Indifferent demand is the attribute of products or services that customers do not care about. Customers pay no attention to this attribute whether it is provided or not. The driverless function should not waste resources to meet the indifferent demand of customers because it will not lead to customer satisfaction or dissatisfaction [13].

3.1.5. Reversal Demand. Reversal demand is the quality attribute that customers dislike. It refers to the quality attributes that may cause strong dissatisfaction or low levels of satisfaction. The reason is that not all customers have similar preferences [14]. When customers' reversal demand is met, they may feel more dissatisfied. Suppliers of driverless technology should resolutely make such attributes disappear.

A successful product function can not only meet the basic needs of users but also meet user expectations. At the same time, such a product can even allow users to experience exciting feelings. In addition, indifferent demand is used to explore user requirements, and reversal demand should be avoided as much as possible. In designing products and functions, it is necessary to consider the five categories of demand. Structural partitions should be made to all functions in order to clearly understand the value and significance of each product function. Furthermore, from these five categories, product designers can know whether a product function is needed or not so as to find goals for product design and analysis. In this way, customers can be better served and product function can be improved.

3.2. Two-Dimensional Satisfaction Pattern. According to the two-dimensional satisfaction pattern, the opposite concept of "satisfied" is not "dissatisfied." "Satisfied" and "dissatisfied" should be regarded as two different and parallel concepts, which means that the opposite of "satisfied" is "not satisfied," while the opposite of "dissatisfied" is "not dissatisfied". Therefore, the relationship between "satisfied" and "dissatisfied" is not "either-or." For example, employees may

Table 1: Evaluation results of the KNAO model.

Function/Service		Dysfunctional				
		Dislike (1 point)	Live-with (2 points)	Neutral (3 points)	Must-be (4 points)	Like (5 points)
Functional	Dislike (1 point)	Q	R	R	R	R
	Live-with (2 points)	M	I	I	I	R
	Neutral (3 points)	M	I	I	I	R
	Must-be (4 points)	M	I	I	I	R
	Like (5 points)	O	A	A	A	Q

A : attractive, O : one-dimensional, M : must-be, I : indifferent, R : reversal, and Q : questionable.

not necessarily feel dissatisfied when satisfying factors are removed. Similarly, the removal of dissatisfying factors will not necessarily lead to employee satisfaction. Table 1 shows the relationship between the two-dimensional pattern of satisfaction and the attribute of the product defined by the KANO model.

We can see the relationship between functional requirements and satisfaction based on the KANO model (see Table 1).

Firstly, in the questionnaire, the questions of the same function or service will be asked in both positive (P) and negative (N) aspects.

Secondly, the positive question is like "if we can provide ** function or service, you feel. . . ." The negative question is like "if we cannot provide ** function or service, you feel. . . ."

Thirdly, we can get six attributes finally according to the answers.

Fourthly, attractive means that functions or services have exceeded user expectations. One-dimensional means certain functions or services may improve user satisfaction, and it will decrease without such functions or services. Must-be refers to the condition that certain functions or services will not improve user satisfaction, but it will decrease without such functions or services. Indifferent means that user satisfaction will remain the same with or without certain functions or services. Reversal refers to the condition that user satisfaction may increase without certain functions or services. Questionable means that users may not understand the questionnaire or give a wrong answer.

4. Empirical Analysis

According to the previous introduction to driverless functions, we have developed a questionnaire. For the same function or service, we have prepared two aspects of questions, positive or negative. Each question can be chosen from 1 to 5, representing dislike, live with, neutral, must-be, and like, respectively. The survey was completed online, and a total of 181 valid questionnaires were returned. Judging from the demographic characteristics, the proportion of males and females is almost equal to 50%. People who participated in the survey are mostly aged 35 to 45 with nearly 30%. Besides, the majority of participants have driving experience for more than 2 years, and all questionnaire users have used the self-driving functions (see Table 2).

According to Table 2, functions such as blind spot detection systems and rear cross-traffic alerts belong to attractive attributes. Adaptive cruise control belongs to the one-dimensional attribute. Forward collision warning, autonomous emergency braking, and stated-speed sign recognition belong to must-be attributes. Lane-keeping assist, lane departure warning, parking distance control system, and door open warning system belong to indifferent attributes. The lane change assist system belongs to the reversal attribute. No functions belong to questionable attributes.

In summary, we can infer that users have expectations when a driverless function can improve driving ability in the blind spot and indirect field of vision. In other words, users hope that driverless technology can solve the problems of the

Table 2: Results based on the KANO model.

Function/Service	A	O	M	I	R	Q	Results	Better	Worse
adaptive cruise control (P) & adaptive cruise control (N)	27.07%	29.83%	19.89%	22.10%	0.55%	0.55%	One-dimensional	57.54%	-50.28%
forward collision warning (P) & forward collision warning (N)	0.55%	1.10%	63.54%	33.70%	0.55%	0.55%	Must-be	1.68%	-65.36%
autonomic emergency braking (P) & autonomic emergency braking (N)	3.31%	4.97%	43.65%	26.52%	8.84%	12.71%	Must-be	10.56%	-61.97%
lane keeping assist (P) & lane keeping assist (N)	0.55%	0.00%	2.21%	85.08%	3.87%	8.29%	Indifferent	0.63%	-2.52%
lane departure warning (P) & lane departure warning (N)	3.87%	0.00%	0.55%	91.71%	3.87%	0.00%	Indifferent	4.02%	-0.57%
stated-speed sign recognition (P) & stated-speed sign recognition (N)	18.23%	9.94%	44.75%	21.55%	5.52%	0.00%	Must-be	29.82%	-57.89%
blind spot detection system (P) & blind spot detection system (N)	60.22%	13.81%	2.21%	19.89%	3.87%	0.00%	Attractive	77.01%	-16.67%
parking distance control system (P) & parking distance control system (N)	1.10%	6.63%	14.36%	59.67%	16.57%	1.66%	Indifferent	9.46%	-25.68%
lane change assist system (P) & lane change assist system (N)	7.73%	3.87%	5.52%	33.70%	49.17%	0.00%	Reversal	22.83%	-18.48%
rear cross traffic alert (P) & rear cross traffic alert (N)	34.25%	22.10%	6.63%	32.60%	4.42%	0.00%	Attractive	58.96%	-30.06%
door open warning system (P) & door open warning system (N)	1.10%	12.71%	29.28%	54.70%	2.21%	0.00%	Indifferent	14.12%	-42.94%

A : attractive, O : one-dimensional, M : must-be, I : indifferent, R : reversal, and Q : questionable.

blind spot and indirect field of vision they face when driving. The more this function can meet user expectations, the higher user satisfaction will be. However, the user will not show obvious dissatisfaction even when the expectations are not met. The reason may be that users also have the ability to deal with problems of the blind spot and indirect field of vision when there is no driverless technology.

Adaptive cruise control is expected by users according to the questionnaire. That is to say, most users hope that driverless functions can help them free their hands and enjoy a more relaxed driving experience.

For forward collision warning, autonomous emergency braking, and stated-speed sign recognition, users consider that they belong to must-be attributes. In a driverless environment, the greatest concern of users is safety. Therefore, users think that driverless technology must be equipped with such functions as warning of road conditions ahead and emergency braking afterwards. In addition, users consider stated-speed sign recognition necessary because they are not willing to passively receive tickets for overspeeding in the case that cars are controlling the speed automatically. As a result, stated-speed sign recognition is also indispensable.

For lane-keeping assist and lane departure warning, users see no impact on their acceptance of driverless technology. After all, land departure is an obvious and easily perceived driving situation for most drivers. Besides, the parking distance control system and door open warning system are not attractive to users. It is mainly because there are not many accidents reported when parking and getting off the car without the driverless functions.

For the lane change assist system, some users think it is unnecessary out of the distrust of the car changing lanes by itself.

Table 3: Summarized results based on the KANO model KANO (numerical).

Function/Service	A	O	M	I	R	Q	Results	Better	Worse
adaptive cruise control (P) & adaptive cruise control (N)	49	54	36	40	1	1	One-dimensional	57.54%	-50.28%
forward collision warning (P) & forward collision warning (N)	1	2	115	61	1	1	Must-be	1.68%	-65.36%
autonomic emergency braking (P) & autonomic emergency braking (N)	6	9	79	48	16	23	Must-be	10.56%	-61.97%
lane keeping assist (P) & lane keeping assist (N)	1	0	4	154	7	15	Indifferent	0.63%	-2.52%
lane departure warning (P) & lane departure warning (N)	7	0	1	166	7	0	Indifferent	4.02%	-0.57%
stated-speed sign recognition (P) & stated-speed sign recognition (N)	33	18	81	39	10	0	Must-be	29.82%	-57.89%
blind spot detection system (P) & blind spot detection system (N)	109	25	4	36	7	0	Attractive	77.01%	-16.67%
parking distance control system (P) & parking distance control system (N)	2	12	26	108	30	3	Indifferent	9.46%	-25.68%
lane change assist system (P) & lane change assist system (N)	14	7	10	61	89	0	Reversal	22.83%	-18.48%
rear cross traffic alert (P) & rear cross traffic alert (N)	62	40	12	59	8	0	Attractive	58.96%	-30.06%
door open warning system (P) & door open warning system (N)	2	23	53	99	4	0	Indifferent	14.12%	-42.94%

Except for discussing the attributes based on the KANO model, the better-worse coefficient can be calculated according to the percentage of each attribute. It indicates the degree of satisfaction increase or dissatisfaction removal by certain functions. After satisfaction increases, $\text{better} = (A + O)/(A + O + M + I)$. After dissatisfaction removal, $\text{worse} = -1 * (O + M)/(A + O + M + I)$. The better coefficient can be interpreted as a coefficient after satisfaction increase. The value is commonly positive, representing that if a certain function is provided, user satisfaction will increase. The larger the positive value or the closer the value is to 1, the greater the impact on user satisfaction and the stronger the effect of satisfaction increase. In this case, user satisfaction will increase faster. The worse coefficient can be interpreted as a coefficient after dissatisfaction removal. The value is commonly negative, representing that if a certain function is not provided, user satisfaction will decrease. The larger the negative value or the closer the value is to -1, the greater the impact on user dissatisfaction and the stronger the effect of satisfaction decrease. In this case, user satisfaction will decrease faster. Therefore, functions or services should be considered first if the absolute value of the better-worse coefficient is higher.

After calculating better and worse coefficients, we can get the numerical results based on the KANO model (see Table 3).

According to Table 3, we find out that users are most satisfied with functions such as adaptive cruise control, blind spot detection system, and rear cross-traffic alert, which reflects that users are pursuing a more relaxed and safer driverless experience. On the contrary, users are least satisfied with functions like forward collision warning and autonomous emergency braking. However, these two functions are still considered essential by users, which shows that driverless technology should urgently improve these two functions to better satisfy users. There is a high worse coefficient in the door open warning system, indicating that users are in great need of this function. If this function is cancelled or poorly designed, users will have a bad experience with the whole driverless driving function.

5. Discussion and Conclusion

More newly produced cars are now equipped with driverless technology and user satisfaction with driverless technology is increasingly affecting their purchase choices. From the satisfaction research on driverless functions based on the KANO model, it is found that users are dependent on functions like forward collision warning, autonomous emergency braking, and stated-speed sign recognition, which are considered essential in driverless vehicles.

Therefore, car manufacturers or driverless technology suppliers should pay attention to the research and development of these technologies; otherwise, they will lose customers.

Secondly, users have high expectations for functions such as blind spot detection systems and rear cross-traffic alerts, but they are also very dissatisfied with these two functions. Car manufacturers and driverless technology suppliers should not only consider it a warning but also an opportunity. The better these two functions are, the more recognition can be obtained from users.

Lane-keeping assist, lane departure warning, parking distance control system, and door open warning system belong to indifferent attributes. Users are not too fond of these functions and consider them dispensable. Therefore, relevant enterprises should seek to improve these functions in order to improve user recognition, but the priority is not high.

The lane change assist system has been criticized by users, which is an unexpected situation. Therefore, relevant enterprises should investigate user requirements and feedback in time so as to improve this function.

Data Availability

The data that support the findings of this study are available from the corresponding author upon reasonable request.

Conflicts of Interest

The authors declare no conflicts of interest with respect to the research, authorship, and/or publication of this article.

References

[1] D. Bissell, T. Birtchnell, A. Elliott, and E. L. Hsu, "Autonomous automobilities: the social impacts of driverless vehicles," *Current Sociology*, vol. 68, no. 1, pp. 116–134, 2020.

[2] N. J. Goodall, "How to think about driverless vehicles," *American Journal of Public Health*, vol. 108, no. 9, pp. 1112-1113, 2018.

[3] J. Weber and F. Kröger, "Introduction: autonomous driving and the transformation of car cultures," *Transfers*, vol. 8, no. 1, 2018.

[4] W. Shiers, "Safety first and second," *Commercial Motor*, vol. 2305802 pages, 2018.

[5] D. Beasley, *The Importance of Rich Data*, Utility Week, 2018.

[6] D. Johnson, "Lessons from a semi-driverless vehicle," *ISHN*, vol. 51, no. 10, 2017.

[7] *Global Driverless/SelfDriving Car Market to Witness Rapid Growth till 2025, Reveals New Market Research Report*, M2 Presswire, 2017.

[8] S. B. SeoinKim, "Network approach of autonomous Car's industry structure," *International Business Review*, vol. 21, no. 3, pp. 39–68, 2017.

[9] K. Al Rabaiei, F. Alnajjar, and A. Ahmad, "Kano model integration with data mining to predict customer satisfaction," *Big Data and Cognitive Computing*, vol. 5, no. 4, p. 66, 2021.

[10] U. A. Kirgizov and C. Kwak, "Quantification and integration of Kano's model into QFD for customer-focused product design," *Quality Technology & Quantitative Management*, vol. 19, no. 1, pp. 95–112, 2022.

[11] S. K. Dewi and A. Nugraha, "Quality of service evaluation based on importance performance analysis method and the kano model," *Journal of Physics: Conference Series*, vol. 1764, no. 1, p. 012199, 2021.

[12] A. P. Lu, Y. F. Sun, Z. Lei, and C. J. LiJingLiuHu, "Kkma - a calculation method for KANO classification based on user reviews," *IOP Conference Series: Materials Science and Engineering*, vol. 1043, no. 2, p. 022062, 2021.

[13] A. Ishak, R. Ginting, B. Suwandira, and A. Fauzi Malik, "Integration of kano model and quality function deployment (qfd) to improve product quality: a literature review," *IOP Conference Series: Materials Science and Engineering*, vol. 1003, no. 1, p. 012025, 2020.

[14] F. Macieira, T. Yanaze, and M. Oliveira, "Models of satisfaction antecedents: a brief review. An integrative literature review of the most discussed satisfaction models in marketing studies," *International Journal of Services and Operations Management*, vol. 36, no. 3, p. 348, 2020.

Hindawi
Mobile Information Systems
Volume 2022, Article ID 7427899, 11 pages
https://doi.org/10.1155/2022/7427899

Research Article

Control System and Speech Recognition of Exhibition Hall Digital Media Based on Computer Technology

Yu Zhao

School of Visual Communication Design, LuXun Academy of Fine Arts, Shenyang 110000, Liaoning, China

Correspondence should be addressed to Yu Zhao; 1631180879@xzyz.edu.cn

Received 15 June 2022; Revised 26 July 2022; Accepted 30 July 2022; Published 30 August 2022

Academic Editor: Yajuan Tang

With environmental noise in the exhibition hall, speakers tend to change their speech production to preserve intelligible communication. While great evolution has been prepared in Automatic Speech Recognition (ASR), important performance deprivation occurs in a noisy environment. The assessment of the degree of speech impairment and the efficacy of computer recognition of impaired speech are distinctly and independently executed. Convolutional Neural Networks (CNN) have been effectively employed in speech recognition and computer vision tasks. Hence, this study uses the Deep Convolutional Neural Network-based Automatic Speech Recognition Model (DCNN-ASRM) for effective speech recognition in the noisy exhibition hall. This study configures the filter sizes, poolings, and input feature map. The filter size and pooling are decreased, and the dimension of the input feature is comprehensive to permit increasing convolution layers. Furthermore, an in-depth analysis of the proposed DCNN-ASRM model discloses critical features, like fast convergence speed, compact model scales, and noise robustness in speech recognition. The simulation analysis shows that the suggested DCNN-ASRM model enhances the recognition accuracy ratio of 98.1%, performance ratio of 97.2%, and noise reduction ratio of 96.5% and reduces the word error rate by 9.2% and signal-to-noise ratio by 10.3% compared to other existing models.

1. Introduction of Speech Recognition in Exhibition Hall

Describing the acoustic environment of performance spaces like concert halls, theatres, exhibition halls, and auditoria has been one of the key topics in room acoustics and speech recognition studies during the past decades [1]. For spaces where the major function is sound-associated (e.g., spaces for performing or listening), clear criteria connected to measurable variables must be in place to evaluate acoustic performance and quality [2]. The general deliberation on inclusion ensures that the case fits the suitable building type for crowd transit (e.g., exhibition/museum spaces, shopping malls, and transportation stations/hubs) [3]. Numerous visitors, conversations, and product presentations cause noise levels in trade fairs and exhibitions to rise quickly [4, 5]. Many of the most advanced speech recognition systems use the Mel-Frequency Cepstral Coefficient (MFCC) and the Perceptual Linear Prediction (PLP) cepstral coefficient (like MFCCs) based on human auditory models, two types of cepstral coefficients that are computed utilizing discrete cosine transform on smoothed power spectra [6]. However, these systems still execute poorly in a noisy environment (e.g., in situations with additive noise), and magnified performance deprivation has been perceived under the detached (far-fields) talking state [7]. To attain robust automatic speech recognition, it is more significant to cooperatively optimize the acoustic and beam-forming model to maximize the ASR performance [8]. In noise, speakers modify their vocal efforts. For an extensive noise level range, the dependency among voice Sound Pressure Level (SPL) and noise sound pressure level is almost linear, with diverse slopes when reading text or communicating with others [9]. Vowels tend to get more attention than consonants in increasing vocal effort, which is not universal among phones [10]. The pitch rises with an increase in subglottal pressure and tension in the laryngeal musculature due to the adjustment in a vocal effort [11]. When

represented in semitones and SPL, the pitch varies roughly linearly with speech intensity [12].

Speech recognition is an artificial intelligence-enhanced technology that converts a person's speech from an analog form to a digital one. An improved computer program then uses digital speech for additional processing [13]. Speech recognition is the ability to speak to a computer and have it comprehend and interpret what people speak. Spoken language is decoded and translated into machine form. A natural language such as English is used to communicate between people and computers in Natural Language Processing (NLP) [14]. Although extraordinary performance has been realized in ASR with the introduction of Convolutional Neural Networks (CNNs), the performance still reduces dramatically in far-field and noisy situations [15]. To attain robust speech recognition, multiple microphones can improve speech signals, reduce noises and reverberation, and enhance Automatic Speech Recognition performance [16]. The low signal-to-noise ratio (SNR) in these noisy situations creates CNN more susceptible to the mismatch issue [17]. CNNs have numerous benefits: firstly, speech spectrograms have local associations in both frequency and time, and CNNs are well-matched to model those connections overtly via local connectivity, whereas Deep Neural Networks (DNN) have a comparatively more complex encoding of this data [18]. Secondly, translational invariance, like frequency shift because of speaking style or speaker variation, can be more effortlessly seized by CNNs than DNNs [19, 20]. Thus, in CNNs, a more affluent set of features can be demoralized than traditional low-dimensional feature vectors, like PLP coefficients and MFCCs.

The major contribution of the research is

(i) Designing the Deep Convolutional Neural Network-based Automatic Speech Recognition Model (DCNN-ASRM) for speech recognition in the noisy exhibition hall.

(ii) Evaluating the DCNN shows noise robustness greater than other models in noisy situations.

(iii) The simulation outcomes have been executed, and the recommended DCNN-ASRM model enhances the accuracy and performance compared to other existing models.

The rest of the study is systematized: Sections 1 and 2 discuss the introduction and existing speech recognition methods. In Section 3, DCNN-ASRM has been proposed. In Section 4, experimental results have been executed. Finally, Section 5 concludes the research paper.

2. Literature Survey

Song et al. [21] proposed the Learning-to-Rescore (L2RS) mechanism for ASR. L2RS uses a wide variety of textual data from state-of-the-art NLP models and spontaneously decides their weights to restore the N-best lists for ASR systems. These characteristics included Bidirectional Encoder Representation for Transformer (BERT) sentence topic vector, embedding, perplexity score generated by n-gram Language Model (LM), topic modeling BERT LM, LM, and RNNLM to train an algorithm for scoring. According to their research, L2RS surpasses standard rescoring techniques and its Deep Neural Network equivalents by a significant enhancement of 20.67% in terms of the NDCG@10 in terms of L2RS. L2RS enables the development of a more accurate rescoring model for ASR.

Han et al. [22] suggested the ContextNet for ASR with Global Context. New CNN-RNN-transducer architecture, termed ContextNet, focuses on a new study in this paper. ContextNet has a fully convolutional encoder that adds global context data into the convolution layer by including squeeze-and-excitation modules. In addition, they presented a simple scaling mechanism for ContextNet's widths which offers a fair trade-off between computation and accuracy. CNN models previously released have had a hard time competing with this model on the LibriSpeech test. Small Automatic Speech Recognition (ASR) models may be found using the suggested design, limiting the network's breadth to a minimum. A preliminary analysis of a bigger and more difficult data set supports their findings.

Isobe et al. [23] recommended the Deep Canonical Correlation Analysis (DCCA) for speech recognition in noisy environments. DCCA provides projections from two modalities into a single space to increase the correlation of projected vectors. Automatic Speech Recognition (ASR) may be more robust by employing DCCA approaches with audio and visual modalities, recovering noisy audio characteristics, and training an ASR model using the additional data. Our technique was tested using an audio-visual corpus CENSREC-1-AV and a noise database DEMAND. Our DCCA-based speech recognizers outperformed traditional ASR and featured fusion-based audio-visual speech recognition systems in terms of accuracy.

Hidayat and Winursito [24] discussed the Mel-Frequency Cepstral Coefficients for Improved Wavelet-Based Denoising (MFCC-IWBD) on Robust Speech Recognition. The Fast Fourier Transform (FFT) step of the MFCC was used. The denoising procedure utilizing Wavelet was only applied to data with noise, as determined by the FFT analysis findings. A total of eleven isolated English words were used in the research, along with various kinds of background noise. According to the research, this approach was more accurate than standard wavelet denoising methods for SNRs of 10 dB, 15 dB, and 20 dB when utilizing a Fejer Korovkin 6 wavelet type.

Based on the survey, there are several challenges to existing approaches such as Learning-to-Rescore (L2RS), ContextNet, Deep Canonical Correlation Analysis (DCCA), and Mel-Frequency Cepstral Coefficients for Improved Wavelet-Based Denoising (MFCC-IWBD) in achieving high accuracy, performance, signal-to-noise ratio, noise reduction, and word error rate (WER). The following section discusses the proposed DCNN-ASRM briefly.

3. Deep Convolutional Neural Network-Based Automatic Speech Recognition Model (DCNN-ASRM)

The most important component of the Human-Computer Interface (HCI) system is speech recognition, which

translates the human auditory function. Automatic Speech Recognition (ASR) is making its way into our everyday lives at the same time as advances in computer technology are being made, and its applications are becoming more prevalent. There are two main causes for the present difficulties with speech recognition: extended range and noisy environments in the exhibition hall. This emphasizes the need for even higher accuracy systems capable of handling complex ASR tasks. The interruption of the channel and the unwanted background noise will always have a negative impact on the performance of the ASR system's recognition capabilities. Strategies for reducing noise may be applied differently to the ASR system. For instance, these techniques are speech enhancement upon the signal levels, extraction of the robust feature vector, and adjustment of the back-end acoustic model. In the real world, the problem of ambient noise cannot be considered in the preliminary phase, and it is not easy to anticipate how it will play out. The strategies for reducing noise will not depend on any suppositions about noisy settings or training variables, and they should function well across various noise circumstances. The basic objective of a feature extractor designed to be sound is to make as few assumptions as possible or none at all regarding the noise information. This is one of the difficult challenges that has recently been favoring research fields that are still being conducted. The capacity of different speech classes is appropriate and relevant with the interference of background noise and the variable nature of speaker characteristics. Hence, this paper proposes the DCNN-ASRM model for speech recognition in exhibition halls.

Figure 1 shows the proposed DCNN-ASRM model. The functionality of an ASR system can be described as the extraction of several speech variables from acoustic speech signals for every word or subword unit. The cascaded model contains two steps. The initial step is the denoising step, in which the denoised spectrogram is produced by eliminating the noise from the noisy speech signal. An Audio-Visual Speech Recognition (AVSR) model utilizes visual speech data, and the acoustic data are utilized by a normal ASR model. Audio and video data can be incorporated by feature or decision fusion. Mel-Frequency Cepstral Coefficient (MFCC) is one of the most accurate feature extraction methods used in Automatic Speech Recognition. The feature vector is extracted from the frequency spectrum of the windowed speech frame. The output is a speech signal or vocal sound accepted in all languages on a computer.

3.1. Problem Formulation. Let us preassume that a microphone input signal $y(t)$ is modeled as

$$y(t) = w(t) * g(t) + m(t). \tag{1}$$

As shown in equation (1), $w(t)$ denotes the non-reverberant speech signal, $g(t)$ indicates exhibition Room Impulse Response (RIR) among the speaker and the microphone, $*$ represents the convolution operator, and $m(t)$ signifies additive noise signal.

In the short-time Fourier transform (STFT) domain, the convolution is estimated as a multiplication operation, and equation (1) can be modified as

$$y(k, f) = J(k) \cdot w(k, f) \cdot g(k, f) + m(k, f). \tag{2}$$

As inferred from equation (2), $k \in \{0, \ldots, K-1\}$ and $f \in \{0, \ldots, F-1\}$ are frame and frequency index. The term $J(k)$ denotes the activity of $w(k, f)$ with,

$$J(k) = \begin{cases} 0, & \sum_{f=0}^{F-1} w(k, f) < Th, \\ 1, & \sum_{f=0}^{F-1} w(k, f) \geq Th. \end{cases} \tag{3}$$

As shown in equation (4), Th denotes a predefined threshold applied on the clean signals.

The automatic speech detection goal is to accurately detect frames in which the speaker is active given a noisy reverberant signal,

$$U(k) = q(J(k) = 1|y). \tag{4}$$

3.2. Convolutional Neural Network in Speech Recognition. A convolution layer does the convolution on the prior layer's feature maps utilizing filters and then augments bias scalars to the respective feature maps, trailed by nonlinear operations. Convolutions can be observed as operations employed to feature maps utilizing filters, where both feature maps and filters can be signified as a matrix. During this process, the enclosed region of feature maps is termed receptive fields, and the size is equal to the size of filters. At every stage, receptive fields execute dot products with filters and give one output, and every output collected during the progression will form fresh feature maps. The whole progression of a convolution layer is articulated as an expression given as follows:

$$g^{(k)} = \rho\left(S^{(k)} * g^{(k-1)} + a^{(k)}\right). \tag{5}$$

As discussed in equation (5), $g^{(k-1)}$ and $g^{(k)}$ denote feature map in two successive layers. $*$ represents the convolutional operator is achieved within filters $S^{(k)}$ and the feature maps $g^{(k-1)}$. The bias $a^{(k)}$ is auxiliary, and lastly, activation functions $\rho(\cdot)$, usually ReLU or sigmoid, can be employed to produce the output of the convolution layer. Expression equation (5) shows the modest setting where only one feature map occurs in prior layers. When numerous feature maps are contemporary in prior layers, the outcomes of convolution operation are initially added before accumulating biases.

Figure 2 shows the convolution and pooling operation. Pooling layers execute down-sampling on the feature map of prior layers and produce novel ones by decreased resolutions. Presently, the most famous configuration for convolutional neural networks is utilized in speech recognition, which has 2 convolution layers with 256 feature maps, 9×9 filters with 1×3 poolings in the initial convolution layer and

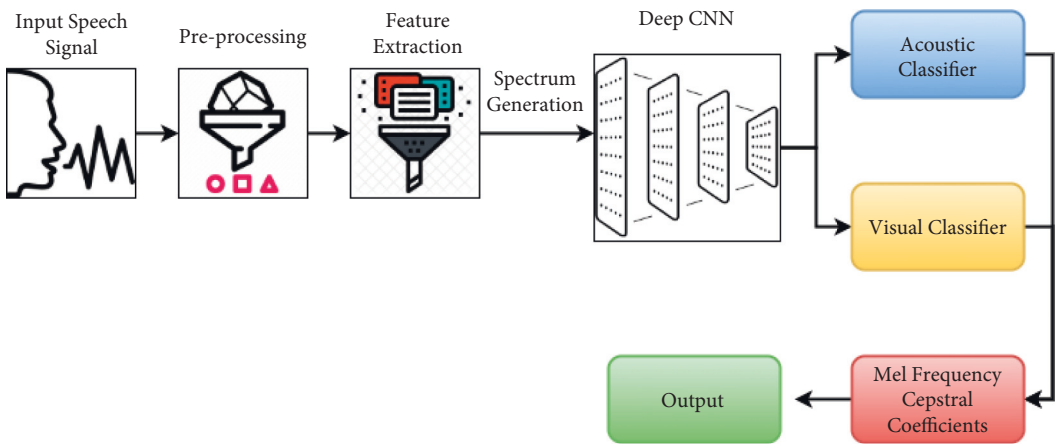

Figure 1: Proposed DCNN-ASRM model.

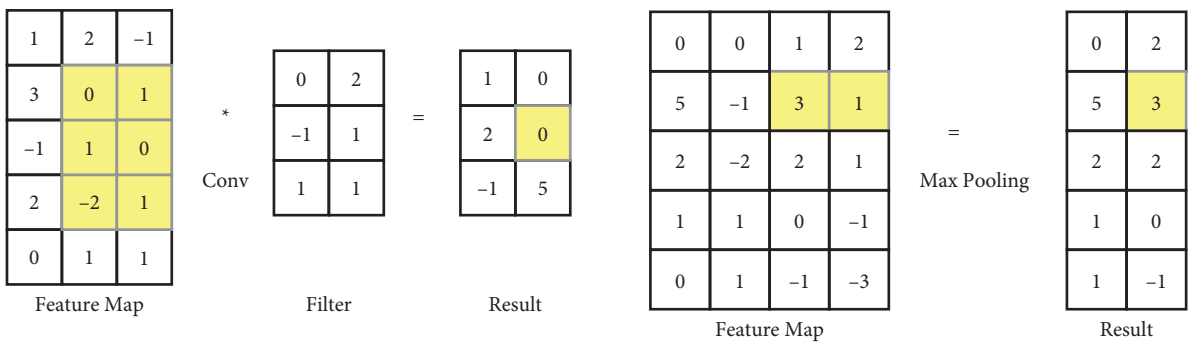

Figure 2: Convolution and pooling operation.

3×4 filters in the additional convolution layer and without poolings. This structure is utilized as the reference Convolutional Neural Network in this study. The number of convolution layer variables is comparatively minor since the filters are collective between every receptive field in one feature map. The variable number of one convolution layer can be computed as

$$\text{parameters}^{(k)} = \text{filtersize}^{(k)} \times n^{(k)} \times n^{(k-1)}. \quad (6)$$

As shown in equation (6), $n^{(k)}$ denotes the feature map in kth layers. Pooling layers achieve down-sampling on prior layers' feature maps and produce novel ones with a condensed resolution. In this research, max-pooling is utilized in the Convolutional Neural Network model.

Figure 3 shows the mismatches between testing and training conditions. The mismatch between testing and training conditions because of reverberation can be distinctly viewed in signals, features, and model spaces. Typical features are the Mel-Frequency Cepstral Coefficients, the formants, the pitch, the intensity of the speech signal, the vocal tract cross-sectional areas, and the speech ratio. Feature compensation and model adaptation are approaches that correspondingly work in the feature and model spaces. The notion is to decrease the mismatch between the perceived utterance and the actual speech models during utterance recognition. In feature compensation, this study maps the distorted features to evaluate the actual features so that the actual acoustic model can be utilized. This study maps the actual acoustic models to a converted model that better matches the detected utterance in model adaptation.

3.3. Aware Factor Training (AFT). Aware factor training normally integrates a vector representing acoustic state data into the network training progression to standardize the nonspeech unpredictability. An LSTM mechanism has concatenated the assisting factor depictions with the acoustic feature, the energy for noise, j-vector for the speaker, and room reverberations. This study uses an auxiliary feature in a combined framework to evaluate a speaker-dependent bias rather than concatenate them with the acoustic feature. The speaker-dependent bias can be integrated into any position in a NN, e.g., convolution layers or fully connected layers. The construction of the suggested united aware factor training is

$$a^{wk} = U_2^k \rho \left(U_1^k x^w + q_1^k\right), \quad (7)$$

$$p^{wk} = \rho \left(S^k p^{k-1} + a^{wk} + a^k\right). \quad (8)$$

As inferred from equations (7) and (8), p^{wk} denotes the speaker that altered the hidden output of layers k. a^{wk} indicates speaker-dependent biases. This work uses shallow adaptations neural network with one hidden layer. U_2^k, U_1^k, and q_1^k are the weight matrix and biases for the adaptation

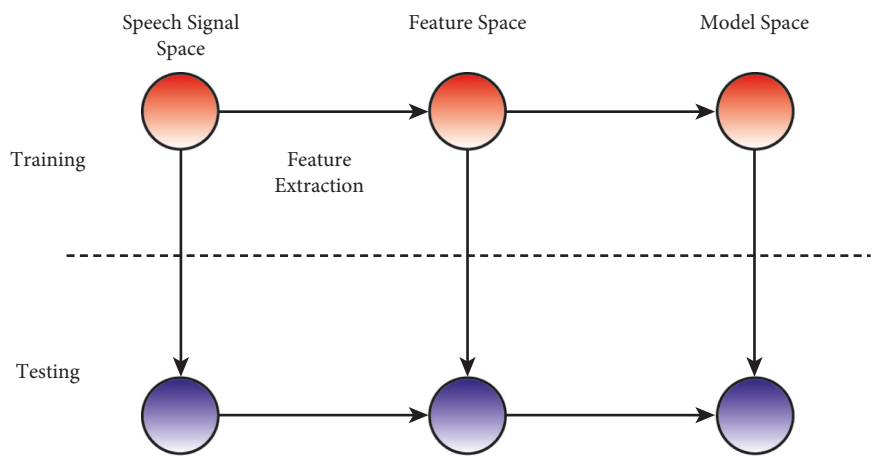

Figure 3: Mismatches among testing and training conditions.

neural network. x^w represents an auxiliary feature. S^k signifies the weight matrices employed to the output from the prior layer. a^k denotes independent speaker biases.

In this work, three positions have been compared, including (i) the acoustic feature input layers, (ii) the output of the first convolution layers, and (iii) the output of the initial fully linked layers, which trails the entire Convolutional Neural Network blocks. When biases are auxiliary to a convolution layer, they must be redesigned to 3-dim tensors. The speaker-dependent dimension bias a^{wk} that adapted output feature maps are provided by

$$\begin{aligned} a^{wk} &= U_2^k \rho\left(U_1^k x^w + q_1^k\right), \\ r^{wk} &= \text{reshape}\left(a^{wk}\right), \\ p_j^{wk} &= \rho\left(\sum_{i=1}^{M} S_{j,i}^k \oplus p_i^{k-1} \oplus a_j^k + r_j^{wk}\right). \end{aligned} \tag{9}$$

As shown in equation (9), p_i^{k-1} denotes jth feature maps of the speaker-adapted hidden output of layers k. r^{wk} denotes reshaped tensor. r_j^{wk} is the jth element in the tensor.

Figure 4 shows the frequency masking. In a naturalistic environment, simultaneous masking is a common occurrence. Using the Minimum Masking Threshold (MMT) to obscure watermarks, audio watermarking attempts to achieve this goal. This study offers an improved MFCC by merging it with the masking effect to extract strong acoustic information from loud utterances based on this consideration. This research can use masking models in feature extraction to evaluate which frequency components are more susceptible and how much noise influence may mix into the signal without being predicted. Furthermore, it can calculate the loudness of speech.

3.4. Adaptive Cluster Training (ACT). Figure 5 shows the adaptive cluster training. Different from making adaptations with the auxiliary feature as in the preceding subdivision, numerous factorized adaptation approaches have been suggested to straightly adapt the NN in the model domain in the past few years. Speaker-dependent matrices are utilized to form

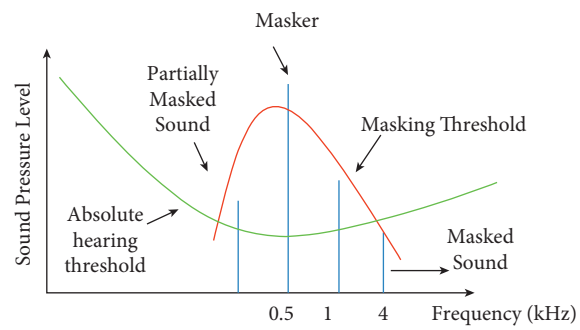

Figure 4: Frequency masking.

speaker-dependent hidden layers. The variance among those approaches is the model utilized to evaluate speaker-dependent matrices. Weight matrices bases have been computed as

$$N = \left\{\left\{N^1, \ldots N^k\right\}, \left\{S^1, \ldots, S^L\right\}\right\}. \tag{10}$$

As inferred from the equation (10), $N^k = [S_1^k, \ldots S_Q^k]$ denotes weight matrix basis of layer k and Q indicates the clusters. K represents the overall ACT layer. N^k signifies the weight matrices of non-ACT layer l, and L illustrates the overall non-ACT layer.

The transformation function of the speaker-dependent interpolation vectors is λ^{wk}.

$$\lambda^{wk} = \left[\lambda_1^{wk}, \ldots, \lambda_Q^{wl}\right]^T. \tag{11}$$

As discussed in equation (11), λ_c^{wk} denotes interpolation weights for cth clusters. The last adapted weight matrices for an assumed speaker w and the output are provided by

$$S^{wk} = \sum_{c=1}^{Q} \lambda_c^{wk} S_c^k, \tag{12}$$

$$p^{wk} = \rho\left(S^{wk} p^{k-1} + a^k\right). \tag{13}$$

The weight matrices are first decomposed by singular value decomposition (SVD), $S_{m\times n} \approx V_{m\times Q} U_{Q\times n}$, then speaker-dependent square linear layers were employed for

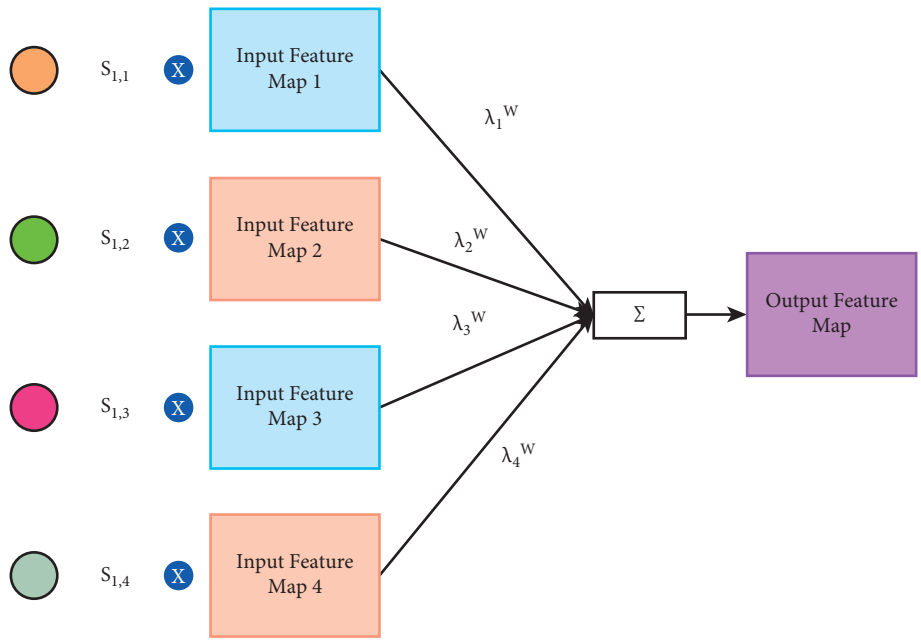

Figure 5: Adaptive cluster training.

bottlenecks. A speaker-adapted weight matrices can be found as

$$S^{w}_{m\times n} = V_{m\times Q} W^{w}_{Q\times Q} U_{Q\times n}. \tag{14}$$

As inferred from the equation (14), $W^{w}_{Q\times Q}$ indicates speaker-dependent square matrices. The speaker-dependent square matrices are decomposed into diagonal matrices plus low-rank matrices.

$$W^{w}_{Q\times Q} = Z^{w}_{Q\times Q} + Q^{w}_{Q\times c} O^{w}_{c\times Q}. \tag{15}$$

As shown in equation (15), $Z^{w}_{Q\times Q}$ represents diagonal matrix and $Q^{w}_{Q\times c}$ and $O^{w}_{c\times Q}$ are two low-rank matrices. The formulation of the diagonal part can be rewritten as follows

$$V_{m\times Q} Z^{w}_{Q\times Q} U_{Q\times n} = \sum_{c=1}^{Q} z^{w}_{c} v_{c} u^{T}_{c}. \tag{16}$$

As found in equation (16), v_c denotes cth column of V and u_c indicates the cth column of U^T. This structure can be understood as incorporating manifold rank-1 matrices based on speaker-dependent vectors. Motivated by these effective factorization-based adaptation models for CNNs, this study intends further to discover its potential capability for robust noise and speech recognition.

Direct training of the integrated neural network quickly falls into a local optimum as the gradients for the DCNN and acoustic model have different dynamic ranges. The training should be performed in sequence for a robust estimation of the model variables as shown in Algorithm 1. The calculation of improved speech presence probability is a recursive process, which concurrently possesses a strong track/adapt capability and a precise estimation ability for connected statistics by integrating the strong prior data of the speech and noise signal from the exhibition hall. The proposed DCNN-ASRM model enhances the recognition accuracy, performance, signal-to-noise ratio, and noise reduction ratio and decreases the word error rate compared to other existing models.

4. Simulation Results and Discussion

This paper presents the DCNN-ASRM model for accurate speech recognition in the exhibition hall. This study utilizes the speech signal from the CHiME-3 challenge data set [25]. The CHiME-3 environment is Automatic Speech Recognition for multimicrophone tablet devices utilized in an everyday, noisy environment. It signifies an important step forward in terms of realism concerning the previous CHiME challenges. Speech is seized by six microphones embedded in the frame and recorded 24 bits at a multitrack field recorder. The audio was consequently down-sampled to 16 bit 16 kHz for dissemination. This study discusses the recognition accuracy, performance, signal-to-noise ratio, noise reduction ratio, and word error rate compared to other popular models.

The challenge features are as follows:

(i) 6-channel microphone array information,

(ii) Actual acoustic mixing, i.e., talkers speaking in a challenging noisy environment,

(iii) There are five varied noise settings: cafe, exhibition, street junction, public transports, and pedestrian zone.

4.1. Recognition Accuracy Ratio. An audio-visual feature extraction technique based on the DCNN model presented in this research takes feature concatenation a step further by learning to automatically align the two media, resulting in more accurate visual and auditory representations. After the

Input: One noisy speech utterance
Output: improved speech presence probability estimation
Initialize the statistics at the initial frame for every frequency
for every time frame *k***do**
for every frequency *l***do**
Compute the mask estimation using equations (12) and (13)
Compute the posterior SNR using the noise estimation in equation (15)
Compute the priori SNR
Compute the gain function or improved speech presence probability based on CNN input, hidden and output layer
end for
end for

Algorithm 1: Deep Convolutional Neural Network Algorithm.

convolutional layer, an additional layer called a pooling layer is added, to be more specific, after a nonlinearity (such as ReLU) is added to the feature maps generated by a convolutional layer. The adoption of the wavelet denoising strategy in the MFCC significantly surpassed the identification accuracy, notably at low SNRs, although at high SNR values, the recognition accuracy remained almost unaltered. SNR levels were averaged to obtain the average identification accuracy in various noise environments. All models received validation using noise-free utterances between every training epoch, and training was terminated when recognition accuracy on the data set declined from the prior epoch or achieved 100%. Two to six epochs of training were sufficient for all models. The recognition accuracy has been computed from equation (10). The suggested DCNN-ASRM model achieves high recognition accuracy ratio of 98.1% compared to other existing models. Figure 6 signifies the recognition accuracy ratio.

4.2. Performance Ratio. Despite considerable success in speech recognition, MFCCs' performance is still unsatisfactory for many real-world applications, despite their widespread use in speech recognition systems. Ambient noise is one of the most common problems with popular spectral characteristics. There is a lot of background noise in many places where automated speech recognition applications would be perfect, making voice-activated devices unfeasible in many cases. Mean values of the proposed method's performance are presented here for noise sources to analyze and verify its performance at all input SNRs. To improve the performance of DCNN, the dropout method is used. There are 100 audio signals chosen for analyzing the performance of the proposed DCNN-ASRM model in speech recognition at the exhibition hall. A Deep Convolutional Neural Network (DCNN) has been employed for training and testing the database because of its superior performance. Training the system thoroughly through weight connectivity, local connectivity, and polling achieves excellent testing performance. This study introduces acoustic features based on higher-order indicators of the speech signal. When paired with MFCCs, these features have been proven to generate greater recognition accuracies in a noisy environment. The performance ratio has been computed from equations (12) and (13). The suggested DCNN-ASRM model achieves a high performance ratio of 97.2% compared to other systems. Figure 7 illustrates the performance ratio.

4.3. Signal-to-Noise Ratio. The first metric for evaluating the effectiveness of speech enhancement and speech recognition algorithms is one based on the signal-to-noise ratio (SNR). However, the typical SNR measure does not correspond with the quality of the speech since the average across the entire signal duration may remove key information. As a result, the SNR is estimated in short segments and then averaged to address this issue. The term "segmental SNR" refers to the method used to calculate SNR. SegSNR is a step up from traditional SNR. When SNR is computed, an upper and lower threshold is specified to replace any frames with an abnormally high or low signal-to-noise ratio. Quality estimates are based on the average SNR of all frames in a sequence. The SNR ratio has been computed from equation (14). The suggested DCNN-ASRM model achieves less SNR ratio of 10.3% than other models. Figure 8 indicates the signal-to-noise ratio.

4.4. Word Error Rate. Word error rate (WER) is a typical statistic used to measure the accuracy of speech conversion performed by Automatic Speech Recognition (ASR) systems. A 5–10% WER is considered good quality and is ready to use. The WER is the number of errors divided by the total amount of words. To obtain the WER, add the substitutions, insertions, and deletions in a series of recognized words. Gaussian white noise may cause word error rates to rise from less than 5% to more than 20% when applied to Large Standard Vocabulary Continuous Speech Recognition (LVCSR) tasks such as recognizing the 5,000 words in the Wall Street Journal corpus, even using compensatory strategies. Even for continuous digit identification, the word error rate often exceeds 10% in the presence of high noise levels. The word error rate has been computed from equation (15). The suggested DCNN-ASRM model achieves a lower WER rate of 9.2% than other models. Figure 9 demonstrates the word error rate.

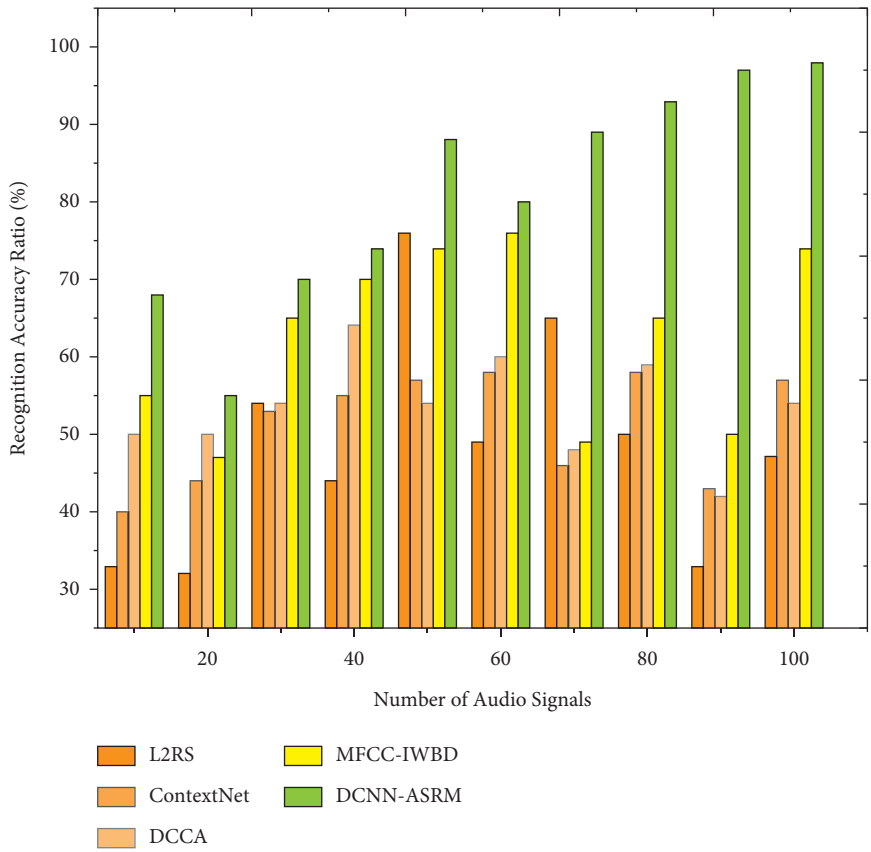

Figure 6: Recognition accuracy ratio.

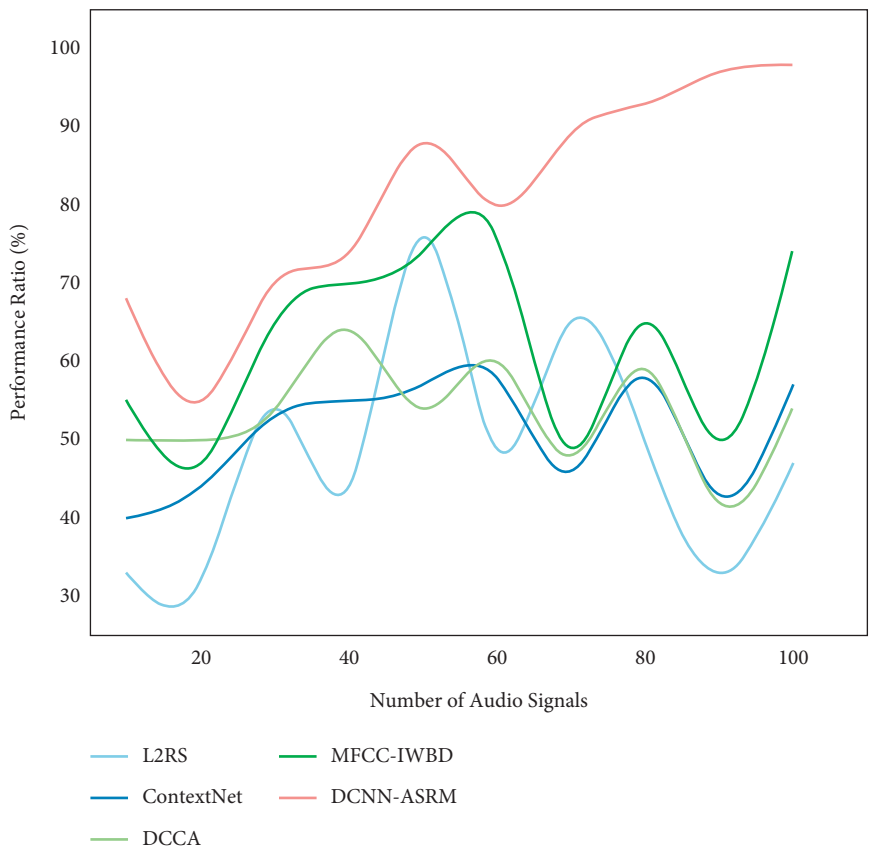

Figure 7: Performance ratio.

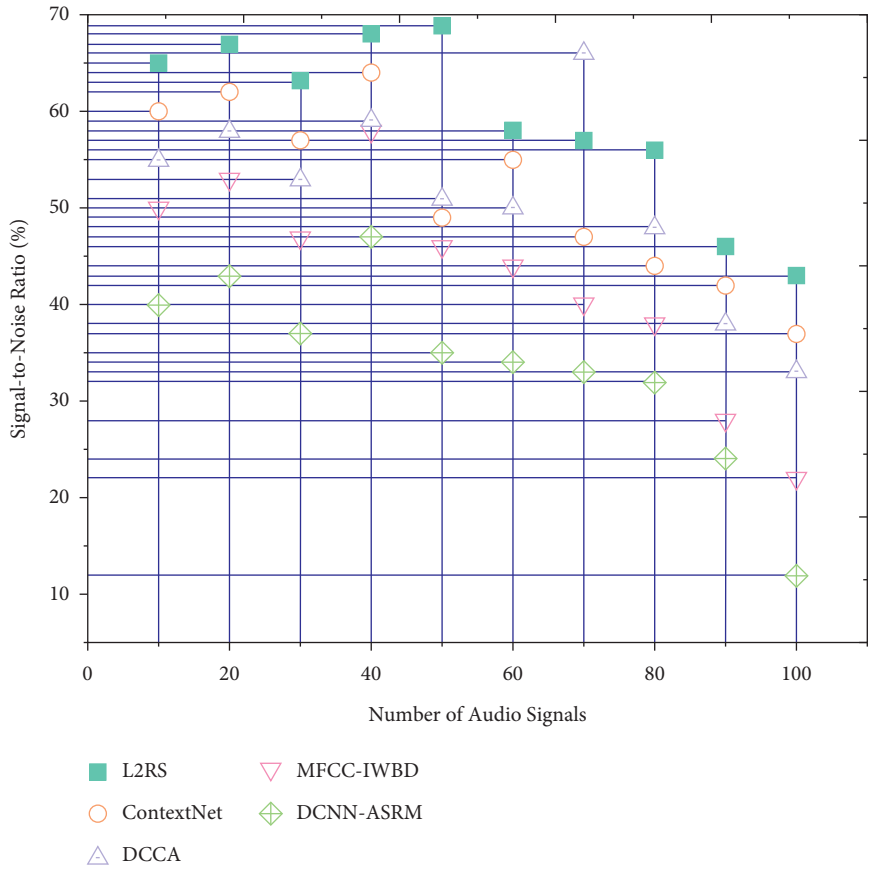

Figure 8: Signal-to-noise ratio.

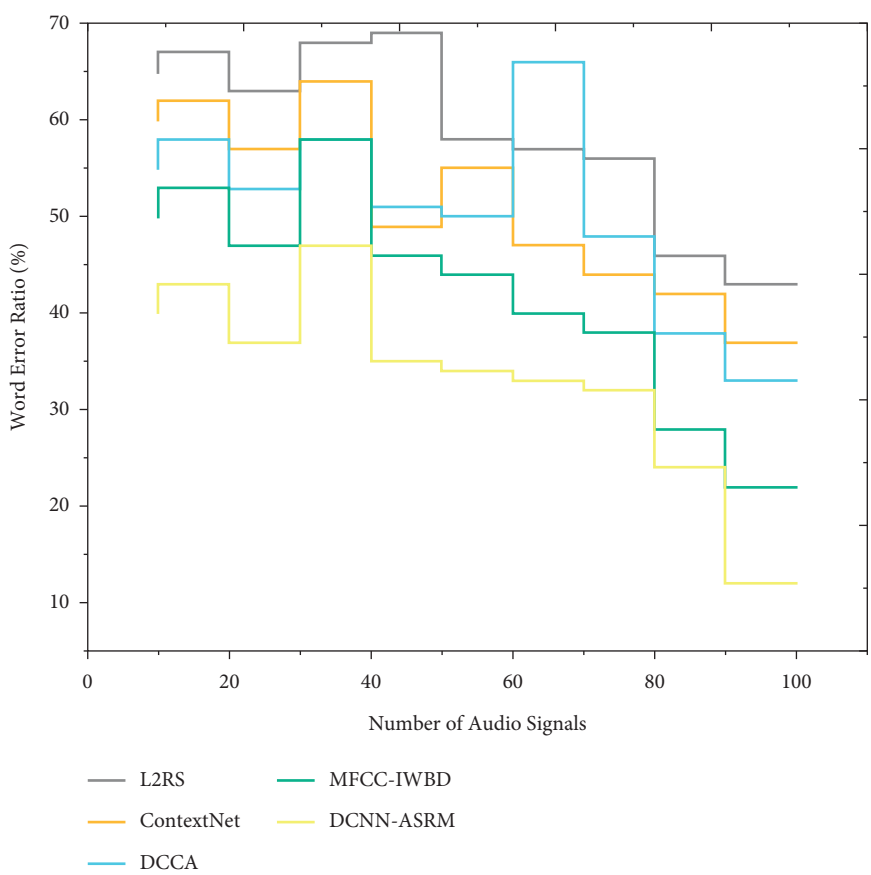

Figure 9: Word error rate.

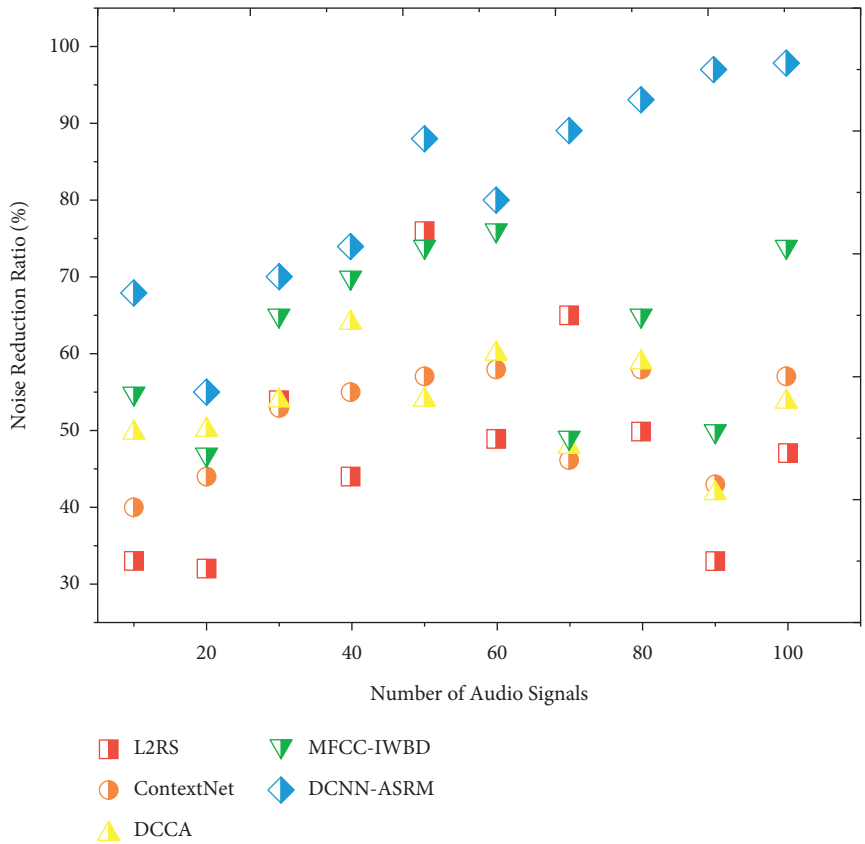

Figure 10: Noise reduction ratio.

4.5. Noise Reduction Ratio. For low SNRs and noise types that are not steady, many of the mentioned deep learning models aim for high noise attenuation and, as a result, may still impair voice quality. To solve this issue, it is proposed that noise reduction be used initially, followed by the restoration of natural-sounding speech. Even when the model was evaluated with data and noise not included in the training set, the findings show that the recommended CNN structure gives higher denoising capabilities than filtering in noise reduction. The suggested system with a single skip connection, on the other hand, has far greater noise-reducing capabilities. The noise reduction ratio has been computed from equation (16). The suggested DCNN-ASRM model attains a high noise reduction ratio of 96.5% compared to other existing models. Figure 10 shows the noise reduction ratio.

The proposed DCNN-ASRM model enhances the recognition accuracy, performance, signal-to-noise ratio, and noise reduction ratio and decreases the word error rate compared to other existing Learning-to-Rescore (L2RS), ContextNet, Deep Canonical Correlation Analysis (DCCA), and Mel-Frequency Cepstral Coefficients for Improved Wavelet-Based Denoising (MFCC-IWBD) methods.

5. Conclusion

This paper presents the DCNN-ASRM model for speech recognition in an exhibition hall. The objective of ASR research is to address the different issues relating to speech recognition. This paper offered a new auditory filter modeling-based feature extraction technique for noisy speech recognition. Based on higher-order sub-band filter speech signal indicators, a new acoustic feature extraction technique was proposed. Preliminary tests demonstrate that combining these features with MFCCs can enhance the robustness of the speech recognition model in exhibition hall noise conditions. The baseline CNN gained a high overall accuracy. Paralleled to the conventional Convolutional Neural Network structure in Automatic Speech Recognition, filter and pooling are small, and the more extensive input feature map. This modification permits us to improve the number of convolution layers to ten. A comprehensive analysis of padding, pooling, and input feature map assortment is executed. The simulation analysis validates that the suggested DCNN-ASRM model enhances the recognition accuracy ratio of 98.1%, performance ratio of 97.2%, and noise reduction ratio of 96.5% and reduces the word error rate by 9.2% and signal-to-noise ratio by 10.3% compared to other existing models.

Data Availability

No data were used to support this study.

Conflicts of Interest

The author declares that there are no conflicts of interest regarding the publication of this article.

References

[1] F. Abreu Araujo, M. Riou, J. Torrejon et al., "Role of non-linear data processing on speech recognition task in the framework of reservoir computing," *Scientific Reports*, vol. 10, no. 1, pp. 1–11, 2020.

[2] H. Bourouba and R. Djemili, "Feature extraction algorithm using new cepstral techniques for robust speech recognition," *Malaysian Journal of Computer Science*, vol. 33, no. 2, pp. 90–101, 2020.

[3] N. Saleem and M. I. Khattak, "Regularized sparse decomposition model for speech enhancement via convex distortion measure," *Modern Physics Letters B*, vol. 32, no. 22, Article ID 1850262, 2018.

[4] Y. M. Kang and Y. Zhou, "Fast and Robust Unsupervised Contextual Biasing for Speech Recognition," 2020, https://arxiv.org/abs/2005.01677.

[5] T. Iio, Y. Yoshikawa, M. Chiba, T. Asami, Y. Isoda, and H. Ishiguro, "Twin-robot dialogue system with robustness against speech recognition failure in human-robot dialogue with elderly people," *Applied Sciences*, vol. 10, no. 4, p. 1522, 2020.

[6] R. H. Gifford, J. H. Noble, S. M. Camarata et al., "The relationship between spectral modulation detection and speech recognition: adult versus pediatric cochlear implant recipients," *Trends in Hearing*, vol. 22, Article ID 2331216518771176, 2018.

[7] C. Spille, B. Kollmeier, and B. T. Meyer, "Comparing human and automatic speech recognition in simple and complex acoustic scenes," *Computer Speech & Language*, vol. 52, pp. 123–140, 2018.

[8] A. Baruwa, M. Abisiga, I. Gbadegesin, and A. Fakunle, "Leveraging End-To-End Speech Recognition with Neural Architecture Search," 2019, https://arxiv.org/abs/1912.05946.

[9] C. X. Qin, W. L. Zhang, and D. Qu, "A new joint CTC-attention-based speech recognition model with multi-level multi-head attention," *EURASIP Journal on Audio Speech and Music Processing*, vol. 2019, no. 1, pp. 1–12, 2019.

[10] U. Sharma, S. Maheshkar, A. N. Mishra, and R. Kaushik, "Visual speech recognition using optical flow and hidden Markov model," *Wireless Personal Communications*, vol. 106, no. 4, pp. 2129–2147, 2019.

[11] A. B. Nassif, I. Shahin, I. Attili, M. Azzeh, and K. Shaalan, "Speech recognition using deep neural networks: a systematic review," *IEEE Access*, vol. 7, pp. 19143–19165, 2019.

[12] R. A. Khalil, E. Jones, M. I. Babar, T. Jan, M. H. Zafar, and T. Alhussain, "Speech emotion recognition using deep learning techniques: a review," *IEEE Access*, vol. 7, pp. 117327–117345, 2019.

[13] Y. Dokuz and Z. Tufekci, "Mini-batch sample selection strategies for deep learning based speech recognition," *Applied Acoustics*, vol. 171, Article ID 107573, 2021.

[14] R. Haeb-Umbach, S. Watanabe, T. Nakatani et al., "Speech processing for digital home assistants: combining signal processing with deep-learning techniques," *IEEE Signal Processing Magazine*, vol. 36, no. 6, pp. 111–124, 2019.

[15] H. Meng, T. Yan, F. Yuan, and H. Wei, "Speech emotion recognition from 3D log-mel spectrograms with deep learning network," *IEEE Access*, vol. 7, pp. 125868–125881, 2019.

[16] A. Hannun, A. Lee, Q. Xu, and R. Collobert, "Sequence-to-sequence Speech Recognition with Time-Depth Separable Convolutions," 2019, https://arxiv.org/abs/1904.02619.

[17] M. Alhussein and G. Muhammad, "Voice pathology detection using deep learning on mobile healthcare framework," *IEEE Access*, vol. 6, pp. 41034–41041, 2018.

[18] C. X. Qin, D. Qu, and L. H. Zhang, "Towards end-to-end speech recognition with transfer learning," *EURASIP Journal on Audio Speech and Music Processing*, vol. 2018, no. 1, pp. 1–9, 2018.

[19] B. Kanisha, S. Lokesh, P. M. Kumar, P. Parthasarathy, and G. Chandra Babu, "Speech recognition with improved support vector machine using dual classifiers and cross fitness validation," *Personal and Ubiquitous Computing*, vol. 22, no. 5, pp. 1083–1091, 2018.

[20] A. Shewalkar, D. Nyavanandi, and S. A. Ludwig, "Performance evaluation of deep neural networks applied to speech recognition: RNN, LSTM and GRU," *Journal of Artificial Intelligence and Soft Computing Research*, vol. 9, no. 4, pp. 235–245, 2019.

[21] Y. Song, D. Jiang, X. Zhao et al., "L2RS: A Learning-To-Rescore Mechanism for Automatic Speech Recognition," 2019, https://arxiv.org/abs/1910.11496.

[22] W. Han, Z. Zhang, Y. Zhang et al., "Contextnet: Improving Convolutional Neural Networks for Automatic Speech Recognition with Global Context," 2020, https://arxiv.org/abs/2005.03191.

[23] S. Isobe, S. Tamura, and S. Hayamizu, "Speech recognition using deep canonical correlation analysis in noisy environments," in *Proceedings of the 10th International Conference on Pattern Recognition Applications and Methods ICPRAM*, pp. 63–70, Vienna, Austria, February, 2021.

[24] R. Hidayat and A. Winursito, "A modified MFCC for improved wavelet-based denoising on robust speech recognition," *International Journal of Intelligent Engineering and Systems*, vol. 14, no. 1, pp. 12–21, 2021.

[25] Spandh, "Chime_challenge," 2015, http://spandh.dcs.shef.ac.uk/chime_challenge/chime2015/.

Hindawi
Mobile Information Systems
Volume 2022, Article ID 4652946, 12 pages
https://doi.org/10.1155/2022/4652946

Research Article

Research on Human Action Feature Detection and Recognition Algorithm Based on Deep Learning

Zhipan Wu[1] and Huaying Du[2]

[1]*School of Computer Science and Engineering, Huizhou University, Huizhou 516007, Guangdong, China*
[2]*School of Information Technology City College of Huizhou, Huizhou 516025, Guangdong, China*

Correspondence should be addressed to Huaying Du; duhuaying@tm.hzc.edu.cn

Received 13 July 2022; Revised 5 August 2022; Accepted 20 August 2022; Published 29 August 2022

Academic Editor: Yajuan Tang

With the improvement of computer computing power and storage capacity, the emergence of massive data makes the methods based on human action feature detection and recognition unable to meet people's needs due to poor generalization ability. Based on the detection and recognition of human action features based on deep learning algorithms, a suitable neural network can be constructed to identify locked human action features from surveillance video and analyze whether it is a specific behavior. In this paper, a deep learning algorithm is proposed to optimize the detection of human action features, and a multiview reobservation fusion action recognition model of 3D pose is designed. Several factors affecting the recognition of human action features are analyzed, and a detailed summary is made from the detection environment. Experiments show that adding one or two layers of feature attention enhancement to the multiview observation fusion network can improve the accuracy by 1% to 3%. In this way, the model can integrate action features from multiple observation angles to judge actions and learn to find observation angles suitable for action recognition, thereby improving the performance of action recognition.

1. Introduction

In recent years, the application of deep learning in the field of computer vision and pattern recognition has been in-depth, especially the research on human action recognition, which has become one of the important technologies in deep learning application research. It has huge development potential in intelligent monitoring, video understanding, human-computer interaction, medical diagnosis, and so on.

This paper conducts in-depth research on computer vision technology in deep learning and uses deep learning technology to solve the problems of intelligence and automation of monitoring systems. According to the three-dimensional recognition of human body, a multiview fusion model based on attention mechanism is proposed, and a set of deep learning monitoring system based on deep learning is developed. The system can detect, identify, track and identify people in the monitored scene, and analyze the obtained information, so as to play the role of supervision, early warning, and prevention. Therefore, the research on deep learning monitoring system has important application value and significance.

In order to study the problem of 3D human action recognition, this paper proposes a multiview reobservation fusion model based on attention mechanism. In the fusion process, the attention mechanism is used to evaluate whether the observation perspective is helpful to the action recognition according to the action sequence information. In this way, the model can learn to find suitable viewpoints for action recognition among multiple viewpoints based on action information.

2. Related Work

Human action recognition is widely used in intelligent applications, and key human detection is a hot topic in the field of action recognition. In order to improve the identification rate of key points in the human body, Thrall et al. used an artificial intelligence program to extract "radioactive" information

from images that cannot be discerned by visual inspection, thereby increasing the diagnostic and prognostic value derived from image datasets [1]. Mamoshina et al. outlined next-generation artificial intelligence and blockchain technology and proposed innovative solutions that can be used to accelerate biomedical research, enable patients to control and monetize personal data with new tools, and incentives for continuous health monitoring [2]. Jiang et al. proposed a novel unified framework that jointly exploits feature relations and class relations to improve classification performance. The proposed Regularized DNN (rDNN) is more suitable for video semantic modeling by endowing the DNN with the ability to better utilize features and class relations [3]. Cheng et al. conducted a comprehensive survey of recent advances in network acceleration, compression, and accelerator design from both algorithmic and hardware perspectives, while the computational complexity and resource consumption of these networks are increasing. In terms of hardware implementation of deep neural networks, a number of accelerators based on Field Programmable Gate Array (FPGA) or Application Specific Integrated Circuit (ASIC) have been proposed in recent years [4]. Dong and Wang studied the robust exponential stability problem of uncertain discrete-time stochastic neural networks with time-varying delays based on output feedback control by choosing an enhanced Lyapunov-Krasovskii functional, which establishes a sufficient condition for asymptotically stable delay correlation in the mean square for a class of discrete-time stochastic neural networks with time-varying delays [5]. Lucas et al. reviewed deep learning techniques for solving such inverse problems in imaging. Specifically popular neural network architectures for imaging tasks, they provided some insights into how these deep learning tools can solve the inverse problem [6]. Yin et al. proposed BinaryRelax, a simple two-stage algorithm for training deep neural networks with quantized weights, and aimed to test BinaryRelax on benchmark CIFAR and ImageNet color image datasets to demonstrate the superiority of relaxed quantization methods and higher accuracy than state-of-the-art training methods [7]. Sarabu and Santra used two CNNs that use pretrained ImageNet models to extract spatiotemporal features, combining the results of the two CNNs in the first step as input to CLSTM to obtain an overall classification score [8]. Liu et al. made full use of video and deep skeleton data and propose a dual-stream network (SV-GCN) based on RGB-D action recognition, which can be said to be a dual-stream architecture that processes two different data. To provide the model with richer skeleton point features, they replaces the traditional random sampling layer with an atrous convolutional layer, which can better utilize the depth features, and finally fuses the two-stream information to achieve action recognition [9]. These studies are instructive to a certain extent, but in some cases, the demonstrations are insufficient or inaccurate and can be further improved.

3. Action Recognition Method Based on Deep Learning

Deep learning is a learning method using distributed features, which can automatically learn from low-level features to high-level features, eliminating the dependence on manual feature extraction methods. And the powerful feature extraction ability of deep learning makes it have huge advantages in classification and recognition. Traditional human action recognition aims to extract design features and classify them according to the features. Human target detection and recognition based on deep learning algorithm constructs a suitable neural network, which can identify a movement of a locked person from surveillance video, and analyze whether it is a specific behavior [10–12]. The traditional human action recognition flowchart is shown in Figure 1. Deep learning performs feature extraction at the position with the greatest saliency by defining a saliency function, and obtains local feature descriptors.

Traditional human action recognition is mainly based on RGB images or videos, and the effect is not satisfactory due to factors such as scale, illumination changes, and background noise. The use of deep learning is popular in the field of computer vision. At present, the recognition effect of this human action recognition method through deep learning is far superior to the traditional recognition method and gradually replaces the traditional human body recognition [13–15]. The basic framework of the human action recognition framework based on deep learning is shown in Figure 2.

3.1. Mask RCNN Algorithm. The Mask RCNN algorithm framework can be widely used in many vision tasks such as target detection, target instance segmentation, target key point detection and so on by fine-tuning the network structure [16]. Since it inherits the advantages of both the classic segmentation network FCN and the classic target detection network Faster RCNN, Mask RCNN can simultaneously ensure high classification accuracy, detection accuracy, and instance segmentation accuracy. Although Mask RCNN is more complex than Faster RCNN, the speed of the two is comparable. Therefore, the above advantages make Mask RCNN extremely outstanding in multiple vision tasks [17].

The schematic diagram of the overall structure of Mask RCNN is shown in Figure 3. The first half of the network structure is similar to the network structure of Faster RCNN. First, the input image is extracted as a feature map through the convolution layer, and then the feature map is input to the RPN network, so that the RPN generates the region of interest corresponding to the feature map. Then, the feature maps of the region of interest are uniformly scaled through the RoIAlign layer, and finally, the obtained uniform-size feature maps are input to multiple branch networks. Two of the fully connected layer branches are used to obtain the classification score results and the regression parameters of the target frame respectively, and another branch generates a mask image of the same size as the input original image through the image segmentation network FCN, that is, the semantic segmentation result of the image classifies each pixel of the image [18].

Mask RCNN introduces the RoIAlign structure to replace the RoI pooling layer of the Faster RCNN part. The

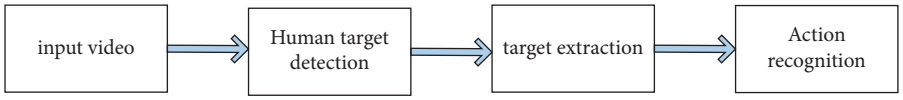

Figure 1: Traditional human action recognition flowchart.

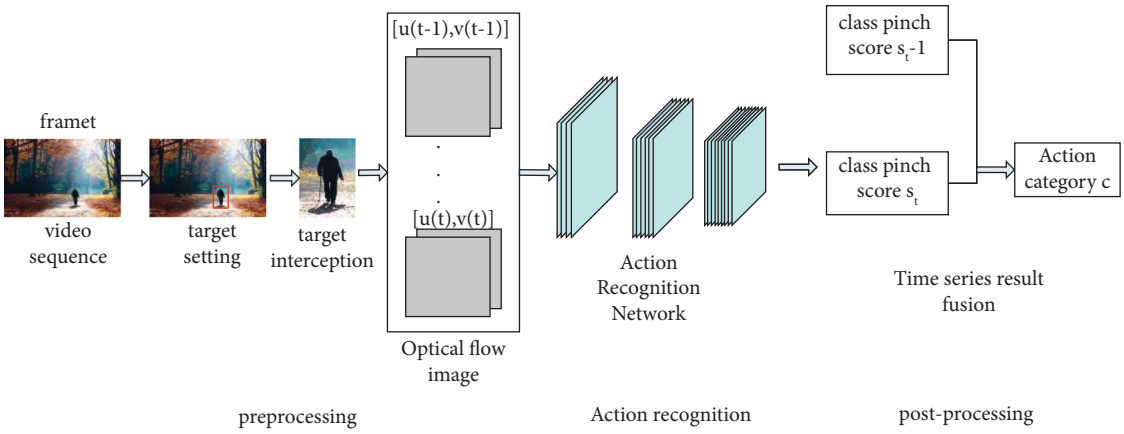

Figure 2: Action recognition framework.

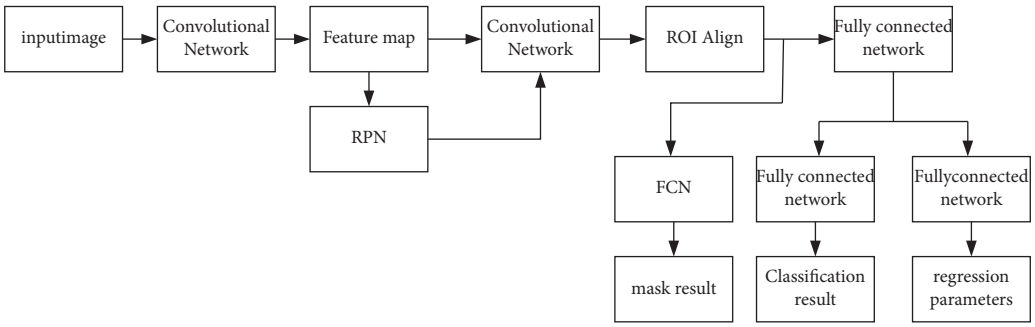

Figure 3: Schematic diagram of Mask RCNN framework.

main purpose of this layer is also to extract the feature map corresponding to the region of interest and unify the feature maps of the region of interest of different sizes to the same size, so as to facilitate the input of the subsequent network [19].

3.2. Fully Convolutional Neural Networks. The network introduces a deconvolution structure to generate a mask map that is the same size as the input feature map, thereby generating a mask value classification for each pixel, and implementing instance segmentation for each pixel [20]. Through the convolution and pooling operations of the input data, the full-volume neural network starts from the shallow features, extracts the deep features layer by layer, and directly inputs the original image data, avoiding the complex preprocessing of the image. Deconvolution can actually be understood as the reverse operation of ordinary convolution operations, and its schematic diagram is shown in Figure 4. It first fills the feature map with 0 between each feature point and then performs the convolution calculation

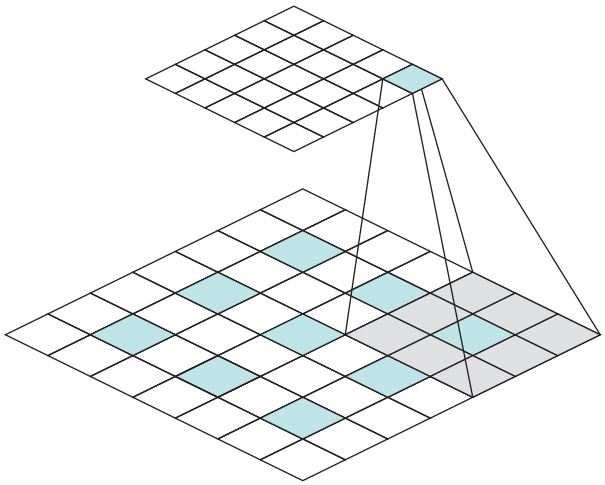

Figure 4: Schematic diagram of deconvolution.

of the convolution kernel to obtain a feature map with a larger size after upsampling [21, 22].

The feature extraction process of the convolutional local connection in Figure 4 can be regarded as a process of

convolution of each region in the image by multiple convolution kernels. After the input image has undergone multiple convolutions, the resolution of the feature map becomes smaller and smaller. Then, the size of the low-resolution feature map needs to be restored to the same size as the input feature map in order to generate a mask feature map to classify and score each pixel [23]. Full-volume neural networks are fault-tolerant and adaptive, and robust to specific poses, lighting, displacements, scaling, or more types of image distortions. FCN deconvolutes the feature map finally output by the original convolutional network by 32 times and can directly obtain the feature map of the same size as the original image, but such a result can only reflect the deep overall features, without using some intermediate features. The detailed local features extracted by the layer, so FCN introduces a skip-level structure.

By training the parameters of the FCN network, the network is finally able to generate a mask of the same size as the input image, that is, each pixel has a corresponding classification score, and the output feature map has layers in depth. That is, there is a category, and the score of each pixel in each layer represents the confidence score that the pixel belongs to the current layer category. First, the classification probability is obtained by performing Softmax on the score of each layer and then the target position or key point position belonging to the category of the current layer is found through a certain threshold limit.

3.3. Human Key Point Detection Based on Improved Mask RCNN. In this experiment, a new method for initializing the size of the anchor candidate frame is introduced. The size of the character annotation frame in the dataset is classified by the clustering method, and then the average value of each type of cluster is calculated, so that the anchor point candidate frame size that is more suitable for the human key point detection task is calculated through the dataset itself [24–26]. The general idea of the K-means algorithm is to first select a sample from the training set as the center of the cluster and evaluate the distance between all the sample points and the center of the cluster. For each sample point, it is divided into the cluster to which the cluster center with the smallest distance value belongs. After such a clustering, the cluster center is recalculated and updated for each cluster, and so on until the model reaches a satisfactory convergence accuracy. The algorithm flow is as follows:

(1) Set the initial value for each cluster center according to the set number of clusters. Generally, a group of samples is randomly selected as the initial cluster center $\mu_1, \mu_2, , \mu_n$.

(2) Update the labels of the clusters to which all samples belong, and the cluster label of the first sample is y_i. In this paper, two feature components $x_i = (x_i^1, x_i^2)$ are set for the position of the labeling target frame. By calculating the Euclidean distance between the feature vectors composed of these two values, the similarity in size and size of the two position annotation boxes can be better represented. Calculated as follows:

Table 1: Box selection size of points based on K-means clustering algorithm.

Candidate frame number	Candidate box size
Candidate box 1	45×20
Candidate box 2	22×55
Candidate box 3	$31 * 76$
Candidate box 4	$59 * 145$
Candidate box 5	$82 * 200$

$$y_i = \underset{j}{\operatorname{argmin}}\, \operatorname{dist}\left(x_i, \mu_j\right) j \in [1, c],$$
$$\operatorname{dist}\left(x_i, \mu_j\right) = \sqrt{\sum_{k=1}^{2} \left|x_i^k - \mu_j^k\right|^2}. \tag{1}$$

(3) Update the center point of each cluster, the formula is as follows:

$$\mu_j = \frac{\sum_{k \in S_j} x_k}{K_j}, j = 1, 2, \ldots. \tag{2}$$

In the formula, K_j represents the number of the j-th sample points assigned in this iteration process, and S_j represents the set of samples that are assigned to the j-th sample point.

(4) Repeat steps 1 to 3 until the classification ability of the cluster center makes the model reach the convergence accuracy.

Through the above K-means clustering training process, the size and height-width ratio of the annotation frame in the human key point detection dataset are used as the two dimensions of the feature vector as the classification criteria of the cluster, and the classification result is obtained [27]. For each cluster in the classification result, the average size of the annotation frame in the same cluster is obtained, so as to obtain a set of anchor candidate frame sizes that are representative of the size of the person in the human key point dataset. In this paper, a clustering algorithm is performed on the character annotation boxes provided by the MSCOCO dataset. Considering that the characters are rich in actions, resulting in a large gap in the aspect ratio of the characters, the number of clusters is increased to 13, and the average size of the annotation box in each cluster is calculated, and finally, the anchor point candidate frame size is obtained as shown in Table 1.

For the multiperson target scene, the confidence is appropriately lowered, and a variety of calculation methods are introduced to adjust the confidence penalty. Finally, it analyzes which penalty function calculation method can better improve the recognition performance of the algorithm in dense human scenes and reduce the sensitivity of the model to the confidence threshold through experiments [28].

Three kinds of common weight calculation methods are selected as the object of discussion, namely linear function, Gaussian function, and exponential function [29–31]. These

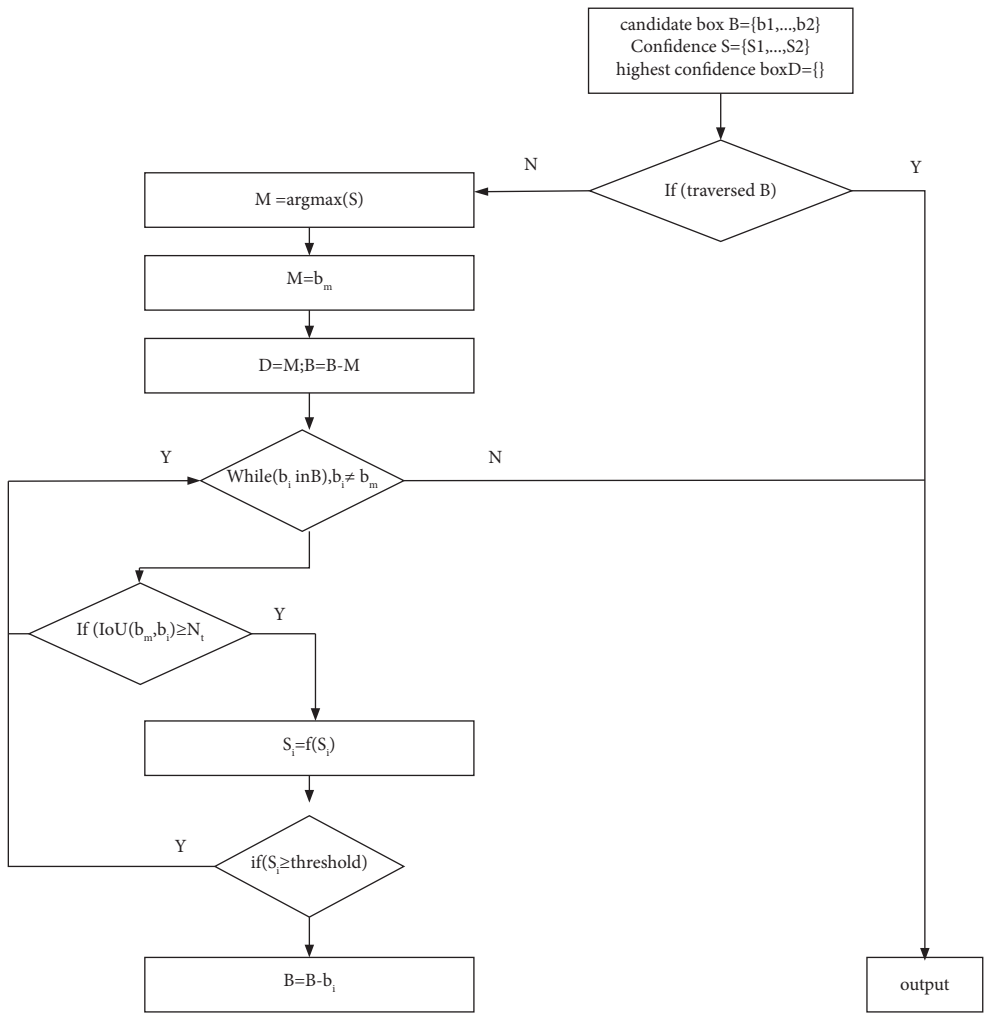

Figure 5: Flowchart of the improved nonmaximum suppression algorithm.

three types of functions can calculate a penalty value. When a candidate box whose intersection with the marked box is greater than the threshold appears in the process of nonmaximum suppression, its confidence will be penalized, so as to further judge whether to retain the candidate box. The program flowchart of the improved nonmaximum suppression is shown in Figure 5, where f represents the type of penalty function used, and N_t is the threshold of the intersection and union ratio. *Threshold* represents the confidence threshold, which is used to judge whether the confidence after punishment meets the conditions that need to be eliminated.

The penalty function is defined below according to three types of weighting methods. The first is a linear penalty function, whose penalty function is defined as follows:

$$s_i = \begin{cases} s_i, & \mathrm{IOU}(b_m, b_i) < N_t, \\ a \bullet s_i (1 - \mathrm{IOU}(b_m, b_i)), & \mathrm{IOU}(b_m, b_i) \geq N_t, \end{cases} \tag{3}$$

where a is a coefficient weight, ranging from 0 to 1, to control the strength of the penalty. S_i represents the confidence score of the candidate frame currently being judged, b_m represents the position coordinate of the candidate frame with the highest confidence score discharged in this round of iteration, and b_i represents the position coordinate of the candidate frame currently being judged. When the intersection ratio of the two is greater than the threshold, it is necessary to impose a certain penalty on the confidence of the candidate frame. If the values of a and N_t are different, the degree of penalty will also be different. The parameter sensitivity will be analyzed in subsequent experiments.

The second is the Gaussian penalty function, which modifies the Gaussian function to wait until the penalty function:

$$S_i = S_i e^{-\mathrm{IOU}(b_m, b_i)^2/\sigma}. \tag{4}$$

Among them, σ represents the penalty for the confidence, S_i represents the confidence score of the candidate frame currently being judged, b_m represents the position coordinate of the candidate frame with the highest confidence score discharged in this round of iteration, and b_i represents the position coordinates of the candidate frame currently being judged.

The third is the exponential penalty function. Compared with the linear function, the transition of the penalty

function at the threshold point is smoother. Compared with the Gaussian function, it can maintain a higher degree of confidence in the stage where the intersection and union are low. The calculation formula is as follows:

$$S_i = \begin{cases} S_i, & \mathrm{IOU}(b_m, b_i) < N_t, \\ S_i e^{(N_t - IOU(b_m, b_i))}, & \mathrm{IOU}(b_m, b_i) \geq N_t. \end{cases} \quad (5)$$

The above three penalty functions are brought into the whole process of nonmaximum suppression. Each time the intersection ratio is judged, the above three types of penalty functions are introduced to calculate the confidence after penalty. If the confidence is still greater than the set confidence threshold, the candidate frame is retained as the region of interest, otherwise the candidate frame is rejected [32].

4. Multiview Reobservation Fusion Action Recognition Model Based on 3D Pose

In the problem of human action recognition, most of the current video-based methods directly process the entire video image, and let the network classify actions from the entire image in a data-driven way [33]. These methods rarely focus on the role of action elements, and it is difficult to explain whether the model learns human actions or more information about the appearance of the environment, especially when the current datasets are small. Compared with other deep learning-based algorithm architectures, the multipose human action recognition architecture mainly has the advantages of high recognition accuracy, low complexity, and strong complementarity of action information between multiple modalities.

Human action recognition is an important technology in the field of video understanding and analysis [34]. In recent years, with the rapid development of video-based position estimation algorithms, bone-based methods for human action recognition have become popular. The framework of action recognition based on skeleton data is mainly divided into three steps: skeleton data acquisition, action feature extraction, and action classification. All of these methods see the human skeleton as a graph, with joint points as graph nodes and bone connections as edges on the graph. Graph-based methods provide a good characterization of the skeletal structure. In the current graph-based method, nodes are convolved and pooled. However, most of the movements do not require the participation of all the joint points throughout the body, and a few of them play a central role. By introducing an attention model, the model can focus more on a small number of important joint points.

In reality, there is a high diversity of movements, and many actions will have different forms in different situations, such as eating when people may be sitting or standing [35]. This diversity of actions poses great difficulty for the generalization of the model. The observation perspective has an important influence in action recognition. On the one hand, human movements can be observed from many perspectives, and the observation data from different perspectives will vary greatly, which causes the diversity of action data. The model needs to consider the data changes brought about by the change of the observation perspective to ensure the identification effect. On the other hand, for many actions, it is difficult to identify from some angles and particularly difficult to identify from other angles. In this case, it will be helpful to identify actions from easy to identify.

Multipose feature fusion is crucial for recognition performance because it can enhance the representational ability of features and reduce the redundancy of features. In the fusion process, the model also adopts the attention mechanism to evaluate all the observation angles according to the action sequence information and give the corresponding weights. The observation perspective will achieve higher weight in the fusion process. In this way, the model can integrate the action information of multiple observation angles to judge the action and learn to find the observation angle suitable for action recognition, so as to improve the performance of action recognition.

4.1. LSTM Neural Network. RNN realizes the accumulation of historical information through the design of cyclic structure, which is suitable for processing sequence data, and has been widely used in sequence problems such as action recognition in recent years [36]. The output h_t of the current step of the RNN is determined by the current input x_t and the output h_{t-1} of the previous step of the RNN (that is, the historical information accumulated in the RNN). In this way, RNN realizes the utilization of historical information of sequence data.

$$h_t = \varphi(W_x \bullet x_t + W_h \bullet h_{t-1} + b). \quad (6)$$

In the above formula, W and b are the parameters to be learned by the RNN unit. In theory, RNN can handle sequence information of arbitrary length and dependencies between sequences in this way. However, there are many practical problems that hinder the realization of the idealization, such as gradient disappearance during training, and gradient explosion. Long Short-Term Memory (LSTM) is an improved variant of RNN for handling such long-term sequence problems. Unlike the simple perceptron-like structure in the original RNN unit, the LSTM unit contains multiple gates to control the flow of information in the LSTM. These gate units also build a temporally linear connection, which alleviates the problems of vanishing and exploding gradients to a certain extent. The data computation in the LSTM cell looks like this:

$$\begin{aligned} \mathrm{f}_t &= \sigma\left(W_{xf*g} X_t + W_{hf*g} H_{t-1} + b_f\right), \\ \mathrm{i}_t &= \sigma\left(W_i \bullet [h_{t-1}, x_t] + b_i\right., \\ \mathrm{o}_t &= \sigma\left(W_O \bullet [h_{t-1}, x_t] + b_O\right., \\ \mathrm{u}_t &= \tan h\left(W_c \bullet [h_{t-1}, x_t] + b_c\right., \\ \mathrm{C}_t &= \mathrm{f}_t * C_{t-1} + i_t * u_t, \\ \mathrm{h}_t &= \mathrm{o}_t * \tan h(C_t). \end{aligned} \quad (7)$$

The cell state C refers to the state information in the LSTM cell. The forget gate, input gate, and output gate are

calculated according to the input x_t of the current step and the unit state C_{t-1} of the previous step to control the flow of information inside the LSTM unit. Forget gate f_t controls how much the cell state of the previous step (that is, the historical information accumulated by the cell) C_{t-1} should be retained; input gate i_t controls how much current input x_t should be input into the cell calculation; output gate o_t controls the conversion calculation from cell state to output.

The proposed action recognition model is also based on the LSTM unit. LSTM can better handle long-term and short-term time series memory by adding control gates. It has excellent performance in time series problems and is the most widely used RNN variant.

4.2. Attention Mechanism is used to Enhance Pose Information and Feature Representation. For many human actions, usually only a few limb joints play a decisive role, and the states of other joints or limbs are irrelevant to the action. For example, no matter what the posture of an object is, as long as he puts something to eat in his mouth, it constitutes the action of "eating." Based on this idea, this chapter introduces an attention mechanism to learn to assign different attention weights to different skeleton joint points according to action information to assist in action recognition. Since in the action recognition task, all the joint points may have an influence on the determination of the action, this chapter adopts the attention method of the soft attention mechanism. At step t of the LSTM network time series, skeleton data $x_t = \lfloor x_t^1, x_t^2, \ldots x_t^n \rfloor$ (x_t^{i} refer to the three-dimensional coordinates of the i-th joint point, n is the number of joint points in the skeleton model) is input into the network for processing for action recognition. During data input, the attention mechanism is used to assign an additional weight to the joint points in the skeleton, indicating the importance of the joint points under the current action sequence information. Attention weights are calculated based on input and historical information:

$$A_{\mathrm{ja}} = U_j\left(\tanh\left(W_{jh}\bullet \mathrm{h}_{t-1} + W_{jx}\bullet \mathrm{x}_t + b_{j1}\right)\right) + b_{j1}. \quad (8)$$

In the computation of attention weights, the state h_{t-1} of the previous step of the LSTM represents the sequence history information accumulated in the LSTM unit. According to the action history information h_{t-1} and the current skeleton data input x_t, the importance of the current step skeleton joints is predicted W_{ja}. W_{ja} is the attention weight of the joint point, corresponding to the J joint points in the skeleton model. This weight is used to revise the skeleton data, emphasizing the joint points according to their importance:

$$\widetilde{x_t} = \left[x_t^1, x_t^2, \ldots x_t^n,\right]\bullet A_{ja}. \quad (9)$$

The corrected input contains the importance $\widetilde{x_t}$ of the joint points. Through this enhancement of the attention mechanism, the movements of the more important joints are amplified, while the movements of the less important joints are suppressed. In this way, the sequence information or interaction information of important joint points is emphasized, which is helpful for the identification of related actions.

In a multilayer LSTM network, the output of the previous layer of LSTM is used as the input of the next layer of LSTM, and the attention LSTM enhances the attention mechanism of the features passed between the LSTM layers. The attention mechanism of general features is similar to the implementation of the attention mechanism on the skeleton joints. For the l-th LSTM layer in the network:

$$A_{\mathrm{t}} = U_t\bullet\left(\tanh\left(W_{l,h}\bullet h_{\mathrm{l},t-1} + W_{l,x}\bullet h_{l-1,t} + b_{l1}\right)\right) + b_{l2}. \quad (10)$$

Here, $h_{\mathrm{l}-1,t}$ is the output of the $l-1$-th layer LSTM, which is the input of the l-th layer LSTM. $h_{\mathrm{l},t-1}$ is the previous state of the lth layer LSTM. Similarly, attention weights are calculated based on feature input $h_{\mathrm{l}-1,t}$ and historical information $h_{\mathrm{l},t-1}$. Then, according to the attention weights, the features are modified:

$$\widetilde{h_{\mathrm{l}-1,t}} = h_{\mathrm{l}-1,t}\bullet A_{\mathrm{t}}. \quad (11)$$

4.3. Multiview Fusion Model Based on Attention Mechanism. The multiview fusion action recognition model of the attention mechanism first reobserves the input action sequence from multiple perspectives, then uses the deep network to process the observation data separately, and finally fuses the processing results of all observations to determine the final action category. The observation angle of action has a great influence on 3D action recognition, which is reflected in two aspects. First, action data can be collected from different observation perspectives, which increases the diversity of action data. Therefore, these increased sample diversity needs to be considered in the model or training to obtain a good algorithm generalization effect. Second, in general, many actions are hard to discern from some perspectives and easy to discern from others. In this way, finding observations from a suitable perspective will be of great help to improve the performance of action recognition.

Figure 6 illustrates the multiview reobservation fusion model. The model first performs N three-dimensional transformations on the skeleton data input x_t to simulate the observation of the skeleton data from N perspectives. The learned temporal features are extracted from the graph through a fully convolutional neural network, and the sequence of human skeleton key points can be represented by a series of undirected graphs. The obtained N observations are separately processed by the main LSTM network. In practice, observations under different viewing angles are obtained by 3D rotation of the skeleton s. Multiple new observations are obtained by performing N different rotations on the original skeleton s.

$$s_{vn} = \mathrm{Rotate}_n(s). \quad (12)$$

Skeleton sequence-based action recognition tasks have a huge dependence on timing information, so skeleton key points are encoded into multiple two-dimensional pseudoimages, which are then input into convolutional neural networks to learn timing features. When rotating the

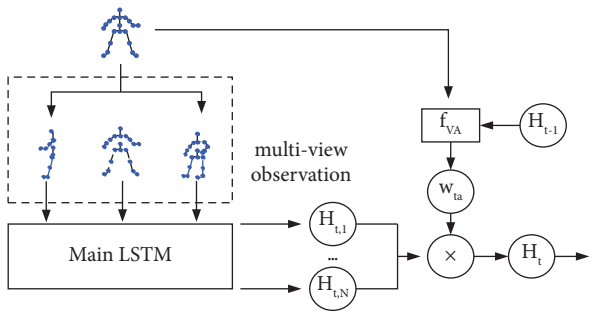

Figure 6: Multiview reobservation fusion based on attention and mechanism.

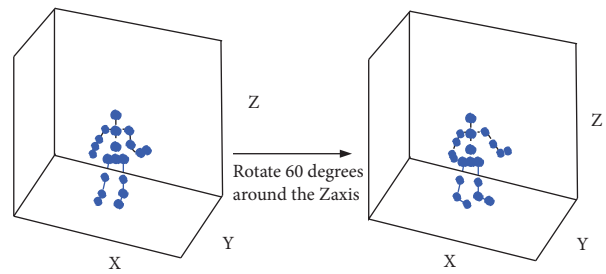

Figure 7: Skeleton model rotated 60 degrees in 3D space.

skeleton, first reposition the skeleton with its hip-center as the origin to reduce the joint drift caused by the rotation. Then, it rotates the skeleton in a 3D coordinate system. In the three-dimensional coordinate system, for a joint point $s^i = [x^i, y^i, z^i]^T$ in the skeleton, the result obtained by its rotation can be expressed as:

$$\tilde{s}^i = R_x R_y R_z s^i. \tag{13}$$

Among them, $R_x R_y R_z$ represent the rotation around the X, Y, and Z axes of the coordinate system, respectively. For example, a rotation around the Z axis can be represented by the following matrix:

$$R_y(\theta) = \begin{bmatrix} \cos\theta & -\sin\theta & 0 \\ \sin\theta & \cos\theta & 0 \\ 0 & 0 & 1 \end{bmatrix}. \tag{14}$$

In the matrix, θ represents the rotation angle around the Z axis. In reality, most of the perspective transformations are caused by changes in the horizontal direction of the observation perspective, which can be roughly represented by the rotation of the skeleton around the Z-axis in a three-dimensional coordinate system. Therefore, in order to reduce the amount of computation, in the model implementation process, only the horizontal rotation around the Z axis is now considered, as shown in Figure 7.

As discussed earlier, among all observational perspectives, some may be helpful for action recognition, and some may be detrimental to action recognition. The multiframe images or video segments input in the 3D full-volume network pass through the network and the output is a 3D feature map. The timing information of the video is effectively preserved, and the features in the timing information are accurately extracted. Therefore, the attention mechanism is used to evaluate all observation perspectives, and the perspectives that are helpful for action recognition are given higher weights, while the perspectives that are unfavorable for action recognition are given lower weights. During fusion, the results of all views are fused according to the attention weights. In this way, the model is able to learn to pick viewpoints that are beneficial for action recognition. The attention weight for the observation perspective is also generated based on the previous output h_t of the model and the current input x_t:

$$A_t = \mathrm{Softmax}\left(U\left(\tanh\left(W_{tx} * X + W_{th} * H_{t-1} + b_{t1}\right) + b_{t2}\right)\right). \tag{15}$$

The processing results of observation data from different perspectives are weighted and summed according to the attention weight to obtain the final output result:

$$\mathrm{h}_t = \sum_{i=1}^{N} A_{t,i} \bullet h_{t,i}. \tag{16}$$

In the above formula, $[h_{t,1}, h_{t,2}, \ldots, h_{t,i}]$ is the result of the main LSTM processing of observation data from different perspectives, and the weighted summation of them obtains the output of the model fused with multiple observation perspectives. h_t is deal after Softmax processing; the final category recognition result is obtained. The model can detect, identify, track, and identify people in the monitored scene, and analyze the obtained information, so as to play the role of supervision, early warning, and prevention.

4.4. Experiment and Result. The model is mainly experimentally verified on the following two current mainstream and challenging 3D action recognition databases: NTU RGB + D is currently the largest 3D action recognition database, which includes a total of 45 action categories and 35,760 records. The 45 types of movements include daily activities, health-related movements, two-person interaction movements, and more. Actions are demonstrated by 38-bit objects and captured simultaneously from 3 different viewpoints. The scale of data in this database is large, and there are multiple perspective changes. In addition, there are many actions with high similarity. It is currently the most challenging database.

LSTM + FA in the table represents a three-layer Attention LSTM combined with a multilayer feature attention mechanism. LSTM + VF represents a multiview integrated network that uses the basic three-layer LSTM network as the main network. LSTM + FA + VF represents the final model combining multilayer feature attention mechanism and multiview observation fusion architecture. In the fusion process, the attention mechanism is used to evaluate different observation perspectives, and the perspective suitable for the recognition of the action will get a higher fusion weight. As can be seen from the comparison in the table, for the cross-view evaluation method, the effect of this method

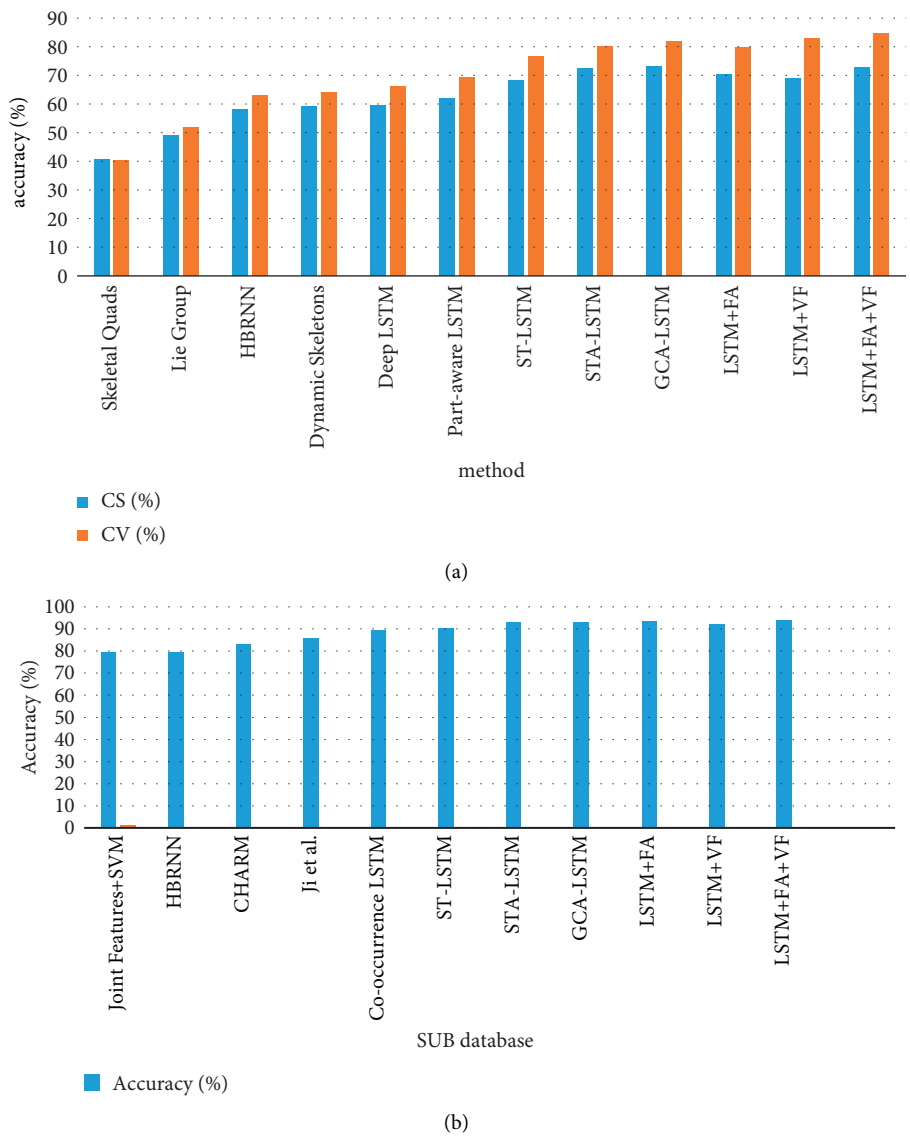

Figure 8: Comparison results with other state-of-the-art methods on NTU RGB + D and SBU databases.

is the current state-of-the-art method, which is 3% higher than the GCA-LSTM method. For the cross-object evaluation method, the effect is similar to that of GCA-LSTM, with a difference of only 0.6% as shown in Figure 8.

Figure 8 shows that processing the features in LSTM with attention improves the performance of action recognition. Moreover, processing with multilayer attention mechanisms in the LSTM network can further improve the performance. However, when stacking the three-layer attention mechanism, the performance improvement is not obvious, and there is a large drop in accuracy on the smaller database such as SBU. Through analysis, it is believed that this is because the multilayer attention operation greatly increases the complexity of the model, thereby increasing the risk of overfitting in model training, which is reflected in the sharp drop in the accuracy of SBU. The results showed that the application of multilayer feature attention mechanism in LSTM can effectively improve the performance of action

Table 2: Experimental results of multiview fusion method on NTU RGB + D database.

Method	CS (%)	CV (%)
Basic LSTM	65.67	76.36
LSTM + VF (ave)	66.27	81.5
LSTM + VF (tanh)	67.15	80.83
LSTM + VF (softmax)	69.12	83.08

Table 3: Experimental results of multiview fusion method on SBU database.

Method	Accuracy (%)
Basic LSTM	86.4
LSTM + VF (ave)	90.25
LSTM + VF (tanh)	90.64
LSTM + VF (softmax)	92.12

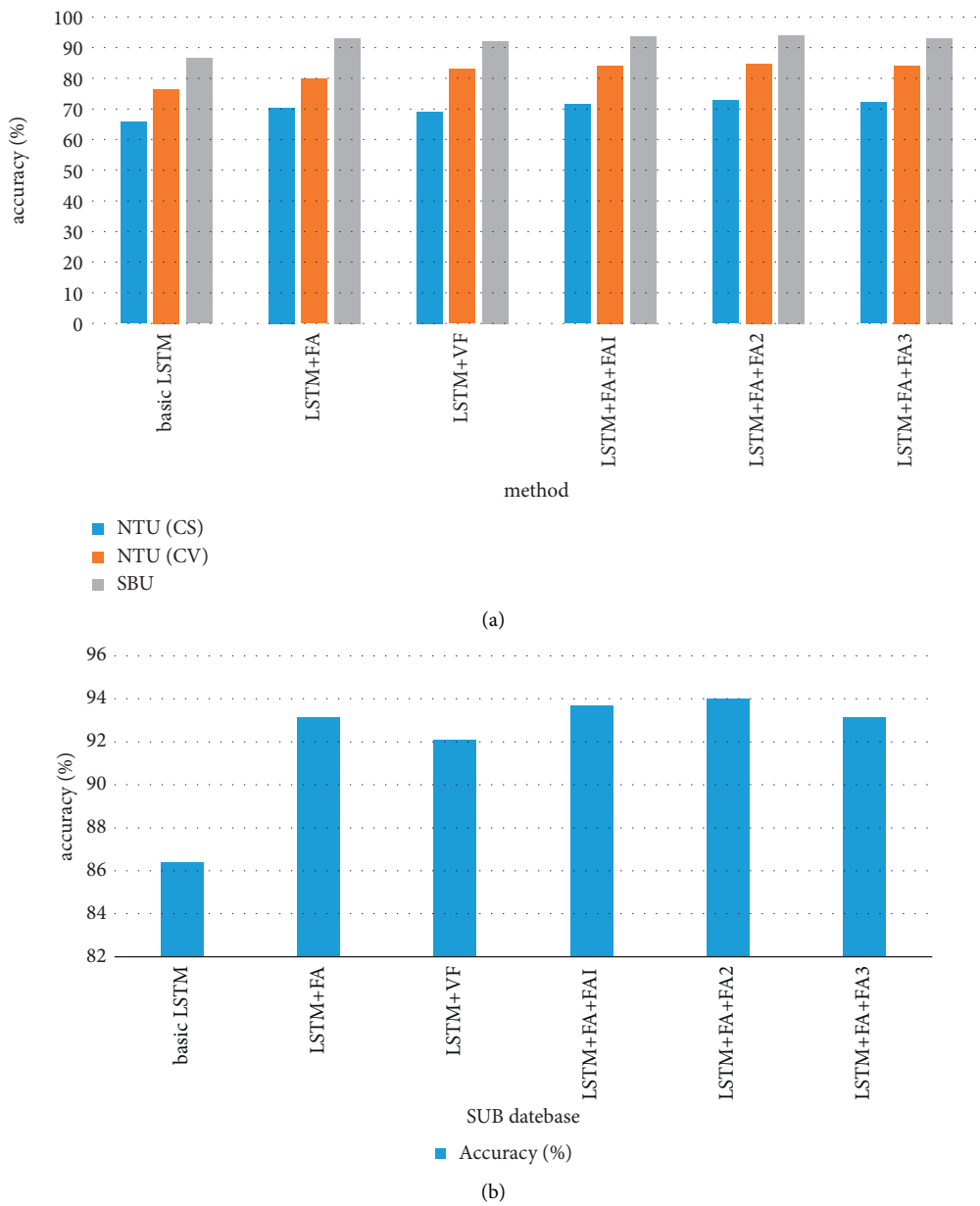

Figure 9: Comparison results with other state-of-the-art methods on NTU RGB + D and SBU databases.

recognition, but the superposition of too many layers of attention mechanism will also bring the risk of model overfitting, so it needs to be handled with caution in use.

Tables 2 and 3 indicate the experimental results of different observation fusion methods. In the experiment, three fusion strategies, average, attention weight, and attention weight were used to fuse the processing results of multiple observations to obtain the final result. For the NTU RGB + D database, three observation angles [0°, ±60°] were used in the experiment. For the SBU Kinect Interaction database, three observation angles [0°, ±90°] are used.

The experimental results indicate that multiview observation fusion is of great help to improve the performance of action recognition. Even simply averaging the processing results of multiple time observations can significantly improve the recognition accuracy. The application of the attention mechanism in the fusion process has brought further significant improvements. Experimental comparisons also show that generating weights by Softmax performs better in fusion tasks than simply generating weights with tanh activation. Overall, this experiment shows that the multiview observation fusion method proposed in this chapter is effective in 3D action recognition. It is worth mentioning that the NTU RGB + D database contains data collected from multiple perspectives, while all the data in the SBU Kinect Interaction database are collected from the same perspective. In experiments, the multiview observation fusion method achieves good results on both databases. This shows that fusing observations from different perspectives is a general 3D action recognition improvement method. The

final model fuses the multilayer feature attention mechanism in LSTM and the multiview observation fusion method to form an end-to-end network model. Experiments on the integration of methods are carried out on two databases, NTU RGB + D and SBU Kinect Interaction.

The relevant experimental results on the two databases of NTU RGB + D and SBU Kinect Interaction are shown in Figure 9. Experiments show that adding 1 or 2 layers of feature attention mechanism enhancement to the multiview observation fusion network can increase the accuracy by 1% to 3%. However, when the three-layer feature attention mechanism is added to enhance, the accuracy rate will drop. In conclusion, the combination of multiview observation fusion and feature attention mechanism method allows boosting the behavior of the model further in action recognition problems. According to the experimental results and in the final model, two layers of feature focus operations are used.

5. Discussion

The development of deep learning has solved many common problems that highly rely on feature design in computer vision. Deep networks automatically learn feature extraction under data drive and can easily obtain more powerful features compared with the traditional tedious and manually designed features. Although deep learning-based methods have achieved far more results than traditional methods in action recognition, the current theoretical research of deep learning is imperfect, and its internal information is more like a black box.

Deep learning method is used to identify human movements. In action recognition, most deep learning methods directly input images, and through data-driven methods, human action recognition is regarded as a simple classification task. Through the whole volume neural network about human action recognition, put forward based on 3D attitude human action recognition situation, through the attention mechanism of multiple observation fusion action recognition model in different environments. By identifying the human skeleton data effective information enhancement and perspective transformation, the recognition method improvement integrated into an end-to-end action recognition network.

6. Conclusion

Validated by demonstrating the rationality and effectiveness of both CS and CV algorithms on NTU RGB + D and SBU datasets. First, the accuracy of the new attention mechanism module and the new mechanism are compared, and the importance of the feedback mechanism in the recognition of human action features in multiview reobservation fusion of 3D poses is verified. Finally, the model is validated on the NTU-RGB + D Cross-Object (CS) and Cross-Perspective (CV) datasets, respectively, proving that the network model is more accurate in performance and recognition than other mainstream human action features. The rate has been improved algorithm.

Data Availability

The data that support the findings of this study can be obtained from the corresponding author upon reasonable request.

Conflicts of Interest

The authors declared no potential conflicts of interest with respect to the research, authorship, and/or publication of this article.

Acknowledgments

This work was supported by the Independent Innovation Capability Improvement Program of Huizhou University (no. HZU202054).

References

[1] J. H. Thrall, X. Li, Q. Li et al., "Artificial intelligence and machine learning in radiology: opportunities, challenges, pitfalls, and criteria for success," *Journal of the American College of Radiology*, vol. 15, no. 3, pp. 504–508, 2018.

[2] P. Mamoshina, L. Ojomoko, Y. Yanovich et al., "Converging blockchain and next-generation artificial intelligence technologies to decentralize and accelerate biomedical research and healthcare," *Oncotarget*, vol. 9, no. 5, pp. 5665–5690, 2018.

[3] Y. G. Jiang, Z. Wu, J. Wang, X. Xue, and S. F. Chang, "Exploiting feature and class relationships in video categorization with regularized deep neural networks," *IEEE Transactions on Pattern Analysis and Machine Intelligence*, vol. 40, no. 2, pp. 352–364, 2018.

[4] J. Cheng, P. S. Wang, G. Li, Q. Hu, and H. Lu, "Recent advances in efficient computation of deep convolutional neural networks," *Frontiers of Information Technology&Electronic Engineering*, vol. 19, no. 1, pp. 64–77, 2018.

[5] Y. Dong and H. Wang, "Robust output feedback stabilization for uncertain discrete-time stochastic neural networks with time-varying delay," *Neural Processing Letters*, vol. 51, no. 1, pp. 83–103, 2020.

[6] A. Lucas, M. Iliadis, R. Molina, and A. K. Katsaggelos, "Using deep neural networks for inverse problems in imaging: beyond analytical methods," *IEEE Signal Processing Magazine*, vol. 35, no. 1, pp. 20–36, 2018.

[7] P. Yin, S. Zhang, J. Lyu, S. Osher, Y. Qi, and J. Xin, "BinaryRelax: a relaxation approach for training deep neural networks with quantized weights," *SIAM Journal on Imaging Sciences*, vol. 11, no. 4, pp. 2205–2223, 2018.

[8] A. Sarabu and A. K. Santra, "Human action recognition in videos using convolution long short-term memory network with spatio-temporal networks," *Emerging Science Journal*, vol. 5, no. 1, pp. 25–33, 2021.

[9] Y. Liu, R. Ma, H. Li, C. Wang, and Y. Tao, "RGB-D human action recognition of deep feature enhancement and fusion using two-stream ConvNet," *Journal of Sensors*, vol. 2021, no. 1, Article ID 8864870, 10 pages, 2021.

[10] M. Taddeo and L. Floridi, "Regulate artificial intelligence to avert cyber Ar ms race," *Nature*, vol. 556, no. 7701, pp. 296–298, 2018.

[11] S. Wan, L. Qi, X. Xu, C. Tong, and Z. Gu, "Deep learning models for real-time human activity recognition with

smartphones," *Mobile Networks and Applications*, vol. 25, no. 2, pp. 743–755, 2019.

[12] H. Wei and N. Kehtarnavaz, "Semi-supervised Faster Rcnn-Based Person Detection and Load Classification for Far Field Video Surveillance," *Computer Vision*, vol. 1, no. 3, pp. 756–767, 2019.

[13] V. Dignum, "Ethics in artificial intelligence: introduction to the special issue," *Ethics and Information Technology*, vol. 20, no. 1, pp. 1–3, 2018.

[14] S. Ding, S. Qu, Y. Xi, and S. Wan, "Stimulus-driven and concept-driven analysis for image caption generation," *Neurocomputing*, vol. 398, pp. 520–530, 2020.

[15] S. Zhou, M. Ke, and P. Luo, "Multi-camera transfer GAN for person re-identification," *Journal of Visual Communication and Image Representation*, vol. 59, pp. 393–400, 2019.

[16] X. M. Zhang and Q. L. Han, "State estimation for static neural networks with time-varying delays based on an improved reciprocally convex inequality," *IEEE Transactions on Neural Networks and Learning Systems*, vol. 29, no. 4, pp. 1376–1381, 2018.

[17] Y. Guo, "Globally robust stability analysis for stochastic cohen–grossberg neural networks with impulse control and time-varying delays," *Ukrainian Mathematical Journal*, vol. 69, no. 8, pp. 1220–1233, 2018.

[18] C. Sánchez-Sánchez and D. Izzo, "Real-time optimal control via Deep Neural Networks: study on landing problems," *Journal of Guidance, Control, and Dynamics*, vol. 41, no. 5, pp. 1122–1135, 2018.

[19] N. Liu, J. Han, T. Liu, and X. Li, "Learning to predict eye fixations via multiresolution convolutional neural networks," *IEEE Transactions on Neural Networks and Learning Systems*, vol. 29, no. 2, pp. 392–404, 2018.

[20] Y. Cheng, D. Wang, P. Zhou, and T. Zhang, "Model compression and acceleration for deep neural networks: the principles, progress, and challenges," *IEEE Signal Processing Magazine*, vol. 35, no. 1, pp. 126–136, 2018.

[21] H. Wei and N. Kehtarnavaz, "Determining Number of Speakers from Single Microphone Speech Signals by Multi-Label Convolutional Neural Network," in *Proceedings of the IECON 2018-44th Annual Conference of the IEEE Industrial Electronics Society*, Washington, DC, USA, October 2018.

[22] Z. Lv, S. Zhang, and W. Xiu, "Solving the security problem of intelligent transportation system with deep learning," *IEEE Transactions on Intelligent Transportation Systems*, vol. 22, no. 7, pp. 4281–4290, 2021.

[23] W. Wei, Y. Sheng, J. Wang, and I. D. S. Hast, "Learning hierarchical spatial-temporal features using deep neural networks to improve intrusion detection," *IEEE Access*, vol. 6, no. 99, pp. 1792–1806, 2018.

[24] P. Cao, W. Xia, M. Ye, J. Zhang, and J. Zhou, "Radar-ID: human identification based on radar micro-Doppler signatures using deep convolutional neural networks," *IET Radar, Sonar & Navigation*, vol. 12, no. 7, pp. 729–734, 2018.

[25] E. Nabiel Al-Khanak, S. Peck-Lee, S. Ur-Rehman-Khan et al., "A heuristics-based cost model for scientific workflow scheduling in cloud," *Computers, Materials & Continua*, vol. 67, no. 3, pp. 3265–3282, 2021.

[26] S. Sengan, P. Vidya-Sagar, O. Ibrahim Khalaf, and R. Dhanapal, "The optimization of reconfigured real-time datasets for improving classification performance of machine learning algorithms," *Mathematics in Engineering, Science and Aerospace (MESA)*, vol. 12, 1 page, 2021.

[27] O. Öztimur Karadağ, "An adversarial framework for open-set human action recognition using skeleton data," *Turkish Journal of Electrical Engineering and Computer Sciences*, vol. 29, no. 2, pp. 717–729, 2021.

[28] M. Attique-Khan, M. Alhaisoni, A. Armghan et al., "Video analytics framework for human action recognition," *Computers, Materials & Continua*, vol. 68, no. 3, pp. 3841–3859, 2021.

[29] L. Xia and Z. Li, "A new method of abnormal behavior detection using LSTM network with temporal attention mechanism," *The Journal of Supercomputing*, vol. 77, no. 4, pp. 3223–3241, 2021.

[30] S. Zhang, W. Tan, Q. Wang, and N. Wang, "A new method of online extreme learning machine based on hybrid kernel function," *Neural Computing & Applications*, vol. 31, no. 9, pp. 4629–4638, 2019.

[31] C. H. Chen, S. Fangying, F. J. Hwang, and L. Wu, "A probability density function generator based on neural networks," *Physica A: Statistical Mechanics and Its Applications*, vol. 541, 2020.

[32] J. Dai, H. Song, and G. Sheng, "Prediction method for power transformer running state based on LSTM network," *Gaodianya Jishu/High Voltage Engineering*, vol. 44, no. 4, pp. 1099–1106, 2018.

[33] H. Zhao, S. Sun, and B. Jin, "Sequential fault diagnosis based on LSTM neural network," *IEEE Access*, vol. 6, no. 99, pp. 12929–12939, 2018.

[34] S. Gai, X. Zeng, and T. Yuan, "Parking volume forecast of railway station garages based on passenger behaviour analysis using the LSTM network," *Journal of Advanced Transportation*, vol. 2021, no. 722, Article ID 6688609, 14 pages, 2021.

[35] J. Venskus, P. Treigys, and J. Markevičiūtė, "Unsupervised marine vessel trajectory prediction using LSTM network and wild bootstrapping techniques," *Nonlinear Analysis Modelling and Control*, vol. 26, no. 4, pp. 718–737, 2021.

[36] D. Gupta, V. Kumar, I. Ayus, M. Vasudevan, and N. Natarajan, "Short-term prediction of wind power density using convolutional LSTM network," *FME Transactions*, vol. 49, no. 3, pp. 653–663, 2021.

Hindawi
Mobile Information Systems
Volume 2023, Article ID 9793406, 1 page
https://doi.org/10.1155/2023/9793406

Retraction

Retracted: Naive Bayes Algorithm Mining Mobile Phone Trojan Crime Clues

Mobile Information Systems

Received 26 September 2023; Accepted 26 September 2023; Published 27 September 2023

This article has been retracted by Hindawi following an investigation undertaken by the publisher [1]. This investigation has uncovered evidence of one or more of the following indicators of systematic manipulation of the publication process:

(1) Discrepancies in scope
(2) Discrepancies in the description of the research reported
(3) Discrepancies between the availability of data and the research described
(4) Inappropriate citations
(5) Incoherent, meaningless and/or irrelevant content included in the article
(6) Peer-review manipulation

The presence of these indicators undermines our confidence in the integrity of the article's content and we cannot, therefore, vouch for its reliability. Please note that this notice is intended solely to alert readers that the content of this article is unreliable. We have not investigated whether authors were aware of or involved in the systematic manipulation of the publication process.

Wiley and Hindawi regrets that the usual quality checks did not identify these issues before publication and have since put additional measures in place to safeguard research integrity.

We wish to credit our own Research Integrity and Research Publishing teams and anonymous and named external researchers and research integrity experts for contributing to this investigation.

The corresponding author, as the representative of all authors, has been given the opportunity to register their agreement or disagreement to this retraction. We have kept a record of any response received.

References

[1] F. Zhao, "Naive Bayes Algorithm Mining Mobile Phone Trojan Crime Clues," *Mobile Information Systems*, vol. 2022, Article ID 6262147, 11 pages, 2022.

Hindawi
Mobile Information Systems
Volume 2022, Article ID 6262147, 11 pages
https://doi.org/10.1155/2022/6262147

Research Article

Naive Bayes Algorithm Mining Mobile Phone Trojan Crime Clues

Fugang Zhao

Police Officer Academy, Shandong University of Political Science and Law, Jinan, Shandong 250014, China

Correspondence should be addressed to Fugang Zhao; zhaofugang@sdupsl.edu.cn

Received 14 June 2022; Revised 20 July 2022; Accepted 1 August 2022; Published 26 August 2022

Academic Editor: Yajuan Tang

After the mobile phone virus infects the mobile phone, it can transmit the real-time information of the user to the designated place set by the virus through the built-in recorder and camera on the mobile phone, thereby causing information leakage. With the rapid development of the Internet, the penetration rate of mobile terminals is also increasing day by day. As an emerging mobile terminal, smart phones have now fully occupied the market. With this trend, the importance of mobile phone information security is also increasing day by day. How to prevent mobile phone virus has gradually become an important issue. Trojan horse crime cases have different manifestations and behavioral characteristics from traditional cases. They have the characteristics of low crime cost, high income, high concealment, novel criminal methods, and great difficulty in detection, which brings greater difficulties to the public security organs in their investigation and detection. And the current research on mobile phone virus behavior is still in the preliminary stage, and some existing detection models can only target random networks. Trojan horses, viruses, and malicious software for smartphones have sprung up like mushrooms after rain, seriously infringing on the data security of mobile communication terminals, such as mobile phones and causing incalculable losses to users. This paper proposes a naive Bayesian algorithm to mine the clues of the criminal cases of mobile phone Trojans. It helps detect and discover new viruses at the beginning of an attack, allowing them to be more effectively defended and contained. And based on the feature set data extracted from the network data packets, it conducts an in-depth analysis of the current business behaviors of mobile phone Trojans, such as propagation and implantation, remote control, leakage of user privacy information, and malicious ordering, and extracts its behavior characteristics. Thus, unknown mobile Trojan horses that are taking place can be detected. The experimental results of the naive Bayesian classification algorithm proposed in this paper show that the algorithm improves the accuracy of mobile phone Trojan virus mining by 28%, which plays a significant role.

1. Introduction

In recent years, with the rapid development of mobile communication technology, the degree of intelligence of mobile phones is also getting higher and higher. The hardware configuration of smart phones is constantly upgraded, and it also integrates technologies, such as short message (SMS), multimedia message (MMS), Bluetooth (Bluetooth), wireless application protocol (WAP) surfing, and general packet radio service (GPRS) Internet access. With the popularization of computers and the rapid development of the Internet, people's lifestyles and values have undergone earthshaking changes. While enjoying a large amount of information resources and an increasingly convenient life brought by the Internet, some lawbreakers use emerging science and technology to commit illegal and criminal acts, infringing on citizens' legitimate rights and interests and disrupting public order. In recent years, a large number of illegal and criminal activities using Trojan horses have occurred throughout the country. Mobile phone viruses can damage the software and hardware of mobile phones and directly affect the normal work of mobile phones. The main symptoms include crashes, automatic restarts, keyboard locks, rapid power consumption, slow operation, and abnormal noises. The form of crime has also evolved from the initial singularity and individualization to the diversification and industrialization of today. The perpetrators of most Trojan horse crime cases have formed a huge interest group with a clear division of labor. They use methods such as stealing virtual property to sell for profit or

maliciously destroying important data, and so on, to commit crimes of infringement of property and disrupting the order of social management. even crimes that endanger national security. The popularity of smart phones has brought a new situation of mobile phone applications. The functions of mobile phone-based applications are more powerful, the types are more diverse, and the download volume is increasing.

The formulation of an information security policy involves more than just the formulation and implementation of the policy. Unless organizations clearly recognize the various steps required to develop a security strategy, they run the risk of developing a strategy that is well thought out, incomplete, redundant, and irrelevant, and will not be fully supported by users. Flowerday and Tuyikeze believe that an information security strategy has a complete life cycle, and it must be passed during its useful life cycle. A formal content analysis of the information security policy formulation method was carried out using secondhand data. Flowerday and Tuyikeze subsequently developed a conceptual framework based on the results of content analysis. The proposed framework outlines the various structures required to develop and implement an effective information security strategy. During their research, they conducted a survey of 310 security professionals to verify and refine the concepts contained in the key components of the framework. However, the conceptual framework they proposed is too general to accurately explain the information security strategy [1]. Gusmo et al. proposed a risk analysis model for information security assessment. This model identifies and evaluates the sequence of events in potential accident scenarios (called alternatives) after the initial event corresponding to the abuse of information technology systems occurs. In order to carry out this assessment, this work proposes to use event tree analysis combined with fuzzy decision theory. The contribution of the proposal is to develop a classification of events and scenarios, rank alternatives according to the severity of the risk, take into account financial losses, and, finally, provide information about the most serious causes of attacks on information systems. For the management relevance of the organization, they included an illustrative example of a data center to illustrate the applicability of the proposed model. In order to evaluate its robustness, they considered two different methods for setting the probability of occurrence of events and analyzed twelve alternatives. However, the information security assessment risk analysis model they proposed is too complicated, and errors may occur in the calculation process [2]. Runtime security is a hot spot in current cyberspace security research, especially embedded terminals, such as smart hardware and wearable and mobile devices. These devices usually use common hardware and software to connect to public networks via the Internet and may be vulnerable to security threats from Trojan horse viruses and other malicious software. Therefore, the security of sensitive personal data is threatened, and the economic interests of the industry are harmed. In order to effectively solve the problem of runtime security, Rui et al. proposed a security architecture based on information security. The experimental results prove the effectiveness and the feasibility of the proposed safety scheme. However, there are still deficiencies in the handling of runtime security issues [3].

The innovation of this paper is to use the proposed naive Bayes algorithm to mine the clues of mobile phone Trojan horse criminal cases, and based on the feature set data extracted from network data packets, including protocol type, content length, connection status, whether to carry the installation files, and so on, truly reflect the mobile phone network behavior of the data, and then the mining engine based on the data can effectively summarize the behavior characteristics of the existing mobile phone viruses and use this to detect unknown mobile phone viruses.

2. Mobile Phone Trojan Virus Data Mining Algorithm

2.1. Bayesian Classification Method. Bayes' theorem is a result of probability theory, which is related to the conditional probability of the machine variable and the marginal probability distribution [4]. Let D and S be two random variables, $D = d$ is a certain result hypothesis, $T = t$ is a set of sample data, $T(D = d)$ is the prior probability of time $D = d$, and $S(D = d/T = t)$ is the posterior probability of event $D = d$ under the premise of sample data $T = t$. The Bayes formula is also called the posterior probability formula:

$$S(D = d|T = t) = \frac{S(D = d)S(T = t|D = d)}{S(T = t)}. \tag{1}$$

In addition to signatures, the behavior of mobile phone viruses is also special. Studying the behavioral characteristics of mobile phone viruses is helpful to detect and discover new viruses at the early stage of the outbreak so as to be able to defend and control them more effectively. The Bayesian classification model is a typical classification model, based on statistical methods, with Bayesian formula as the core. The specific expression is $A = (D1, D2, ..., DN, G)$ is the original training set, where $D1, D2, ..., DN$ are the N special attributes of the training data, and the value of the class label G, the range, is $(G1, G2, ..., gm)$; that is, there are m class labels in total.

$$\begin{aligned} S\left(g_i/a_j\right) &= \frac{S(g_i)S\left(a_j/g_i\right)}{S\left(a_j\right)} = \beta S(g_i)S\left(\frac{a_j}{g_i}\right) \\ &= \beta S(g_i)S\left(\frac{(b_1, b_2, \ldots, b_n)}{g_i}\right). \end{aligned} \tag{2}$$

The naive Bayes classification algorithm assumes that each attribute value of the sample data in the original training set is independent of each other, which greatly simplifies the calculation of the posterior probability. Among them, $S(a_j)$ is the prior probability of the sample data a_j, which has nothing to do with the specific value of the class label, so it can be treated as a constant when judging the class label.

2.2. Naive Bayes Classification Algorithm. The naive Bayes smashing algorithm is based on the premise of class condition independence; that is, it is assumed that each attribute

value of the sample data in the original training set is independent of each other [5]. This assumption greatly simplifies the amount of calculation when obtaining the posterior probability, so it is called "naive."

The specific workflow of the naive Bayes classification method is as follows:

Let D be a collection of training samples and class labels (training set), and suppose that each training sample is represented by an n-dimensional attribute vector $R = \{r_1, r_2, \ldots, r_n\}$, where r_1, r_2, ..., r_n are, respectively, corresponding to n, a collection of specific values of attributes.

Assuming that, for a given data sample R, there are a total of m class labels, denoted as $\{G_1, G_2, \ldots G_m\}$, the classification algorithm will calculate the posterior probability value of each class label under the data sample R, and determine that R belongs to the posterior probability, the class with the largest value, that is, when R belongs to class G_j:

$$S\left(\frac{G_i}{R}\right) > S\left(\frac{G_j}{R}\right), \quad 1 \le j \le m,\ j \ne 1. \tag{3}$$

In this way, to maximize $S(G_i/R)$, the value of $S(G_i/R)$ can be calculated according to Bayes' theorem.

$$S\left(\frac{G_i}{R}\right) = \frac{S(R/G_i)S(G_I)}{S(R)}. \tag{4}$$

Since the naive Bayes classification algorithm assumes that each feature attribute is independent of each other, that is, the attributes do not affect each other, then

$$S\left(\frac{R}{G_i}\right) = \prod_{x=1}^{n} S\left(\frac{R_x}{G_i}\right) = S\left(\frac{R_1}{G_i}\right) \times S\left(\frac{R_2}{G_i}\right) \times \ldots S\left(\frac{R_n}{G_i}\right). \tag{5}$$

Use formula (5) to estimate $S(R/G_i)$, where R_x represents the value of the attribute D_x in the sample data R. For each attribute, consider whether the attribute is discrete or continuous.

$$P(o, \eta, \mu) = \frac{1}{\sqrt{2\pi\mu}} w^{-\left((o-\eta)^2/2\mu^2\right)}. \tag{6}$$

Therefore,

$$S\left(\frac{R_x}{G_i}\right) = h\left(R_x, \eta_{G_i}, \mu_{G_i}\right). \tag{7}$$

Using formula (5), to predict the class number of R, calculate $S(R/G_i)S(G_i)$ for each class G_i. The classification method predicts that the class label of the sample data R is G_i, only if

$$S\left(\frac{R}{G_i}\right)S(G_i) > S\left(\frac{R}{G_j}\right)S\left(G_j\right), \quad 1 \le j \le m,\ j \ne 1. \tag{8}$$

That is, the final class label is class G_i that makes $S(R/G_i)S(G_i)$ the largest under the condition of R.

2.3. Naive Bayes with Tree Augmentation. To create a naive Bayesian classification tree classification model, you must first calculate the mutual information between all variable attributes according to formula (9). Mutual information is used to measure the amount of information contained in one variable in another variable. The greater the amount of mutual information, the more explanation, most information contains the relationship between two variables.

$$I\left(\frac{D_i, D_j}{G}\right)\log\frac{S\left(D_i, D_j/G\right)}{S\left(D_i/G\right)S\left(D_j/G\right)}. \tag{9}$$

Next, obtain all attribute variables as node and mutual status information, and artificially link the nodes to create an undirected complete graph. The maximum tree weight algorithm is used to create the maximum weight tree for the unguided graph. The naive Bayes classification algorithm is based on the premise of class conditional independence; that is, it is assumed that each attribute value of the sample data in the original training set is independent of each other. This assumption greatly simplifies the amount of computation when calculating the posterior probability.

2.4. Incremental Learning Bayesian Classification. Incremental learning Bayesian classification is to overcome its two shortcomings by continuously completing the training set of the naive Bayes algorithm. After the initial modeling is completed, the incremental learning algorithm is used to select the incremental samples without category labels in the incremental set K, and the new modeling parameters are obtained after the discriminated incremental samples are added to the original training set. Then, the unknown samples are judged according to this new classification model. The core of the algorithm is to continuously select new sample data to be added to the training set Y, making the training set more and more complete and testing with training data repeatedly, which makes the conditional correlation between the attribute values of the sample instances weaken and become more independent [6, 7].

A loss weight coefficient σ^y is introduced from all instances in the training set Y, and σ^y reflects the sensitivity of the instances in Y to newly added instances. Suppose that the class conditional probability of W^y is stored in φ^y in the learning new instance, and the new class conditional probability of W^y is calculated in Y and expressed as φ^y. Definition:

$$\sigma^y = \varphi^y \exp\left(\varphi^{y\prime} - \varphi^y\right) = \varphi^y \exp\left(\Delta\varphi^y\right). \tag{10}$$

The estimate of W^y is the absolute loss of $|\Delta\varphi^y|$ in the calculation formula:

$$\text{Loss}_y = \sigma^y\left|\Delta\varphi^y\right| = \left|\Delta\varphi^y\right|\varphi^y \exp\left(\Delta\varphi^y\right). \tag{11}$$

The algorithm of this module is to make the stock calculation formula of all the instances in the training set Y and the smallest instance enter Y from the photos in K, gradually reduce the number of instances in the test set K, knowing that K is empty or the LossSum value is greater than the set maximum threshold.

2.5. Selection Method of Characteristic Attributes. The methodology of feature attribute extraction is based on judging the gain rate of each feature attribute to obtain the

most suitable feature set. Before introducing the gain rate, first introduce the concept of information gain as its foundation. Information gain belongs to the category of information theory. It is used to measure the ability of an attribute to distinguish samples. The larger the value, the stronger the ability, and vice versa.

The expected information required for the classification of tuples (feature attributes) in the data set T is obtained by the following formula:

$$\mathrm{Inf}(T) = -\sum_{i=1}^{n} s_i \log_2(s_i). \tag{12}$$

Among them, s_i is the probability of using the 2-base logarithmic function because any T (attribute property) set belongs to the G_i class and the information is binary bits. Inf (T) is the average value of the information required to identify the class label of T and is calculated as follows:

$$\mathrm{Inf}_C = \sum_{j=1}^{O} \times \mathrm{Inf}(T_j). \tag{13}$$

Information capture is defined as the difference between the initial demand for information (based on analogy only) and the new demand.

$$\mathrm{Gain}(C) = \mathrm{Inf}(T) - \mathrm{Inf}_C(T). \tag{14}$$

Obtaining information also has the disadvantage of multiple output feature deviations, which means that they often have a large number of feature values. In order to overcome this prejudice, the profit margin is used as an extension of information acquisition, using the split information value to normalize the information gain, and "split information" is defined as follows:

$$\mathrm{Inf}_C = -\sum_{j=1} \frac{|T_j|}{|T|} \times \log_2\left(\frac{|T_j|}{|T|}\right). \tag{15}$$

Select the attributes with short answer gain rate to form a new feature set.

3. Characteristics of Illegal and Criminal Cases of Trojan Horse under Information Security

3.1. Main Forms of Trojan Horse Crime Cases. In the crime of property invading Trojan horses, criminal suspects use various means and excuses, such as building false web pages to deceive users from clicking, and so on, downloading Trojan horses to the user's computer to steal user's related information or virtual property. After that, the criminal suspect may use the stolen information to conduct traditional crimes such as blackmail and fraud or sell the virtual property and convert it into real currency to directly benefit. In short, since the ultimate goal of the criminal suspects in such cases is to obtain economic benefits, they are collectively referred to as the crime of invading property Trojan horses [8,9]. Trojan horse virus is a program used by computer hackers to remotely control the computer. The control program is parasitized in the controlled computer system, and the inside and outside are combined to perform operations on the computer infected with the Trojan horse virus.

In the crime of disrupting the order of social management, the suspect uses a Trojan horse to control the user's computer, not for the purpose of obtaining economic benefits, and maliciously delete, modify, add, or interfere with the user's storage data, information system, or network environment. This behavior produced serious consequences and disrupted the management order of the society [10, 11].

In the crime of endangering national security, criminal suspects use Trojan horses to invade information systems, such as national affairs, national defense construction, and cutting-edge science and technology, and their behavior constitutes a violation of national security [12].

3.2. Behavioral Characteristics of Trojan Horse Crime Cases

Concealment. Trojan horse crime occurs automatically when the system is started, most of the Trojan horse programs are hidden in the task manager and taskbar, deceiving the operating system in the form of system services that are difficult for users to detect [13].

In unauthorized, Trojan horse crime cases, any operation of the criminal suspect on the target host is illegal [14], and the operation authority granted by the user is not obtained.

Self-Protection. In Trojan horse crime cases, the Trojan horse used by the criminal suspect has an automatic recovery function, and the user thinks that the Trojan horse is deleted and then runs other programs to cause the Trojan horse to recover; or has a self-destruction function that will self-destruct after achieving the expected goal This type of function brings great difficulties when discovering and investigating Trojan horse crimes, and plays a role of self-protection [15,16].

Function Peculiarities. In Trojan horse crime cases, due to the different needs of the criminal suspect, the function of the Trojan horse is very special, such as keylogging, obtaining passwords, and modifying the registry [17].

3.3. Investigation Thinking of the Trojan Horse Crime Case

(1) The thinking of investigation is that after the criminal act is filed by the case-handling agency, in order to logically associate the case with the suspect, it effectively integrates some messy clues and evidence, through on-site visits, on-site investigations, on-site evidence collection, queuing, and investigation, and through interrogation, search, wanted criminal suspects, and other investigative measures and methods, and finally identifies and arrests criminal suspects. The quality of the case-handling thinking adopted by the investigators will directly affect the smoothness of the case-handling process. In Trojan horse crime cases, due to the characteristics of a wide geographical span, a large number of

people are involved, and with a fast transmission speed, if the thinking of handling the case cannot be directed to criminal behavior quickly and effectively, the economic and spiritual losses brought about will be immeasurable [18, 19].

(2) Use the information involved in investigations.

The user discovers that the computer is attacked by Trojan horse crime, which usually occurs in two stages. One is that users discover the existence of Trojan horses through real-time monitoring of IDS, firewall, FTP, WWW and antivirus software log abnormal detection, Trojan horse discovery tools, and so on; the second is that during the "horizon-troubled" stage, the WEB website finds that the system is running abnormally and reports a case. In either case, the attacker often finds the server or target host with system vulnerabilities on the Internet through vulnerability scanning technology, directly attacks it or induces users to log in to the website, run the download program, and so on, to hang the horse. First of all, investigators need to investigate the victimization of the system, extract the logs of the invaded system to find scan traces, uploaded active files, registry modification information, and so on. After analysis, the source of the attack was found, and the Trojan horse used by the suspect was obtained [20, 21]. Analyze and test the Trojan horse, and locate the virtual address of the criminal suspect through the receiving address of the returned data packet in the Trojan horse function. Secondly, investigators need to inspect the server that is linked to the horse, and find information related to the criminal suspect in the real society through the rental information and maintenance information of the server [22, 23]. The data packet received on the server records the victim's situation. The data packet can not only be used as evidence for future prosecution, but also can be used as a clue to find unknown victims in the real society. In this way, some criminal activities that the investigators have not yet mastered will be obtained, and the criminal behavior of the criminal suspect will be further determined.

3.4. Spread and Implant of Trojan Horse Virus. At present, there are two main ways for mobile phone Trojans to spread and implant. The first is to pretend to be a popular mobile phone application and hang on the website to induce users to download and install. The second is to cooperate with copycat mobile phone manufacturers and directly implant it on their mobile ROM [24]. The first method is to spread and implant through network downloads. Mainly take advantage of the lack of security review management loopholes in today's mobile phone forums, use current popular mobile applications, and use vocabulary such as free version, cracked version, and Chinese version as inducements, and use the psychology of some users not to pay for genuine mobile applications to spread and plant into, such as disguised as QQ landlord, call flipping, mobile phone accelerator, and other applications. The second method is implanting in the ROM of the factory through the copycat mobile phone. Once the user bought this kind of fake mobile phone, he was directly attacked by the Trojan horse after

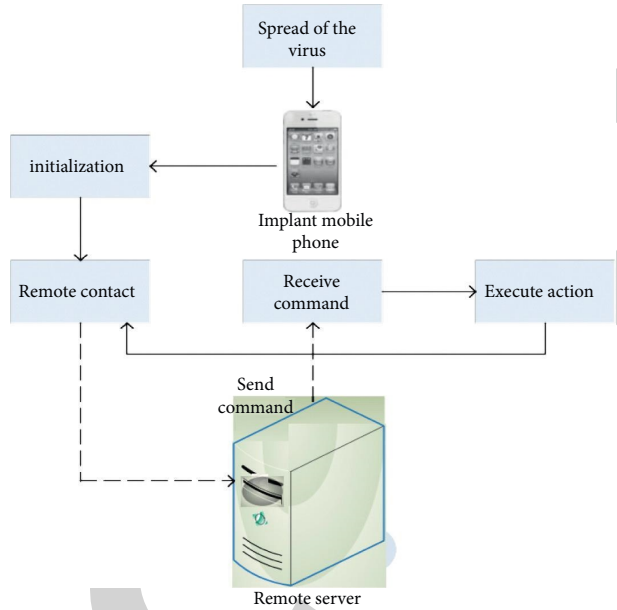

Figure 1: Typical mobile phone Trojan horse behavior pattern diagram.

plugging in the SIM card. A large number of mobile phone users suffer from the harm caused by mobile phone Trojan horses [25]. Summary of behavioral characteristics: The first method is actually to induce mobile phone users to manually download and install mobile phone Trojan horses. It is no different from mobile phone users downloading and installing a normal mobile phone application through the Internet. The installed applications are tested [26,27]. The second method is that the mobile phone Trojan has been implanted into the mobile terminal first, so the mobile phone user's behavior cannot be used to detect its propagation and implantation behavior. After the mobile phone Trojan is successfully implanted in the mobile terminal, it will contact the server, notify the server that the mobile terminal has become the target terminal, and request the server to issue a command [28,29].

3.5. Mobile Phone Trojan Horse Behavior

3.5.1. A Mobile Phone Trojan Horse Is Usually a Virus Program with a Server and a Client. The Trojan horse client program is responsible for performing malicious actions in response to the server's commands in the mobile terminal, and the remote server is mainly responsible for issuing commands to the client. A typical mobile phone Trojan horse behavior model is shown in Figure 1.

The smart phone communicates with the control terminal through the socket. The computer generates various click commands by clicking on the visual interface, and the Android client analyzes the commands and calls the corresponding operators for command control. This control method is based on the C/S architecture, where the computer is the control device and the Android device is the implanted device. Figure 2 shows the overall control flow.

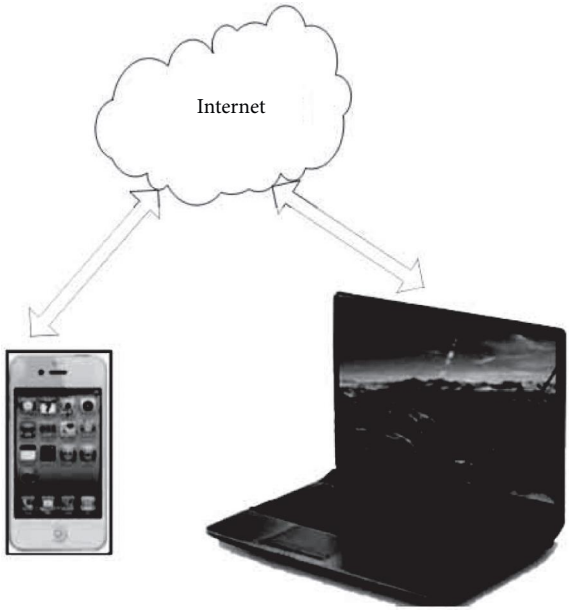

Figure 2: The overall control process.

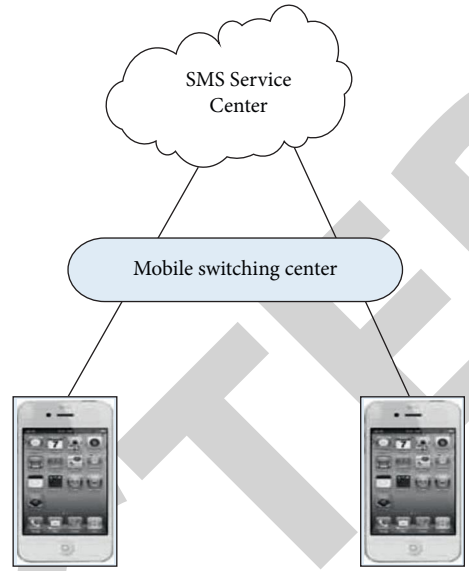

Figure 3: SMS service process.

After the mobile phone Trojans induce users to download and install them to the mobile terminal through various means of propagation, they first complete the initialization work, such as obtaining operation permissions, registering the listener, and running in the background, and then contact the remote server to inform the server that the mobile terminal has been implanted. And wait for the server to issue a command for the next action. After receiving the command issued by the server, the mobile phone Trojan will execute the corresponding action. After completion, it will contact the server again to inform that the command has been executed and wait for the next command.

3.5.2. SMS Command Control Technology. The mobile phone Trojan can also communicate via SMS. The client and the server communicate with each other through command short messages containing special characters or custom keywords as identification. However, this method is not common, mainly because the communication via SMS requires the operator's SMS service, and the requirements for the server are higher, and the ability to send and receive SMS is required. Its complexity and cost are more than those through the network. The way of communication is higher. The way to check the short message command is to send a short message based on SMS (Short Message Service) and check the command. SMS is a store and forward service. Figure 3 shows the flowchart of saving and forwarding messages. SMS is a store and forward service. That is to say, short messages are not sent directly from sender to receiver, but are always forwarded through the short message service center.

The SMS sent by P1 is received from the base station and then forwarded to the Mobile Switching Center (MSC), and the mobile switching center sends the data to the Short Business Service Center (SMSC). After SMSC receives the message, it will send a confirmation message to the sender to notify them that the message has been received. Finally, the SMS service center forwards the received SMS to the mobile switching center, and the mobile switching center sends the mobile phone P2.

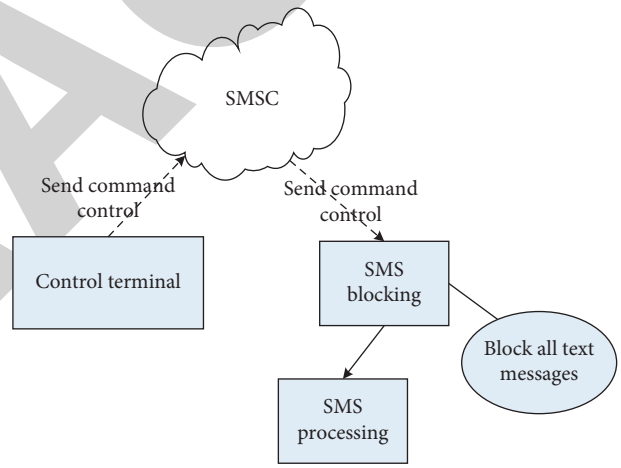

Figure 4: Control principle diagram.

In the final analysis, the entire process of the control terminal controlling the terminal through SMS commands includes three steps: sending SMS instructions, SMS spying, and SMS processing. The control principle diagram is shown as in Figure 4.

The Trojan can determine the encryption algorithm used by adding a format to the additional bits. You can specify the number 5 to indicate the use of RAS encryption to send packet data. As shown in Figure 5, encrypted data can achieve the purpose of restoring information by preventing antivirus software and firewall software from being intercepted.

Figure 5 shows that encrypted data cannot be analyzed by antivirus software. Improve the concealment of data

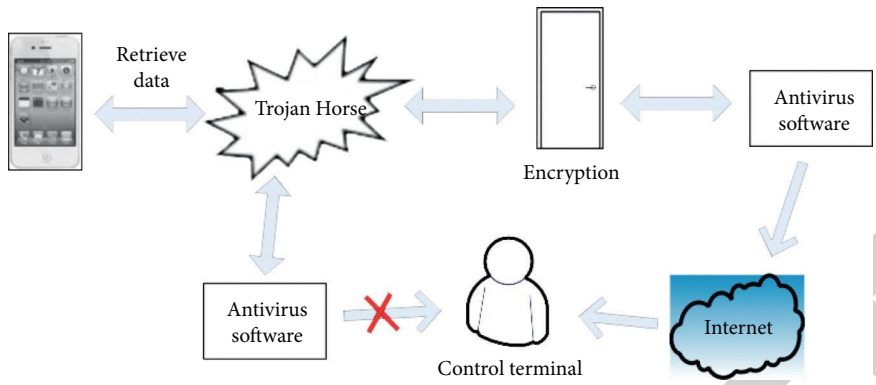

Figure 5: Data encryption transmission process.

recovery and ensure the normal transmission of data. The unencrypted data is intercepted and cannot be obtained by the control end. Only from the mobile phone Trojan horse client program implanted in the mobile terminal, we can only analyze which malicious behaviors it may have, but we cannot know under what circumstances these malicious behaviors will be executed. If the key parameters of certain malicious behaviors are also distributed through the server, we cannot even analyze what kind of malicious behavior the mobile phone Trojan will perform. For example, there is a network access behavior in the client program, but the specific access address is passed in with the instruction issued by the server as a parameter. Another example is the behavior of sending a text message in the program, but the recipient of the SMS and the content of the SMS are delivered by command from the server. Therefore, only when the mobile phone Trojan runs in an executable environment and can get in normal contact with the server, can it show a complete malicious behavior.

4. Naive Bayes Algorithm Trojan Virus Mining

4.1. Weighted Naive Bayes Algorithm Classification Processing. The idea of the experiment in this paper is to use the idea of rough set attribute reduction to perform attribute reduction, check whether there are attributes and redundant attributes that are not relevant to decision-making, and if so, select the best attribute set and use the naive Bayes method classification; if not, proceed to classification directly. Let A, B, C, D, E, F, and G, respectively, represent setting startup items, hiding, phishing interface, remote thread injection into other processes in the registry, reducing security, binding network ports, and killing other processes. The establishment of the recognizable matrix is shown in Table 1.

The seven different attributes in the experiment are different from the normal inverted triangle and the normal triangle discernibility matrix. The following discernible matrix rows represent Trojan horses and the columns represent normal programs. The kernel attributes obtained are {A, B, C, D, E, F, G}, indicating that there is no redundancy in the data; this core attribute can be used for classification.

4.2. Comparative Analysis of Weighted Naive Bayes Algorithm. The weighted Bayes algorithm is used for learning, but the weighted probability value obtained by learning is optimal, and it is not optimal for different test sets. That is, when the best experience risk is the largest, the confidence range is often relatively low. Therefore, this article weights the different probability values of each attribute in turn, tests the test set data, and selects the optimal value from the test results, which is the weighted parameter value found in this article. According to the abovementioned feature attribute selection method, the feature attributes required by the mobile phone Trojan horse clue mining in this article are obtained, as shown in Table 2.

Among them, method_type records the data submission method used when the mobile phone accesses the data requested by the website, is_connect_flag records whether the person has sent a CONNECT request, is_contain_url records whether the sample contains a URL link, transmit_size records the stream length, protocol_type records the protocol type, receive_or_send records whether the sample is a received file or a sent file, and flowtype records whether the sample is an MMS or a normal file.

The experimental results are shown in Figure 6. After comparing the results, the weighted Bayes classifier has a significantly higher detection accuracy than the naive Bayes algorithm.

The result is shown in Figure 7. After comparing the results, the weighted Bayes classifier has a significantly lower detection false alarm rate than the naive Bayes algorithm.

The result is shown in Figure 8. After comparing the results, the weighted Bayesian classifier has a significantly lower detection false negative rate than the naive Bayes algorithm. This shows that the naive Bayes method assumes that the importance of each conditional attribute to classification is the same is not true.

4.3. Naive Bayesian Classification Algorithm Behavior Feature Extraction. Download 10 Trojans from the hacker base, and put their server side on the experimental machine. For the feature extraction of the sample program, this article mainly focuses on 7 attribute features, such as setting self-starting items in the registry, hiding, whether there is visibility Interface, remotely inject other processes, reduce security, bind

Table 1: Recognizable matrix.

	1	2	3	4	5	6	7
1	0	A, C, E	A, C	B, D	C	A, D	C, E
2	A, B, D, F, G	B, C, D, E, F, G	B, C, D, F, G	A, C, D, E, F	B, C, D, E, F	A, B, C, D, F, G	A, B, C, D, E, F
3	B, E	A, B, C	A, B, C, E	B, C, E	B, C	A, D, E	A, B, D, G
4	B, F, G	A, B, C, E, F, G	A, B, C, F, G	B, C, F, G	B, D, E, F, G	A, C, D, F, G	A, B, D, E, F
5	B	A, B, C, E	A, B, C	B, C	A, C, D	B, C, E, F	A, B, C, D, F
6	A, B, D, G	A, B, C, E	B, C, D	A, C, D, F	A, B, C, D, G	A, B, C, D, E, F	A, B, C, D, E
7	A, B, E, F	B, C, D, E, G	B, C, F	B, C, E, F	A, B, C, E, G	A, B, C, F	B, C, D

Table 2: Characteristic attribute table.

Number	Attribute name	Property value properties	Attribute value range	Number of attribute values
1	Method_	Discrete value	GET, POST, Http, Reply, and null	6
2	Connect_flag	Discrete value	1 and 0	3
3	Contain_url	Discrete value	1 and 0	3
4	Transmit_size	Continuous value	0–10M	\
5	Protocol_type	Discrete value	UDP, TCP	9
6	Receive_or_send	Discrete value	1 and 0	2
7	Flowtype	Discrete value	1 and 0	2

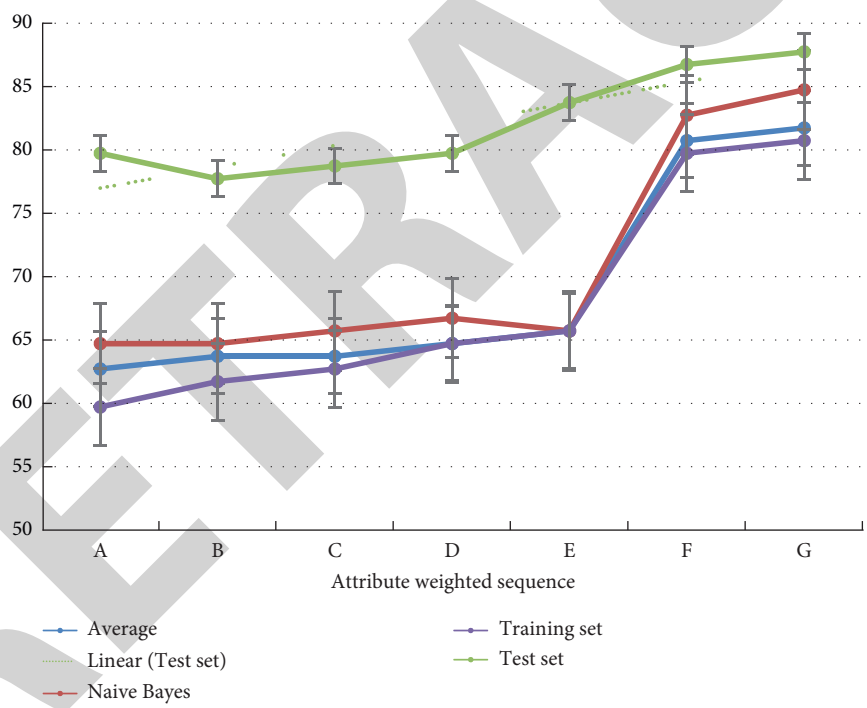

Figure 6: Accuracy statistics of test results.

ports, and kill other processes. The extraction of behavioral characteristics needs to be carried out under the conditions of the running of the sample program. Through the above three software and the tools for viewing services and processes that come with the system, the behavioral characteristics (shown or hidden) of the sample program during operation can be viewed and analyzed, and the feature library recorded in the sample program is used as the data set of the naive Bayes classifier detection and verification experiment. The feature database of the recorded sample set is shown in Table 3.

4.4. Experimental Analysis of Improved Pattern Search Method. Aiming at the problem of parameter optimization in support vector machines, this paper proposes an improved method based on the pattern search method. First, the grid technique and the quadratic Lagrange difference technique are used to obtain the initial point, and then the obtained initial point is used for the pattern search method. Find the best parameter combination according to the improved pattern search method, and use the cross-validation method to verify. The experimental results are shown in Table 4.

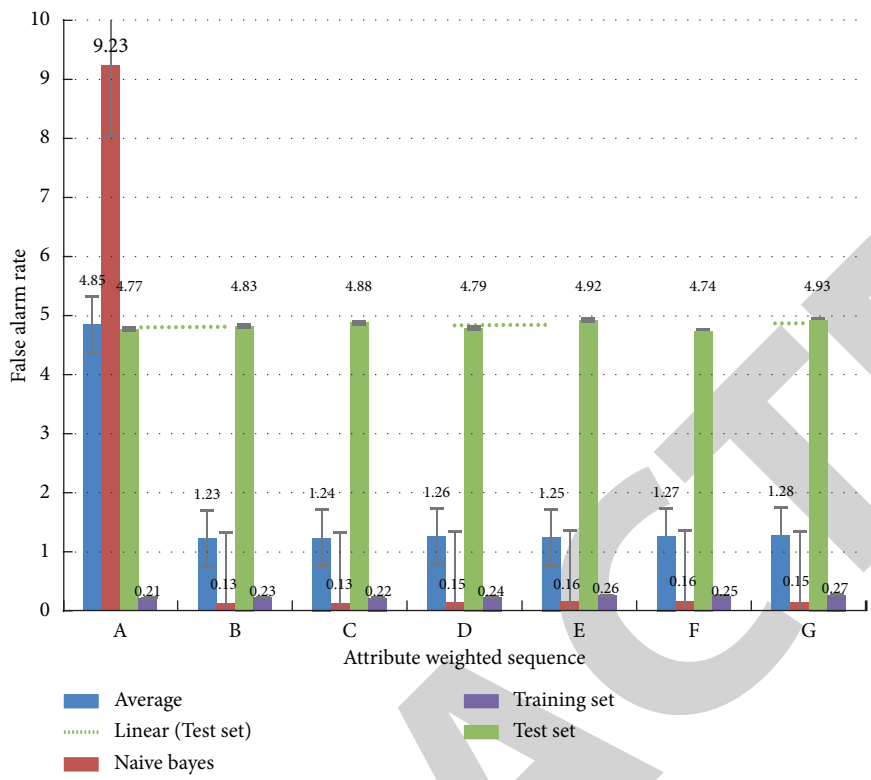

Figure 7: False alarm rate of test results.

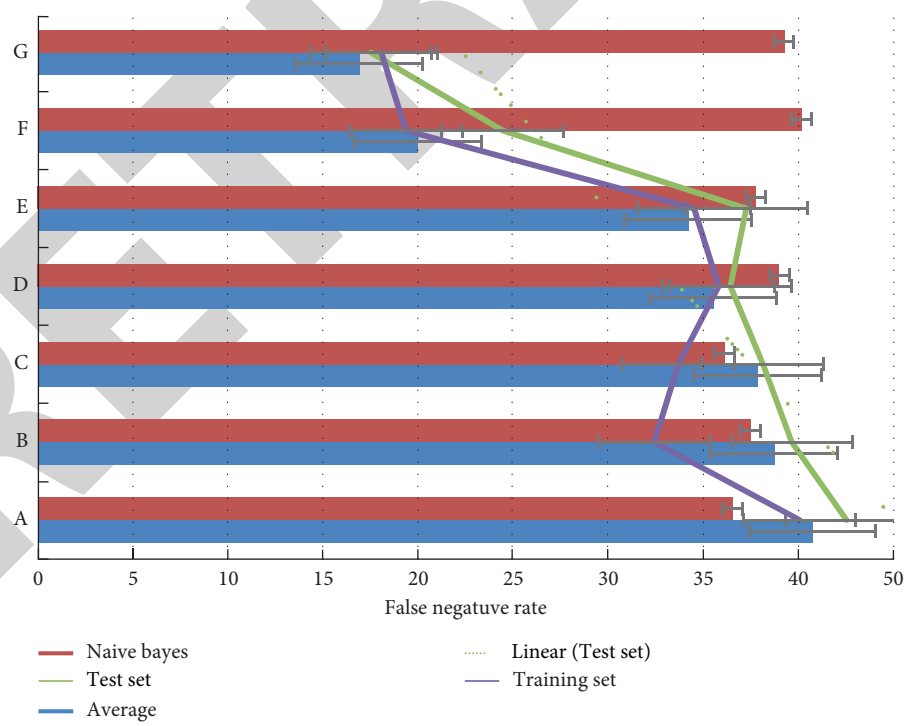

Figure 8: False report rate of test results.

This experiment verifies that the improved algorithm overcomes the local optimal problem of the pattern search method and can obtain the global optimal node. But the algorithm also has the following problems: the basic pattern search method does have a higher requirement for the initial node, and the quality of the initial node plays a vital role in

Table 3: Sample set feature library.

Feature name	Self-starting	Hide	Visual interface	Inject into other processes	Reduce safety	Binding port	Kill other processes
Pcshare	1	1	0	1	0	0	0
NetThief	1	1	0	0	1	1	0
Spirit3	1	1	0	1	0	0	1
NetSys	1	1	0	1	0	1	0
FeiMooMba	1	1	0	0	1	0	1
NewsunRCtrl	1	1	0	0	1	1	0
BlueButterfly	1	1	0	1	0	1	1

Table 4: Experimental results.

	Pattern search			Improved pattern search method		
	Initial parameters	Optimal parameters	Correct rate	Initial parameters	Optimal parameters	Correct rate
The first set of test data	(0.36, 0.4) (1.2, 0.6)	(0.137, 0.312) (0.74, 0.52)	71.47% 88.49%	(1.5, 0.6)	(2.79, 0.05)	99.43%
The second set of test data	(0.36, 0.8) (1.2, 0.6)	(0.58, 0.32) (1.25, 0.75)	85.16% 94.24%	(1.8, 0.8)	(1.8, 0.8)	99.71%
The third set of test data	(0.36, 1.2) (1.2, 0.8)	(0.04, 0.8) (1, 0.8)	97.45% 99.48%	(1.5, 1.2)	(1.5, 1.2)	98.25%

the final result. The improved algorithm has a good effect on the selection of the abovementioned initial points, and the accuracy rate can be at a relatively high level, which reflects the advantages of the improved algorithm in parameter optimization. For example, in the test data, the correct rate achieved by the improved algorithm has reached more than 99%. This article also has areas for improvement. The improved algorithm does not have a theoretical guide to the grid setting problem. When the grid setting is too large, it will degenerate into a basic pattern search method. When the grid setting is too small, it will degenerate into a basic pattern search method, grid search method.

5. Conclusions

With the wide application of smart phones, the information security of mobile phones has become one of the key points that people pay attention to. As one of the key factors affecting mobile phone security, Trojan horse crime has spread rapidly in recent years. Trojan horse crime cases have different manifestations and behavioral characteristics from traditional cases, which bring more difficulties to the public security organs' investigation and cracking, such as disturbing the social order and network order and even seriously affecting the socialist economic construction. Because the Trojan horse crime case is a new type of case with the development of the Internet, this type of case has the characteristics of low cost, new technology, strong concealment, novel criminal methods, high difficulty in investigation and punishment, and huge benefits. In order to punish such crimes, this paper proposes to use the naive Bayes algorithm to mine the clues of the criminal cases of mobile phone Trojans and detect the mobile phone Trojan virus by extracting the characteristic attributes in the data packets. The accuracy of the search method has been greatly improved. In order to more effectively maintain social stability and development, it is not enough for the investigators to solve the case only by using the professional knowledge of computer crime investigation because the computer network is composed of two levels of human and technology. As the level of technology becomes more and more perfect, in the face of certain cases, it becomes easy for those who use technology to break through the whole link. Effective use of knowledge from other disciplines can give full play to people's subjective initiative in investigative activities. Collecting a large amount of relevant information is an indispensable prerequisite for applying other integrated disciplines to solving investigative problems.

Data Availability

No data were used to support this study.

Conflicts of Interest

The author declares that there are no conflicts of interest regarding the publication of this article.

References

[1] S. V. Flowerday and T. Tuyikeze, "Information security policy development and implementation: the what, how and who," *Computers & Security*, vol. 61, no. aug, pp. 169–183, 2016.

[2] A. P. H. D. Gusmo, L. Silva, and M. M. Silva, "Information security risk analysis model using fuzzy decision," *International Journal of Information Management*, vol. 36, no. 1, pp. 25–34, 2016.

[3] C. Rui, J. Liehui, C. Wenzhi, X. Yaobin, and Z. Lu, "A TrustEnclave-based architecture for ensuring run-time security in embedded terminals," *Tsinghua Science and Technology*, vol. 05, no. 22, pp. 3–13, 2017.

[4] N. S. Safa and R. Von Solms, "An information security knowledge sharing model in organizations," *Computers in Human Behavior*, vol. 57, no. apr, pp. 442–451, 2016.

[5] Y. Mengke, Z. Xiaoguang, Z. Jianqiu, and X. Jianjian, "Challenges and solutions of information security issues in the

Hindawi
Mobile Information Systems
Volume 2022, Article ID 1872139, 10 pages
https://doi.org/10.1155/2022/1872139

Research Article

The Impact of Environmental Regulation on Agricultural Ecological Efficiency from the Perspective of High-Quality Agricultural Development: Based on Evidence from 30 Provinces in China

Shuo Tang, Jie Shang, and Ximing Chen

College of Economics and Management, Northeast Forestry University, 150040 Harbin, China

Correspondence should be addressed to Jie Shang; shangjie2005@nefu.edu.cn

Received 2 July 2022; Revised 21 July 2022; Accepted 2 August 2022; Published 25 August 2022

Academic Editor: Yajuan Tang

Based on the data of 30 provinces in China, the super-efficiency EBM model is used to calculate the agricultural ecological efficiency in China, and analyze the impact of different environmental regulations on the agricultural ecological efficiency. The results show that: China's agricultural ecological efficiency is not optimal. Specifically, the main grain production areas and grain balance areas have not reached the optimal efficiency, and the main grain sales areas have basically reached the optimal efficiency. In addition, among the influencing factors, the influence degree of different environmental regulations is well distinguished, which is the focus of this paper. We can find that command control environmental regulation and market incentive environmental regulation have a significant positive effect on different regions. Among them, market incentive environmental regulation has a significant positive impact on the agricultural ecological efficiency of the whole country and the grain balance areas. Command controlled environmental regulation has a significant positive impact on the agricultural ecological efficiency of the whole country and the main grain producing areas. So, it is necessary to formulate environmental policies according to the actual needs of development.

1. Introduction

As of 2022, my country's grain output has achieved a "nineteenth consecutive harvest," which has remained above 1.3 trillion kilograms. With the harvest of grain, we also need to pay attention to the worsening ecological environment. In 2015, the Ministry of Agriculture's "Implementation Opinions on Fighting the Battle for the Prevention and Control of Agricultural Non-point Source Pollution" clearly pointed out that it needs to be strictly controlled. In the same year, the Action Plan for Zero Growth of Fertilizer and Pesticide Use by 2020 was promulgated. This marks the official launch of the reduction and efficiency increase action. Relevant statistics show that by the end of 2020, fertilizer utilization rate of three grain crops in China will reach 40.2%, and the utilization rate of pesticides will reach 40.6%, basically reaching the utilization rate of 40%–60% of pesticides and chemical fertilizers in the world. In 2019, the intensity of chemical fertilizer application in my country dropped to 325.7 kg hm^{-2}, which is still far above the safe upper limit of chemical fertilizer application; the intensity of pesticide use dropped to 8.8 kg hm^{-2}, which is also higher than the world average level, still stands out. In 2022, the Central No. 1 document also pointed out that we need to continue to promote the reduction of volume and efficiency. At this stage, the policy of reducing the amount and increasing efficiency has achieved certain results in controlling the application amount of agricultural production factors, and the grain output has not decreased with the reduction of chemical fertilizers and pesticides. This policy has a positive impact on the green development of agriculture.

The green development of agriculture is based on protecting the natural ecological environment, achieving high-quality agricultural growth as the condition, and improving

and improving people's life satisfaction as the ultimate goal [1]. Realizing agricultural modernization is an important part of agricultural development, it is necessary to reduce resource consumption, reduce environmental damage. Agricultural ecological efficiency is an important part of analyzing the green sustainable development of agriculture. Environmental regulation is an important policy tool to deal with social problems. There are many types of environmental regulation, different types for different situations, but the fundamental purpose is to maintain the ecological environment. In terms of environmental pollution control, Government promulgation of policies and regulations is one of the main tools used by the government. This kind of environmental regulation is authoritative and mandatory. Short-term command control environmental regulation has good effects, but long-term command control environmental regulation may have negative effects. Analysis of environmental regulation is of momentous significance for solving practical problems. Therefore, this study chose two kinds of environmental regulations as the research focus, and analyzed their impact on agricultural ecological efficiency.

For the research on agricultural ecological efficiency, different scholars have expounded the relevant content of agricultural ecological efficiency from different perspectives. From the perspective of research methods, many scholars mainly use data envelopment analysis (DEA) to measure agricultural ecological efficiency. This method has been widely used in efficiency measurement [2]. Scholars are relatively mature in the application of DEA models, and different types of DEA methods have emerged to meet the research needs. It mainly includes SBM model, super-efficiency SBM model, SSBM-ESDA model [3], network DEA model [4], and so on. In the scope of study, it mainly focuses on the measurement of agricultural ecological efficiency in the macro fields and medium fields. Ji Xueqiang et al. pointed out that there is a large gap between the leading provinces and the backward provinces in agricultural ecological efficiency [5]. In the medium fields, Liang Yaowen et al. calculated the agricultural ecological efficiency in the Bohai Rim region and found that although the overall level of agricultural ecological efficiency in this region was low, it showed a gradual upward trend with large differences between regions [6]. Liu Peng et al. pointed out that the agricultural ecological efficiency of the main grain-producing areas has not reached an effective state as a whole [7]. From the research of influencing factors, many scholars have analyzed the influencing factors of agricultural ecological efficiency from different perspectives. Wang Chenxuan et al. pointed out that the scale of agricultural science and technology investment has a significant spillover effect on agricultural ecological efficiency [8]. Hu Pingbo et al. also pointed out that the integration of agriculture and tourism under the support of the government is beneficial to improve the agricultural ecological efficiency, especially when the level of integration is high, the promotion effect will be enhanced [9]. Hou Mengyang et al. pointed out that the transfer of rural labor force to the ecological efficiency of grain production has a significant role in promoting [10]. Li Lu et al. pointed out that the aging of rural population has a negative impact on agricultural eco-efficiency. This kind of negative influence decreases first, then rises after reaching a certain degree, namely "U" type change [11]. Shang Jie et al. pointed out that the development of urbanization can promote the improvement of agricultural ecological efficiency as a whole. Among them, the per capita disposable income of urban residents and urban economic density has a positive impact on agricultural ecological efficiency. Area negatively affects agricultural ecological efficiency [12]. Huang et al. expressed the impact of environmental regulation intensity analysis on agricultural ecological efficiency from two aspects: order regulation and publicity regulation [13]. Fang Yongli pointed out that there are obvious spatial differences in the level of agricultural ecological efficiency among provinces in China, and the development and change trends are different. The main reasons for the loss of efficiency are redundant input of factors and excessive undesired output [14]. Among them, plastic film, water resources, and fertilizer input elements have the highest degree of redundancy [15]. In addition, the low skills of agricultural laborers and the inefficiency of land use are also causes of efficiency losses [16].

These documents show that there are abundant results in the measurement of agricultural ecological efficiency, and scholars are relatively mature in their research on the influencing factors of agricultural ecological efficiency. However, there is still a lack of research from the perspective of environmental regulation. On the one hand, different scholars have different cognitive perspectives on environmental regulation, this leads to differences in the specific selection of variables and the results obtained are also different; on the other hand, there is a lack of analysis of the impact mechanism of phased policy of reducing quantity and increasing efficiency. This paper considers the use of the super-efficiency EBM model to measure agricultural ecological efficiency. It can clearly distinguish the regions with an efficiency value of 1 for effective comparison. Taking the policy of reduction and efficiency increase as the variable of control command type environmental regulation, combined with the market incentive type environmental regulation, this paper examines the impact on agricultural ecological efficiency, and judges whether the current environmental regulation has any effect on agricultural ecological efficiency, in order to provide policy basis for how to control pollution and promote the green and sustainable development of agriculture in China in the next step.

2. Materials and Methods

2.1. Research Methods. DEA model. The traditional DEA models are divided into two types, one is the radial BCC model and the CCR model, the other is the SBM model. Since the input-output variables in the traditional DEA must increase or decrease in equal proportions, the changes in the slack variables cannot be calculated. Although the SBM model based on undesired output can incorporate slack variables into the model, it is difficult to reflect the situation between actual situation and best case scenario, and there is

also a certain defect. Therefore, in order to improve the defects of the traditional DEA, Tone et al. proposed the EBM model, which combined the radial and non-radial distance functions. The model can clearly calculate the gap between actual situation and best case scenario, and accurately calculate the relative efficiency of the research target. Usually, the maximum efficiency value measured by the traditional DEA is 1, but when the number of research objects increases, and when there are multiple research objects with an efficiency value of 1, we cannot differentiate effectively. The super-efficiency model can be greater than 1, which is an effective tool to realize discrimination [17]. Just like the methods used by other researchers in the previous article, SBM model cannot distinguish multiple research objects with efficiency of 1. The super efficiency SBM model is difficult to embody the difference between the actual value and the best value; SSBM-ESDA is a spatial difference analysis; Network DEA is to calculate the efficiency by stages according to the different stages of the research object. Combined with the above analysis, this paper mainly selects the EBM model to measure the agricultural ecological efficiency, and compare regional differences, the specific formula is as follows:

$$\begin{aligned}
&\gamma = \min \frac{\theta - \varepsilon_x \sum_{i=1}^{m} \omega_i \overline{x}_i / x_{ik}}{\eta + \varepsilon_y \sum_{r=1}^{s} \omega_r^{+} \overline{y}^{+} / y_{rk} + \varepsilon_b \sum_{p=1}^{q} \omega_p^{b-} \overline{y}^{b-} / b_{pk}}, \\
&\sum_{j=1}^{n} x_{ij}\lambda_j + \overline{x}_i = \theta x_{ik}, \quad i = 1, \ldots, m, \\
&\sum_{j=1}^{n} y_{rj}\lambda_j - \overline{y}_r^{+} = \theta y_{rk}, \quad r = 1, \ldots, s, \\
&\sum_{j=1}^{n} b_{pj}\lambda_j + \overline{y}_p^{b-} = \eta b_{pk}, \quad i = 1, \ldots, q, \\
&\lambda_j \geq 0, \quad \overline{x}_i, \overline{y}_r^{+}, \overline{y}_p^{b-} \geq 0,
\end{aligned} \tag{1}$$

where γ represents the value of the agricultural ecological efficiency. The input of agricultural production in decision-making unit k, the expected output of agricultural production, and the undesired output of agricultural production are x_{ik}, y_{rk}, and b_{pk}, respectively. The slack values of agricultural production input, agricultural production expected output, and agricultural production undesired output are $\overline{x}_i$, $\overline{y}_r^{+}$, and $\overline{y}_p^{b-}$, respectively. ω_i, ω_r^{+}, and ω_p^{b-} are the weights of agricultural production input, agricultural production expected output, and agricultural production undesired output. εx, εy, and εb are the key parameters of agricultural production input, expected output of agricultural production, and undesired output of agricultural production, $\varepsilon \in [0, 1]$.

Panel Tobit Model. The agricultural ecological efficiency values measured by the EBM model are all greater than 0, which are restricted dependent variables. The value of agricultural ecological efficiency is discontinuous, and there is no situation without agricultural ecological efficiency, so Tobit model is suitable for this study. Whether it is better to use a FE Tobit model or a RE Tobit model, existing studies have not reached a consensus. Fixed-effect Tobit models measure panel data, and the results are often inconsistent or biased [18]. This paper adopts the random-effect Tobit model to analyze the influencing factors hence. The specific formula is as follows:

$$Y_{it} = \alpha + \beta_1 ER_{it} + \beta_2 \text{POLICY}_{it} + \lambda CV_{it} + \varepsilon_{it}. \tag{2}$$

Among them, Y_{it} represents agricultural ecological efficiency, ER_{it} represents the intensity of environmental regulation, POLICY_{it} represents the policy of reducing quantity and increasing efficiency, CV_{it} represents other control variables, and εit represents the random error term.

2.2. Data Source and Processing. From the agricultural perspective in a narrow sense, combined with agricultural practice, and referring to the research results of previous scholars, this paper selects relevant input-output indicators. Table 1 shows the details.

We select agricultural practitioners, crop-sown area, fertilizer application amount, plastic film usage amount, pesticide usage amount, agricultural machinery power, and effective irrigation area as input indicators; the total agricultural output is selected as the expected output index; the amount of fertilizer pollution, pesticide residue, and plastic film residue is selected as the undesired output index. Among them, the official data on agricultural employees do not provide direct statistical data, so this article refers to the processing method of relevant scholars, obtain the number of agricultural employees through calculation; in order to eliminate the objective influence of some indicators such as prices, output indicator adjusts the data to the output value at constant prices in 2007. In the undesired output indicators, combined with the practices of Lai, Shi, and Wu [19–21] and other scholars, the amount of fertilizer pollution, pesticide residues, and plastic film residues were measured. The pesticide residue rate was set to 50%, and the plastic film residue rate was set to 10%; the fertilizer pollutants are mainly nitrogen and phosphorus emissions. Calculated according to the pure chemical composition of chemical fertilizers: The TN pollution coefficients of nitrogen fertilizer, phosphorus fertilizer, and compound fertilizer (n, P, K ratio of 1: 1:1) were 1, 0, and 0.33, respectively. TP pollution coefficients were 0, 0.44, and 0.15, respectively. Therefore, the specific expression is: nitrogen (phosphorus) fertilizer production amount = chemical fertilizer application amount ∗ loss rate ∗ pollution production coefficient, compound fertilizer pollution production amount = chemical fertilizer application amount ∗ loss rate ∗ nitrogen (phosphorus) pollution production coefficient ∗ (1/3). Table 1 shows the basic data of 30 provinces in China within the research range. We can see that the gap between the values of various indicators has increased. We can see that there is a big gap between regions in each indicator. In particular, from the perspective of mean, maximum and minimum values, the distance between mean and maximum value is larger, which indicates that, on the whole, the index values of most of the 30 provinces in China are relatively low,

Table 1: Descriptive statistics of input-output indicators of agricultural ecological efficiency.

	Variable	Observed value	Average value	Standard error	Minimum	Maximum
Input indicators	Agricultural employees (10,000 people)	420	506.2	427.0	11.44	2226
	Crop sown area (square kilometers)	420	54285	37070	886	149101
	Fertilizer application amount (10,000 tons)	420	187.8	143.7	5.500	716.1
	Plastic film usage (10,000 tons)	420	4.360	4.120	0.0400	24.27
	Pesticide usage (10,000 tons)	420	5.560	4.240	0.120	17.35
	Effective irrigation area (square kilometers)	420	21211	15977	1092	61776
	Total power of agricultural machinery (10,000 kilowatts)	420	3240	2870	94	13353
Output indicators	Gross agricultural output value (100 million yuan)	420	1580	1219	44	5579
Unexpected output indicators	Fertilizer pollution production (10,000 tons)	420	17.64	14.75	0.310	65.56
	Pesticide residues (10,000 tons)	420	2.780	2.120	0.0600	8.670
	Residual amount of plastic film (10,000 tons)	420	0.560	0.430	0.0100	2.380

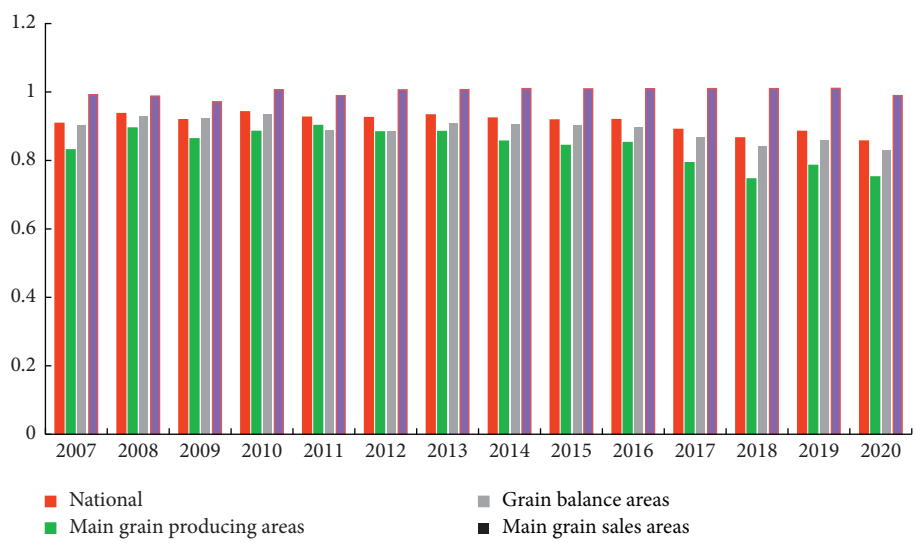

Figure 1: Changes in the agricultural ecological efficiency by region from 2007 to 2020.

and the provinces with large index values occupy a minority. Therefore, the division and specific analysis of 30 provinces in China can better reflect the changes in agricultural ecological efficiency and help to put forward targeted policies.

3. Agricultural Ecoefficiency Calculation Results

MAXDEA was mainly used for calculation in this study, and Figure 1 shows the details. The agricultural ecological efficiency of the whole country and each region was calculated by software. In 2001, China implemented the reform of the grain circulation system. Based on the overall characteristics of grain production and consumption in each province, and taking into account the differences in resource endowments and the historical traditions of grain production, 31 provinces (including Tibet) were divided into major selling areas, production areas, and marketing balance areas. On the whole, China's agricultural ecological efficiency has not reached the optimal level. Due to the traditional agricultural production mode in China in the past, the agricultural production efficiency has been improved, but the continuous production mode of high input and high consumption has reduced the growth rate of efficiency, and agricultural environmental problems have become increasingly apparent. China has a vast territory, and the agricultural production level of each province varies greatly, which leads to the limited improvement of China's overall agricultural ecological efficiency. The agricultural ecological efficiency is also different in different areas, among which only the main food sales area has achieved the best efficiency. Grain main sales areas > grain balance areas > grain production areas. However, all areas show a fluctuating downward trend. In recent years, the increasing frequency of extreme weather has brought serious challenges to agricultural production. The

Table 2: Average value of agricultural ecological efficiency in 30 provinces in China from 2007 to 2020.

Regional classification	Areas	Efficiency value	Regional classification	Areas	Efficiency value
Main grain production areas	Anhui	0.67	Grain balance areas	Guizhou	0.94
	Hebei	0.81		Ningxia	0.82
	Henan	0.84		Qinghai	1.02
	Heilongjiang	1.02		Shanxi	0.73
	Hubei	0.82		Shǎnxi	1.03
	Hunan	0.78		Xinjiang	1.02
	Jilin	0.67		Yunnan	0.65
	Jiangsu	1.00	Grain main sales areas	Chongqing	0.98
	Jiangxi	0.73		Beijing	1.02
	Liaoning	0.87		Fujian	1.01
	Inner Mongolia	0.70		Guangdong	1.02
	Shandong	0.83		Hainan	1.03
	Sichuan	0.99		Shanghai	1.00
	Gansu	0.77		Tianjin	0.99
	Guangxi	0.98		Zhejiang	0.98

weak ability of agricultural production to withstand natural disasters leads to farmers' increasing inputs to ensure grain output. Especially since the outbreak of COVID-19, the urgency of production materials transportation and the decrease of production conditions will urge farmers to increase production inputs, which indirectly leads to the reduction of efficiency, so it is necessary to take effective measures to adjust production and management.

At the same time, we also obtained the agricultural ecological efficiency values of all provinces, and Table 2 shows the details. There are also obvious gaps between provinces. In this paper, agricultural ecological efficiency is divided into three levels, including high efficiency, medium efficiency, and low efficiency. High efficiency refers to achieving the best efficiency, that is, the research object is at the forefront of agricultural production, and the value of agricultural ecological efficiency is greater than or equal to 1; Efficiency refers to inefficiency research objects, and there is efficiency loss. Specifically, the value of agricultural ecological efficiency of medium-efficiency groups is between 0.8 and 1, and the value of agricultural ecological efficiency in the low-efficiency group is less than 0.8 [14]. On the whole, the provinces with high efficiency level in China are Heilongjiang, Jiangsu, Qinghai, Shǎnxi, Xinjiang, Beijing, Fujian, Guangdong, Hainan, and Shanghai; the provinces with medium efficiency level are Hebei, Henan, Hubei, Liaoning, Shandong, Sichuan, Guangxi, Guizhou, Ningxia, Chongqing, Tianjin, and Zhejiang; provinces with low efficiency levels are Anhui, Hunan, Jilin, Jiangxi, Inner Mongolia, Gansu, Shanxi, and Yunnan. In addition, there is great potential for improvement in regional agricultural development. Although there are differences in functional positioning, in order to improve the overall agricultural ecological efficiency level of the country, it is necessary to balance the production levels of each functional area, stabilize the optimal efficiency, and improve the inefficient areas. Specifically, in the main grain producing areas, only Heilongjiang and Jiangsu, and among the grain balance areas, only Qinghai, Xinjiang and Shanghai have the best efficiency. The main grain producing areas bear the supply of commercial grain in China. At the current production level, a large number of chemical factors still need to be invested to ensure grain production, so it has a strong impact. Although the grain balance areas are not mainly responsible for the supply of commodity grain, these still bear part of the pressure of agricultural production, the grain balance areas are at a higher level of agricultural production and production.

4. Analysis of Influence of Environmental Regulation on Agricultural Ecological Efficiency

4.1. Variable Description

4.1.1. Core Explanatory Variable. All kinds of policies on environmental governance designated by the government are collectively referred to as environmental regulation, which is not a new policy tool. In actual research, different scholars also choose different indicators to represent the intensity of environmental regulation from different angles. This study mainly selects the proportion of environmental pollution control investment to represent the market-oriented environmental regulation, and at the same time, we take 2015 as the time node, dummy variables were set and represented as command-and-control environmental regulations. Environmental regulation plays an important part in controlling pollutant discharge. Therefore, this study believes that environmental regulation can improve agricultural ecological efficiency.

4.1.2. Control Variable

Industrial organization (IO). Changes in the industrial structure will lead to the change of agricultural production input according to the direction of industrial change, which will promote or hinder the development of agriculture to varying degrees. Therefore, it is difficult to accurately judge the impact of industrial structure on agricultural ecological efficiency.

Agricultural financial support (AFS). The intensity of agricultural financial support represents the degree of government intervention in agricultural production. The higher the support, the more problems need to be solved in agricultural production. There is a risk of over-investment and environmental risks are aggravated. Therefore, the intensity of agricultural financial support hinders agricultural ecological efficiency.

Agricultural disaster rate (ADR). The agricultural disaster rate represents the degree to which agricultural production is affected by natural disasters. In order to reduce the loss of their own economic interests, the production entities that are greatly affected by natural disasters will reduce the negative impact of natural disasters by increasing the input of agricultural production factors. Although it has ensured its own economic interests to a certain extent, the risk of environmental pollution has significantly increased. Therefore, the agricultural disaster rate hinders agricultural ecological efficiency.

Planting structure (PS). There are obvious differences in the growth patterns and environmental conditions of different crops. Therefore, in the production process, the input of agricultural production factors should also be adjusted according to the actual production conditions and crop growth requirements, that is, there is a possibility of increasing the input of production factors and reducing it. Increasing or reducing agricultural input requires specific analysis of specific problems. Therefore, it is difficult to accurately judge the impact of planting structure on agricultural ecological efficiency.

Urbanization rate (UR). The urbanization rate represents the transfer of rural labor. In areas with a high degree of mechanization, agricultural production does not require a large amount of labor input, and labor can be liberated and agricultural production efficiency can be steadily improved with the help of agricultural machinery. In areas with a low degree of mechanization, agricultural production still needs to invest a large amount of labor to meet production. The increase in urbanization rate will lead to reduction in labor force. Instead, increase the input of other agricultural production factors to meet the actual needs, resulting in the emergence of environmental problems. Therefore, it is difficult to accurately judge the impact of planting structure on agricultural ecological efficiency.

Agricultural science and technology investment intensity (ASTII). Combined with the research of relevant scholars, the index of R&D investment intensity of research and experimental development is selected to reflect the status of agricultural science and technology investment [22]. A sound agricultural science and technology support system is the inherent requirement and inevitable path to realize agricultural modernization [23]. Increasing the output of high-quality research results, and converting the results into agricultural productivity are irreplaceable keys to promoting high-quality agricultural development, improving agricultural risk resistance, and improving the agricultural production environment. Therefore, it hinders agricultural ecological efficiency.

Explanations of all variables and assumptions are described in detail in Table 3.

5. Empirical Results of Influencing Factors of Agricultural Ecoefficiency

This study mainly uses STATA16.0 software for analysis. Considering that there may be multicollinearity among variables, first perform a multicollinearity test on each explanatory variable. The multicollinearity diagnosis was carried out using the variance inflation factor method, and it is found that the variance inflation factors of all independent variables in the model are between 1 and 5, indicating that there is basically no multicollinearity between variables [24], and Table 4 shows the details. It can be seen that at the 10% level, the market-driven environmental regulation significantly and positively affects the agricultural ecological efficiency of the whole country and the grain balance areas, but it has no significant impact on others. Under the current technological level, the main grain producing areas need to invest a certain amount of chemical production factors to ensure grain output. Although subsidies and other policies can encourage farmers to carry out green production, compared with economic and ecological benefits, farmers are more inclined to economic benefits. Due to the small production scale of farmers and the lack of subsidies and other policies, the impact on farmers in the main grain sales areas is limited, and farmers' production behavior is more inclined to their own experience. The input of agricultural production factors in China is still unreasonable. Agricultural infrastructure construction, financial subsidies, etc. are all important parts of environmental pollution control investment. Encouraging enterprises and research institutions to update agricultural production technology and widely publicizing and promoting it, on the other hand, improving agricultural production conditions will improve agricultural production efficiency. For the grain balance areas, the positioning of this functional area is that the grain production meets the production and living needs of the region, and a certain scale of agricultural production is required, but its agricultural production capacity is weaker than that of the main grain producing areas and stronger than that of the main grain sales areas. The risk of pollution problems in the production process is also relatively large. At the 1% level, command-and-control environmental regulation significantly and positively affects the ecological efficiency of the whole country and major grain producing areas. In 2015, Government policy was very effective, and agricultural economy and agricultural environment played a positive role. In controlling the amount of input, the policy has a good effect. The main grain producing areas are responsible for the supply of national commodity grains and play a key role in stabilizing food security and ensuring social stability. The traditional extensive agricultural production method has improved agricultural production efficiency for a certain period of time, but high input and high pollution have made environmental

Table 3: Agricultural ecological efficiency factors.

Variable	Variable explanation	Influence judgment
ER	Proportion of total investment in environmental pollution in regional GDP (%)	Positive
IO	The proportion of the output value of the primary industry in the total regional output value (%)	Unknown
AFS	The proportion of spending on agriculture, forestry, and water conservancy in local government spending (%)	Negative
ADR	Proportion of area affected by natural disasters to crop-sown area (%)	Negative
PS	Ratio of sown area of food crops to sown area of non-food crops (%)	Unknown
UR	Proportion of urban population in total population (%)	Unknown
ASTII	Research and experimental development (R&D) funding intensity (%)	Positive
POLICY	Before implementing the policy of reducing volume and increasing efficiency = 0, after implementing the policy of reducing volume and increasing efficiency = 1	Positive

Table 4: Empirical results of influencing factors of agricultural eco-efficiency.

Variable	National (1)	Grain main sales areas (2)	Main grain production areas (3)	Grain balance areas (4)
ER	0.0146* (0.00786)	0.0156 (0.0109)	0.0170 (0.0162)	0.0211* (0.0117)
IO	0.00759*** (0.00243)	0.00305*** (0.000848)	0.0103* (0.00526)	0.0114** (0.00486)
AFS	−0.00307 (0.00278)	0.000203 (0.00244)	0.00155 (0.00466)	0.000323 (0.00534)
ADR	−0.000264 (0.000379)	−0.000438 (0.000384)	−0.000356 (0.000666)	−0.000457 (0.000687)
PS	−0.00839*** (0.00281)	0.00157 (0.00565)	−0.00734* (0.00434)	−0.0424*** (0.0162)
UR	−0.000860 (0.00129)	0.00169* (0.000892)	−0.000433 (0.00289)	−0.00112 (0.00285)
ASTII	0.0226 (0.0139)	−0.00570 (0.00989)	0.0343 (0.0373)	−0.0272 (0.0380)
POLICY	0.0325*** (0.0116)	0.00986 (0.0113)	0.0581*** (0.0211)	0.0298 (0.0238)
C	0.881*** (0.0812)	0.856*** (0.0690)	0.692*** (0.170)	0.926*** (0.138)
Number of samples	420	84	182	140
Number of regions	30	6	13	10

***, **, * respectively means passing the significance test of 1%, 5%, and 10%.

problems increasingly serious. Therefore, under the premise of ensuring grain output and quality, it is very important to control the input of chemical agricultural production factors, especially in the main grain-producing areas, where the application of chemical fertilizers and pesticides is large, and there is a phenomenon of unreasonable use.

Among other control variables, industrial structure has a significant positive impact on all regions. It can be seen that the industrial structure can have a general positive impact. Through the integration of agricultural resources, scattered farmers will be gathered to form a large-scale operation; increase modern agricultural machinery facilities and equipment and reduce labor input; develop regional characteristic agriculture according to local conditions; allowing a large number of industrial and commercial capital and financial funds to enter agriculture, building a scientific and reasonable investment model, allowing enterprises and banks to build a platform, and allowing entrepreneurs and farmers to become professional industrial workers are important measures to realize the transformation and upgrading of agricultural industrial structure. The planting structure has a negative impact on the agricultural ecological efficiency of the whole country and the grain balance area at the level of 1%, Negative response to agricultural ecological efficiency in main grain producing areas at the level of 10%. Whether it is the whole country, or the main grain producing areas, grain balance areas, these areas are important production areas of commodity grain, bearing the task of grain production. If the planting structure is adjusted at will, it will inevitably lead to the inadaptability of production methods and production conditions, and hinder the improvement of agricultural ecological efficiency. At the level of 1%, the urbanization rate has a significant positive impact

Table 5: Robustness test results.

Variable	National (1)	Grain main sales areas (2)	Main grain production areas (3)	Grain balance areas (4)
ER	0.0165** (0.00799)	0.0217* (0.0114)	0.0217 (0.0167)	0.0210* (0.0120)
IO	0.00821*** (0.00265)	0.00321 (0.00302)	0.0118** (0.00544)	0.0156*** (0.00505)
AFS	3.34e-05 (0.00295)	−0.00551 (0.00412)	0.00362 (0.00479)	0.00419 (0.00554)
ADR	−0.000342 (0.000387)	−4.49e-05 (0.000430)	−0.000318 (0.000693)	−0.000535 (0.000713)
PS	−0.0103*** (0.00308)	0.0196* (0.0103)	−0.0115** (0.00450)	−0.0559*** (0.0199)
UR	−0.00245* (0.00140)	0.00694*** (0.00219)	−0.000317 (0.00323)	−0.00216 (0.00306)
ASTII	0.0187 (0.0149)	0.00122 (0.0114)	0.0199 (0.0416)	0.0281 (0.0410)
POLICY	0.0204* (0.0121)	0.0171 (0.0137)	0.0467** (0.0219)	0.0245 (0.0247)
C	0.935*** (0.0828)	0.495*** (0.165)	0.674*** (0.180)	0.909*** (0.138)
Number of samples	420	84	182	140
Number of regions	30	6	13	10

***, **, * , respectively, mean passing the significance test of 1%, 5%, and 10%.

on the agricultural ecological efficiency of major grain sales areas. The agricultural production scale in the main grain selling areas is small, and does not need a lot of labor input. The improvement of urbanization level will promote the citizenization of farmers, promote non-agricultural employment, and liberate the surplus productive forces.

6. Robustness Check

In order to verify the stability and accuracy of the previous research conclusions, this study uses the fixed effect model to perform regression again, and Table 5 shows the details. It can be seen that the results of the new calculation are basically consistent with those of our previous calculation. Environmental regulation still has a significant positive effect on agricultural ecological efficiency. The results of the study are basically the same as those mentioned above, indicating that the study results are reliable.

7. Conclusion and Suggestion

7.1. Conclusion. After calculation and analysis, we get the following conclusions: (1) China's agricultural ecological efficiency has not yet reached the optimal level, and the differences between regions are obvious. The agricultural ecological efficiency value is the main grain sales areas > the whole country > the grain balance areas > the main grain production areas. The provinces with high efficiency level in China are Heilongjiang, Jiangsu, Qinghai, Shǎnxi, Xinjiang, Beijing, Fujian, Guangdong, Hainan, and Shanghai. These provinces achieve the best efficiency, they can give consideration to economic and ecological benefits in agricultural production. (2) Environmental regulation has a positive impact on agricultural ecological efficiency, indicating that it is an important means to improve agricultural ecological efficiency. Among them, the market-incentivized environmental regulation significantly positively affects the whole country and the grain-balanced areas, and the command-and-control environmental regulation significantly positively affects the ecological efficiency of the whole country and the main grain-producing areas. Among other control variables, the industrial structure significantly positively affects the agricultural ecological efficiency of all regions; the planting structure significantly negatively affects the agricultural ecological efficiency of the whole country, the grain balance areas and the main grain producing areas; the urbanization rate significantly positively affects the main grain sales areas agricultural ecological efficiency. When analyzing the influencing factors in this study, due to the fact that the data do not include the public participation type environmental regulation in the research scope, the control variables only try to find out the factors that affect the agricultural ecological efficiency, so as to avoid multicollinearity and endogenous problems.

7.2. Suggestion. (1) Improve the environmental regulation system. Every environmental regulation has its own field of adaptation, and there are also obvious differences in natural and social conditions between regions. Governments need to tailor policies to specific problems. In the previous conclusions, Market incentive environmental regulation is very important in the overall level of the country and the regional level of the grain balance areas. The effect of efficiency is not obvious in other areas, so more targeted measures are needed for both areas. As the name implies, the main grain

producing areas are important grain production bases, and are superior to other areas in terms of infrastructure level and production experience. Simply providing basic support and other policies have limited effects. We need to rely on scientific and technological progress to enhance agricultural productivity. Environmental regulation requirements, put forward technology-based environmental regulation to develop; the agricultural production scale in the main grain sales areas are the smallest, and it depends more on the food supply of other regions. The regional agricultural development is not paid much attention, and the non-agricultural industries are developed. No matter what kind of environmental regulation, the role of these environmental regulations is weak, so the management of scattered small agricultural production units is required for these areas. The policy of reducing quantity and increasing efficiency has an apparent promoting effect on the overall level of the country and the regional level of major grain producing areas. The policy of reducing quantity and increasing efficiency has been promulgated and carried out from top to bottom across the country. In 2015, in the implementation process of the national policies issued by the government, the effects vary from region to region, some regions are effective, while others are not significant. The implementation of the reduction and efficiency increase can achieve good expected results. However, the effect of the reduction and efficiency policy in the grain balance areas and the main grain sales areas are not obvious. This shows that the pertinence of the policy is not enough, and specific problems need to be analyzed. Therefore, it is necessary to formulate different control and order-based environmental regulation policies for different regions, continue to promote reduction and increase efficiency nationwide, continue to realize no growth or negative growth of chemical fertilizers and pesticides for major grain producing areas, and manage existing environmental problems to achieve destocking; for the main grain sales areas and the grain balance areas, we need to combine the present situation of agricultural production with rational allocation of factor input and formulate appropriate environmental regulations in the region to improve agricultural ecological efficiency.

(2) Multiple measures to promote high-quality transformation of agriculture. Industrial structure is one of the important factors. Under the requirements of high-quality agricultural development, we need to get rid of the traditional production methods of high input, high consumption, and high emissions, improve the allocation of factors, vocational education, science and technology, management capabilities, etc. and apply new high-efficiency agricultural production equipment in hardware conditions. Promote soil testing, formula fertilization, biological control technology, etc., improve the quality of agricultural occupations in terms of software, teach new skills in agricultural production, improve agricultural production management capabilities, and achieve high-quality transformation of agriculture. Pollutant discharge, clean production, reduce the negative impact of secondary and tertiary industries on agricultural production, and improve agricultural ecological efficiency.

(3) Develop moderate-scale agricultural operations. Planting structure significantly negatively affects agricultural ecological efficiency, which indicates that blindly expanding grain sown area is not conducive to agricultural development. Based on the scarcity of land, expanding the acreage of grain will encroach on other forms of land use, and land use conversion also requires a series of management of land to meet planting needs, in the process there is a risk of environmental damage, and the expansion of grain sown area means that the input of chemical production factors. It will be increased in the production process, increasing the possibility of agricultural pollution. Therefore, it is feasible to develop agricultural moderate-scale management. There is no uniform standard for agricultural moderate-scale operation, and different regions need to realize moderate-scale agricultural management according to the actual situation of the region.

Data Availability

The basic data of this study are all from the public statistical data published by the Chinese government, including the China Statistical Yearbook, the China Rural Statistical Yearbook and the China Environmental Statistical Yearbook. https://data.cnki.net/Yearbook/Navi?type=type&code=A.

Conflicts of Interest

The authors declare that there are no conflicts of interest in this manuscript.

Acknowledgments

This work was supported by the National Social Science Foundation of China (20FGLB059).

References

[1] X. Y. Bu, "Construction of legal mechanism of Agricultural ecological compensation under the Vision of green Development," *Agricultural economy*, vol. 4, pp. 86–88, 2019.

[2] X. S. Zhang and B. W. Gui, "Analysis of total factor productivity in China: evaluation and application of Malmquist Index method," *Quantitative Economy, Technical and economic Research*, vol. 6, pp. 111–122, 2008.

[3] H. F. Wang, "Spatitemporal evolution of agricultural efficiency in Anhui county based on SSBM-ESDA model," *Economic Geography*, vol. 40, no. 4, pp. 175–183, 2020.

[4] J. R. Hong, C. Chen, C. Feng, and J. B. Huang, "Spatiotemporal differences in agricultural ecological efficiency and its influencing factors," *Journal of South China Agricultural University (Social Science edition)*, vol. 15, no. 2, pp. 31–41, 2016.

[5] Y. Zheng and J. Huang, "Characteristics and driving factors of agricultural ecological efficiency in China," *Economic Jingwei*, vol. 38, no. 6, pp. 32–41, 2021.

[6] X. Q. Ji and J. Shang, "A study on agricultural ecological efficiency in China based on the three-stage SBM model," *Agricultural Resources and regionalization in China*, vol. 42, no. 7, pp. 210–217, 2021.

[7] Y. W. Liang and B. H. Wang, "Study on the spatial and temporal evolution and influencing factors of agricultural

ecological efficiency in the Bohai Rim region," *Ecological Economy*, vol. 37, no. 6, pp. 109–116, 2021.

[8] X. B. Shu, W. X. Feng, F. Q. Liao, and C. Y. Ling, "Research on the spatial and temporal evolution of agricultural ecological efficiency in urban agglomerations in the middle reaches of the Yangtze River," *Soil and Water Conservation Research*, vol. 29, no. 1, pp. 394–403, 2022.

[9] P. L. Liu, K. Sun, and Y. Zhou, "Study on Agricultural ecological Efficiency and influencing Factors in major grain producing areas," *Journal of Shandong Agricultural University (Natural Science Edition)*, vol. 23, no. 2, pp. 74–79, 2021.

[10] P. B. Hu and Y. P. Zhong, "The mechanism and empirical analysis of the promotion of agricultural ecological efficiency through the integration of agriculture and tourism under the support of the government: taking the national leisure agriculture and rural tourism demonstration counties as an example," *China Rural Economy*, vol. 12, pp. 85–104, 2019.

[11] M. Y. Hou and S. B. Yao, "Spatial spillover effect and threshold characteristics of the influence of rural labor force transfer on agricultural ecological efficiency in China," *Resources Science*, vol. 40, no. 12, pp. 2475–2486, 2018.

[12] L. Li and W. X. Xu, "Changes in agroecological efficiency under the effect of rural population aging," *Journal of South China Agricultural University (Social Science edition)*, vol. 20, no. 2, pp. 14–29, 2021.

[13] M. R. Huang, L. L. Zeng, and X. Y. Li, "The study of agricultural ecological efficiency combining LCA and DEA method, combines the influence of green cognition and environmental regulation," *Journal of Huazhong Agricultural University (Social Science edition)*, 10 pages.

[14] Y. Li Fang and X. L. Zeng, "Evaluation of China's interprovincial agricultural ecological efficiency and its improvement path analysis," *Journal of Agricultural and Resource Economics*, vol. 38, no. 1, pp. 135–142, 2021.

[15] Y. J. Wang and Z. Z. Chen, "Research on the evaluation and improvement path of agricultural ecological efficiency in the economic belt of the northern slope of the Tianshan Mountains: based on the Super-SBM model and the Global-Malmquist index," *Ecological Economy*, vol. 36, no. 2, pp. 111–117, 2020.

[16] Y. Zhang and J. J. Chen, "International comparison of agricultural ecological efficiency and China's positioning research," *China Soft Science*, vol. 10, pp. 165–172, 2019.

[17] P. Andersen and N. C. Petersen, "A procedure for ranking efficient units in data envelopment analysis," *Management Science*, vol. 39, no. 10, pp. 1261–1264, 1993.

[18] B. Y. Wang and W. G. Zhang, "Inter-provincial differences and influencing factors of China's agricultural ecological efficiency: based on panel data analysis of 31 provinces from 1996 to 2015," *China Rural Economy*, vol. 1, pp. 46–62, 2018.

[19] S. Y. Lai, P. F. Du, and J. N. Chen, "An investigation and evaluation method of non-point source pollution based on unit analysis," *Journal of Tsinghua University*, vol. 9, pp. 1184–1187, 2004.

[20] C. L. Shi, Y. Li, and J. F. Zhu, "Labor transfer , chemical fertilizer excessive use and non-point source pollution," *Journal of China Agricultural University*, vol. 21, no. 5, pp. 169–180, 2016.

[21] X. Q. Wu, Y. P. Wang, L. M. He, and G. F. Lu, "Evaluation of agricultural ecological efficiency based on AHP and DEA models——based on AHP and DEA models wuxi city as an example," *Resources and Environment in the Yangtze River Basin*, vol. 21, no. 6, pp. 714–719, 2012.

[22] Q. Chen and Q. B. Lin, "Analysis of the effect of rural financial poverty alleviation: an empirical study based on panel data of 26 provinces in my country," *Taxation and Economy*, vol. 2, pp. 37–43, 2019.

[23] D. H. Liu, T. Q. lai, and Q. Wang, "Research on the dynamic correlation between agricultural science and technology investment and agricultural economic growth -- Based on the empirical data of Sichuan Province from 2000 to 2015," *Rural economy*, vol. 10, pp. 118–122, 2017.

[24] X. Wang, M. Zhang, and F. S. Yu, "Managerial overconfidence and enterprise investment behavior alienation: empirical evidence from my country's securities market," *Nankai Management Review*, vol. 2, pp. 77–83, 2008.

Hindawi
Mobile Information Systems
Volume 2022, Article ID 4277149, 12 pages
https://doi.org/10.1155/2022/4277149

Research Article

A Resource Scheduling Method for Enterprise Management Based on Artificial Intelligence Deep Learning

Lujie Zhu[1,2] and Li Huang[1]

[1]*School of Business, Yulin Normal University, Yulin 537000, Guangxi, China*
[2]*Business Administration in Baliuag University in the Philippines, Baliuag 3006, Bulacan, Philippines*

Correspondence should be addressed to Li Huang; hl1338@zjgsdx.edu.cn

Received 20 June 2022; Revised 13 July 2022; Accepted 21 July 2022; Published 21 August 2022

Academic Editor: Yajuan Tang

Under the current trend of economic globalization and international competition, more and more production enterprises are introducing the project management model, that is, customer or order projection, and using the concept of project management to manage operations. In an enterprise, there are multiple customers at the same time, and the production line can also generate multiple orders from different customers at the same time. That is to say, multiple projects are running at the same time, resulting in continuous changes in management processes, heavy project coordination tasks, and a serious waste of corporate resources. The resources that can be used are limited. In the production business using project management, how to rationally utilize the limited business scheduling resources has become the focus of research. Aiming at the method of business management resource scheduling, this paper investigates the application of enhanced particle swarm algorithm on the cloud deep learning platform, and the mapping problem between virtual machines and physical machines. As a heuristic algorithm, particle swarm optimization is suitable for solving combinatorial optimization problems. By improving the diversity of particle hosts and setting parameters, it improves the integration speed and accuracy of the algorithm. Through the analysis of the current situation of multi-project business management, it examines the allocation of resources. In terms of business management, it has established a resource allocation model for multiple projects. The results show that the method improves the efficiency of the enterprise by 35% compared to the traditional method with a 20% reduction in personnel. A better configuration scheme is simulated by MATLAB, which verifies the scientificity and effectiveness of the method studied in this paper.

1. Introduction

As the diversification of consumer demand becomes more obvious, enterprises continue to introduce new products in order to better meet the demand. It drives the next round of product development competition and increases the variety of products. However, some enterprises blindly follow the trend, and if the sales chain is interrupted slightly, they will accumulate a large amount of inventory. It takes up a lot of capital, which seriously affects the speed-up and capital turnover of enterprises. This in turn affects the sustainable competitiveness of the company. As consumer demand has become more unpredictable, there are many homogeneous products on the market. It is full of personalized needs, consumers cannot get what they want, and companies cannot provide what consumers want. With the intensification of market competition, the rhythm of economic activities is getting faster and faster; therefore, every business spends more time on researching consumers. If a business is relatively slow in meeting consumer demand, it will soon be overtaken by competitors. Because for today's companies, market opportunities are scarce, and the time for companies to think and make decisions is very limited. Therefore, shortening the product development and production cycle and meeting the needs of consumers at the fastest speed has become one of the concerns of all enterprises and managers.

Big data can solve the storage and processing of data, and cloud computing can realize the efficient and flexible utilization of computing resources. It is very practical to combine the two. How to analyze big data, extract elements,

and visualize large amounts of data has become an important research topic. It can solve this problem through in-depth research. Deep learning is a type of machine learning. It uses the structure of the human brain to create multi-layered neural networks and continuously trains data to capture nonarithmetic functions, such as parts of high-level complexity. Cloud deep learning is provided by the deep learning platform, and the GPU performance is poor due to the use of virtualization technology in the cloud environment. So, it can also choose GPU training servers to improve performance. The GPUs discussed here range from cloud GPU servers to cloud service providers to physical machines. However, many problems arise when researchers use TensorFlow's deep learning framework to train neural networks. When training on GPU servers, GPU usage relies on manual and static device allocation, and the uncertainty of resource allocation creates problems for consumers who cannot use computer resources efficiently. In addition, it is also important to use the deep cloud learning platform to do deep learning work and solve the mapping problem between virtual machines and physical machines in various places. Therefore, for deep learning platform training and GPU server training in two different cloud environments, it is very important for deep learning developers to use deep learning workflow plans and computing resources more efficiently.

In the case of limited resources, the immediate change is that the tasks performed by the business never increase, while the resources and organizational structure of the business are relatively strong. In particular, the total resources such as human, material, and financial resources of enterprises are limited. Under a project condition, the enterprise only needs to put all the resources into the project, and the project schedule will not be disturbed. However, if the enterprise is running multiple projects, there will be problems that multiple projects compete with each other or share some resources and interfere with each other's schedule. In addition, project managers of various business projects will only consider how to meet resource requirements, construction phase, and cost of the project for which they are responsible, and focus on how to achieve the goals of the project for which they are responsible. It reinforces the overall level of self-development, joint planning, allocation, and management of project resources specific to each project. It must address limited resources. This requires research into multi-project planning and planning to ensure resource scheduling and allocation methods for specific projects.

2. Related Work

In recent years, with the continuous deepening of globalization, in order to obtain strong corporate competitiveness in the fierce market competition, and to seek the survival and long-term development of enterprises, the world experts have carried out a lot of research on enterprise management resources. By reducing the optimization problem into two sequential problems according to You C, it corresponds to the optimal scheduling order and the joint data partitioning and time division problem given the optimal order. It was found that the optimal time-sharing strategy tends to offload the defined effective computing power among mobile devices through time-sharing balancing [1]. Zhang believed that driven by the increase of massive wireless data traffic from different application scenarios, 5G networks based on network slicing should utilize efficient resource allocation schemes to improve the flexibility and capacity of network resource allocation [2]. This problem is addressed by leveraging the common interest, physical and energy-aware clustering, and resource management framework of wireless powered communication (WPC) technologies according to Tsiropoulou E E. Within the proposed framework, numerous M2M devices initially form different clusters based on the low-complexity Chinese restaurant process (CRP) [3]. Chen C developed a supply and demand system model for the study area using system dynamics modeling tools. To explore the optimal resource management scheme by testing the system response under various scenarios, he identified the main factors that affect the response to achieve a balance of sustainable socioeconomic development [4]. Although the above research brings us some references, the research is too one-sided.

We bring artificial intelligence and deep learning algorithms into the research of enterprise management resource scheduling methods. Chen first introduced the concept of deep learning into hyperspectral data classification. First, he qualified stacked autoencoders by following classical spectral information-based classification [5]. Shen believed that recent advances in artificial intelligence, especially in deep learning, are helping with identification, scheduling, and resource allocation. Central to these advances is the ability to utilize hierarchical feature representations that are learned only from data, rather than hand-designed features based on domain-specific knowledge [6]. Ravi believed that deep learning is a technology based on artificial neural networks. It is emerging as a powerful machine learning tool in recent years, which is expected to reshape the future of artificial intelligence [7]. Although the above research is relatively comprehensive, the analysis is not deep enough, so it is not adopted in this paper.

3. TensorFlow Deep Learning Framework

In order to replace humans with repetitive tasks, humans have created computers with massive storage space and ultra-high computing speed, which can perform difficult tasks that humans need to accomplish, such as scientific computing and statistics. However, some problems that can usually be solved by humans cannot be solved by computers at present, such as natural language understanding, image recognition, and speech recognition, so they need the analysis of artificial intelligence [8]. The computer itself lacks intelligence and has obvious advantages in computing speed, but it is often inefficient in decision-making and analysis. Insufficient intelligence of computer operations is a serious problem, and based on this situation, early artificial intelligence such as IBM's deep blue can only solve problems in specific

environments [9]. To enable computers to control information in an open environment, researchers use knowledge bases to give computers access to artificially generated information. But building a knowledge base of human and material resources is limited to but not excluded from all content except information disclosure. Information can be published in a fixed format that computers can understand [10]. Machine learning works by computing the correlation between a set of features derived from these data and its predictions, training data. However, these results are highly dependent on preplanned data acquisition and many issues need to be addressed, making direct data acquisition difficult for a number of reasons. Therefore, exploration is expected to automate tasks from data [11].

As shown in Figure 1, the most common network systems are input layer, hidden layer, and production layer. The number of circuits that neurons have a specific function to connect neurons to different neurons and the direction of each connection resource should be data access and training of network neurons. Since the product layer adjusts each neuron connection to obtain the best results, a scaled structural network should be used to obtain some input information of the production function, i.e., to complete the prediction [12].

With the development of deep learning, more and more deep learning frameworks are introduced, and TensorFlow is becoming more and more popular. Regarding GitHub, TensorFlow has long been considered an open-source machine learning project. TensorFlow is the best-designed project in GitHub's annual developer report and is highly rated by deep learning experts. From Table 1, we can see the key position of the current deep learning framework in the industry [13].

TensorFlow borrows and maximizes the advantages of DisBelief's original AI system. Its name contains two key concepts in the framework, representing N-dimensional arrays, which is a calculation method described by a combination of points and lines. TensorFlow is a series of data features and performs end-to-end computations in a process graph. TensorFlow can be used to transfer data structures representing data features into neural networks with multiple input, hidden, and output layers [14]. For convenience, TensorFlow provides several APIs. Using these APIs, students can easily create various web templates, such as CNN, RNN, and LSTM. As shown in Figure 2, the TensorFlow architecture is divided into front-end components, hardware device layer, and application layer [15].

3.1. Cloud Computing Architecture. Cloud configuration has two aspects: service and management. Services can be divided into hardware (IaaS) services, application-based services (PaaS), and application-based software services (SaaS). Supervision includes the management of personnel, storage, data, infrastructure, etc., under various functions to ensure the normal operation of the cloud platform. Its complete structure is shown in Figure 3 [16].

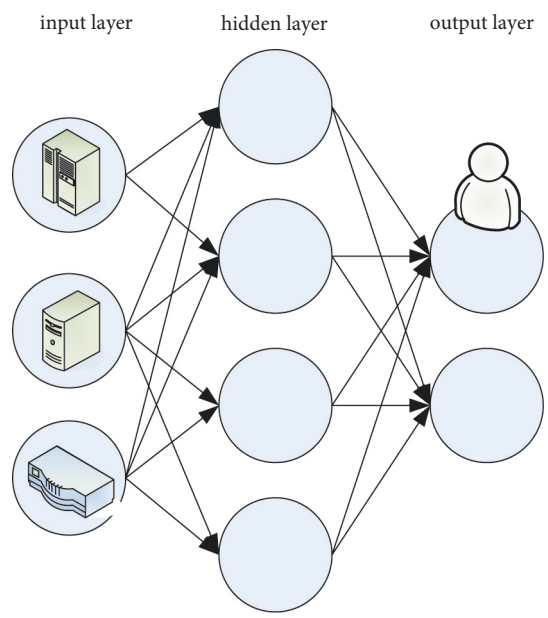

Figure 1: Neural network structure.

3.2. Virtualization Technology. Cloud computing can transform the ability of information technology to achieve meaningful discovery. It is based on virtualization technology and valuable cloud computing technology. It uses computer resources to reduce memory, CPU, network, and storage. This unique approach modifies the original integration, which simplifies data center management and improves resource efficiency [17]. When invisible to the user, configuring the system becomes more intuitive and the use of practical methods is not limited to the physical components of the original composition. Virtualization technology is a method of freeing resources without compromising the hardware structure. For the application industry, virtualization technology can integrate resource management, distribution, and scalability. CPU and GPU are components of computer systems, but there are still differences [18]. A person must not only begin to manipulate, but also participate in the control of logic [19]. The latter contains a large number of computer units. Due to the high improvement in computer performance in recent years, the use of multiple GPUs at parallel computing time leads to better performance in difficult computer tasks such as deep learning [20]. Currently, there are four main ways to view GPUs: direct GPU integration, GPU simulation, mid-level API implementation, seamless virtualization of GPU tools, and communication between the two in the system, as shown in Figure 4 [21].

The resource layer is not only the bottom layer of cloud computing architecture, but also the most important layer in cloud computing. The realization of any upper-layer business needs to rely on the support of hardware devices. This level is mainly the application of virtualization technology, which makes the use of resources more flexible by converting it into virtual resources. As an important technology in cloud computing, it realizes the

Table 1: Comparison of various deep learning frameworks.

Frame	Torch	Theano	Caffe	MXNet	TensorFlow	PyTorch
GitHub starts	6541	5642	15456	7856	45643	2455
Open-source time	2002	2008	2013	2015	2015	2017
Development language	C/Lua	C/python	C++	C++	C++/Python	C++/Python
Language used	Lua Python	C++/Python MATLAB	C++/Python MATLAB	C++/Python R/Go	C++/Python	Python

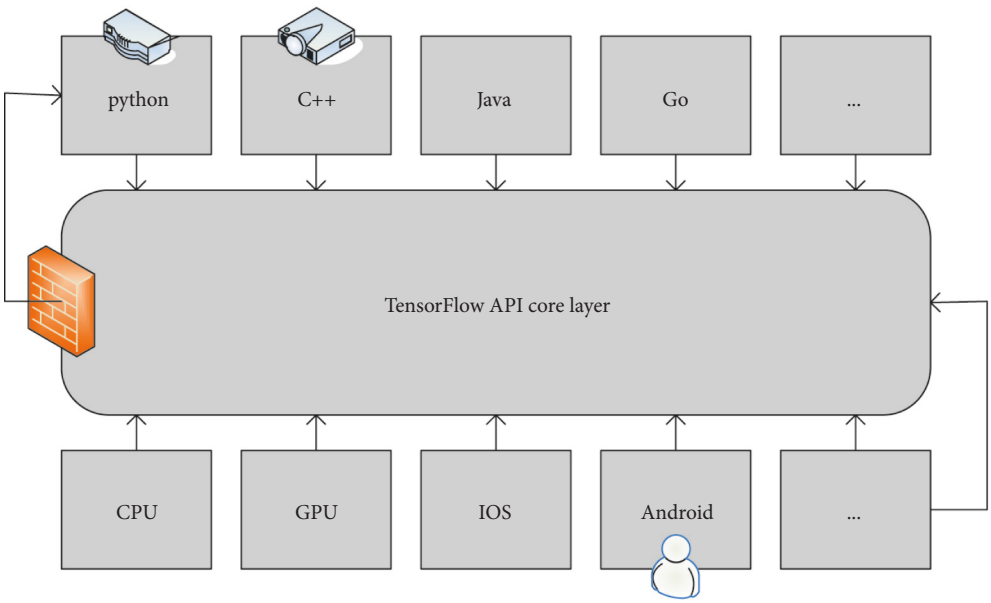

Figure 2: TensorFlow architecture diagram.

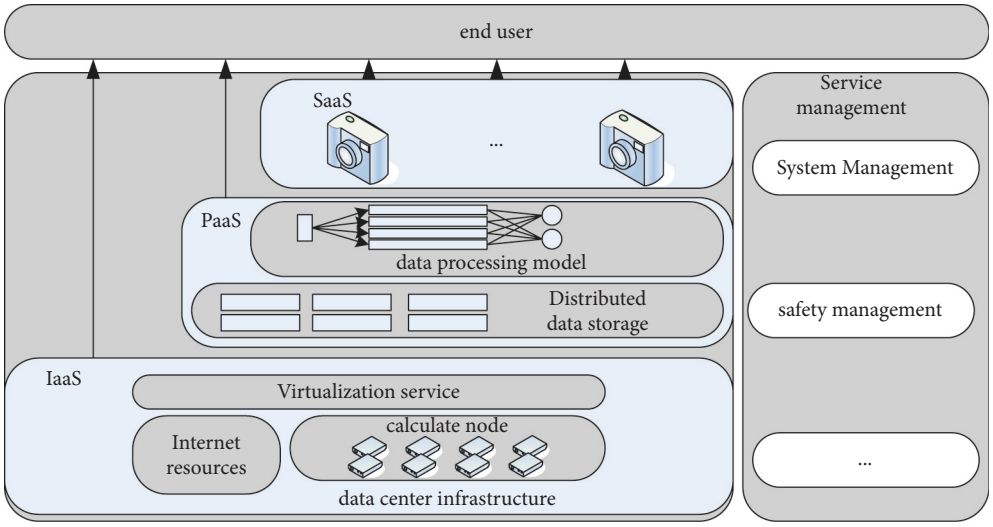

Figure 3: Overall architecture of cloud computing.

integration of heterogeneous resources with the help of network connection. Platform layer: This layer is also essential in the three-tier architecture. It connects the application layer and the resource layer, it needs to provide services to the other two layers, and it needs to provide real-time monitoring of virtual machines for the resource layer. It ensures the normal operation of the virtual machine and performs virtual machine migration when necessary. It needs to realize resource discovery and recovery. It requires scheduling of tasks. It needs to provide functions such as disaster recovery mechanism. It provides permission management for the application

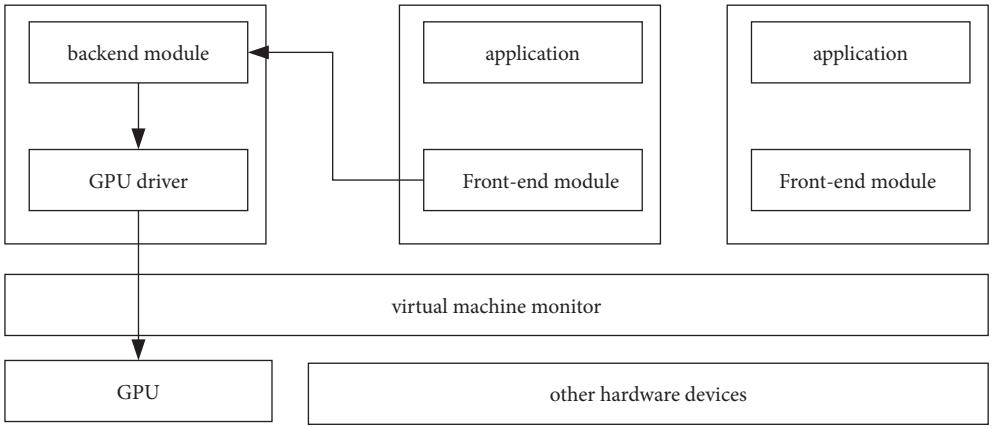

Figure 4: API redirection method architecture diagram.

layer. It implements resource billing module and provides security mechanism, API, and other functions. Application layer: Through this layer, users can apply for resources on the cloud platform and deploy different applications. In order to facilitate the operation process, it is presented in the form of web pages, and different functions are realized by calling different APIs. The resource scheduling service in cloud computing is subdivided into task scheduling and virtual machine scheduling according to different objects. The former maps virtual machines, and the latter maps physical machines. From Figure 5 we can see that they are mainly used in the resource layer.

Whenever a user submits a task to the data center, a certain task scheduling strategy is required. By dividing tasks, it places different subtasks in different virtual machines to execute. Sometimes, different subtasks have requirements on the execution order, and the mapping between subtasks and virtual machines requires task scheduling to play a role. This process relies on first-level scheduling. The virtual machine contains the resource requirements for user task execution, which must be mapped to a specific physical machine before the task execution can begin. Because the relationship between virtual machines and physical machines is many-to-one, the total resources of multiple virtual machines running at the same time are limited by the total resources of physical devices. How to complete the creation of the virtual machine on the physical machine, what strategy to adopt for the migration of the virtual machine, and how to balance the load of each physical machine, these series of processes all depend on the second-level scheduling [22].

3.3. Main Resource of Deep Learning. The GPU has more ALUs (ArithmeticAndLogicUnit, arithmetic logic unit) than the CPU, and more computing units enable the GPU to gain advantages in floating-point processing capabilities. Then comes the need for bandwidth. To this end, on the one hand, the GPU has designed a large number of distributed caches internally to ensure the versatility and compatibility of high-bandwidth scenarios of data reuse. In addition, the GPU has always used the most advanced technology in terms of video memory technology, and its video memory bandwidth is also much higher than that of the CPU. It enables the GPU to read and process data at high speed. The following is a comparison of specific experimental data to reflect the difference between GPU and CPU in performing deep learning tasks. The figure below is a comparison of the time consumption of training a common MNIST (handwritten digit recognition) task in a fully convolutional neural network through the TensorFlow platform. The batch size of the task is set to 100, the epoch is 4, and the learning rate is 0.05. For other hardware parameters, the experimental environment description below is shown. Figure 6 shows the comparison of the training time when using the CPU alone to open 1, 2, 4, 8, 16, and 32 threads and using the GPU alone. From the figure, we can intuitively see the acceleration of GPU training for deep learning tasks. Without optimizing the network model, by using GPU, the training speed of CPU is increased by 67 times compared with a single thread, showing a significant acceleration effect. With the continuous development of deep learning, more complex neural networks will appear and face larger-scale training data. The training time will also be longer, and the use of GPU is particularly important.

In the training process of the neural network, it needs to perform multiple training on the full amount of data and fully learn the data features to improve the performance. The usual practice is to set a larger epoch value and train the data multiple times. This process increases the proportion of GPU usage and reduces the error of time estimation. The time required to complete the task under different epochs is calculated and analyzed through experiments. The results show that when the epoch is set to 32, the estimation error of the completion time of this task is reduced to about 5%, which confirms the effectiveness of this method. In order to test the accuracy of the deep learning task time estimation mentioned above, this paper counts the deep learning task estimated time and actual running time (unit: seconds) under different epoch

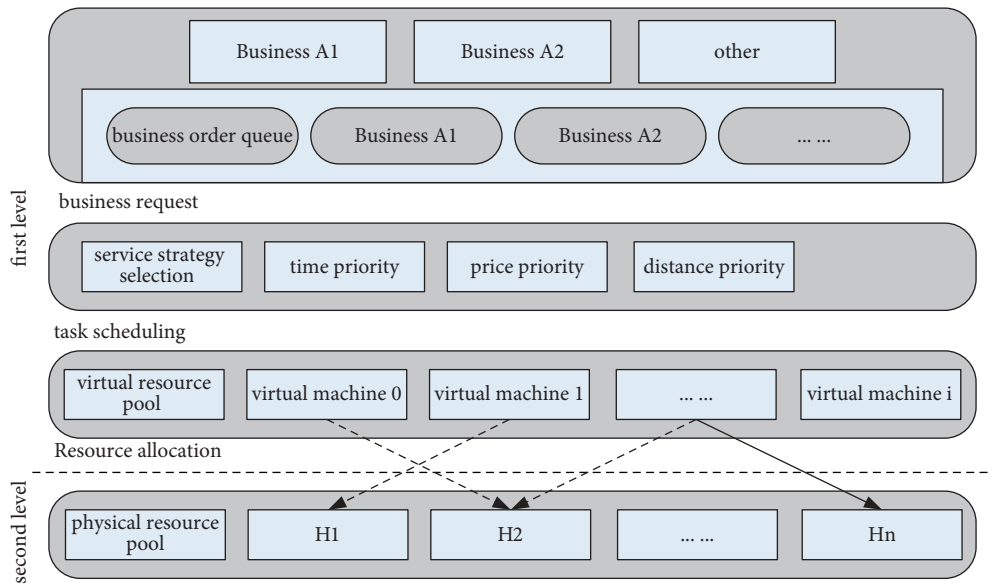

Figure 5: Cloud computing resource scheduling model.

settings. It calculates the error ratio. It is set to 1, 2, 4, 8, 16, 32, 48, 56, and 64, respectively. The related results are shown in Table 2.

3.4. Mathematical Description of Particle Swarm Optimization. Particle swarm optimization is a heuristic algorithm. From the mathematical model, it means that m number of particles are in the D-dimensional space. According to the objective function, it continuously iteratively searches and finally finds the optimal solution. The position of the particle is expressed as

$$\begin{aligned} x_i &= (x_{i1}, x_{i2}, \ldots, x_{iD})\,(i = 1, 2, \ldots, m), \\ V_i &= (V_{i1}, V_{i2}, \ldots, V_{iD}), \\ p\mathrm{Best}_i &= (P_{i1}, P_{i2}, \ldots, P_{iD}), \\ g\mathrm{Best}_i &= (g_{i1}, g_{i2}, \ldots, g_{iD}). \end{aligned} \tag{1}$$

Every time an iteration is completed, particle i needs to update its own speed and position according to the formula:

$$\begin{aligned} v_{id}^{k+1} &= v_{id}^{k} + c_1 r_1 \left(p\mathrm{Best}_{id} - x_{id}^{k}\right) + c_2 r_2 \left(g\mathrm{Best}_{id} - x_{id}^{k}\right), \\ x_{id}^{k+1} &= x_{id}^{k} + v_{id}^{k+1}, \\ v_{id} &= -V_{\max}\,(v_{id} < -V_{\max}), \\ v_{id} &= V_{\max}\,(v_{id} > V_{\max}). \end{aligned} \tag{2}$$

However, particle swarm optimization also has its shortcomings. In the process of continuous research, in order to balance the search speed and accuracy of particles, the standard particle swarm optimization algorithm was produced. It applies the inertia weight to the particle swarm algorithm, which is combined with the previous velocity of the particle. It represents the effect of the previous speed on the current speed update. This evolves into the formula:

$$\begin{aligned} v_{id}^{k+1} &= w v_{id}^{k} + c_1 r_1 \left(p\mathrm{Best}_{id} - x_{id}^{k}\right) + c_2 r_2 \left(g\mathrm{Best}_{id} - x_{id}^{k}\right), \\ x_{id}^{k+1} &= x_{id}^{k} + v_{id}^{k+1}, \\ v_{id}^{k+1} &= x\left[v_{id}^{k} + c_1 r_1 \left(p\mathrm{Best}_{id} - x_{id}^{k}\right) + c_2 r_2 \left(g\mathrm{Best}_{id} - x_{id}^{k}\right)\right], \\ x &= \frac{2}{\left|2 - c - \sqrt{c^2 - 4c}\right|}, \quad c = c_1 + c_2,\ c > 4. \end{aligned} \tag{3}$$

That is, the iterative process linearly reduces the inertia weight value, and a large value in the early stage ensures that the optimal solution can be searched in a wide range. As the iteration progresses, the inertia weight value keeps shrinking, and the particle swarm presents an overall aggregation. At this time, a stronger local search ability is needed, and the following algorithm is proposed:

$$\begin{aligned} w &= (w_1 - w_2) \times (T - t) \div (T + w_2), \\ x_i &- x_{\min} + (x_{\max} - x_{\min}) \times \mathrm{r\ and} \\ w &= w_{\max} - (w_{\max} - w_{\min}) \times \frac{l}{l_{\max}}, \\ w &= w_{\max} - (w_{\max} - w_{\min}) * \left(\frac{l}{l_{\max}}\right)^{k}. \end{aligned} \tag{4}$$

$W_{\max}$, $W_{\min}$ are generally 0.9, 0.4, the optimization effect of this value is good, and k is a constant. In order to choose a suitable k, a series of experiments are carried out, as shown in Figure 7, and it can be seen that k is 0.3 and the effect is better. This also shows that the improved method is better than the linear adjustment of the formula with $k = 1$.

Based on the above analysis, an improvement and optimization of dynamically adjusting the value of the learning factor with the number of iterations are proposed, as shown in the formulas:

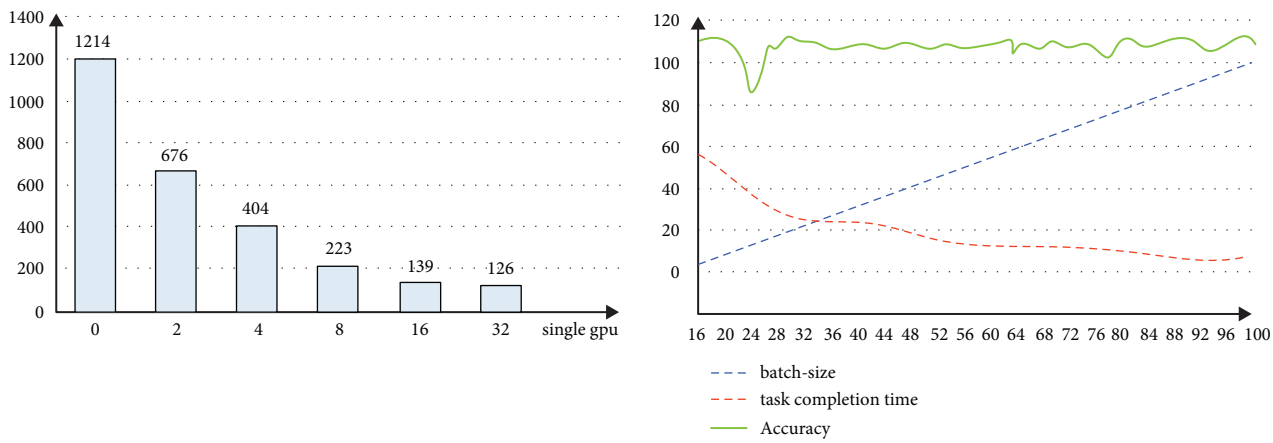

Figure 6: Comparison of acceleration effects and the impact of different batch sizes during GPU training.

Table 2: Time estimate vs true value comparison.

Epoch value	Average time for batch data	Estimated task time	Actual task time	Error value	Error percentage (%)
1	0.00641	3.45	6.6512	2.31	42
2	0.00642	7.656	10.65641	2.32	25
4	0.00651	11.65	17.65231	3.02314	14
8	0.00542	21.35	31.35641	3.45122	10.6
16	0.00582	51.63	58.65612	4.56123	45.6
32	0.00541	123.32	165.65652	5.64123	5.3
40	0.00563	145.32	145.65565	6.32465	4.2
48	0.00542	154.65	175.65465	7.34512	4.1
56	0.00621	201.32	212.98712	8.65446	3.5
64	0.00602	223.32	234.641123	8.79854	3.8

$$\begin{aligned} \min f(x) &= \frac{\sin(10\pi x)}{x}, \\ \max f(x) &= \sum_{i=1}^{2}\left(x_i^2 - 10 * \cos(2\pi x_i)\right) + 20, \\ \min f(x) &= \sum_{i=1}^{30}\left[100\left(x_{i+1} - x_i^2\right)^2 + (x_i - 1)2\right], \\ c_2 &= \frac{2 + l}{2 * l_{\max}}. \end{aligned} \tag{5}$$

The test results are shown in Table 3.

4. Application Example of Enterprise Management Resource Scheduling Method

A Steel Heavy Industry Co., Ltd., adopts the MTO-type production method to organize production. At the same time, the company undertook the manufacturing projects of three mechanical lifting trolleys of different models (the orders were placed at the same time), and the project numbers were Project A, Project B, and Project C, respectively. The project indicators of each project are shown in Table 4, and each project contains 11 tasks. According to the experience and expert judgment of similar projects in the past, it has determined the task information data of each project, as shown in Figure 8. According to the logical relationship of task sequence, the network diagram structure

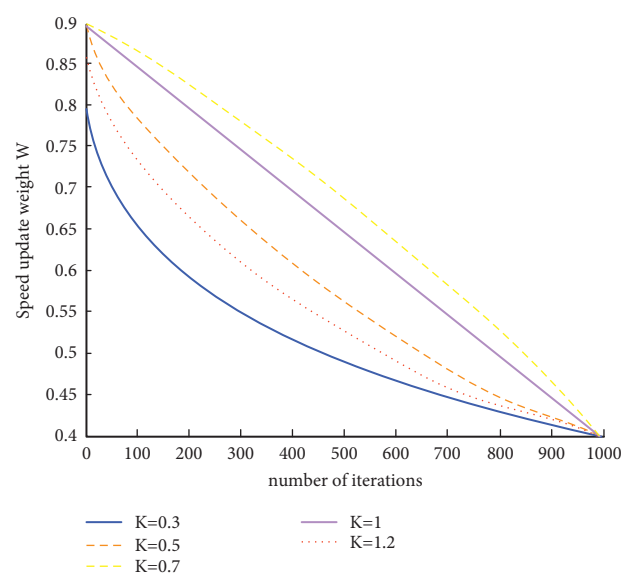

Figure 7: Comparison plot for different k values.

of the three projects is the same, and the logical relationship of each task is given in Figure 8. The contract amounts of the three projects are 1 million, 900,000, and 800,000, respectively, and the delivery time is 50, 60, and 70 days. The late delivery penalty is 6/10 of the contract amount. Figure 8 shows the maximum supply of the project's shared resources. Now it is necessary to formulate a reasonable resource allocation plan, so that the three trolleys can meet the

Table 3: Standard particle swarm algorithm running results.

Function	The optimal value	Worst value	Average value	Convergence average number of iterations
F1	0.9651	0.8456	0.9456	132
F2	86.6541	75.6542	79.6521	241
F3	10.6521	35.6542	13.6562	563
The running results of the improved particle swarm algorithm				
F1	0.9653	0.9856	0.9586	56
F2	82.3564	75.6542	79.6564	123
F3	4.6523	12.3541	6.9564	334

Table 4: Data for each item.

Project evaluation factor data	Project A	Project B	Project C
Customer contribution	200	300	250
Project social benefits	96%	92%	92%
Client needs	4	4	4
Project expected net profit margin	21%	13%	6%
Project contract amount	100	95	86%
Project overdue fines	0.45	0.54	0.54
Project resource requirements	5	4	3
Project duration	45	45	75
Project technical complexity	3	3	1
Project dependencies	24%	26%	30%

requirements of on-time delivery within the contract period or the minimum total penalty for overdue under the resource constraints.

No matter what the reality is, there are still many enterprises that are transforming from traditional functional department management to project-based management mode. This phenomenon is more pronounced in order-design-production enterprises. Companies such as Motorola, Bell, and Ailant can not only customize the special requirements of customers, but also produce low-cost, high-quality products with short lead times. Compared with traditional manufacturing, the coexistence of multiple projects in project-based business has the following advantages. It can quickly respond to dynamic market demands. It adopts the idea of modular design, and the technology adopts mass production as much as possible. Therefore, customers can get products that exactly meet their needs at a lower price. It reduces production costs. It is made to order, so the company's inventory is reduced. The spending is on the backlog, which reduces the cost of the bill. It shortens the delivery time and makes full use of business resources. By adopting a modular approach, it shortens product launch time and improves product quality. As product designs revolve around more integrated parts, its effective production monitoring is better with standardization of parts, materials, and manufacturers. The quality can be greatly improved. Through efficient use of resources, it continues to improve quality, further enhance MC production and management and control capabilities, and improve the economic benefits of the enterprise. Because it can produce products and deliver products according to the needs of consumers, it increases the sales volume of products, occupies a wider market, and promotes the benefits of enterprises. During the production process, it takes full account of the actual location of other existing projects. It reasonably allocates limited resources and many time differences, and the business output-input ratio is significantly improved. First of all, due to the parallelism of multiple projects, it is necessary to prioritize the multiple projects being implemented in order to reasonably plan resources. Now it takes the three projects of the enterprise, Project A, Project B, and Project C as the priority evaluation object. In this paper, the established evaluation index system is adopted; that is, 10 priority evaluation elements are directly scored. After collecting the project data and five experts' comments on the evaluation elements, the score statistics shown in Table 5 is obtained.

After solving the resource scheduling scheme of the program group, the number of resources allocated to each task of each project and the construction period used are obtained. The specific data are shown in Figure 9.

The article discusses the formulation process and method of enterprise program resource scheduling plan. First of all, this paper discusses the need to prioritize the order items of the enterprise before planning. By constructing the project priority evaluation system, the gray relational evaluation method is adopted in this paper to determine the project priority. On this basis, this paper establishes a corresponding mathematical model for the actual resource scheduling problem of enterprises through the deep learning method of artificial intelligence. It constructs the objective function with minimum weighted total overdue sum and minimum overdue penalty based on program group, and gives its constraints. By using the resource scheduling solution algorithm, it solves the model to determine the resource scheduling scheme of the project group. Finally, this paper applies the planning process and method to an enterprise example to solve practical problems.

5. Discussion

In the process of implementing program resource scheduling management, the objects of control are multiple projects. The entire enterprise presents a multidimensional state. Its implementation and control process is relatively complicated, so it is necessary to build a perfect dynamic control system to ensure the effective implementation of resource scheduling management. Based on the deep learning method combined with enterprise artificial intelligence, this paper studies the implementation of resource scheduling from three aspects: the key nodes of resource scheduling and monitoring of enterprise order items, the enterprise organization model, and the resource information platform.

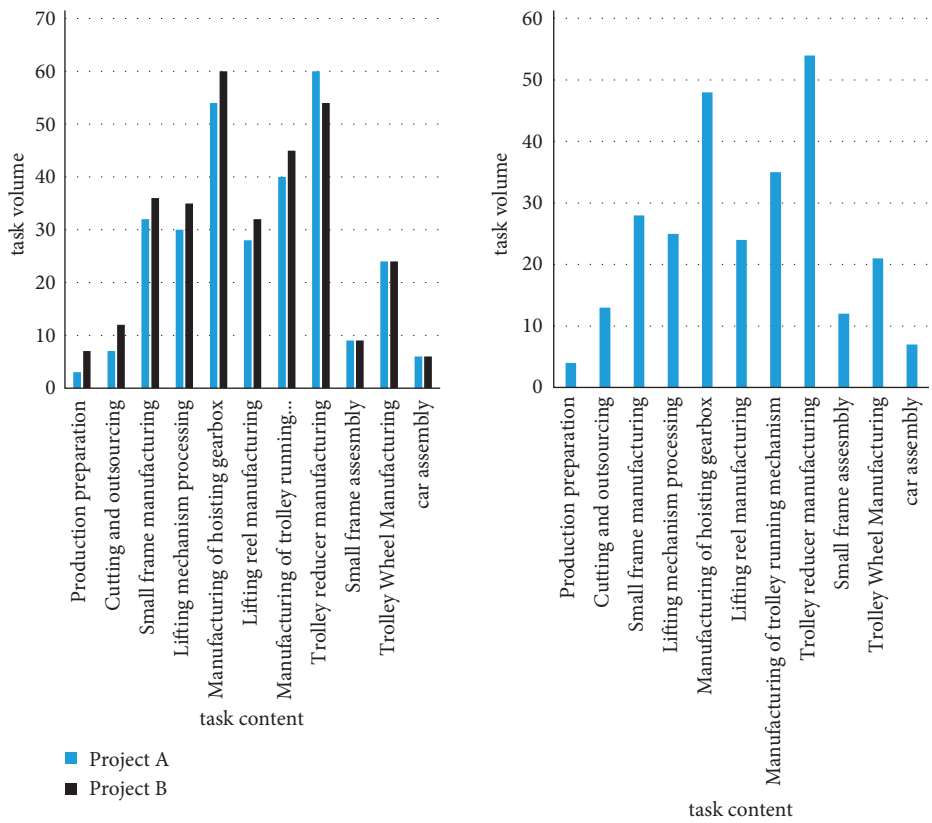

Figure 8: Task map of each project.

Table 5: Index scores and ideal values of the items to be evaluated.

Metric dimension	Indicator factors	Project A	Project B	Project C	Project ideal index value
Customer dimension	Customer contribution	200	300	250	300
	Project social benefits	0.94	0.96	0.97	1
	Client needs	4	4	2	6
Financial dimension	Project expected net profit margin	0.12	0.13	0.04	0.14
	Project contract amount	100	80	98	100
	Project overdue fines	0.42	0.34	0.39	0.45
Internal process dimension	Project resource requirements	4	4	2	4
	Project duration	56	60	70	52
	Project technical complexity	4	2	1	5
	Project dependencies	0.25	0.21	0.35	0.35

Enterprise program resource scheduling monitoring refers to the management activities such as inspection, supervision, correction, and other management activities carried out by the enterprise organization in the dynamic changing environment to ensure the realization of the established resource scheduling goals. To make enterprise program resource scheduling monitoring work effectively, it must follow the following basic requirements—goal-oriented: the enterprise's program resource scheduling control work should be oriented to the goal of resource scheduling. That is, on the basis of maximizing resource utility, it can meet the delivery time of each order item. And the goal orientation should be consistent with the strategic goals of the enterprise to ensure the effectiveness of the enterprise-level goal management, so that the market competitiveness of the enterprise continues to grow. Key management: In the enterprise's program resource scheduling and control work, it should carry out key management and control for the key points in the resource scheduling management. It ensures the effective advancement of enterprise resource scheduling and management. Scientific management schedules the resource scheduling of business program groups in resource management activities. In order to improve the robustness and effectiveness of management, it requires the collection of large amounts of data and proper analysis. It enables resource scheduling to be logical and economical. Applying this scientific method to resource scheduling management activities is the principle of applying scientific management. Adapting measures to local conditions: The principle of enterprise resource scheduling management adapting to local conditions means that the resource scheduling management system must be individually designed. It is suitable for the actual situation of specific business, department, work, and project, and it cannot

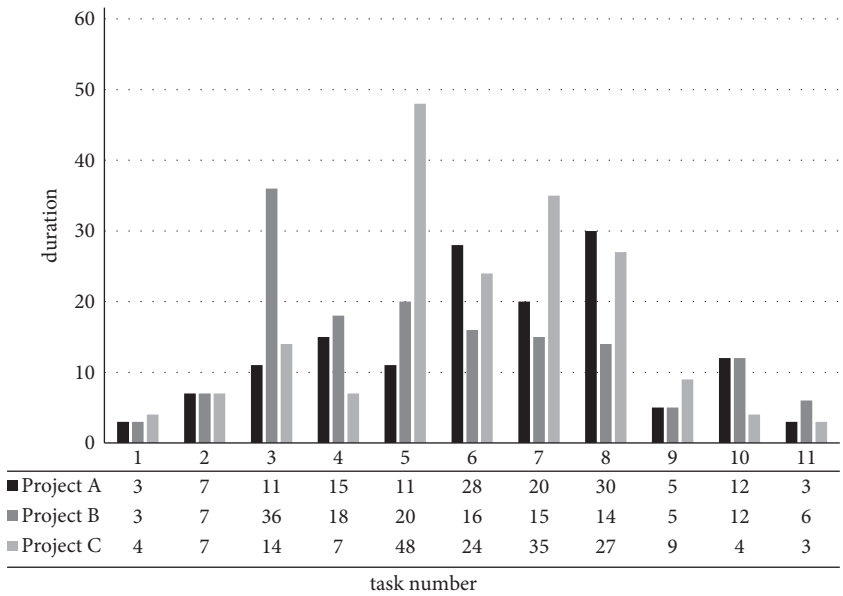

Figure 9: The number of resources allocated to each project task.

copy the habits of others. Due to different industries, different scales, and even different development stages of the same business, its management focus, organizational structure, and management style are different. Therefore, scheduling management is impossible. Each business-related resource, as well as enterprise management standards and procedures, is different.

According to the characteristics of the whole project life cycle, it divides the project into preproject preparation, project implementation, project completion, and project warranty phases and corresponding monitoring objectives. Indicators and corresponding management requirements are set in the main objectives of each business project. Only when the indicators and requirements are met can the next stage or management objectives be entered. When setting the main goal of planning resource scheduling, it should consider the unity of multiple projects. It covers aspects of project quality, investment, development, safety, and risk management. The specific monitoring content must be consistent with the target system, and the business expectations system must be managed consistently. In the prepreparation stage of the project, order item selection, project resource information tracking, and project resource scheduling plan review have become the focus of monitoring. This is mainly based on the enterprise's response to the market and customers' demands and the evaluation of its own resources and investment capabilities in the preproject preparation stage. In the project implementation stage, the enterprise should bring the project production work into the monitoring focus. It is mainly to manage whether the project department has the corresponding production conditions. Its purpose is to assess the availability of the relevant human, material, and financial resources of the project, and to have the corresponding technical force. In the project implementation stage, the enterprise can carry out the implementation inspection of resource scheduling in different stages of the product production process by adopting corresponding inspection methods. It also comprehensively considers the implementation of product quality, safety, progress, and investment. It can ensure the effective implementation of resource scheduling and the realization of the overall project goals by increasing the frequency of inspections. In the preacceptance stage of the project completion, the enterprise can conduct a comprehensive inspection of the project resource utilization efficiency and product quality by setting up the precompletion acceptance inspection. This is also an important node for the project to monitor the effect of the order project before delivery. After the project is officially completed, the enterprise conducts final monitoring of the project department after completing the project management tasks. The purpose is to check the completion of the project and provide real-time feedback on the monitoring results.

6. Conclusion

In enterprise management, resource scheduling is an important issue that program management is concerned about and needs to solve urgently. Combining with the actual situation of production and operation of the enterprise, this paper conducts an in-depth study on the resource scheduling management of its program group. In this paper, the problem of mapping the application of improved particle swarm algorithm to virtual machine and physical machine is proposed for the situation of task training through cloud deep learning platform. It is improved in the initialization stage of particle swarm and focuses on improving the diversity of particle swarm. The improvement of particle velocity out of bounds adds randomness to the original processing method. For the improvement of particle inertia weight value, different values are used in different stages of iteration to balance the global search and local search capabilities of particles. It controls the resource scheduling of enterprise program groups from three aspects: resource scheduling management and monitoring key nodes, organizational structure design, and information platform

establishment. It determines the key nodes of enterprise program resource scheduling and monitoring. It fully considers the organizational needs of program resource scheduling, and designs and optimizes the organizational form, so as to provide a good organizational guarantee. It takes modern information technology as an effective technology management tool. It provides a platform for resource scheduling that can collect, transmit, process, and analyze the resource information of each project within the organization, so as to ensure more effective resource scheduling of enterprise program groups. This paper makes some exploratory work on the resource scheduling of enterprise program groups. However, this paper is still in its infancy, and there are still many aspects to be further improved. Due to the current data sources and practical experience, the project priority evaluation index system proposed in this paper has certain pertinence, and it is necessary to further improve. The mathematical model of resource scheduling is based on simplifying complex problems. In the actual problem processing, the problem should be considered more comprehensively. The organizational model of optimal design is only a preliminary idea, and its scope of application and internal structure needs to be further studied.

Data Availability

The data that support the findings of this study are available from the corresponding author upon reasonable request.

Conflicts of Interest

The authors declared no potential conflicts of interest with respect to the research, authorship, and/or publication of this article.

Acknowledgments

This work was supported by NSFC Project "Research on Long-Term Mechanism for Solving Relative Poverty in Ethnic Minority Areas" (No. 20BMZ14).

References

[1] C. You, Y. Zeng, R. Zhang, and K. Huang, "Asynchronous mobile-edge computation offloading: energy-efficient resource management," *IEEE Transactions on Wireless Communications*, vol. 17, no. 11, pp. 7590–7605, 2018.

[2] H. Zhang, N. Liu, X. Chu, K. Long, A. H. Aghvami, and V. C. M. Leung, "Network slicing based 5G and future mobile networks: mobility, resource management, and challenges," *IEEE Communications Magazine*, vol. 55, no. 8, pp. 138–145, 2017.

[3] E. E. Tsiropoulou, G. Mitsis, and S. Papavassiliou, "Interest-aware energy collection & resource management in machine to machine communications," *Ad Hoc Networks*, vol. 68, pp. 48–57, 2018.

[4] C. Chen, S. Ahmad, A. Kalra, and Z. Xu, "A dynamic model for exploring water-resource management scenarios in an inland arid area: shanshan County, Northwestern China," *Journal of Mountain Science*, vol. 14, no. 6, pp. 1039–1057, 2017.

[5] Y. Chen, Z. Lin, X. Zhao, G. Wang, and Y. Gu, "Deep learning-based classification of hyperspectral data," *Ieee Journal of Selected Topics in Applied Earth Observations and Remote Sensing*, vol. 7, no. 6, pp. 2094–2107, 2014.

[6] D. Shen, G. Wu, and H. I. Suk, "Deep learning in medical image analysis," *Annual Review of Biomedical Engineering*, vol. 19, no. 1, pp. 221–248, 2017.

[7] D. Ravi, C. Wong, F. Deligianni et al., "Deep learning for health informatics," *IEEE Journal of Biomedical and Health Informatics*, vol. 21, no. 1, pp. 4–21, 2017.

[8] P. Gyorgyi, "A PTAS for a resource scheduling problem with arbitrary number of parallel machines," *Operations Research Letters*, vol. 45, no. 6, pp. 604–609, 2017.

[9] P. Faria and Z. Vale, "Distributed energy resource scheduling with focus on demand response complex contracts," *Journal of Modern Power Systems and Clean Energy*, vol. 9, no. 5, pp. 1172–1182, 2021.

[10] P. Garcia Ansola, A. Garcia Higuera, F. J. Otamendi, and J. de las Morenas, "Agent-based distributed control for improving complex resource scheduling: application to airport ground handling operations," *IEEE Systems Journal*, vol. 8, no. 4, pp. 1145–1157, 2014.

[11] S. Y. Shin, Y. Brun, H. Balasubramanian, P. L. Henneman, and L. J. Osterweil, "Discrete-event simulation and integer linear programming for constraint-aware resource scheduling," *IEEE Transactions on Systems, Man, and Cybernetics: Systems*, vol. 48, no. 9, pp. 1578–1593, 2018.

[12] Y. Sun, P. Yao, and S. Zhang, "Dynamic battlefield resource scheduling model and algorithm with interval parameters," *Systems Engineering-Theory & Practice*, vol. 37, no. 4, pp. 1080–1088, 2017.

[13] S. K. Patel and A. K. Sharma, "Optimization of dynamic resource scheduling algorithm in grid computing environment," *INTERNATIONAL JOURNAL OF COMPUTER SCIENCES AND ENGINEERING*, vol. 6, no. 3, pp. 19–26, 2018.

[14] D. Nagaraju and V. Saritha, "An evolutionary multi-objective approach for resource scheduling in mobile cloud computing," *International Journal of Intelligent Engineering and Systems*, vol. 10, no. 1, pp. 12–21, 2017.

[15] B. K. Dewangan, M. Venkatadri, A. Agarwal, A. Pasricha, and T. Choudhury, "An automated self-healing cloud computing framework for resource scheduling," *International Journal of Grid and High Performance Computing*, vol. 13, no. 1, pp. 47–64, 2021.

[16] G. Litjens, T. Kooi, B. E. Bejnordi et al., "A survey on deep learning in medical image analysis," *Medical Image Analysis*, vol. 42, no. 9, pp. 60–88, 2017.

[17] D. S. Kermany, M. Goldbaum, W. Cai et al., "Identifying medical diagnoses and treatable diseases by image-based deep learning," *Cell*, vol. 172, no. 5, pp. 1122–1131.e9, 2018.

[18] J. Lee, "Integration of digital twin and deep learning in cyber-physical systems: towards smart manufacturing," *IET Collaborative Intelligent Manufacturing*, vol. 38, no. 8, pp. 901–910, 2020.

[19] T. Oshea and J. Hoydis, "An introduction to deep learning for the physical layer," *IEEE Transactions on Cognitive Communications and Networking*, vol. 3, no. 4, pp. 563–575, 2017.

[20] R. T. Schirrmeister, J. T. Springenberg, L. D. J. Fiederer et al., "Deep learning with convolutional neural networks for EEG decoding and visualization," *Human Brain Mapping*, vol. 38, no. 11, pp. 5391–5420, 2017.

[21] W. Hou, X. Gao, and D. Tao, "Blind image quality assessment via deep learning," *IEEE Transactions on Neural Networks and Learning Systems*, vol. 26, no. 6, pp. 1275–1286, 2015.

[22] T. Young, D. Hazarika, S. Poria, and E. Cambria, "Recent trends in deep learning based natural language processing [review article]," *IEEE Computational Intelligence Magazine*, vol. 13, no. 3, pp. 55–75, 2018.